ISTANBUL TECHNICAL UNIVERSITY ★ INSTITUTE OF SCIENCE AND TECHNOLOGY

DIFFERENT TOPOLOGIES ON BAROPLASTICS

Ph. D. Thesis by
Şebnem İNCEOĞLU

Department : Polymer Science and Technology

Programme : Polymer Science and Technology

APRIL 2010

ISTANBUL TECHNICAL UNIVERSITY ★ INSTITUTE OF SCIENCE AND TECHNOLOGY

DIFFERENT TOPOLOGIES ON BAROPLASTICS

Ph. D. Thesis by
Şebnem İNCEOĞLU
(515022006)

Date of submission : 04 March 2010
Date of defence examination : 22 April 2010

Supervisor (Chairman) : Prof. Dr. Metin H. ACAR (ITU)
Members of the Examining Committee : Prof. Dr. A. Tuncer ERCİYES (ITU)
Prof. Dr. Yusuf Z. MENCELOĞLU (SU)
Prof. Dr. F. Seniha GÜNER (ITU)
Assoc. Prof. Dr. A. Ersin ACAR (BU)

APRIL 2010

İSTANBUL TEKNİK ÜNİVERSİTESİ ★ FEN BİLİMLERİ ENSTİTÜSÜ

FARKLI TOPOLOJİLERE SAHİP BAROPLASTİKLER

DOKTORA TEZİ

Şebnem İNCEOĞLU
(515022006)

Tezin Enstitüye Verildiği Tarih : 04 Mart 2010
Tezin Savunulduğu Tarih : 22 Nisan 2010

Tez Danışmanı : Prof. Dr. Metin H. ACAR (İTÜ)
Diğer Jüri Üyeleri : Prof. Dr. A. Tuncer ERCİYES (İTÜ)
Prof. Dr. Yusuf Z. MENCELOĞLU (SÜ)
Prof. Dr. F. Seniha GÜNER (İTÜ)
Doç. Dr. A. Ersin ACAR (BÜ)

NİSAN 2010

FOREWORD

PhD thesis is not the work of only one person, but the result of cooperation with many other people. Therefore I would like to thank everyone who in one way or another contributed to this thesis. In the first place I would like to express my deep and sincere gratitude to my advisor Prof. Metin H. ACAR for his supervision, advice, and guidance of this research as well as giving me extraordinary experiences throughout the work. Above all and the most needed, he provided me unflinching encouragement and support in various ways. I am grateful in every possible way and hope to keep up our collaboration in the future.

I gratefully acknowledge Prof. Yusuf Z. MENCELOĞLU. I am much indebted to him for his support and valuable advice in science discussion.

I really appreciate Prof. Anne M. MAYES for giving me the opportunity of being a researcher in Mayes Group, Material Science Department at Massachusetts Institute of Technology. I cherish the group members that support me, and the friendships with Juan, Sang-Woog, Will, Ariya, Ayşe and Solar.

Special thanks to the present and past MACAR Group members, especially to Atılay TUZER and Ari Şant BİLAL for their great contribution in this research topic. Additionally, I would like to thank Artun ZORVARYAN, Candan ÇATLI, Damla GÜLFİDAN, Evrim BÜYÜKASLAN, Yıldız AÇIKALIN, C. Erdinç TAŞ and Hamza KOCATÜRK for their help, understanding, support and friendship.

Many thanks go in particular to Sabancı University colleagues Taner AYTUN, Burak BİRKAN, Assis. Prof. Ilhan OZEN and Assoc. Prof. Cleva Ow-YANG for their collaboration.

I am also greatly indebted to Aydın ŞAŞMAZ. Without his encouragement, support and understanding it would have been impossible for me to finish this work.

I would really like to thank my special friends Aydan DAĞ, Eda GÜNGÖR and İpek ÖSKEN for their unconditional support, help and encouragements.

Also my friends and family indirectly contributed to this thesis by showing their interest and providing the necessary social distraction. I would like to especially thank to my parents and my brother for their love, support and absolute confidence in me.

Finally, I would like to thank everybody who was important to the successful realization of this thesis, as well as expressing my apology that I could not mention personally one by one.

This work is supported by ITU Institute of Science and Technology and TUBITAK (107M323).

April 2010

Şebnem İnceoğlu

Polymer Science and Technology

TABLE OF CONTENTS

Page

ABBREVIATIONS

TPE	**:** Thermoplastic elastomers
SBCs	**:** Styrenic block copolymers
PS	**:** Polystyrene
PEHA	**:** Poly(ethyl hexyl acrylate)
PBA	**:** Poly(butyl acrylate)
PI	**:** Polyisoprene
PB	**:** Polybutadiene
PBMA	**:** Poly(*n*-butyl methacrylate)
SANS	**:** Small angle neutron scattering
UDOT	**:** Upper disorder-to-order temperature
CRS	**:** Compressible regular solution
CRP	**:** Controlled/'living' radical polymerization
RP	**:** Radical polymerization
ATRA	**:** Atom transfer radical addition
ATRP	**:** Atom transfer radical polymerization
ARGET	**:** Activators regenerated by electron transfer
PDI	**:** Polydispersity
TEM	**:** Transmission electron microscopy
SPM	**:** Scanning probe microscopy
AFM	**:** Atomic force microscopy
DSC	**:** Differential scanning calorimeter
MDSC	**:** Modulated differential scanning calorimeter
UCST	**:** Upper-critical solution temperature
DMA	**:** Dynamic mechanical analysis
CuCl	**:** Copper (I) chloride
CuBr	**:** Copper (I) bromide
HEA	**:** 2-hydroxy ethyl acrylate
PEHA	**:** Pentaethylenehexamine
BPB	**:** 2-bromopropionylbromide
EDA	**:** Ethylenediamine
DETA	**:** Diethylenetriamine
TETA	**:** Triethylenetetramine
HPTETA	**:** Hexapentyltriethylenetetramine
ALAL	**:** Alkylated linear amine ligand
THF	**:** Tetrahydrofuran
$LiAlH_4$	**:** Lithium aluminium hydride
DCM	**:** Dichloromethane
Et_3N	**:** Triethylamine
Me_6-TREN	**:** Tris(2-(dimethylamino)ethyl) amine
NaOH	**:** Sodium hydroxide
Na_2SO_4	**:** Sodium sulphate
$NaHCO_3$	**:** Sodiumbicarbonate

NaCl	**:** Sodiumchloride
PMDETA	**:** *N, N, N′, N″, N″*-pentamethyldiethylenetriamine
Bipyr	**:** 2,2′-bipyridine
$CDCl_3$	**:** Deuterated chloroform
NMR	**:** Nuclear magnetic resonance
FT-IR	**:** Fourier transform infrared
ATR	**:** Attenuated total reflectance
UV-VIS	**:** Ultraviolet-visible
GPC	**:** Gel permeation chromatography
GC	**:** Gas chromatography
FID	**:** Flame ionization dedector
ASTM	**:** American society for testing and materials

LIST OF TABLES

Page

LIST OF FIGURES

Page

LIST OF SYMBOLS

σ	**:** Stress
A	: Area
F	**:** Force
E	**:** Modulus
δ	**:** Loss angle
γ	**:** Shear strain
τ	**:** Shear stress
η	**:** Viscosity
M	**:** Monomer
I	**:** Initiator
S	**:** Spheres
C	**:** Cylinders
G	**:** Double gyroid
L	**:** Lamellae
T	**:** Temperature
V	**:** Velocity
R-X	**:** Alkyl halide
tan δ	**:** Loss factor
G", E"	**:** Loss modulus
G' , E'	**:** Dynamic storage modulus
k_{act}	**:** Rate constant of activation
k_{deact}	**:** Rate constant of deactivation
k_p	**:** Rate constant of propagation
k_t	**:** Rate constant of termination
X_n	**:** Degree of polymerization
$T_{g,mix}$	**:** Mixed glass transition temperature
T_g	**:** Glass Transition Temperature
R_p	**:** Polymerization rate
M_w/M_n	**:** Molecular weight distribution
T_{ODT}	**:** Order-disorder temperature

DIFFERENT TOPOLOGIES ON BAROPLASTICS

SUMMARY

In today's world, life without plastics is incomprehensible. Every day, plastics contribute to our health, safety and comfort. The manufacturing of commercial plastics (thermoplastic and thermoplastic elastomers) traditionally involves melt processing at temperatures typically close to melting temperatures (T_m)-to enable extrusion or molding under pressure into desired forms-followed by solidification. This process consumes energy and can cause substantial degradation of polymers and additives limiting plastics performance and recyclability. As an alternative to melt processing, Mayes and Acar et al. had proposed a material called "baroplastic" di-block copolymers, core-shell polymer nanoparticles and biodegredable block copolymers that can be processed mainly by the application of pressure at low/room temperature instead of high temperatures. However, there is a limitation for processing (under the pressure) of core-shell baroplastics because is the processing highly dependent on composition, particle size and processing conditions. To overcome this problem, it was thought that star-block copolymers looked like core-shell nano particles containing high T_g shell and soft T_g core having the difference of covalently bonding that may cause the adjustment of the chain length of each segment.

The main aim of this project is an attempt to understand, the effect of structure on rheological flow of polymers having different topologies with different segments. the goal of expanding the range of existing baroplastics has been achieved. For this purpose, in order to synthesize well defined di-, tri- and star-block copolymers, first suitable multi functional initiators were synthesized by known or new developed methods, and from them well-defined homopolymers with different topologies and molecular weights were synthesized. Obtained block copolymers' baroplastic properties were investigated by simple compression and/or extrusion at room temperature. For extrusion molding, "custom-made" molds were designed to improve the processing at room temperature. Moreover, the imprinting and coloring of baroplastic polymers were demonstrated. Control experiments were performed in order to ensure the processability of block copolymers containing different segments, blend polymers and random copolymers were investigated.

In this study, the effect of topologies, compositions, molecular weights, recycling numbers and pressure were examined in depth for obtained novel baroplastic materials. One additional step was taken and the physical changes (from ordered to disordered state) of "baroplastic" block copolymers after processing at room temperatures were included in the study. In order to obtain a comprehensive understanding of the processability of baroplastics and resulting properties, thermal, morphological, rheological and mechanical property measurements were performed.

Additionally, the possibility of using optimized amount of baroplastic materials as processing aid, in order to process high temperature processing polymers at room temperature under pressure, was demonstrated for the first time with polystyrene that is a commodity and high temperature processing polymer.

During thesis work, baroplastic materials could be recovered 100% without any degradation after multiple recycling cycles. From this result, it can be concluded that the baroplastic materials may be recycled for infinity times.

Herein, when high and low temperature processing were compared, the equipments that are used for the manufacturing of current commercial plastics could be suitable for baroplastic processing as well, since the room temperature processing does not require high pressure i.e. range of pressure used in the thermal processing. Thus, with all this reduced resource utilization, baroplastics can be considered as new environment-friendly materials with different topologies contributing to the economy.

FARKLI TOPOLOJİLERE SAHİP BAROPLASTİKLER

ÖZET

Günümüzde, plastiğin yer almadığı bir yaşam düşünülememektedir. Plastikler günlük yaşantımızda sağlık, güvenlik ve komfor bakımından katkı sağlamaktadırlar. Genellikle, endüstride kullanılan ticari plastiklerin (termoplastik ve termoplastik elastomerler) işlenmesinde (processing), plastiğin erime sıcaklığı (T_m) yakınına ısıtılarak, basınç yardımı ile ekstrüder veya kalıplarda istenen şekillerin verilmesi ve de katılaştırılması yöntemi kullanılır. Bu yöntem, çok yüksek sıcaklıklara çıkıldığından dolayı enerji sarfiyatına, polimer ve katkı malzemelerinin bozunmasına neden olurken aynı zamanda kullanılan katkı malzemelerinin üretilen plastiğin kalitesinin düşmesine yol açmakta ve malzemenin geri dönüşümünün de sınırlandırılmasına neden olmaktadır. Plastiklerin yüksek sıcaklıktaki proseslerine alternatif olarak Mayes ve Acar' ın çalışma grubu düşük/oda sıcaklığında basınç altı nda proses edilebilen baroplastik di-blok kopolimer, çekirdek-kabuk nanoparçacık polimer ve biyobozunabilen blok kopolimerleri ortaya çıkarmışlardır. Fakat çekirdek-kabuk baroplastik polimerlerin proses işlemi için kompozisyonuna, partikül boyutuna ve proses koşullarına bağlı olması açısından sınırlamaları bulunmaktadır. Bu problem çözmek amacıyla, yüksek T_g'ye sahip kabuk ve düşük T_g'ye sahip çekirdek içeren çekirdek-kabuk yapısına benzeyen, herbir segmentin zincir uzunluğu ayarlanabilen kovalent bağlı yapıya sahip yıldız blok kopolimerler düşünülmüştür.

Bu projenin esas amacı olarak, farklı topoloji ve segmentlere sahip olan polimerlerin yapısının reolojik akışa etkisini incelemek amacıyla, varolan baroplastik malzemelerin çeşitlendirilmesi gerçekleştirilmiştir. Bu amaç doğrultusunda, önce çok fonksiyonlu başlatıcılar bilinen ve yeni geliştirilen yöntemlerle elde edilmiş ve bu başlatıcılar kullanılarak değişik topolojilerde ve molekül ağırlıklarında homopolimerler ve bu homopolimerden yola çıkılarak farklı kompozisyonlarda ve molekül ağırlıklarında iyi tanımlanmış blok kopolimerler sentezlenmiştir. Elde edilen blok kopolimerlere oda sıcaklığında basit sıkıştırma ve/veya ekstrüzyon işlemleri uygulanarak baroplastik özellikleri incelenmiştir. Oda sıcaklığında proses işlemini kolaylaştırmak amacıyla yeni ekstrüzyon kalıpları dizayn edilmiştir. Bununla beraber, baroplastik polimerlerin yazı baskılama ve renklendirilmeleri çalışmaları yapılmıştır. Farklı segmentlere sahip blok kopolimerler ile karışım ve rastgele kopolimerler için kontrol deneyleri gerçekleştirilmiştir.

Bu çalışmada, yeni tür baroplastik malzemeler için topoloji, kompozisyon, molekül ağırlığı, geri dönüşüm sayısı ve basıncın etkisi araştırılmıştır. Bunlara ek olarak, oda sıcaklığında basınç altında proses edilebilen baroplastik malzemelerin proses sonrasındaki fiziksel değişimleri (düzenli halden düzensiz hale geçişi) incelenmiştir. Baroplastiklerin proses edilebilirlikleri ve proses sonrası elde edilen özelliklerin tümüyle anlaşılabilmesi için termal, morfolojik, reolojik ve mekanik özellikleri ölçümleri gerçekleştirilmiştir.

Ayrıca, baroplastikler proses yardımcı maddesi olarak değerlendirilerek, yaygın kullanımı olan ve yüksek sıcaklıklarda proses edilen ticari polimerler ile fiziksel karıştırılarak polistirenin oda sıcaklığında ilk kez proses edilebilirlikleri gösterilmiştir.

Tez çalışmasında, birçok kez tekrarlanan geri dönüştürülme işlemlerinde baroplastik malzemenin bozunmaya uğramadan ve madde kaybı olmadan %100 geri kazanım sağlandığı gözlemlenmiştir. Bu durum baroplastik malzemelerin sonsuz kez geri dönüştürülerek kullanılabileceği şeklinde değerlendirilebilir.

Bu çalışmada, yüksek ve düşük sıcaklıkta proses koşulları karşılaştırıldığında, oda sıcaklığında proses işleminin yüksek basınçlar gerektirmediğinden dolayı endüstride termal prosesler için kullanılan cihazların baroplastik malzemeler için de kullanılabileceği değerlendirilmesi yapılabilir. Tüm bu sonuçlar göz önüne lındığında kaynak kullanımı azaltılabileceğinden farklı topolojilere sahip baroplastikler, ekonomiye katkı sağlayan ve çevre dostu yeni bir malzeme olarak değerlendirilebilir.

1. INTRODUCTION

Plastics have grown into a major industry that affects our whole lives, since the 1950s, by providing improved packaging, giving us new textiles, permitting the production of wondrous new products and cutting edge technologies such as in televisions, cars and computers. Owing to their multifaceted application possibilities, plastics have become indispensable fixtures of modern life.

The construction of polymeric materials with controlled compositions, topologies, and functionalities has been the enduring focus in the current research. The significance of controlled polymerization as a synthetic tool is widely recognized and polymers having uniform predictable chain length are readily available. Controlled polymerization provides the best opportunity to control the bulk properties of a target material through control of the multitude of possible variations in composition, functionality and topology now attainable at a molecular level. Atom Transfer Radical Polymerization (ATRP) is one of the most successful methods to polymerize styrenes, meth(acrylates) and a a wide range of monomers in a controlled fashion, yielding polymers with molecular weights predetermined by the ratio of the concentrations of consumed monomer to introduced initiator with low molecular weight distribution.

The block copolymers, which become phase separate due to thermodynamic immiscibility of the constituent blocks, are the subject of a large interest during the last decades due to their unique morphologies and useful properties. The numerous possibilities of variation of architecture and properties within this polymer class allow manufacturing of plastic materials with tailor-made properties for specific applications of special interest, so-called thermoplastic elastomers which are composed of glassy outer blocks and rubbery inner blocks. If the styrene content in the block copolymer is small enough the block copolymer will have a microphase separated morphology. This morphology can be proved by the existence of two glass transition temperatures corresponding to the glassy and elastomeric phases.

By heating to temperatures above their glass transition temperature (T_g) the rigid domains can be weakened. Therefore such materials can be processed at elevated temperatures, e.g. by extrusion or injection moulding. The manufacturing of plastics (block copolymers) traditionally involves melt processing at temperatures typically close to melting temperatures (T_m) -to enable extrusion or moulding under pressure into desired forms- followed by solidification. Thermoplastics, because of little or no cross-bonding between molecules, soften when heated and harden when cooled. Unlike inorganic glasses or metals, recycling of conventional polymers results in substantially lower grade materials, greatly limiting their reuse. A primary reason is the poor thermal stability that polymers exhibit at elevated temperatures necessary for reprocessing, which causes substantial discoloration and loss of mechanical performances.

As an alternative to melt processing, Mayes et. al. and Acar et al. had proposed a material called “baroplastics” di-block copolymers, core-shell polymer nanoparticles and biodegradable block copolymers that can be processed mainly by the application of pressure at low/room temperature instead of high temperatures. The processing is achieved by exploiting the pressure-induced miscibility of low T_g and high T_g components. Baroplastic properties could be defined as the processability of polymers to obtain transparent objects when pressure is applied to the polymer in the mold causing the phase separation of block segments that substantially preserves a new mixed phase. In contrary to conventional polymers, baroplastic materials can be remolded (recycled) many times at room temperature without losing their mechanical properties.

The goal of this thesis is expanding the range of existing baroplastics and to investigate the effect of room temperature processing on thermal, morphological, rheological and mechanical properties of baroplastics with different topologies. One additional step was taken to process homopolymer polystyrene at room temperature, baroplastic polymers were used as processing aid and the processibility of blends under pressure was studied.

2. THEORETICAL PART

2.1 Plastics

Plastic is the material of the 21st century. We are hardly aware of it anymore but we live in the age of plastics. Owing to their multifaceted application possibilities, plastics have become an indispensable fixture of modern life. From coffee machines to telecommunications satellites, from non-slip steering wheels to ultra-light airplane seats, from yoghurt cups to well-insulated energy-saving houses, from swimwear to hard-shell suitcases: plastics are always there, meeting our basic needs and creating equipment for our modern lifestyle. Plastics can be expected to be successfully used in all applications where they are open up completely new potential. They thus point the way toward sustainable development [1]. Plastics play a crucial role in technology-economy-environment circle. A material that is utilized in some end product and then discarded passes through several stages or phases; these stages are represented in Figure 2.1**,** which is sometimes termed the "total plastics cycle".

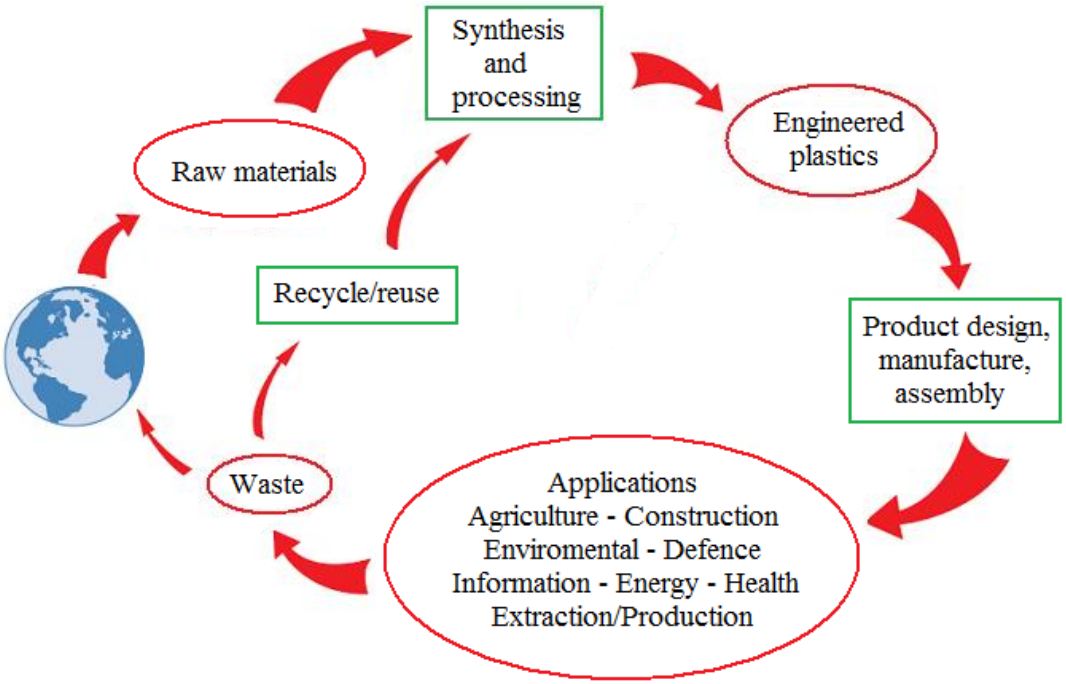

Figure 2.1 : Schematic representation of the total plastic cycle.

Important stages in the plastics cycle where materials science and engineering plays a significant role are recycling and disposal. The issues of recyclability and disposability are important when new materials are being designed and synthesized [2]. There are a lot of different types of plastics which using in industry. To make sorting and thus recycling easier, in 1988 the Society of the Plastics Industry developed a standard marking code from 1 to 7 to categorize the polymer types [3-4]. Recycling to plastics is essentially the typical secondary recycling. It begins with collection of postconsumer items, such as used bottles, cleaning and sorting them according to their identification code, shredding into granular form or converting into pellets by melting, melt filtration, and subsequent pelletization, granules and pellets are most frequently added in required proportion to virgin resins. Lastly, recycle them by processing methods -blow molding, injection molding, extrusion- to reuse of plastic products. This is the known thermal reprocessing for thermoplastics. It should be noted that most plastics cannot be remelted indefinitely without adverse effects on the polymer, such as loss of mechanical properties, discoloration, and possibly partial cross-linking. For that reason, the use of 100% recycled material is seldom practiced [5].

2.1.1 Thermoplastic elastomers

Thermoplastic elastomers (TPE), sometimes referred to as thermoplastic rubbers, are a class of copolymers or a physical mix of polymers (usually a plastic and a rubber) which consist of materials with both thermoplastic and elastomeric properties. While most elastomers are thermosets, thermoplastics are in contrast relatively easy to use in manufacturing, for example, by injection molding. Thermoplastic elastomers show both advantages typical of rubbery materials and plastic materials. Currently known TPEs can be classified into the following seven groups: (1) styrenic block copolymers (SBCs); (2) crystalline multiblock copolymers; (3) miscellaneous block copolymers; (4) combinations of hard polymer/elastomer; (5) hard polymer/elastomer graft copolymers; (6) ionomers; and (7) polymers with core-shell morphologies. Styrenic block copolymers (SBCs) are based on simple molecules of the type A–B–A, where A is polystyrene and B is an elastomeric segment. The most common structure of SBCs is that where the elastomeric segment is a polydiene, such as polybutadiene or polyisoprene.

The styrene-butadiene materials possess a two-phase microstructure due to incompatibility between the polystyrene and polybutadiene blocks, the former separating into spheres or rods depending on the exact composition. With low polystyrene content, the material is elastomeric with the properties of the polybutadiene predominating. The structure representing a styrenic thermoplastic elastomer (TPE) is shown schematically in Figure 2.2 [6].

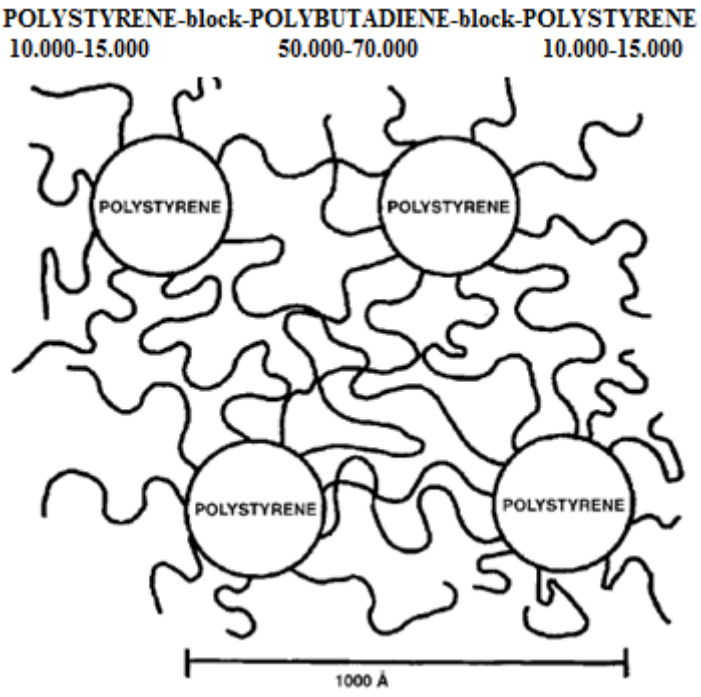

Figure 2.2 : Schematic representation of a styrene–butadiene–styrene block copolymer.

The polystyrene phase, which is present as a minor part of the total volume consists of separate spherical regions (domains). These domains are attached to the ends of elastomeric chains and form in this way multifunctional junction points similar to cross-links in a conventionally vulcanized elastomer (vulcanizate). The difference is that these cross-links are of a physical nature that is in contrast to the chemical nature of cross-links in the vulcanizate and therefore considerably less stable. At ambient temperatures, this block copolymer behaves in many ways like vulcanized rubber. When it is heated, the polystyrene domains soften, the network becomes weaker, and eventually the material is capable of flowing, and when it is cooled again, its original elastomeric properties are regained as the polystyrene domains become rigid.

Block copolymers, such as poly(styrene-*b*-isoprene-*b*-styrene) (PS-*b*-PI-*b*-PS) and poly(styrene-butadiene) (PS-*b*-PB)$_x$ (where x represents a multifunctional junction point), can form similar continuous networks, provided the polystyrene blocks are the minor component. However, structures such as PI-*b*-PS-*b*-PI, PB-*b*-PS-*b*-PB, PS-*b*-PI, PS-*b*-PB are not capable of forming continuous networks because only one end of each polydiene chain is terminated by a polystyrene block and the resulting materials are weak with no resemblance to conventional vulcanized rubber [5, 7].

Thermoplastic elastomers are materials, which can be generally processed by melt-processing methods used for plastics. Thermoplastic elastomers, as any other thermoplastic materials are formed into articles almost exclusively by melt processes that rely on the flow of the melted material at elevated temperatures. Injection molding, blow molding, extrusion, and rotational molding/lining are all examples of melt processing. The melt processing of thermoplastic elastomers involves first heating the material to a point at which it can be made to flow, and then cooling it again to a temperature at which the formed object is stable. This requirement constitutes a major energy demand in the forming process, and is central to the efficiency and economy of the process [5]. Additionally, this process can cause substantial degradation of polymers and additives, limiting plastics performance and recyclability [8].

2.1.2 Baroplastics

A novel class of materials called “baroplastic” block copolymers that can be processed by an applied pressure at low temperature due to a pressure-induced miscibility between two-immiscible polymer phases. A series of block copolymers containing a low T_g block such as poly(alkyl acrylate) and a high T_g block such as polystyrene or poly(alkyl methacrylate) exhibited room temperature processability by compression molding under pressure [9-19]. In recent works, only with di-block copolymers, core-shell nanoparticles and biodegradable block copolymers have been studied with emulsion and controlled/living radical polymerizations and demonstrated the baroplastic abilities at room temperature.

Representative schematic structures of baroplastics are shown in Figure 2.3 and the images of processed baroplastic di-block copolymers belongs to PS-*b*-PEHA (polystyrene-*b*-polyethylhexylacrylate) and PS-*b*-PBA, (polystyrene-*b*-polybutylacrylate) respectively were shown in Figure 2.4.

The transparency of the moulded objects and their accuracy of form are testimony that the copolymer flowed under applied pressure to take shape of its container. For example, the lid of a plastic sample holder box was copied to sufficent accuracy to provide a tight seal with original box [12].

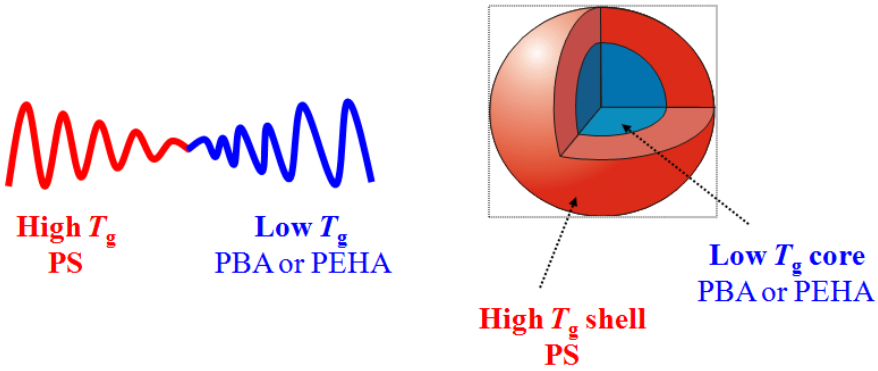

Figure 2.3 : Schematic representation of di-block copolymers and core-shell nanoparticles.

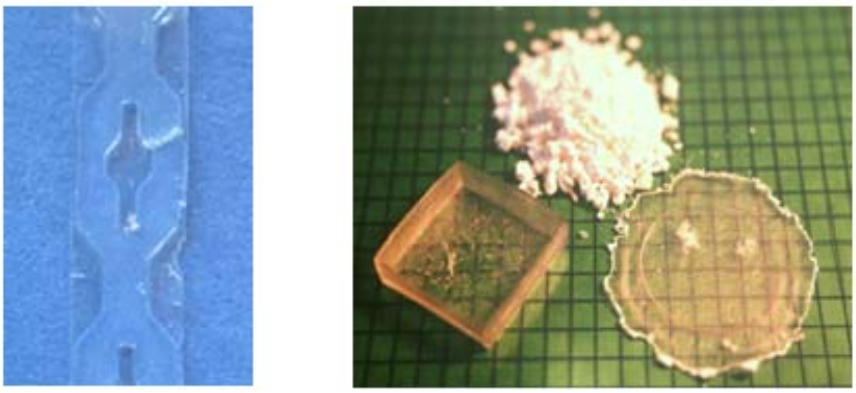

Figure 2.4 : Processed baroplastic di-block copolymers.

It was found from the related research, the requirements for a baroplastic utilizing pressure-induced miscibility are that it:

1. comprise material which is pressure-induced miscible
2. is composed of a hard (high T_g) and a soft (low T_g) component
3. has components which are unmixed at ambient temperature
4. has a high degree of interfacial surface area.

Recent research has demonstrated that pressure is a thermodynamic alternative to temperature for inducing polymer flow, or otherwise enhancing processability. A series of publications [12, 20-23] on the behavior of polymer pairs under applied pressure demonstrate that certain pairs undergo a pressure-induced miscibility that, in combination with their chosen respective "soft" and "hard" textures (low and high T_g, respectively) at room temperature, makes them "baroplastic" in nature. This opens the door for a class of plastic materials that become processable with the application of hydrostatic pressure at greatly reduced temperatures relative to traditional thermoplastic processing.

In 1998, Russell and coworkers reported that the miscibility of the blocks of polystyrene-*b*-poly(*n*-butyl methacrylate) (PS-*b*-PBMA), as measured by small angle neutron scattering (SANS), is enhanced by pressure at 180 ^{o}C [20]. Follow-up studies showed similar behavior for block copolymers of PS with other *n*-alkyl methacrylate species [21, 23-28]. Polybutadiene-*b*-polyisoprene does the same [29], as does poly(ethylene propylene) when in a block copolymer with poly(ethyl ethylene) [30] or poly(dimethyl siloxane) [31]. This transition from order to disorder brings with it all the phenomena observed in the upper disorder-to-order temperature (UDOT) when reached thermally, including the change in stiffness from solid to melt as measured rheologically [24, 28, 32] and the decrease of the scattering intensity of the SANS correlation hole of the block copolymer.

In 2001, Mayes and coworkers present a simple model for the free energy of mixing of compressible blend polymers, based on a modification of the Flory-Huggins regular solution model, the compressible regular solution (CRS) model (2.1) [21]. They add compressibility effect as 2nd and 3rd terms and reduced density of components into the 1st term. This equation tells us, if there is a relationship between reduced density of two segments as $1.06\rho_A<\rho_B<0.94\rho_A$ and when the temperature is goes to 0 K the 3rd term is negative, the incompatible segments can be compressible theoretically and they have been found to exhibit pressure-induced miscibility, including polystyrene(PS)/poly(butyl methacrylate), PS/poly(hexyl methacrylate), PS/poly(ethylene propylene), polybutadiene/polyisoprene, poly(ethylene propylene)/poly(ethyl ehylene), PS/poly(butyl acrylate) and PS/poly(ethyl hexyl acrylate).

By contrast, these conditions are not met for PS/polyisoprene or PS/polybutadine, two commercially important block copolymer systems that have been found to exhibit reduced miscibility with applied pressure [12].

$$\Delta g_{mix} = kT\left[\frac{\phi_A\tilde{\rho}_A}{N_A\nu_A^*}\ln\phi_A + \frac{\phi_B\tilde{\rho}_B}{N_B\nu_B^*}\ln\phi_B\right] + \phi_A\phi_B\tilde{\rho}_A\tilde{\rho}_B(\delta_{A0}-\delta_{B0})^2 + \phi_A\phi_B\left[(\tilde{\rho}_A-\tilde{\rho}_B)(\delta_A^2-\delta_B^2)\right] \quad \textbf{(2.1)}$$

The CRS model was utilized to predict the phase behavior of certain polymer pairs, and to obtain some insight about the pressure dependence of many polymer systems. For a baroplastic to work, the phase behavior of the mixture should be such that phase separation is present at room temperature and atmospheric pressure. Knowledge, at least qualitatively, of the phase diagram for baroplastic candidate materials becomes then a necessity. The PS/poly(*n*-butyl acrylate) (PS-*b*-PBA) and PS/poly(ethyl hexyl acrylate) (PS-*b*-PEHA) systems were synthesized and tested; first, as block copolymers. Then, due to the relatively high cost of block copolymers in industry, core-shell particles were also synthesized via a sequential emulsion process [13, 19]. In both structures, the final precipitate could be molded at ambient temperature using a hydraulic press. The resulting rigid parts were transparent and very true to the mold. Furthermore, the material was shredded and remolded multiple times, with no or little change in properties. In core-shell nano particle baroplastics; however, the processing cost was decreased, it was unfortunately found that when the size of the core-shell has increased, processibility is decreased (Figure 2.5) [11].

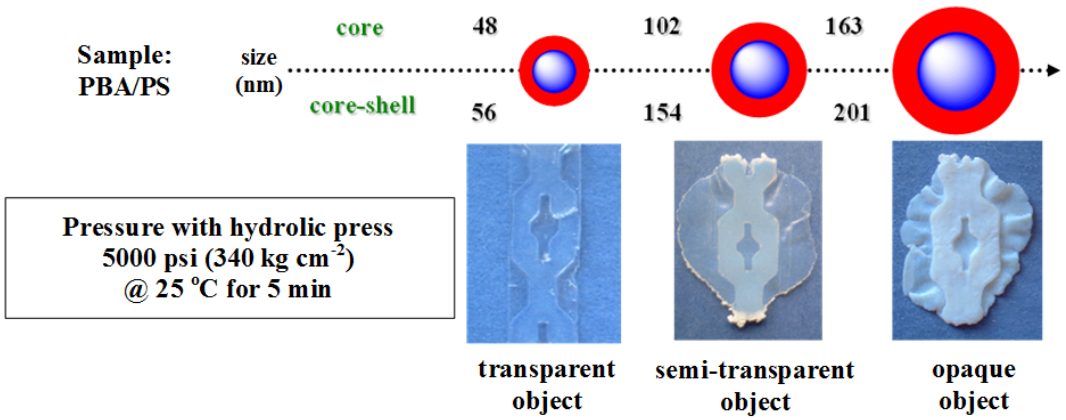

Figure 2.5 : Core-shell size effect on room-temperature processing under pressure.

In 2005, the economic feasibility of market integration of baroplastics have been investigated that compared with traditional TPEs. It was found that there are several main differences in the fabrication of baroplastics and thermoplastics that are cycle time, price of unprocessed polymer and mold life.

As alternatives to traditional plastics, preliminary cost models have shown baroplastic's potential to be cheaper and more enviromentally friendly. Unfortunately these calculations were not applied on the recycling mateials [14].

In summary, baroplastic materials can provide several advantages over current commodity plastics; for example, lower processing temperatures that save energy in processing, which generally requires heating and cooling cycles. Another advantage is that thermal degradation can be reduced with baroplastic materials, which is typically present in melt processing and is one of the problems with current polymer recycling, where reprocessing leads to a material with poor optical and mechanical properties. Consequently, baroplastic materials can conceivably be processed many times without degradation, no additive required, resulting in a material with a long recycle life.

2.3 Block Copolymers

Macromolecular engineering is an integrated chemical process aimed at designing polymeric materials for specific advanced applications. In order to achieve this goal, tailor-made block copolymers with specific macromolecular architecture, chemical composition/functionality, desired molecular weight and low polydispersity have to be synthesized [33]. Block copolymers made by the covalent bonding of two or more polymeric chains that, in most cases, are thermodynamically incompatible giving rise to a rich variety of microstructures in bulk and in solution. The variety of microstructures causes to occur to materials with applications ranging from thermoplastic elastomers and high-impact plastics to pressure-sensitive adhesives, additives, foams, etc. In addition, block copolymers are very strong candidates for potential applications in advanced technologies such as information storage, drug delivery, and photonic crystals. Therefore, it is not surprising that these materials play a central role in contemporary macromolecular science covering the full spectrum of polymer chemistry, polymer physics, and applications [34-35].

2.3.1 Topologies of block copolymers

A block copolymer is a linear arrangement where two often incompatible blocks obtained from different monomers are covalently linked together. It is possible to prepare di-block (A-B), tri-block (A-B-A and B-A-B) and multi-block (or segmented) copolymers [36]. An indispensable requirement for the preparation of well-defined block copolymer structures is the utilization of a living, or at least a controlled chain-growth polymerization method, in connection with suitable purification methods for all reagents employed (monomers, solvents, linking agents, additives etc.) and techniques for excluding the introduction of any impurity in the polymerization system. Under such conditions undesired irreversible termination or irreversible transfer reactions are absent, or at least minimized allowing for the synthesis of chemically and molecularly homogeneous structures.

Two methods have been developed for the synthesis of *linear AB diblock copolymers*: (a) sequential addition of monomers (one-pot or two-pot); and (b) coupling of two appropriately end-functionalized chains. The first method is the most widely used for the synthesis of block copolymers. An essential consideration for the successful employment of the technique is the order of monomer addition. The living chain from the polymerization of the first monomer must be able to efficiently initiate the polymerization of the second monomer. Another important requirement in the one-pot method is that the conversion of the first monomer must be quantitative in order to achieve control over the molecular weights as well as chemical and structural homogeneity.

The synthesis of *linear ABA triblock copolymers* can be accomplished using one of the following methods: (a) three-step sequential addition of monomers; (b) two-pot sequential addition of monomers followed by a coupling reaction with a suitable difunctional linking agent; and (c) use of a difunctional initiator and a two-step or one-pot sequential addition of monomers [35]. The most straightforward and widely explored method so far is the use of a difunctional initiator. The middle block B is made first, bearing at both ends active sites capable of initiating the polymerization of the second monomer A, which is added sequentially to the reaction medium after the consumption of the first monomer. The advantages of this method is that it can be performed in a one-pot procedure [33, 37].

Star-block copolymers are actually star-shaped macromolecules where each arm is a block copolymer. The number of branches can vary from a few to several tens. The topological difference of this kind of macromolecules, with respect to linear block copolymers, is focused on the existence of a central branching point, which, by itself, brings a certain symmetry in the macromolecule and sometimes defines a certain amount of intramolecular ordering [34, 38-39]. Interest in star polymers arises from their compact structure and globular shape, which predetermines their low viscosity when compared to linear analogues and makes them suitable materials for several applications. Synthesis of star polymers, which began in the 1950s with living anionic polymerization, has recently received increased attention due to the development of controlled/living radical polymerization (CRP) [40].

There are several methods used for the synthesis of star-block copolymers. Typically, star polymers are synthesized via CRP by one of two strategies: core-first [41-46] and arm-first. The arm-first strategy can be further subcategorized according to the procedure employed for star formation. One method is chain extension of a linear arm precursor with a multivinyl crosslinking agent, and the other is coupling linear polymer chains with a multifunctional linking agent or "grafting-onto" a multifunctional core [47-56]. With using of multifunctional initiators, multifunctional compounds capable of simultaneously initiating the polymerization of several branches are used to form a star polymer, A_n, where n is the functionality of the star in the core-first method. These living ends can then initiate the polymerization of the second monomer to give the star-block copolymer, $(A\text{-}b\text{-}B)_n$ or they can react with the end-functionalized pre-synthesized B chains to afford the same product. Several requirements are necessary for a multifunctional initiator to produce star polymers with uniform arms, low molecular weight distribution and controllable molecular weights.

Summarized as, the controlled radical polymerization techniques opened up a new era in block copolymer synthesis, and further growth and developments are certain [35].

2.3.2 Synthesis of block copolymers

2.3.2.1 Controlled/living radical polymerization

Recent advances in polymer synthesis, that have been used for many years, allow for polymer chains to be grown to precise molecular weights and contain functional groups at specific positions within each chain. The most important of these techniques, that a relatively new method to synthesize well-defined polymers and copolymers, are collectively called controlled/living radical polymerizations (CRP). In order to understand any of the CRP mechanisms, it is necessary to grasp the underlying mechanisms of conventional radical polymerization since each CRP technique still involves the elementary radical reactions found in conventional radical polymerization systems [57].

Radical polymerization (RP) is industrially the most widespread method to produce polymeric materials such as plastics, rubbers and fibers. It can be used for the (co)polymerization of a very large range of vinyl monomers under undemanding conditions; requiring the absence of oxygen, but tolerant to water, and can beconducted over a large temperature range (-80 to 250 ^{o}C). This is why nearly 50% of all commercial synthetic polymers are prepared using radical chemistry providing a spectrum of materials for a range of markets [58]. Although a wide variety of methods exist for the production of polymers, radical polymerizations have constituted the method of choice for an estimated 50% of all commercially made polymers. The major drawbacks of conventional radical polymerizations are related to the lack of control over the polymer structure. Due to the slow initiation, fast propagation and subsequent irreversible transfer or irreversible termination, polymers with high molecular weights and high polydispersities are generally produced. These features are reflected in the physical and mechanical properties of the produced polymers and to alter and improve these properties, random copolymerizations have been traditionally used [59]. The primary reason for choosing CRP over a conventional radical polymerization is to gain:

1. predictable molecular weights,

2. narrow molecular weight distributions (i.e. low polydispersities), and

3. chain end functionality.

In order to achieve these idealized outcomes the following three are in turn discussed in more detail below, must occur:

1. the initiation situations, which chains must be fast and quantitative,

2. the percentage of irreversibly terminated chains must be small, and

3. exchange between dormant and active species must be fast relative to propagation.

The problem faced with attempting to achieve control over molecular weights and functionality that rivals anionic polymerization yet using radical intermediates manifests itself in the inherent self-reactivity of the radical species. What one would like to do is initiate all chains at the same time (i.e. fast initiation), thus allowing them to grow under identical conditions and therefore yielding polymer chains that are virtually identical. This means that the chains should have the same degree of polymerization (X_n), and low polydispersity. This is what happens during a living anionic polymerization since anions do not self-react. However, to do this at typical polymer chain concentrations (say, between 10^{-4} to 10^{-1} M) with radical intermediates, the rate of radical-radical termination would be so high that the large majority of chains would simply terminate without significant growth. This is obviously a major obstacle to gaining high molecular weight, low polydispersity, and high chain end functionality, and is a consequence of attempting to initiate all chains at the same time. It has been realized for some time that in order to use radical intermediates in a living-type of polymerization it is necessary to keep the concentration of growing chains at appropriate levels, as stated above, somewhere around 10^{-4} to 10^{-1} M, while keeping the radical concentration low, preferably less than 10^{-8} M. As a result, the rate of radical-radical termination will be drastically reduced (rate of termination $R_t = k_t [R^{\cdot}]^2$, where k_t is an overall termination rate coefficient and $[R^{\cdot}]$ is the total radical concentration). The common approach to achieve this is to cap the end of each chain with a non-radical moiety that can be easily removed to yield a radical on the polymer chain. Ideally, the vast majority of chains at any given moment have the capping group (i.e. they are “dormant”). A small concentration (~10^{-7} to 10^{-9} M) may have a propagating radical located at the chain end (i.e. they are “active”). Furthermore, the capping group is labile enough to allow the dormant chains to become active, and the same capping group is able to react with an active chain to render it dormant.

In this way, an equilibrium is established between dormant and active chains, with the capping group mediating the concentration of each chain type. In addition, the capping group, once released from the polymer chain, should not react with any other molecules other than the propagating radical (i.e. it should not initiate polymerization itself).

The use of a capping group itself is not sufficient to gain predictable molecular weights and low polydispersities. The exchange between dormant and active chains (i.e. the equilibrium) must not only favor the dormant species but it also must be fast. In other words, the capping group must leave and rejoin the polymer chain at a rate that is fast enough to allow only a few propagation steps (e.g. something around 10 propagation events or preferably fewer) in each activation cycle. If both the activation and deactivation are fast relative to propagation then the polymer chains will grow in an incremental fashion, and if all chains are initiated at the same time the resulting chains should have low polydispersities. Thus, exchange dynamics are very important in attaining control over molecular weights and polydispersities [57].

In CRP field, several systems have been applied to control molecular weights and end functionalities: iniferters, nitroxides, Co-based systems, degenerative transfer with alkyl iodides, most recently the RAFT-process, and Ru- and Ni-mediated polymerizations. One of the most successful and useful methods, however, is atom transfer radical polymerization (ATRP), based on a copper halide/nitrogen based ligand catalyst [59].

A brief overview of the types of polymer materials that have been produced using CRP methods is given here. In general, these materials can be sub-divided into 4 categories (some of these are given in Figure 2.6)

i. Variations in composition: homo- and co-polymers, including block, graft, and gradient copolymers.

ii. Variations in topology: linear, star, and highly branched polymers.

iii. Composite materials: polymers grafted to surfaces, particles, inorganic/organic composites, polymer/biomaterial composites.

iv. Functionalized polymers: end-group functionality, side chain functionality, sitespecific functionality, multi-functional polymers.

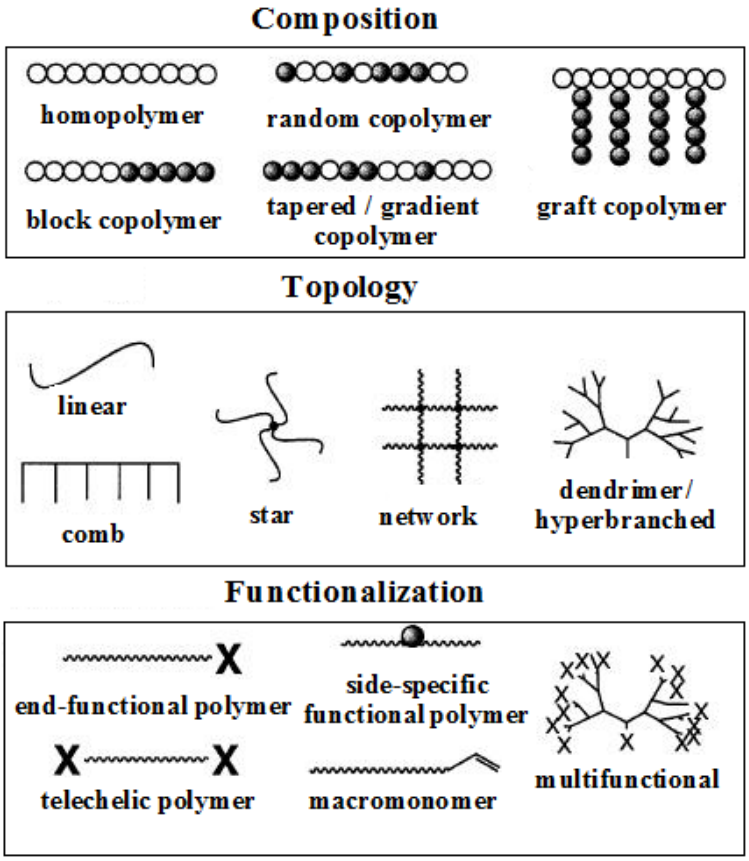

Figure 2.6 : Some of the variety of polymer materials made by CRP techniques.

The rapid emergence methods to manipulate, assemble, and direct molecules of all sizes (polymer and non-polymer), especially on a nanometer scale, means that the definition of polymer size and functionality has to be much greater today than was necessary in the past. Hence, CRP methods are likely to be used a great deal in the future [57].

2.3.2.2 Atom transfer radical polymerization

ATRP is mechanistically derived from atom transfer radical addition (ATRA), a method of producing one-to-one adducts developed from the 1940s through the 1960s, initially by Kharasch and subsequently improved by Minisci and Asscher and Vofsi. The generally accepted mechanism for ATRA involves atom transfer from an organic halide (R-X) to the metal complex, addition to an alkene, then atom transfer back to the organic radical. It was not until 1995 when Wang and Matyjaszewski, Sawamoto et al., and Percec and Barboiu separately published results from ATRP. The main difference between ATRA and ATRP is the fact that the addition product is able to reactivate to a radical that is able to undergo propagation reactions with available monomer, thus forming a polymeric (or oligomeric) chain.

Thus, an equilibrium is established between the dormant alkyl halide molecule and the active radical species, the latter of which may propagate, reversibly terminate or deactivate [57].

A general mechanism for ATRP shown in Figure 2.7 [60]. The radicals, or the active species, are generated through a reversible redox process catalyzed by a transition metal complex (M_t^n-Y/Ligand, where Y may be another ligand or the counterion) which undergoes a one electron oxidation with concomitant abstraction of a (pseudo) halogen atom, X, from a dormant species, R-X. This process occurs with a rate constant of activation, k_{act}, and deactivation k_{deact}. Polymer chains grow by the addition of the intermediate radicals to monomers in a manner similar to a conventional radical polymerization, with the rate constant of propagation k_p. Irreversible termination reactions (k_t) also occur in ATRP, mainly through radical coupling and disproportionation; however, in a well-controlled ATRP, no more than a few percent of the polymer chains undergo termination. Other side reactions may additionally limit the achievable molecular weights. Typically, no more than 5% of the total growing polymer chains terminate during the initial, short, nonstationary stage of the polymerization. This process generates oxidized metal complexes, the deactivators, X-M_t^{n+1}, as persistent radicals to reduce the stationary concentration of growing radicals and thereby minimize the contribution of termination.

A successful ATRP will have not only a small contribution of terminated chains, but also a uniform growth of all the chains, which is accomplished through fast initiation and rapid reversible deactivation [61-62].

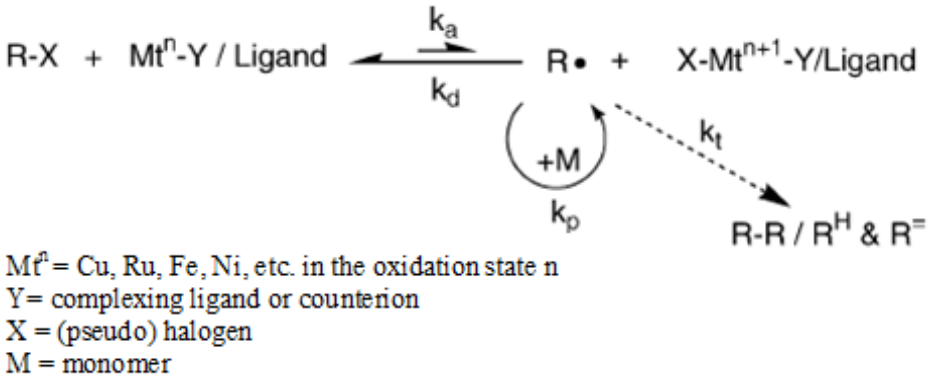

Figure 2.7 : Mechanism for ATRP.

As a multicomponent system, ATRP is composed of the monomer, an initiator with a transferable (pseudo) halogen, and a catalyst (composed of a transition metal species with any suitable ligand). Sometimes an additive is used. For a successful ATRP, other factors, such as solvent and temperature, must also be taken into consideration.

A variety of *monomers* have been successfully polymerized using ATRP. Due to a number of factors, the ATRP of each type of monomer requires a specific set of conditions. Each monomer possesses an intrinsic radical propagation rate, so the concentration of propagating radicals and the rate of radical deactivation may need to be adjusted to maintain polymerization control. For the polymerization of each monomer, the corresponding alkyl halide end group will possess its own unique redox potential. Therefore, in combination with the same metal catalyst, each end group will exhibit a different atom transfer equilibrium constant, deactivation rate constant, and corresponding concentration of propagating radicals [37]. Typical monomers include styrenes, (meth)acrylates, (meth)acrylamides, and acrylonitrile, which contain substituents that can stabilize the propagating radicals [61].

Another useful tool is the *initiator*, which, depending upon the propagation rate constant for a particular monomer and the equilibrium constant for the end group/catalyst pair, can be varied to assure that the apparent rate of initiation is faster than the apparent rate of propagation [37]. The initiator should be carefully selected in accordance with the structure and reactivity of the monomers and metal complexes. The role of the initiator in metal-catalyzed living radical polymerization is to form an initiating radical species via homolytic cleavage of its labile bond such as C-halogen by the metal catalysts [63]. The initiator is generally a simple, commercially available, alkyl halide. The (pseudo) halide group, X, must rapidly and selectively migrate between the growing chain and the transition metal complex [62].

Perhaps the most important component of ATRP is the *catalyst*. It is the key to ATRP since it determines the position of the atom transfer equilibrium and the dynamics of exchange between the dormant and active species. There are several prerequisites for an efficient transition metal catalyst [61]. First, the metal complex must have an accessible one-electron redox couple to promote atom transfer, but this requirement alone is not sufficient, because as its name indicates ATRP is an atom transfer not an electron transfer process.

Therefore, a second requirement is that upon one electron oxidation, the coordination number of the metal center must increase by one in order to accommodate a new atom, X. Finally, the metal center must not be a strong Lewis acid, otherwise the ionization of certain initiators/end groups to carbocations may occur [37].

The dynamic equilibrium between dormant species and propagating radicals can be easily and appropriately adjusted for a given system by modifying the complexing ligand of the catalyst [64]. The main roles of the *ligand* in ATRP is to solubilize the transition metal salt in the organic media and to adjust the redox potential and halogenophilicity of the metal center forming a complex with an appropriate reactivity and dynamics for the atom transfer. The ligand should complex strongly with the transition metal. It should also allow expansion of the coordination sphere and should allow selective atom transfer without promoting other reactions [62].

Typically, ATRP is conducted in bulk, but *solvents* may be used and are sometimes necessary when the polymer is insoluble in its monomer [37]. The rate of polymerization in ATRP increases with increasing *temperature* due to the increase of both the radical propagation rate constant and the atom transfer equilibrium constant.

It is widely accepted that a controlled polymerization process, including ATRP should display the following features: 1-First-order kinetics behavior, 2-pre-determinable degree of polymerization, 3-narrow molecular weight distribution, 4-long-lived polymer chains.

First-order kinetics behavior, i.e. the polymerization rate (R_p) with respect to the monomer concentration ([M]) is a linear function of time (2.2 and 2.3). This is due to the lack of termination, so that the concentration of the active propagating species ([P*]) is constant (k_p is the propagation constant).

$$R_p = \frac{-d[M]}{dt} = k_p[P^*][M] \qquad \textbf{(2.2)}$$

$$\ln\frac{[M]_0}{[M]} = k_p[P^*]t = k_p^{app}t \qquad \textbf{(2.3)}$$

The consequence of equation b and the effect of changes in P* are illustrated in Figure 2.8. It shows that a typical linear variation of conversion with time in semilogarithmic coordinates. Such linear behavior indicates that there is a constant concentration of active species [P*] in the polymerization [61].

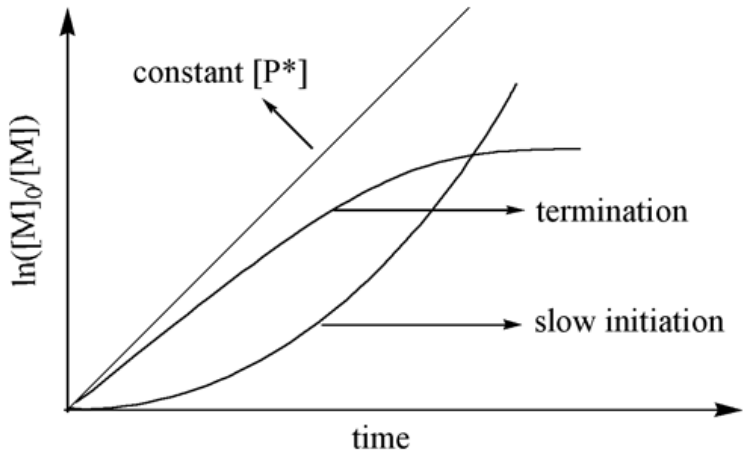

Figure 2.8 : Illustration of the dependence of $\ln([M]_o/[M])$ on time.

This semilogarithmic plot is very sensitive to any change of the concentration of the active propagating species. An upward curvature indicates an increase in [P*], which occurs in case of slow initiation.

On the other hand, a downward curvature suggests a decrease in [P*], which may result from termination reactions increasing the concentration of the persistent radical, or some other side reactions such as the catalytic system being poisoned or redox processes on the radical. It should also be noted that the semilogarithmic plot is not sensitive to chain transfer processes or slow exchange between different active species, since they do not affect the number of the active propagating species.

Predeterminable degree of polymerization (X_n), i.e. the number average molecular weight (M_n) is a linear function of monomer conversion.

$$X_n = \frac{M_n}{M_0} = \frac{\Delta[M]}{[I]_0} = \frac{[M]_0}{[I]_0}(conversion) \qquad \textbf{(2.4)}$$

This result comes from a constant number of chains throughout the polymerization, which requires the following two conditions: that initiation should be sufficiently fast so that nearly all chains start to grow simultaneously; no irreversible chain transfer occurs that increases the total number of chains.

The following Figure 2.9 shows that the ideal growth of molecular weights with conversion, as well as the effects of slow initiation and chain transfer on the molecular weight evolution.

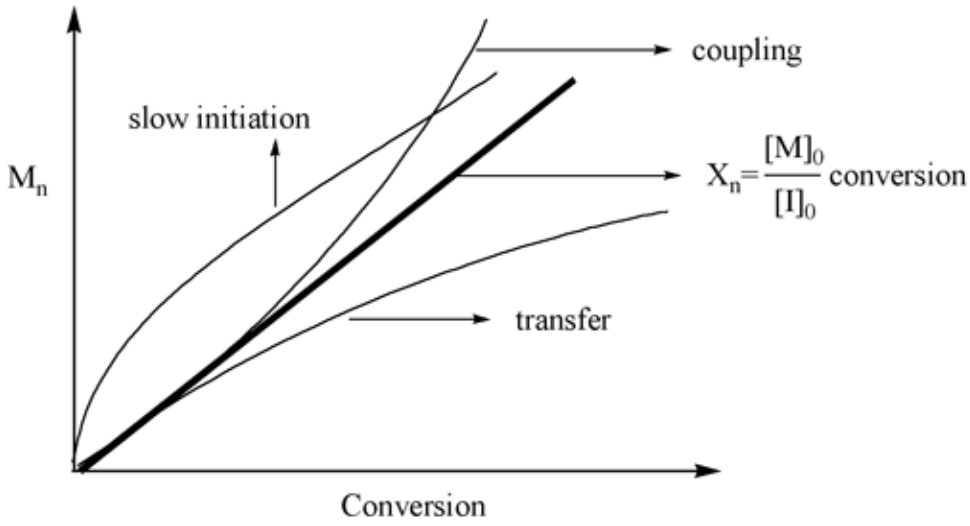

Figure 2.9 : The dependency of molecular weight on conversion.

It is important to recognize that the evolution of molecular weight is not very sensitive to irreversible chain termination, since the number of chains remains unchanged. The effect of termination is only observable on the plot when coupling reactions for polymers with very high molecular weights start to play a significant role.

Narrow molecular weight distribution (polydispersity), although this feature is very desirable, it is not necessarily the result of a controlled polymerization, which only requires the absence of irreversible chain transfer and irreversible termination, but ignores the effect of rate of initiation, exchange and depropagation. Substantial studies [65-67] indicate that in order to obtain a polymer with a narrow molecular weight distribution, each of the following five requirements should be fulfilled.

1. The rate of initiation is competitive with the rate of propagation. This condition allows the simultaneous growth of all the polymer chain.

2. The exchange between species of different reactivity is faster than propagation. This condition ensures that all the active chain termini are equally susceptible to reaction with monomer for a uniform growth.

3. There must be negligible irreversible chain transfer or irreversible termination.

4. The rate of depropagation is substantially lower than propagation. This guarantees that the polymerization is irreversible.

5. The system is homogenous and mixing is sufficiently fast. Therefore all active centers are introduced at the onset of the polymerization.

This should yield a Poison distribution, as quantified in equation 2.5.

$$\frac{X_w}{X_n} = \frac{M_w}{M_n} = 1 + \frac{X_n}{(X_n + 1)^2} \cong 1 + \frac{1}{X_n} \qquad \textbf{(2.5)}$$

According to equation 2.5, polydispersity (M_w/M_n, PDI) decreases with increasing molecular weight. Systems with slow exchange do not follow this perfect distribution but PDI's are defined by the following equation.

$$PDI = \frac{M_w}{M_n} = 1 + \left(\frac{k_p [RX]_o}{k_{deact} [Cu^{II} LnX]} \right) \left(\frac{2}{Conv.} - 1 \right) \qquad \textbf{(2.6)}$$

Equation 2.6 explains how the polydispersities in polymerization systems with relatively fast exchange decrease with conversion, $[R\text{-}X]_o$ corresponds to the concentration of dormant polymer chains and $[Cu^{II}\ LnX]$ is the concentration of deactivator. Polydispersities are higher for low conversion stages due to the fact that, X_n ratio of long chains to short chains (i.e. difference of chain length) is bigger than high conversion stages. Second, the final polydispersities should be higher for higher values of the ratio, k_p/k_{deact}. Thus, under similar condition, the polymerization of acrylates yields higher polydispersities than that of styrene, because k_p for acrylates is much larger than for styrene [68]. A polymerization that satisfies all five prerequisites listed above is expected to form a final polymer with a polydispersity less than 1.1 for X_n greater than 10.

Long-lived polymer chains is a consequence of negligible irreversible chain transfer and irreversible termination. Hence, all the chains retain their active centers after the full consumption of the monomer. Propagation resumes upon introduction of additional monomer. This unique feature enables the preparation of block copolymers by sequential monomer addition [69-70].

In summary, Cu-based *Atom Transfer Radical Polymerization (ATRP)* is a particularly successful CRP that has attracted commercial interest [67] because of its easy experimental setup, use of readily accessible and inexpensive catalysts, many of which are commercially available, and simple commercially available or easily prepared initiators [70]. Because of its mechanism, ATRP allows for the preparation of more precisely controlled polymers and many new materials have been synthesized. New materials are made by varying the topology of the polymer (linear, branched, hyperbranched, stars, etc.) and/or the composition of the polymeric chains (statistical/gradient, block, graft copolymers etc.). Moreover, with this process, the end groups of the polymers are well-defined as they derive from the initiator used. As a variety of initiators can be used, including initiators containing functional groups, end functionalities can easily be incorporated [59].

2.4 Microphase Separation in Block Copolymers

The particular chemical structure of block copolymer materials is reflected in the most fundamental and interesting way by incompatibility effects. These effects give block copolymers a number of specific properties such as new morphologies and original physical and mechanical properties which have led to valuable technological applications.

Block copolymers can produce numerous phase-seperated nanostructures that present high fundamental and technological interest. The blocks can be connected in a variety of ways; schematics of AB diblock and ABA triblock structures are shown in Figure 2.10. The block copolymer phase behavior can be expressed by the product of χN, which is called the reduced interaction parameter; χ and N stand for the Flory–Huggins segmental interaction parameter and the degree of polymerization, respectively.

As a block copolymer cools from the melt, below a characteristic temperature called the order–disorder transition temperature (T_{ODT}), differently ordered nanostructures, popularly known as microphase-separated structures (Figure 2.10) [71-73].

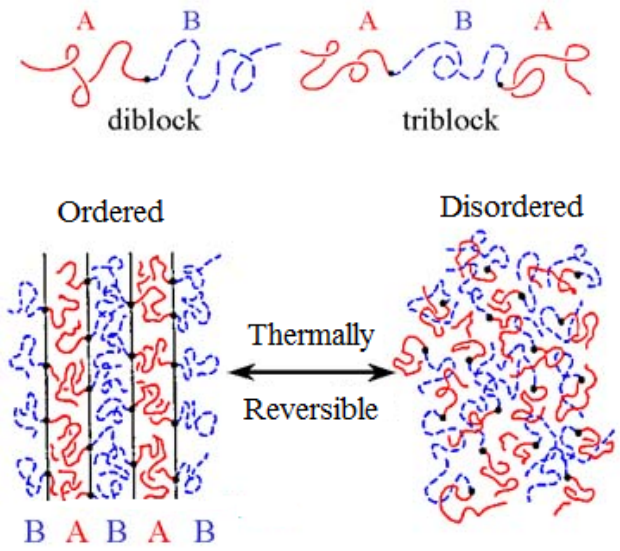

Figure 2.10 : The schematic representation of microphase separation behaviour from the melt.

Upon microphase separation, a rich variety of microstructure develops in systems of block copolymers. The evolution of microstructure is a result of two competing effects. Dissimilar blocks in copolymer prefer to segregate due to their inherent chemical incompatibility. However, the spatial extent of phase separation is limited due to the connectivity of the blocks imposed by the architecture of the molecule. Therefore, as a compromise, periodic microstructures arise which strive to minimize the area of contact between the unlike chemical species. An interesting feature of these structures is that their length scale is comparable to the size of the block copolymer molecules typically on the order of tens of nanometers. Therefore, the appearance of a particular microdomain geometry is quite sensitive to the volume fraction, chemical species and architecture of the copolymers. In other words, the microstructure is highly coupled to the physical and chemical characteristic of the molecules and serves as a molecular probe [74].

Further advances allowed chemists to synthesize block copolymers of a variety of architectures. Starting with changing thermodynamics by temperature variation or by adding low molecular weight solvents to block copolymers, homopolymers or other block copolymers, a large field has opened up for morphological transitions, i.e. manipulating block copolymer morphologies [75].

The best-known and simplest class of block copolymers are linear diblock copolymers (AB). Being composed of two immiscible blocks, A and B, they can adopt the following equilibrium microphase morphologies, basically as a function of composition: spheres (*S*), cylinders (*C* or *Hex*), double gyroid (*G* or *Gyr*), lamellae (*L* or *Lam*), cf. Figure 2.11 and the inverse structures. With the exception of the double gyroid, all morphologies are ideally characterized by a constant mean curvature of the interface between the different microdomains. For nearly symmetric compositions the unlike blocks form domains composed of alternating layers, known as lamellar phase (*L*). Slightly off symmetry composition results in the formation of a different layered structure.

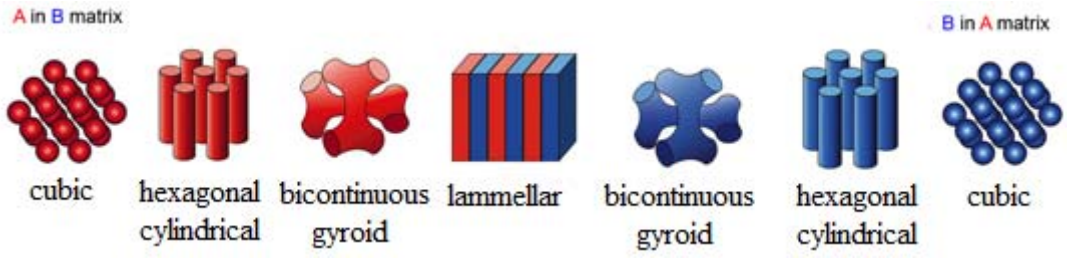

Figure 2.11 : Morphologies of diblock copolymers: cubic packed spheres (*S*), hexagonal packed cylinders (*C* or *Hex*), double gyroid (*G* or *Gyr*), and lamellae (*L* or *Lam*).

However, the influence of additional factors, such as the pressure and shear stress, that appear during the processing of commercial polymers (e.g., extrusion, injection, and compression molding) may cause a significant shift in the block copolymer phase behavior, leading to the evolution of morphologies not expected under equilibrium conditions. These changes arise not only from the reorganization of constituent block copolymer chains but also from the orientation of the nanostructures induced by shear stress. As demonstrated by various authors for different systems, the shear-induced orientation behavior of the microphase-separated structures strongly depends on the temperature, shearing conditions, and molecular properties of the copolymer [71].

Although the most investigations were focused on ordered state of block copolymers, very little has been known until recently about the mechanism of microdomain structure evolution from the disordered state. Hashimoto and coworkers highlighted this problem using lamellar-forming block copolymers and presented interesting results supported by TEM (Transmission Electron Microscopy) results.

The more interesting finding there was the formation of the lamellar microdomain after T-drop from the disordered state to the ordered state [76].

Phase Imaging is a powerful extension of *Tapping Mode Atomic Force Microscopy* (AFM) that provides nanometer-scale information about surface structure often not revealed by other Scanning Probe Microscopy (SPM) techniques. Tapping Mode AFM, the most commonly used of all AFM modes, is a patented technique (Veeco Instruments) that maps topography by lightly tapping the surface with an oscillating probe tip. The cantilever's oscillation amplitude changes with sample surface topography, and the topography image is obtained by monitoring these changes and closing the z feedback loop to minimize them. This eliminates shear forces which can occur in contact mode and so minimizes the damage to soft samples. The Multi Mode system features multiple scanners that permit the user to tailor the system for individual research. By mapping the phase of the cantilever oscillation during the TappingMode scan, phase imaging goes beyond simple topographical mapping to detect variations in composition, adhesion, friction, viscoelasticity, and perhaps other properties. Applications include identification of contaminants, mapping of different components in composite materials, and differentiating regions of high and low surface adhesion or hardness [77].

2.5 Thermal Properties of Polymers

The *differential scanning calorimeter* (DSC) is perhaps the instrument that has dominated the field of thermal analysis of polymers in the past decade. It measures heat flows and temperatures associated with exothermic and endothermic transitions. The ease with which important properties such as transitions, heat capacity, reaction, and crystallization kinetics are characterized have made the DSC widely used in the plastics laboratory. Significant efforts to simplify the technique have put this form of analysis within the reach of most plastics analysts. The DSC can operate in one of two ways: with a power-compensated design in which energy absorbed or evolved by the sample is compensated by adding or subtracting an equivalent amount of electrical energy to a heater located in the sample holder. Or, alternatively, it can operate based on a heat flux design by which it measures the differential heat flow between a sample and an inert reference.

Modulated DSC (MDSC) is an extension of conventional DSC in which the material is exposed to a cyclic, rather than linear, heating profile. Deconvolution of the heat flow results obtained provides unique benefits, including improved resolution of closely occurring or overlapped transitions, increased sensitivity for subtle transitions, and separation of reversing and nonreversing thermal phenomena DSC is routinely used for investigation, selection, comparison, and end-use performance of materials. It is used in academic, industrial, and government research facilities, as well as quality control and production operations. Material properties that are routinely measured include glass transitions, melting point, freezing point, boiling point, decomposition point, crystallization, phase changes, melting, crystallization, product stability, cure and cure kinetics, and oxidative stability [78].

A *glass transition temperature*, T_g, is the temperature below which molecules have little relative mobility. When the polymer is cooled below the glass transition temperature (T_g), it becomes hard and brittle, like glass. Some polymers are used above their glass transition temperatures, and some are used below. Hard plastics like polystyrene and poly(methyl methacrylate), are used below their glass transition temperatures; that is in their *glassy state*. Their T_g's are well above room temperature, both at around 100 ^oC. Rubber elastomers like polyisoprene and polyisobutylene, are used above their T_g's, that is, in the *rubbery state*, where they are soft and flexible [79].

Polymers are miscible if they form a single phase. Usually the components in a polymer blend are not miscible unless there is an attractive interaction between groups on two or more polymer chains. The most widely used technique to determine miscibility uses the measurement of the glass transition. The observation of a single glass transition with T_g somewhere between the T_g values of the individual component polymers is an indication of a miscible system. Conversely, an immiscible blend will show two glass transitions with T_g values corresponding to those of the individual components. In some immiscible, binary polyblend (partial miscibility), the lower T_g in the blend is shifted toward the higher T_g when compared to the pure component, while the higher T_g is lowered with respect to its pure component's T_g. This latter case involves some mixing between the two phases. Several equations have been proposed for calculation of the glass transition temperature of miscible polymer blends.

The earliest of these was the Fox equation:

$$\frac{1}{T_{g,mix}} = \frac{x_A}{T_{g,A}} + \frac{x_B}{T_{g,B}} \qquad \textbf{(2.7)}$$

where x is the mass fraction of components [80].

In DSC thermograms, the T_g values of two immiscible phases of polymer mixtures can be seen separately. Whereas in block copolymers the T_g values are observed separately but shifted towards each other (Figure 2.12). This is because the phases are completely independent for the polymer mixtures, but for block copolymers, the phases are connected to each other by covalent bonds. $T_{g,mix}$ value of block copolymers or polymer blends consisting of two miscible phases, is between the T_g values of each segment, in proportion with the weight percent ratio (Figure 2.12).

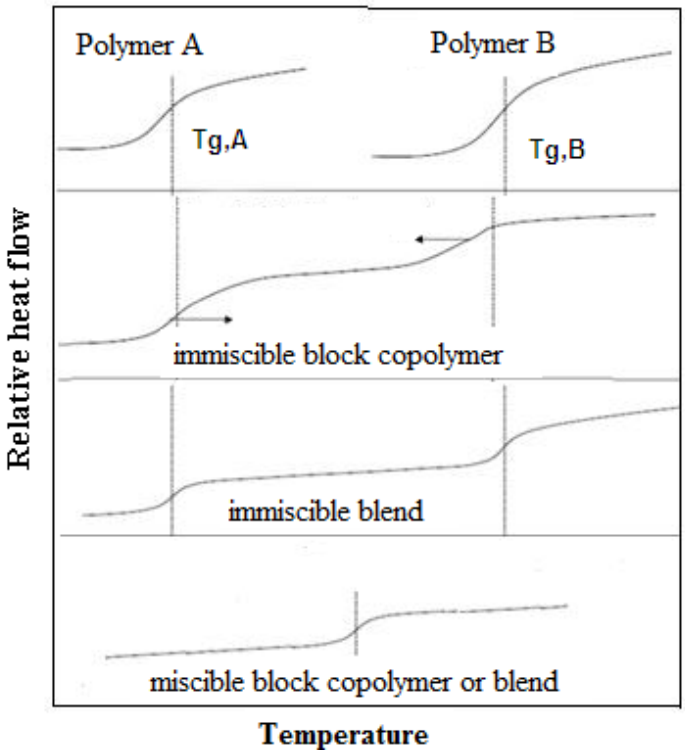

Figure 2.12 : DSC thermograms of miscible and immiscible polymer blends and block copolymers.

Interestingly, two glass transitions and a new transition ($T_{g,mix}$) between them are observed in baroplastics after processing (Figure 2.13). The mixed T_g is probably due to the increased interfacial region created by pressure-induced miscibility [12, 81].

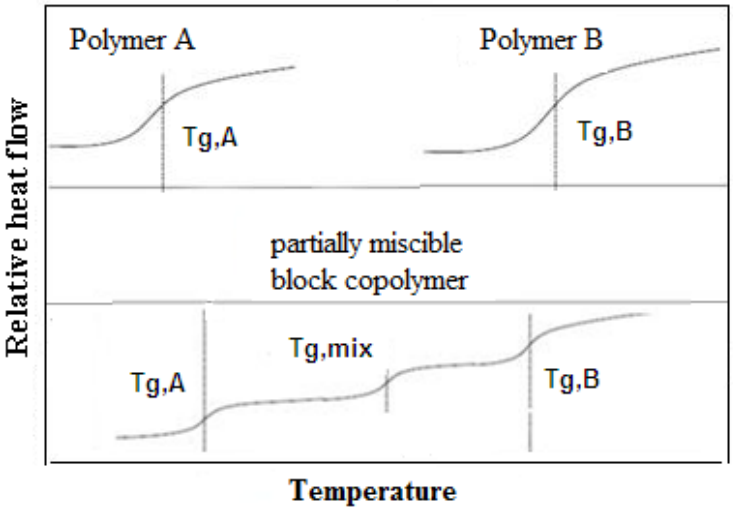

Figure 2.13 : DSC thermograms of baroplastic block copolymers.

2.6 Rheological Properties of Polymers

Rheology is the study of the deformation of materials. This includes the elastic deformation of solids such as metals as well as the viscous behavior of fluids such as water or oil. There is a wide range of materials that exhibit both a viscous and an elastic response to an applied force, and polymers fall into this group. Rheology studies the relationship between force and deformation in a material. To investigate this phenomenon we must be able to measure both force and deformation quantitatively. Steady simple shear is the simplest mode of deforming a fluid. It allows simple definitions of stress, strain, and strain rate, and a simple measurement of viscosity The following Greek symbols are used in the field of rheology: γ (gamma): shear strain, $\dot{\gamma}$ (gamma dot): shear rate, τ (tau): shear stress, η (eta): viscosity [82].

One of the key parameters during processing is the viscosity of the polymers that is the most important flow property. It represents the resistance to flow. Strictly speaking, it is the resistance to shearing, i.e., flow of imaginary slices of a fluid like the motion of a deck of cards. Referring to Figure 2.14, we can define viscosity as the ratio of the imposed *shear stress* (force F, applied tangentially, divided by the area A), and the shear rate (velocity V, divided by the gap h) :

$$\eta = \frac{ShearStress}{ShearRate} = \frac{F/A}{V/h} = \frac{\tau}{\dot{\gamma}} \qquad \textbf{(2.8)}$$

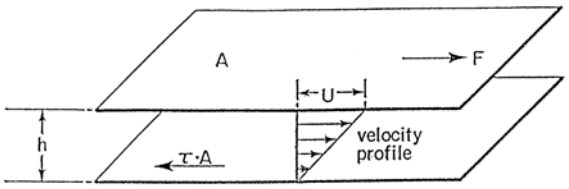

Figure 2.14 : Simple shear flow.

The units for viscosity is Pascal.second (Pa.s). A Newtonian fluid is a fluid that follows Newton's law of viscosity, which states that the viscosity is independent of shear rate. This implies a linear relation between force and plate speed; doubling the force on the plate will double its velocity. To understand and control melt processes, it is necessary to define the way in which melt viscosity changes with temperature and shear rate. The shear rate is a measure of how fast the melt passes through a channel or orifice. A simple fluid such as water has a constant viscosity value regardless of shear rate. This is known as Newtonian behavior in which the fluid can be described fully by a single constant—the viscosity.

By contrast, the viscosity of a melt of a plastic at a constant temperature changes markedly as the shear rate changes. This is non-Newtonian behavior. There is no single viscosity value. The viscosity value for such a melt must always be related to the shear rate at which it was determined and strictly it should always be referred to as the apparent viscosity, although this qualification is usually assumed rather than explicitly stated. An important consequence follows: for a viscosity to be truly useful in determining how a process will turn out, it should be measured at about the same shear rate experienced in the process [5].

One remarkable property of polymeric liquids is their shear-thinning behavior (also known as pseudo-plastic behavior). If we increase the rate of shearing (i.e., extrude faster through a die), the viscosity becomes smaller, as shown in Figure 2.15. This reduction of viscosity is due to molecular alignments and disentanglements of the long polymer chains. As one author said in a recent article: "polymers love shear" [83]. The higher the shear rate, the easier it is to force polymers to flow through dies and process equipment. Low shear rate on a die wall implies slow movement of the polymer melt over the metal surface.

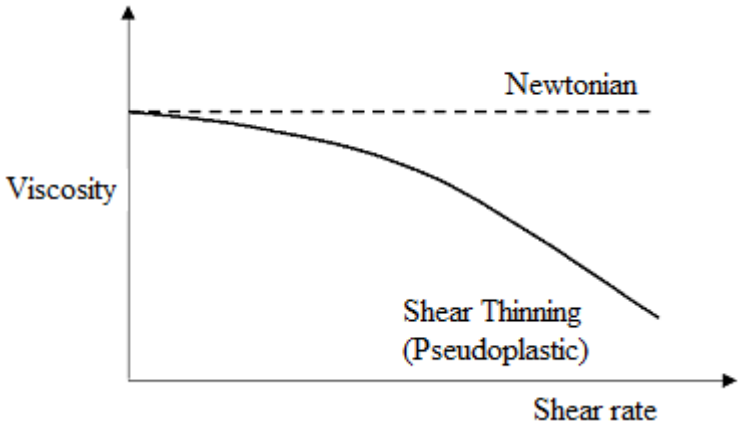

Figure 2.15 : Newtonian and shear-thinning viscosity behavior.

Rheological measurements can be used for (a) material characterization, (b) determination of processability, and (c) as input data for computer simulations. With careful rheological measurements, it is possible to determine whether, or under what conditions, a material will be processable [84-86].

Block copolymer melts usually (i.e., the upper-critical solution temperature-UCST situation) form disordered phases at elevated temperatures where the different blocks are homogeneously mixed. The order-disorder temperature of block copolymers is defined as the temperature at which the ordered microdomain structures disappear completely during heating or begin to appear during cooling.

The rheological properties of block copolymers near the order-disorder temperature T_{ODT} are quite different from homopolymer melts. Rheological measurements are very useful in locating order–disorder temperature (T_{ODT}), since the viscoelastic response differs markedly between the homogeneous phase and microphase separated states. Well above T_{ODT}, the dynamic storage (G´) and loss moduli (G´´) of block copolymers in the homogeneous phase resemble those of homopolymers. The moduli are higher in the phase-separated state ($T < T_{ODT}$) at low frequencies. As a consequence, plots of G vs. T at low frequencies often show an abrupt drop or change in slope at the T_{ODT} [87-88].

Measurement of Viscosity. Perhaps the most important factor to a process engineer in predicting extrusion or molding behavior is melt viscosity. Several methods are used to obtain the viscosity of polymer solutions and melts experimentally as a function of shear rate.

Instruments for making such measurements must necessarily accomplish two things: (1) the fluid must be sheared at measurable rates, and (2) the stress developed must be known. Two kinds of instruments having simple geometry and wide use a rotational viscometer and capillary or extrusion rheometer [89].

A *capillary rheometer* measures the viscous properties of a fluid by determining the pressure required to cause it to flow through a small cylindrical tube or rectangular slit (the capillary) at a set flow rate. Many rheometers control the flow rate (by setting the piston speed) and measure the pressure drop across the capillary; some gas- or weight-driven models fix the pressure and measure the flow.

The American Society for Testing and Materials has issued a standard entitled ‘‘Standard Test Method for Determination of Polymeric Materials by Means of a Capillary Rheometer’’ designated D3835–96 [90]. This method covers the measurement of the viscosity of materials at temperatures and shear rates found in common plastics processes. Issues such as temperature control and calibration, rheometer and die specifications, common temperature ranges, procedures, data analysis, and reproducibility are addressed. Figure 2.16 shows a schematic of a typical capillary rheometer.

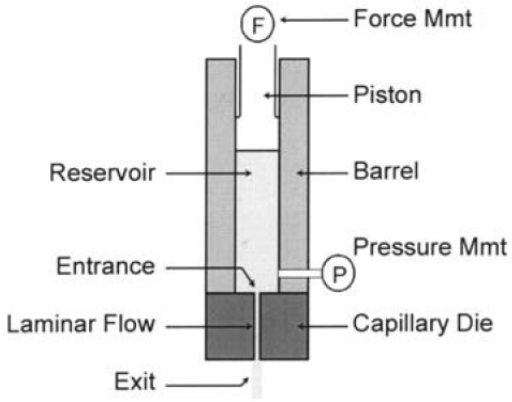

Figure 2.16 : Schematic representation of a capillary rheometer.

The molten polymer is held in a cylindrical reservoir and heated to the desired temperature. A motor-driven piston is used to force the material down the barrel and through the die, with the flow rate determined by the speed of the piston. Once the pressure has reached equilibrium it is noted, and the piston speed may be changed to measure the material at a different rate.

The important parameters in this measurement to be controlled and/or measured are the temperature, pressure (or force on the piston), the material flow rate (calculated from the piston speed and the barrel cross section), and the die geometry [82]. Before running tests on a polymer sample, a number of parameters must be chosen for the instrument. These include the test temperature, shear rate ranges, and the die and pressure transducer selections. Temperature is one of the most important parameters to be specified, as viscosity is a strong function of temperature. The temperature must be high enough to melt the sample completely and low enough that the sample will not degrade during the test. Before selecting a die or transducer, the desired shear rate range for the flow curve must be determined. The process for which the material is intended usually determines this parameter.

Depending on whether somebody wants to determine 'pure' rheological properties or rather processing behavior in technologies with strong elongation flow component (e.g. film blowing, foaming, coating, etc.) the choice of an 'appropriate' measuring technique will have to be different. Generally, the appropriate range of deformation or load will have to be used in obtaining the relevant parameters for a given process (Figure 2.17).

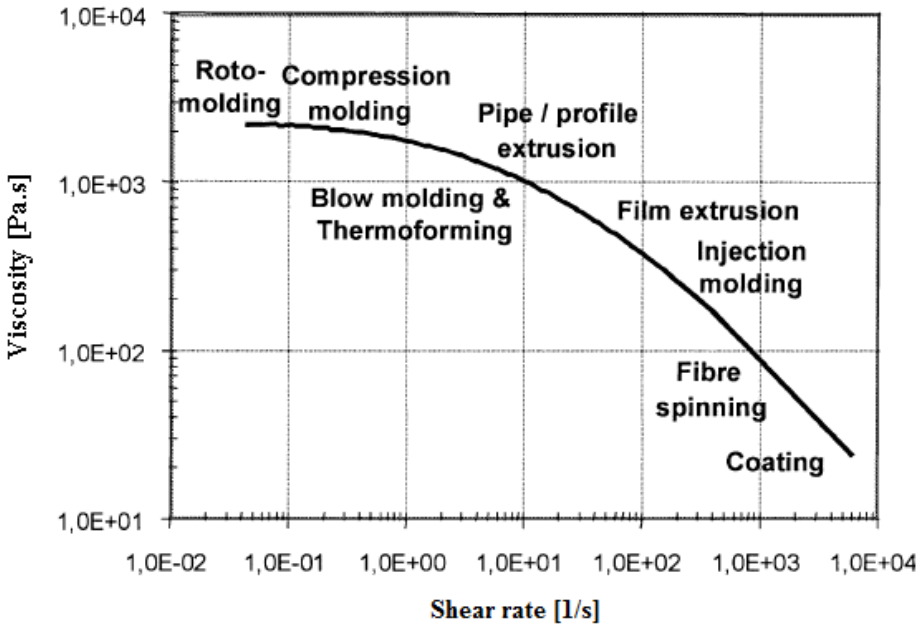

Figure 2.17 : Typical viscosity curve of a polypropylene homopolymer at 230 ^{o}C.

The main types of processing, for which rheological requirements need to be considered, are:

* Extrusion-flat (cast) film, blown film, pipe and profile,

* Extrusion coating and foaming,

* Extrusion blow molding, injection blow molding and thermoforming,

* Fibre spinning [91].

A typical test range for an average extrusion process might be from 20 to 2000 s^{-1}, whereas testing for an injection molding process might be more relevant across a range of 200-20,000 s^{-1}. Once you are familiar with a material, you may find that you can add extra points at either the high or low end of the range.

In summary, the capillary rheometer is a versatile and robust instrument. Easily interchangeable transducers and dies give the instrument the flexibility to study a wide range of materials over a wide range of shear rates, especially in the high-shear-rate ranges. It can handle tough materials at the temperatures, pressures, and flow rates typically found in high-performance plastics processes. The viscosity curve that the instrument produces finds many practical applications in quality control, process design, and troubleshooting, as well as in the study of the material properties themselves [78].

In a *rotational viscometer* (using cylinders, cones, spheres, and discs) the fluid is sheared at a given temperature in the fluid is sheared at a given temperature in the annular or enclosed space due to rotation of the inner cylinder or the like device while the outer cylinder or device is kept stationary or vice versa. In either case the torque required for the rotation is a measure of the shearing stress and the speed of rotation gives a measure of the rate of shear. Rotational viscometers using coaxial cylinders (Figure 2.18-a) measure relatively low viscosity liquids. Typical is the Haake-Rotovisco. In this device, the cup is stationary and the bob is driven a through a torsion spring. In a cone-and-plate rotational viscometer (Figure 2.18-b), the molten polymer is contained between the bottom plate and the cone, which is rotated at a constant velocity (U).

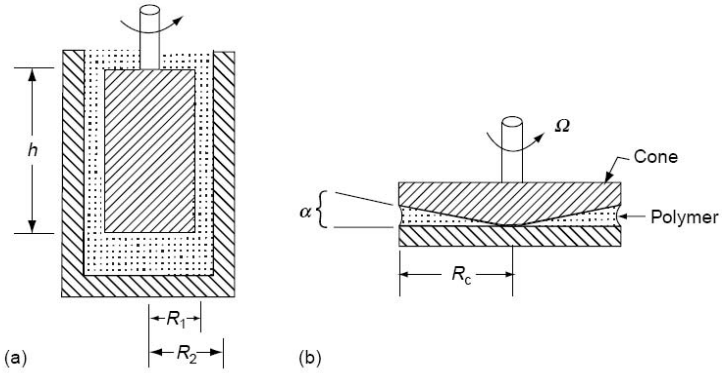

Figure 2.18 : a) Coaxial cylinder viscometer. b) Cone and plate rheometer.

The cone and plate viscometer gives reliable experimental data over an extensive range of shear rates (10^{-4}-10^{4} sec^{-1}). Not only it can be used to measure viscosities in simple shear, but also be used to determine the dynamic properties of viscoelastic materials. The unit is also set up to measure the normal stresses exhibited by viscoelastics, i.e., those perpendicular to the plane of shear [89].

2.7 Mechanical Properties of Polymers

Due to the favorable combination of easy processability and attractive mechanical properties, the use of polymer materials in structural applications has assumed large proportions over the last decades. To ensure proper operation under heavy duty conditions, these applications have to meet specific requirements regarding quality, safety, and mechanical performance (e.g. stiffness, strength and impact resistance). Numerical techniques provide a fast and cost-effective means to analyze and optimize the mechanical performance of polymer materials and products. One of the pre-requisites for a reliable analysis is an accurate constitutive model describing the materials' true stress-strain behavior [92]. The applied force is called stress and is denoted by the Greek letter, σ. When subjected to a stress, a material will exhibit a deformation or strain, γ. Most of researchers working with materials are used to seeing stress–strain curves. The ratio of stress to strain is the modulus (E), which is a measurement of the material's stiffness, or its resistance to deformation. Young's modulus, the slope of the initial linear portion of the stress–strain curve, is commonly used as indicator of material performance in many industries. Since stress–strain experiments are one of the simplest tests for stiffness, Young's modulus provides a useful evaluation of material performance.

Dynamic Mechanical Analysis (DMA) has become more popular because of their significant properties and to provide information about materials in particular polymers. DMA gives the information about rheological and thermal properties of polymers and measures the mechanical properties of materials as function of temperature, frequency and time and also it is a thermal analytical method by which the mechanical response of a sample subjected to a specific temperature program is investigated under periodic stress. Dynamic Mechanical Analyzer is useful for these tests: mechanical properties, morphology of polymers, loss factor (tan delta), loss angle (delta), impact resistance, dynamic viscosity, curing kinetics, correlation with materials formulation, ageing, damping, glass transition temperature (T_g), industrial products stiffness, polymer compatibility, relationships mechanical properties/molecular structure, relaxation time, rheological properties, secondary transitions, specimen stiffness, stress relaxation test, thermal properties, viscoelastic properties, young modulus, thermal stability, prediction of long term mechanical behavior, optimization of curing process, dynamic viscosity, complex viscosity, modulus values, dynamic test, creep behavior, gel time, melting point, dimensional stability, impact resistance, secondary transitions, tension test, stress-strain.

The basic properties obtained from a DMA test include storage modulus (E' or G'), loss modulus (E" or G") and tan delta (tan δ). Tan delta is particularly important for elastomers because it's related to the material's ability to dissipate energy in the form of heat. Glass transition temperature (T_g) and elastomer melting point can also be determined. The DMA data allow the development of structure-property-performance relationships for an elastomer; in other words, how do changes in chemistry, processing or composition impact performance. As the material becomes elastic, the phase angle, δ, becomes smaller, and E" approaches E' [93].

The *storage modulus,* E'**,** represents the stiffness of a viscoelastic material and is proportional to the energy stored during a loading cycle. It is roughly equal to the elastic modulus for a single, rapid stress at low load and reversible deformation, the *loss modulus,* E", is defined as being proportional to the energy dissipated during one loading cycle. It represents, for example, energy lost as heat, and is a measure of vibrational energy that has been converted during vibration and that cannot be recovered. The *phase angle,* δ*,* is the phase difference between the dynamic stress and the dynamic strain in a viscoelastic material subjected to a sinusoidal oscillation.

The phase angle is expressed in radians (rad). The *loss factor,* tan δ, is the ratio of loss modulus to storage modulus. It is a measure of the energy lost, expressed in terms of the recoverable energy, and represents mechanical damping or internal friction in a viscoelastic system. The loss factor tan δ is expressed as a dimensionless number. A high tan δ value is indicative of a material that has a high, nonelastic strain component, while a low value indicates one that is more elastic.

The material is said to be in the *glass state or energy elastic state* at the low temperatures described above, and in the *rubber or entropy elastic state* at the elevated temperatures mentioned there. A change from the glass state into the rubber-elastic state is called the *glass transition*. When the timescale of molecular motion coincides with that of mechanical deformation, each oscillation is converted into the maximum-possible internal friction and nonelastic deformation. The loss modulus, which is a measure of this dissipated energy, also reaches a maximum. In the glass transition region, the storage modulus falls during heating to a level of one-thousandth to one ten-thousandth of its original value. Because the loss factor is the ratio of the loss modulus to the storage modulus, the drop in storage modulus suppresses the rise in the loss factor initially; the temperature at which the loss factor is a maximum is therefore higher than the temperature corresponding to maximum loss modulus [94]**.** Typical curves of the changes undergone by amorphous thermoplastics are shown in Figure 2.19.

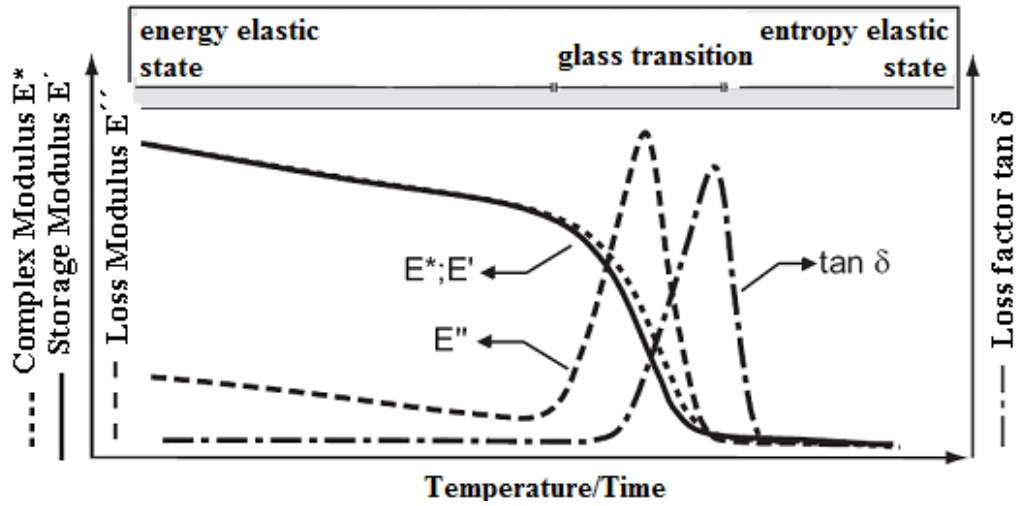

Figure 2.19 : Schematic diagram of typical DMA curves for an amorphous polymer.

3. EXPERIMENTAL PART

3.1 Chemical Used

Styrene (S, 99%, extra pure), 2-ethyl hexyl acrylate (EHA, 99+%, stabilized), copper (I) chloride (CuCl), copper (I) bromide (CuBr, 98%), ethylene glycol (99+ %), ethyl-2-bromo propionate (99%), 2-hydroxy ethyl acrylate (HEA, 97%), pentaethylenehexamine (PEHA, 30.5%) were purchased from Acros. Diethylenetriamine (DETA, 99%) 2-bromopropionylbromide (BPB, 97%), 2-bromoisobutyryl bromide (97%), ethylenediamine (EDA, 99%), and triethylenetetramine (TETA, 60%) were purchased from Aldrich. Sodium sulphate, anhydrous (99%) was purchased from J. T. Baker Co. Hexapentyl triethylene tetramine (HPTETA) is one of the alkylated linear amine ligands (ALALs) that was synthesized according to literature by our group [95].

THF was distilled over $LiAlH_4$ and then stirred overnight with Na and benzophenone and distilled again under N_2. Dichloromethane was distilled from phosphorus pentaoxide (P_2O_5). Trieth ylamine (Et_3N) was stirred over sodium hydroxide pellets, filtered and distilled under N_2 before used. Tris(2-(dimethylamino)ethyl)amine (Me_6-TREN) was synthesized according to the literature [96-98]. All solvents and chemicals were reagent grade, and all reagents were used as received.

3.2 Synthesis of Multifunctional Initiators

3.2.1 Di-functional ATRP initiator

Ethylene glycol (7.28 mL, 130 mmol) and triethylamine (39.87 mL, 286 mmol) were placed into a 500 mL round-bottom flask with 50 mL of dichloromethane (anhydrous). The reactor was cooled to 0 °C in an ice/water bath, and a solution of (29.96 mL, 286 mmol) of 2-bromopropionyl bromide and 70 mL of dichloromethane was added dropwise with stirring over a period of 1 hour. After complete the adding solution, the reactor was kept at 0 ^{o}C for 3 hours while stirring. A white precipitate of triethylammonium bromide formed upon addition of the acid bromide.

The reaction was left to react for 2 days and allowed to warm to room temperature of its own accord. Upon completion the ammonium salt removed by filtration and the mixture was transferred to a separatory funnel with 300 mL of dichloromethane and extracted consecutively with 200 mL of distilled water, 200 mL of $NaHCO_3$(aq), and 200 mL of distilled water. The organic phase was dried over Na_2SO_4 (anhydrous) and filtered and the solvent removed by rotary evaporation and then by under reduced pressure. The product was distilled under vacuum (bp: 140 ^oC, 4 mbar) to give colourless oil (2-Br*, 330 g/mol, ethylene glycol bis(2-bromopropionate), yield: 24.25 g, 63.5%).

^1H NMR ($CDCl_3$), δ: 4.37-4.29 (m, 6H, C-$\underline{CH_2}$-O-C(O)-$\underline{CH}$-(CH_3)Br), 1.78-1.75 (d, 6H, CH(Br)-$\underline{CH_3}$) ppm.

3.2.2 Tri-functional ATRP initiator

Trimethylolpropane (TMP, 12 g, 88.8 mmol) and triethylamine (Et_3N, 40 mL, 287 mmol) were placed into a 500 mL round-bottom flask with 150 mL of dichloromethane (anhydrous). The reactor was cooled to 0 °C in an ice/water bath, and a solution of 30 mL (287 mmol) of 2-bromopropionyl bromide (BPB) and 150 mL of dichloromethane was added dropwise with stirring over a period of 1 hour. After complete the adding ingredients, the reactor was kept at 0 ^oC for 4 hours while stirring (Figure 9). A white precipitate of triethylammonium bromide formed upon addition of the acid bromide. The reaction was left to react for 3 days and allowed to warm to room temperature of its own accord.

Upon completion the ammonium salt removed by filtration and the mixture was transferred to a separatory funnel with 300 mL dichloromethane and extracted consecutively with 200 mL of distilled water, 200 mL of $NaHCO_3$ (aq) and 200 mL of distilled water. The organic phase was dried over Na_2SO_4 (anhydrous) and filtered and the solvent removed by rotary evaporation and then by under reduced pressure to give dark brown oily product (3-Br*, 536 g/mol, trimethylolpropane-tris(2-bromopropionate), yield: 44.25 g, 92.2%).

^1H NMR ($CDCl_3$), δ: 4.37-4.29 (m, 3H, -CH_2-O-C(O)-$\underline{CH}$-(CH_3)Br), 4.18-4.00 (m, 6H C-$\underline{CH_2}$-O-C(O)-), 1.76-1.73 (d, 9H CH(Br)-$\underline{CH_3}$), 1.52-1.46 (m, 2H, C-$\underline{CH_2}$-CH_3) 0.89-0.83 (t, 3H, C-CH_2-$\underline{CH_3}$) ppm.

3.2.3 Tetra-functional ATRP initiator

Pentaerythritol (5.89 g, 43.26 mmol) and triethylamine (25.32 mL, 182 mmol) were placed into a 500 mL round-bottom flask with 100 mL of THF. The reactor was cooled to 0 °C in an ice/water bath, and a solution composed of (19.06 mL, 182 mmol) 2-bromopropionyl bromide or a solution of (22.86 mL, 182 mmol) 2-bromoisobutyrylbromide and 100 mL of THF was dropwise added with stirring over a period of 1 hour. After complete the adding solution, the reactor was kept at 0 ^{o}C for 3 hours while stirring. A white precipitate of triethylammonium bromide formed upon addition of the acid bromide. The reaction was left to react for 2 days and allowed to warm to room temperature of its own accord. Upon completion the ammonium salt removed by filtration and the mixture was transferred to a separatory funnel with 300 mL of diethyl ether and extracted consecutively with 200 mL of distilled water, 200 mL of $NaHCO_3$ (aq), and 200 mL of distilled water. The organic phase was dried over Na_2SO_4 (anhydrous) and filtered and the solvent removed by rotary evaporation and then by under reduced pressure, the product was crystallized with methanol. The white powder product was obtained.

4-Br*, Pentaerythritol tetrakis (2-bromopropionate), 676 g/mol, yield: 9.5 g, 32.5%, Mp: 99-101 °C (melting analyzer) and 90.5-94.2 °C (DSC). ^{1}H NMR ($CDCl_3$), δ: 4.1-4.5 (m, 12H, C-$\underline{CH_2}$-O-C(O)-$\underline{CH}$(CH_3)-Br), 1.7-1.9 (d, 12H, CH(Br)-$\underline{CH_3}$) ppm. Pentaerythritol tetrakis (2-bromoisobutyrylbromide), 732 g/mol, Mp: 92.5-95.8 °C (DSC). ^{1}H NMR ($CDCl_3$), δ: 4.32 (s, 8H, C-$\underline{CH_2}$-O-C(O)-C(CH_3)$_2$-Br), 1.93 (d, 24H, C(O)-C(Br)($\underline{CH_3}$)$_2$) ppm.

3.2.4 Penta-functional ATRP initiator by Schotten-Baumann reaction

The reaction was carried out in the presence of two-immiscible phase systems of dichloromethane and base solution which then does the job of neutralizing the HBr. The organic amine, diethylenetriamine (DETA, 5 mL, 46.28 mmol) was diluted with 30 mL dichloromethane (DCM) and added to the lower layer via syringe. However, DETA was dissolved in water instead of DCM. To solve the problem, the water part was saturated by NaCl solution. Then 2-bromopropionylbromide (BPB, 25 mL, 241 mmol) added to the (lower) dichloromethane layer via syringe, while the base (NaOH, 9.63 g, 241 mmol) remains in the (upper) aqueous layer (50 mL water). After addition of the acyl chloride, pH was around 2.

To controlled pH, it was added saturated NaOH and pH was setted between 11-13. The acyl bromide reacts only with the amine, but the HBr produced can dissolve in, and be neutralized by, the aqueous solution of NaOH. The reaction was stirred over 19 days with fast stirring. Upon completion the reaction, the mixture was transferred to a separatory funnel and extracted consecutively with 100 mL of distilled water three times. The organic phase was dried over Na_2SO_4 (anhydrous) and filtered and the solvent removed by rotary evaporation and then by under reduced pressure to give white solid product (5-Br*, 777.5 g/mol, yield: 13.5 g, 37.5%).

^{1}H NMR ($CDCl_3$), δ: 4.65-4.32 (m, 5H, -C(O)-CH(CH_3)-Br), 3.86-3.77—3.48-3.30 (m, 8H, -C(O)-N-CH_2-CH_2-N-C(O)-), 1.85-1.78 (d, 15H, -C(O)-CH(Br)-CH_3) ppm.

3.2.5 Octa-functional ATRP initiator by Schotten-Baumann reaction

The reaction was carried out in the presence of two-immiscible phase systems of dichloromethane and base solution which then does the job of neutralizing the HBr. The NaOH (4.4 g, 110 mmol) solution in 50 mL of water and 50 mL of DCM was added to the flask. The organic amine, pentaethylenehexamine (PEHA, 3 mL, 12.26 mmol) was diluted with 30 mL dichloromethane (DCM) and added to the lower DCM layer via syringe. However, PEHA was dissolved in water instead of DCM. To solve the problem, the water part was saturated by NaCl solution. Then the acyl bromide, 2-bromopropionylbromide (BPB, 11.56 mL, 110 mmol) added to the (lower) dichloromethane layer via syringe (Figure 13). The acyl bromide reacts only with the amine, but the HBr produced can dissolve in, and be neutralized by, the aqueous solution of NaOH. The reaction was stirred over 4 days with gentle stirring in order to keep the layer separated. After 4 days, the mixture was transferred to a separatory funnel and extracted consecutively with 100 mL of distilled water, 100 mL of saturated $NaHCO_3$ solution and 100 mL of distilled water to remove unreacted precursors. The organic phase was dried over Na_2SO_4 (anhydrous), after filtration the solvent removed by rotary evaporation and then by under reduced pressure to give dark brown solid product (8-Br*, 1311 g/mol, yield: 3.5 g, 22%).

^{1}H NMR ($CDCl_3$), δ: 4.93-4.41 (m, 8H, -C(O)-CH_3-CH-Br), 3.76-3.36 (m, 40H, -C(O)-N-CH_2-CH_2-N-C(O)-), 1.73-1.64 (d, 24H, -C(O)-CH-CH_3) ppm.

3.2.6 Penta-OH functional initiator precursor

The organic amine, diethylenetriamine (DETA, 0.9 mL, 0.0083 mmol) and 2-hydroxyethylacrylate (HEA, 5 mL, 0.048 mmol) were stirred in 15 mL pure ethanol for 6 days in N_2 atmosphere. Then the ethanol was removed by rotary evaporation and then by under reduced pressure to give dark brown oily product (5-OH*, yield: 5.15 g, 73%).

^{1}H NMR ($CDCl_3$), δ: 4.26-4.09 (t, 10H, N-CH_2-CH_2-C(O)-O-$\underline{CH_2}$-CH_2-OH), 3.76-3.48 (t, 10H, N-CH_2-CH_2-C(O)-O-CH_2-$\underline{CH_2}$-OH), 2.77 (t, 10H, -N-CH_2-$\underline{CH_2}$-C(O)-O-CH_2), 2.51 (t, 18H -CH_2–$\underline{CH_2}$-N–$\underline{CH_2}$-CH_2-) ppm.

3.2.7 Penta-functional initiator from penta-OH functional initiator precursor

A solution of 2-bromopropionylbromide (5.7 mL, 54 mmol) was added dropwise into a solution of 5-OH* (5.15 g) in dichloromethane. The reaction was stirred at room temperature for overnight. The dichloromethane was removed by rotary evaporation (5N-Br*, yield: 10 g, 59%).

^{1}H NMR ($CDCl_3$), δ: 4.29-3.65 (m, 10H, -C(O)-O-CH_2-CH_2-O-C(O)-$\underline{CH}$(CH_3)-Br), δ: 3.35-3.10 (t, 20H, -CH_2-CH_2-C(O)-O-$\underline{CH_2}$-$\underline{CH_2}$-O-C(O)-O-), δ:2.91-2.79 (t, 28H, -$\underline{CH_2}$-$\underline{CH_2}$-N-$\underline{CH_2}$-$\underline{CH_2}$-C(O)-O-CH_2-), δ:2.50-2.22 (d, 15H -C(O)-O-CH_2–CH_2-O-C(O)-CH($\underline{CH_3}$)-Br) ppm.

3.2.8 Octa-OH functional initiator precursor

The organic amine, pentaethylenehexamine (PEHA, 4.66 mL, 19 mmol) was added dropwise into the 2-hydroxy ethyla crylate (HEA, 15.98 mL, 152 mmol) at 0 ^oC and they were stirred in 30 mL pure ethanol for 6 days at room temperature. The ethanol was removed by rotary evaporation and then by under reduced pressure to give dark brown oily product (8-OH*, yield: 22 g, 66%).

^{1}H NMR ($CDCl_3$), δ: 4.39-4.10 (t, 16H, -O-$\underline{CH_2}$-CH_2-OH), 4.00-3.71 (t, 16H, -O-CH_2-$\underline{CH_2}$-OH), 2.77 (t, 16H, -O-C(O)-CH_2-$\underline{CH_2}$-N), 2.63-2.54 (t, 36H -$\underline{CH_2}$-$\underline{CH_2}$-N–CH_2-$\underline{CH_2}$-C(O)) ppm.

3.2.9 Octa-functional initiator from octa-OH functional initiator precursor

A solution of 2-bromopropionyl bromide (BPB, 20.94 mL, 200 mmol) in 50 mL of CH_2Cl_2, was added dropwise to a stirring solution of octa-OH functional initiator precursor (8-OH*, 22 g, 19 mmol). The dichloromethane was removed by rotary evaporation and then by under reduced pressure to give dark brown oily product (8N-Br*, yield: 14 g, 21%). ^{1}H NMR ($CDCl_3$), δ: 3.70-3.66 (10H, -O-C(O)-CH(CH_3)-Br), 3.38 (20H, C(O)-O-CH_2-CH_2-O-C(O)), 3.16-2.82 (28H, -CH_2-CH_2-N-CH_2-CH_2-C(O)-O), 2.50 (15H O-C(O)-CH-(CH_3)-Br) ppm.

3.2.10 Vinyl AB* monomer (inimer)

A solution of 2-bromopropionyl bromide (BPB, 36.5 mL, 348 mmol) in 50 mL of CH_2Cl_2, was added dropwise to a stirring solution of 2-hydroxy ethyl acrylate (HEA, 40.0 mL, 348 mmol) and triethylamine (Et_3N, 53.28 mL, 383 mmol) in 250 mL of CH_2Cl_2. The reaction was cooled in an ice bath. During the addition, a white precipitate formed (Et_3N^+-HBr^-). After complete addition of the acid bromide, 1.5 h, the reaction was stirred at room temperature for overnight. The precipitate was then filtered and CH_2Cl_2 part was washed with water (50 mL, 3 times) and then dried over Na_2SO_4. The CH_2Cl_2 was evaporated to give a yellow oil (inimer, yield: 78.49 g, 89%). ^{1}H NMR ($CDCl_3$): δ: 6.40-6.33 (d, 1H); 6.12-6.01 (dd, 1H); 5.83-5.78 (d, 1H); 4.46-4.20 (m, 5H); 1.77-1.74 (d, 3H) ppm.

3.2.11 Tetra-functional ATRP initiator starting from inimer

Ethylenediamine (EDA, 1 mL, 14.95 mmol) were placed into a 100 mL round-bottom flask with 10 mL of dichloromethane (anhydrous). A solution of 10 mL, 59.8 mmol of inimer and 15 mL of dichloromethane was added to the solution (on mixture) dropwise with stirring over a period of half hour. After complete the adding solution, the reactor was kept for overnight while stirring. The mixture was transferred to a separatory funnel and extracted consecutively with 10 mL of distilled water, 20 mL of saturated $NaHCO_3$ solution and 10 mL of distilled water to remove unreacted precursors. The organic phase was dried over Na_2SO_4 (anhydrous), after filtration the solvent removed by rotary evaporation and then by under reduced pressure to give dark brown viscous solid product (4N-Br*, yield: 6 g, 37%). ^{1}H NMR ($CDCl_3$), δ: 1.80-1.83 (d, 12H), 2.51-3.73 (m, 20H), 4.31 (m, 12H) ppm.

3.2.12 Penta-functional ATRP initiator starting from inimer

Inimer (10 mL, 59.8 mmol) were placed into a 100 mL round-bottom flask with 15 mL of dichloromethane (anhydrous). A solution of diethylenetriamine (DETA, 2.16 mL, 20 mmol) and 50 mL of dichloromethane was added to the solution (on mixture) dropwise with stirring over a period of half hour. After complete the adding solution, the reactor was kept for 18 days while stirring. Upon completion the white salt removed by filtration and the mixture was transferred to a separatory funnel and extracted three times with 30 mL 10% NaOH solution (saturated with NaCl) to remove unreacted precursors. The organic phase was dried over Na_2SO_4 (anhydrous), after filtration the solvent removed by rotary evaporation and then by under reduced pressure to give dark brown viscous solid (5N-Br*, yield: 9 g, 53%). ^{1}H NMR ($CDCl_3$), δ: 1.80-1.83 (d, 15H), 2.48-2.78 (m, 28H), 4.275-4.35 (m, 25H) ppm.

3.2.13 Octa-functional ATRP initiator starting from inimer

Inimer (10 mL, 59.8 mmol) were placed into a 100 mL round-bottom flask with 20 mL of dichloromethane (anhydrous). A solution of pentaethylenehexamine (PEHA, 1.835 mL, 7.5 mmol) and 10 mL of dichloromethane was added to the solution dropwise with stirring over a period of half hour. After complete the adding solution, the reactor was kept for overnight while stirring. Upon completion the reaction, the white salt removed by filtration and the mixture was transferred to a separatory funnel and extracted three times with 30 mL 10% NaOH solution (saturated with NaCl) to remove unreacted precursors. The organic phase was dried over Na_2SO_4 (anhydrous), after filtration the solvent removed by rotary evaporation and then by under reduced pressure to give dark brown viscous solid product (8N-Br*). Despite the fact that the product was not dissolved any solvent, ^{1}H NMR measurement couldn't be measured.

3.3 Synthesis of Linear and Star-shaped Macroinitiators

Polystyrene (PS) and polyethyl hexyl acrylate (PEHA) macroinitiators were prepared by ATRP of styrene and 2-ethyl hexyl acrylate. A typical ATRP procedure was performed as follows; the catalyst, CuBr or CuCl was placed in a flask which was sealed with a Teflon stopper and contained a side arm with a Teflon valve (Chemglass).

The flask was deoxygenated by vacuum-thaw-nitrogen cycles for three times. Styrene (S) or 2-ethylhexylacrylate (EHA) as a monomer, bipyridine (Bipyr), Me_6-TREN, *N,N,N′,N″,N″*-pentamethyldiethylenetriamine (PMDETA) or HPTETA as a proper ligand and toluene as solvent and finally, an appropriate mono-, di-, tri-, tetra-, penta- or octa-functional ATRP initiator were added. All liquid components were sparged with nitrogen prior to transferring them into the flask. The mixture was sparged with nitrogen for 10 min prior to placing it in a thermostatically controlled oil bath (at 100 ^{o}C for EHA or 110 ^{o}C for S, 400 rpm stirring rate). After the required time, the polymerization was terminated with methanol and diluted with THF, then passed through neutral alumina to remove the catalyst and precipitated into methanol. The product was dried in vacuum.

3.4 Synthesis of Block Copolymers

ATRP allows the synthesis of di-block copolymers by sequential (one-pot) or separated steps (two-pot) methods [99-100]. To synthesize di-block, tri-block, 3-, 4-, 5- and 8- arm star-block copolymers with different architectures by the two-pot method, the synthesized macroinitiators were used. A typical ATRP procedure was performed. First, a homopolymer was synthesized as mentioned above and then this homopolymer was used as a macroinitiator. In addition to the two-pot procedure, some of the block copolymers were also synthesized by the one-pot ATRP procedure. Once first monomer polymerized to complete conversion, the second monomer was added to the flask under nitrogen to obtain the block copolymers. In both cases, the samples were taken periodically via a syringe to follow the molecular weight of the polymer by GPC and the conversion of polymerization by GC measurements.

3.5 Measurement and Characterization

3.5.1 Nuclear magnetic resonance spectroscopy

To identify the character of initiators and the compositions of block copolymers, they were dissolved in deuterated chloroform ($CDCl_3$), and the ^{1}H NMR spectra were measured on a Bruker AC250 (250,133 MHz) NMR spectrometer with the internal reference.

3.5.2 Fourier transform infrared spectrometer

IR spectra were recorded on Nicolet 6700 FT-IR Spectrometer with attenuated total reflectance (ATR) accessories to identify the obtained initiators for comparison between the starting organic compounds and used for the transparency measurements after processing.

3.5.3 UV-Vis spectrometer

UV-Vis spectra were recorded on a Hitachi U-0080D spectrometer in order to perform transparency measurements to point out of similarities between FT-IR spectrometer.

3.5.4 Gel permeation chromatography

The molecular weights and polydispersities were measured by a gel permeation chromatography (GPC) system consisting of an Agilent 1200 series pump, three Waters Styragel HR columns (guard, 4, 3) and an Agilent 1100 series RI detector with a THF flow rate of 1 mL/min; poly(methyl methacrylate) or polystyrene were used as calibration standards. The second GPC system with an Agilent 1200 model isocratic pump, four Waters Styragel columns (guard, HR 5E, HR 4, HR 3, and HR 2), and a Viscotek TDA 302 triple detector (RI, dual laser light scattering, k: 670 nm, 90^{o} and 7^{o}, and differential pressure viscometer) was conducted in THF with a flow rate of 0.5 mL/min at 35 ^{o}C to measure the absolute molecular weights. Three detectors were calibrated with a PS standard having a narrow molecular weight distribution (M_n : 115000 g/mol, M_w/M_n : 1.02, [η] : 0.519 dL/g at 35 ^{o}C in THF, *dn/dc*: 0.185 mL/g) provided by Viscotek company. The *dn/dc* value for PEHA is calculated to be 0.058 mL/g at 35 ^{o}C in THF using at least three different concentrations of the corresponding polymer.

3.5.5 Gas chromatography

Monomer conversions were determined using a Perkin Elmer AutoSystem XL gas chromatography (GC) equipped with an FID dedector using a SGE-G4 capillary column (30 m lenght, 0.25 mm ID, 0.25 μm film thickness) . Injector and dedector were kept constant at 280 and 285 ^{o}C, respectively. Analysis was carried out isothermally starting from 40 ^{o}C holding for 1 min followed by an increased temperature to 200 ^{o}C at a heating rate of 40 ^{o}C/min and holding at 200 ^{o}C for 1 min.

Conversions were calculated by dedecting the decrease of the monomer peak areas (monomer consumption) relative to the peak areas of toluene as an internal standard.

3.5.6 Hazemeter

Transparency measurements with 21 mm diameter circular films were recorded on BYK-Gardner hazemeter that can be measured the all essential criteria for transmitting properties with one instrument (total transmittance,transmission haze and see-through quality).

3.5.7 Atomic force microscopy

Atomic force microscopy characterization was performed at 25 ^{o}C in air. The morphological observation of the samples was conducted on a Nanoscope IIIa scanning probe microscope (Veeco, Digital Instruments, Multimode Model, High Resolution Scanner Serial No: 4683ev, Santa Barbara, CA) in a tapping mode. A silicon tip (Olympus) with spring constant 28.81 N/m and resonans frequency of 281.4 kHz were used. Tapping mode in 2-3 Hz scanning rate was used for measurements. WSxM software was used to process data [101].

3.5.8 Differential scanning calorimetry

Differential scanning calorimetry (DSC) measurements using Q1000 (TA Instruments) were evaluated from the second heating run from -90 ^{o}C to 200 ^{o}C with a ramp rate of 10 ^{o}C/min for both heating and cooling.

3.5.9 Dynamic mechanical analyzer

TA Q800 dynamic mechanical analyzer (DMA) was used to measure mechanical properties of baroplastics (stress-strain curve) at room temperature using tensile film clamp and also the glass transition temperature (T_g) was found by examining the related modulus or tan delta curves. For T_g measurements the material in tension clamps was heated from 30 ^{o}C to 100 ^{o}C with a heating rate 5 ^{o}C/min while the applied frequency was 0.25 Hz.

3.5.10 Tensile tests

Tensile tests were carried out on a Zwick Z020 universal tensile machine equipped with a 10 N load cell, the strain being measured as the clamp displacement.

Stress–strain curves were obtained at a strain rate of 500 mm/min, the starting clamp distance being 25 mm.

3.5.11 Hardness testing

The Shore hardness test was used to measure the resistance of processed baroplastics to penetration by pin-shaped indentor. Blunt intendor was used for Shore A test which is suitable for examining elastomers (20A-95A) and pointed intendor was used for Shore D test which is suitable for examining soft thermoplastics and covers a range of 40D-90D.

3.5.12 Capillary and rotational rheometers

Capillary rheometry analysis was carried out with Göttfert high pressure capillary rheometer at 28 and 43 ^{o}C. The shear rates used were approximately 25, 50, 100, 350, 650, and 1000 s^{-1}. In order to reveal T_{ODT} of the baroplastic used, measurements were performed on a rotational rheometer (Bohlin CVO-100). After gab calibration of the rheometer, samples generated in disc form were placed between 20 mm diameter parallel plates.

4. RESULTS AND DISCUSSION

The aim of this thesis is to show the baroplastic properties of block copolymers with different topologies. This section of the thesis demostrates the synthesis and characterization results that are discussed in detail.

4.1 Synthesis of Multifunctional Initiators

To obtain different molecular weighted tri-block and star-block copolymers, di-, tri-, tetra-, penta- and octa- functional ATRP initiators were synthesized with different methods.

Method 1: Di-, tri- and tetra- functional initiators were prepared, as shown in Figure 4.1, by esterification with ethylene glycol, trimethylolpropane or pentaerytritol with α-bromo acid halide according to the literature, respectively [102].

Method 2: Starting from different dentated linear amine ligands, tetra-, penta- and octa- functional initiators were synthesized by Schotten-Baumann [103] and Michael addition [104] reaction methods. Using these methods, the synthetic routes (are novel synthetic approaches) were developed by our group as explained below (Figure 4.2).

Method-2a) Tetra-, penta- and octa- functional initiators were synthesized in one step by Schotten-Baumann reaction of different dentated linear amine ligands with α-bromo acid halide. Method-2b) Penta- and octa- functional initiators were synthesized in two steps. First, Michael addition reaction of 2-hydroxy ethyl acrylate with different dentated linear amine ligands to obtain –OH functional initiator precursor and then the esterification reaction of initiator presursors with α-bromo acid halide. Method-2c) Tetra-, penta- and octa- functional initiators were synthesized in two steps. First, esterification reaction of 2-hydroxy ethyl acrylate with α-bromo acid halide to obtain vinyl AB* monomer (inimer) then Michael addition reaction of inimer with different dentated linear amine ligands. Representative examples of the results were given in details for some synthetic methods.

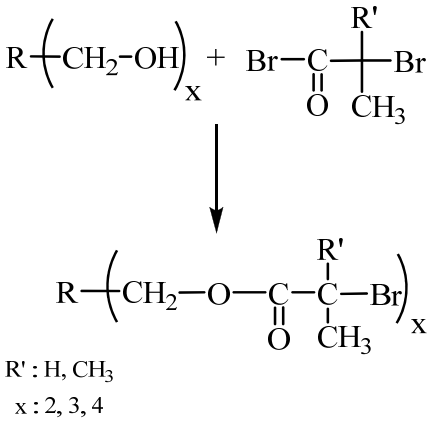

Figure 4.1 : Synthesis of functional ATRP initiators by method 1.

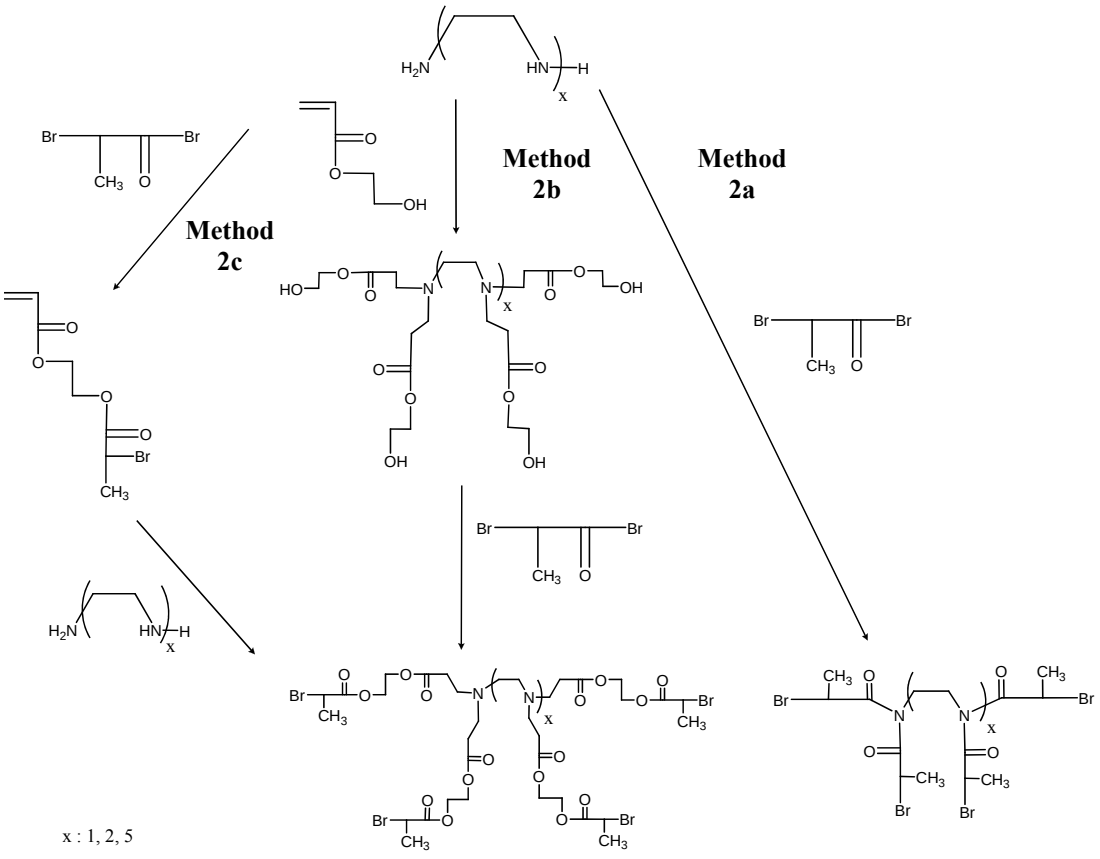

Figure 4.2 : Different routes for synthesis of tetra-, penta- and octa- functional initiators starting from different dentated linear amine ligands by method 2.

4.1.1 Difunctional ATRP initiator by esterification reaction

Difunctional initiator (2-Br*), ethylene glycol bis(2-bromopropionate), was prepared by esterification of ethylene glycol with α-bromo acid halide as shown in Figure 4.3. As shown in Figure 4.4, the ^{1}H NMR spectrum ($CDCl_3$) shows the presence of multiple peaks characteristic of an ester group (m, 6H, C-$\underline{CH_2}$-O-C(O)-$\underline{CH}$(CH_3)-Br, δ: 4.29-4.37 ppm) along with a doublet peak from the methyl protons in the ester groups (d, 6H, -CH(Br)-$\underline{CH_3}$), δ: 1.80-1.83 ppm). The observed from FT-IR measurement, the appearances of peaks at 1736 cm^{-1} (C=O), 1150 cm^{-1} (-C-O-C-) and the disappearances of OH peak at 3294 cm^{-1} that belong to ethylene glycol, confirmed that the reaction was proceeded.

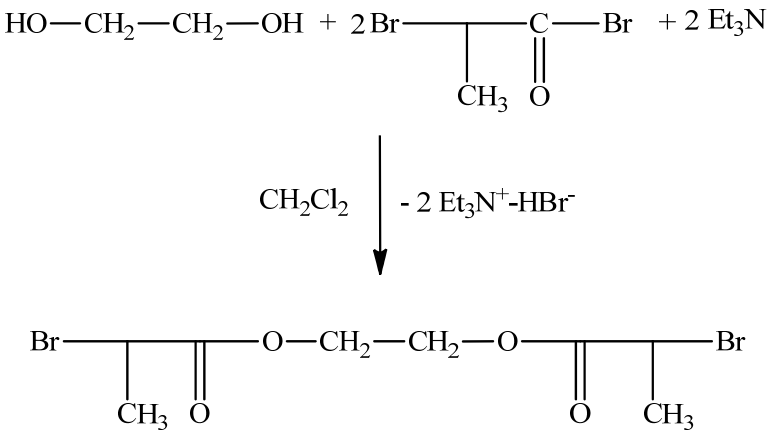

Figure 4.3: Synthesis of di-functional ATRP initiator (2-Br*).

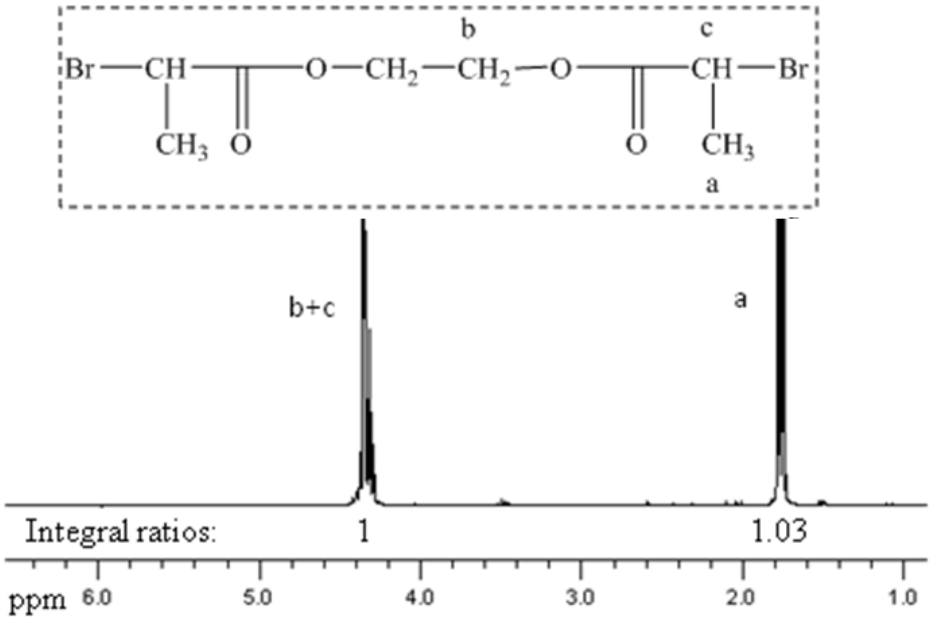

Figure 4.4 : ^{1}H NMR spectrum of 2-Br*.

4.1.2 Tri-functional ATRP initiator by esterification reaction

Trifunctional initiator (3-Br*), trimethylolpropane tris(2-bromopropionate), was prepared by esterification of trimethylolpropane with α-bromo acid halide as shown in Figure 4.5. ^{1}H NMR spectrum of trifunctional initiator (Figure 4.6) shows the presence of multiple peaks characteristic of an ester group (m, 3H, -CH_2-O-C(O)-CH-(CH_3)Br δ: 4.29-4.37 ppm and m, 6H, -C-CH_2-O-C(O)- δ: 4.00-4.18 ppm) along with a doublet peak from the methyl protons in the ester groups (d, 9H, -CH(Br)-CH_3), δ: 1.73-1.76 ppm). There is unknown peak at 2.6 ppm which is belonging to TMP. In FT-IR measurement, the appearances of peaks at 1735 cm^{-1} (C=O), 1146 cm^{-1} (-C-O-C-) and the disappearances of OH peak at 3237 cm^{-1} belongs to trimethylolpropane, confirmed that the reaction was proceeded (Figure 4.7).

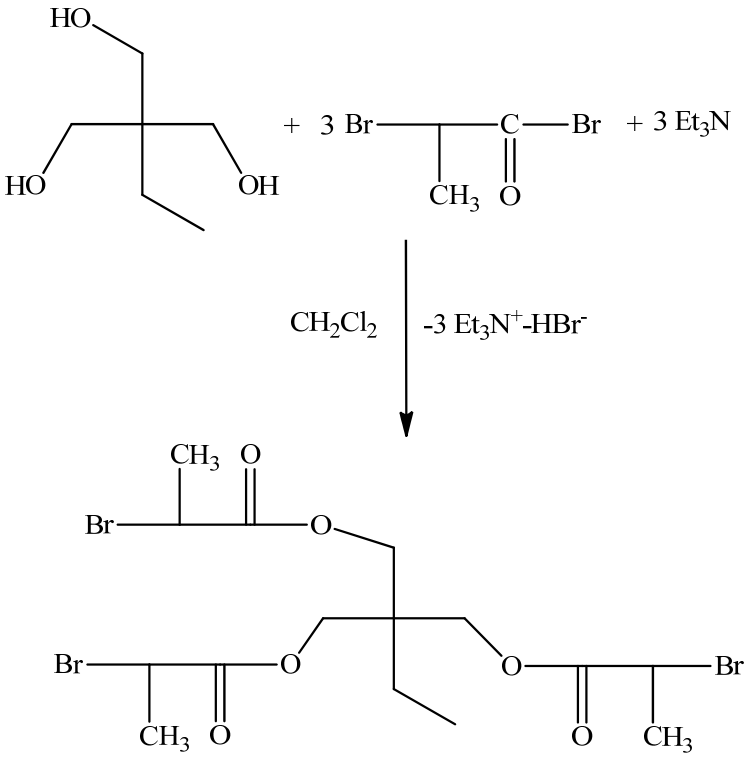

Figure 4.5 : Synthesis of tri-functional ATRP initiator (3-Br*).

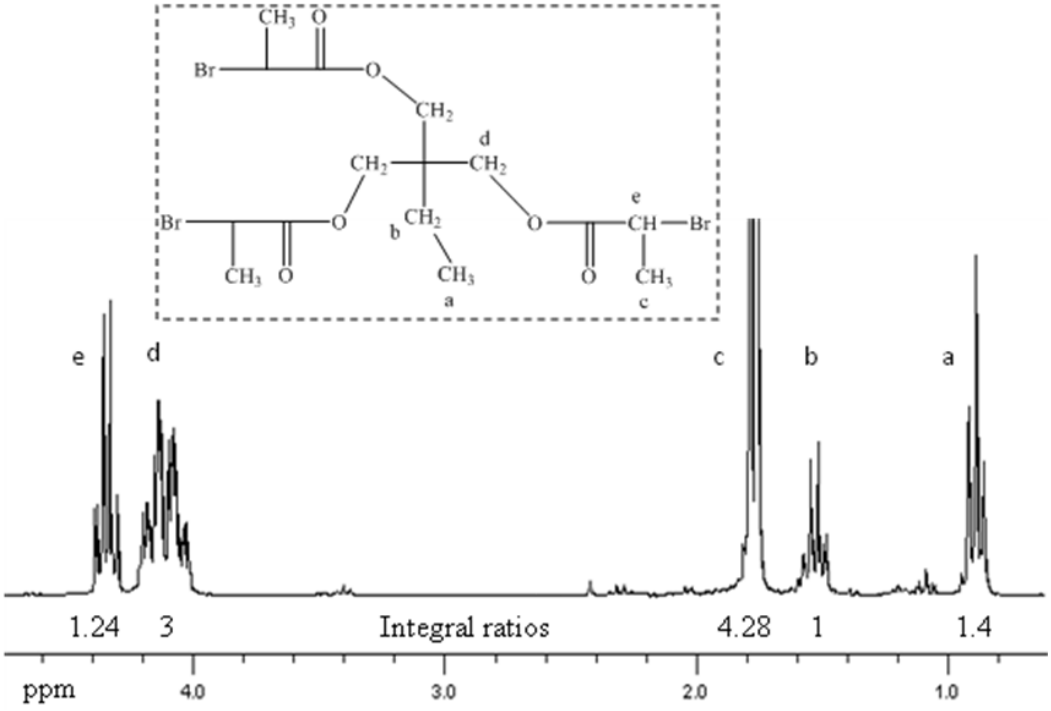

Figure 4.6 : ^{1}H NMR spectrum of 3-Br*.

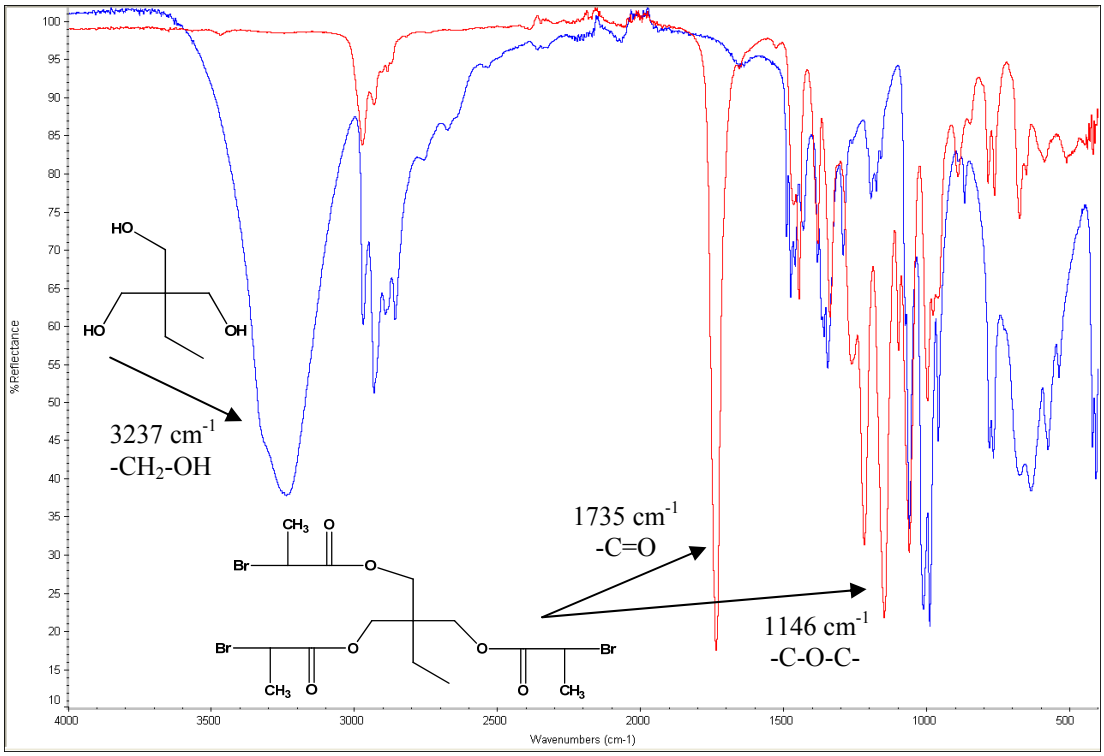

Figure 4.7 : FT-IR spectra of trimethylolpropane and 3-Br*.

4.1.3 Tetra-functional ATRP initiator by esterification reaction

Tetrafunctional initiator (4-Br*), pentaerythritol tetrakis(2-bromopropionate), was prepared by esterification of pentaerythritol with α-bromo acid halide as shown in Figure 4.8.

As shown in Figure 4.9, the ^{1}H NMR spectrum ($CDCl_3$) shows the presence of multiple peaks characteristic of an ester group (m, 12H, C-$\underline{CH_2}$-O-C(O)-$\underline{CH}(CH_3)$-Br, 4.17-4.42 ppm) along with a doublet peak from the methyl protons in the ester groups (d, 12H, -CH(Br)-$\underline{CH_3}$), δ: 1.80-1.83 ppm). The peak at 1.56 ppm is belongs to a little amount of water in $CDCl_3$.

The observed from FT-IR measurement, the appearances of peaks at 1736 cm^{-1} (C=O), 1150 cm^{-1} (-C-O-C-) and the disappearances of OH peak at 3305 cm^{-1} that belong to pentaerythritol, confirmed that the reaction was proceeded.

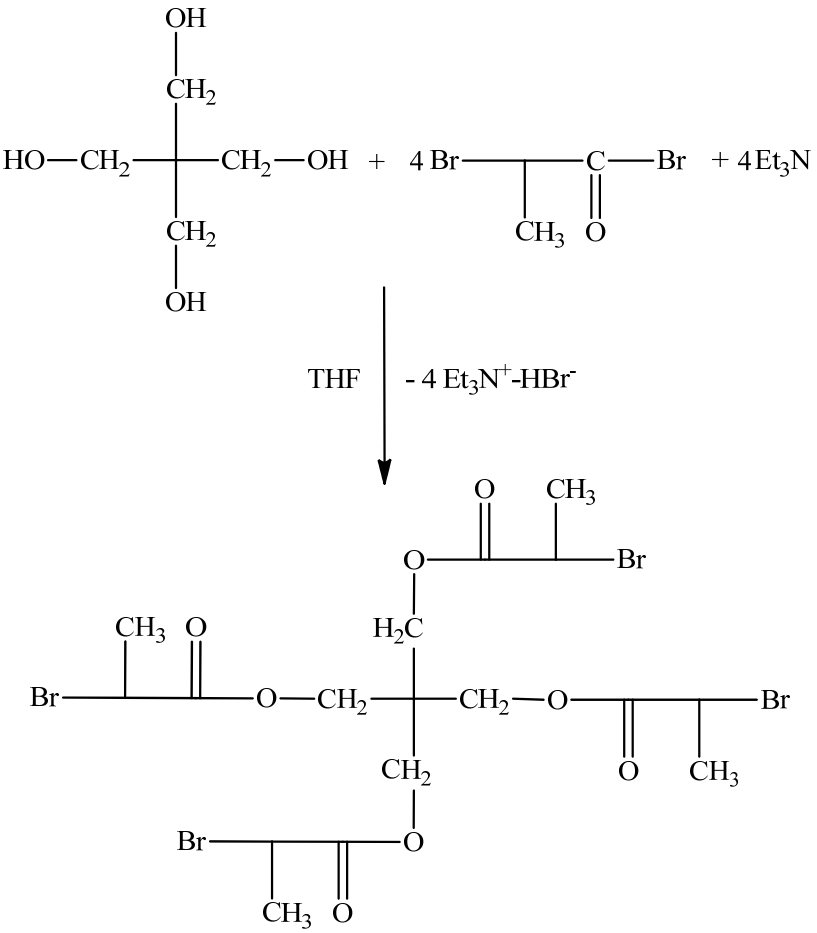

Figure 4.8 : Synthesis of tetrafunctional ATRP initiator (4-Br*).

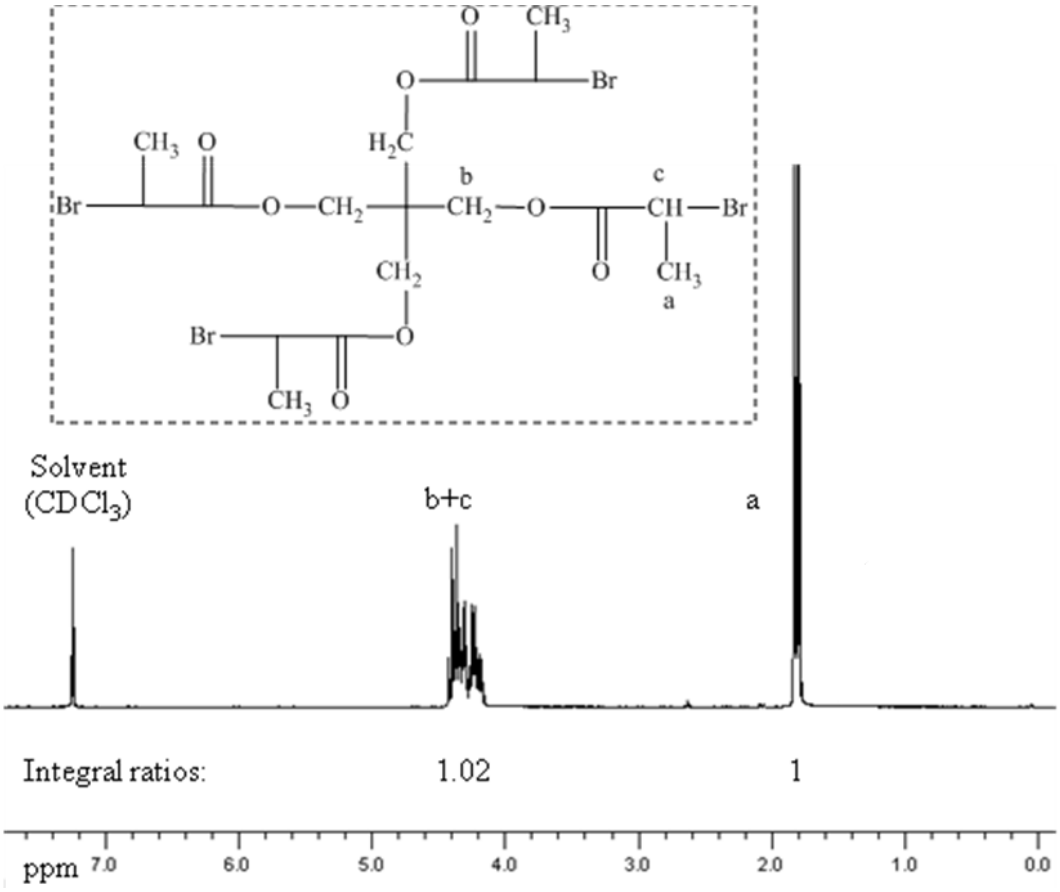

Figure 4.9 : ^{1}H NMR spectrum of 4-Br*.

4.1.4 Penta-functional ATRP initiator by Schotten-Baumann reaction

Schotten-Baumann synthesis of an amide was used as a method for making synthesis of five functional initiator (5-Br*) as shown in Figure 4.10.

As shown in Figure 4.11 , ^{1}H NMR spectrum ($CDCl_3$) shows the presence of multiple peaks characteristic of an ester group (m, 5H, -C(O)-(CH_3)-CH-Br, δ: 4.65-4.32 ppm) along with a doublet peak from the methyl protons in the ester groups (d, 15H, -C(O)-CH(Br)-CH_3, δ: 1.85-1.78 ppm) and multiple peaks characteristic of an amide group (m, 8H, -C(O)-N-CH_2-CH_2-N-C(O)-, δ: 3.86-3.77—3.48-3.30 ppm) and the practical integral ratios are compatible with the theoretical values. The schematic representation of Schotten-Baumann reaction is shown in Figure 4.12.

In FT-IR measurement, the appearances of new peaks at 1634 cm^{-1} (-N-C=O, strong), 1062-1182 cm^{-1} (-CO-N), 558 cm-1 (-C-Br) and the disappearance of N-H bending peak at 823 cm^{-1} belong to DETA and converting of doublet N-H streching peak at 3274 cm^{-1} to broad N-CH_2- streching peak at 3287 cm^{-1} confirmed that as an another proof that the reaction proceeded (Figure 4.13).

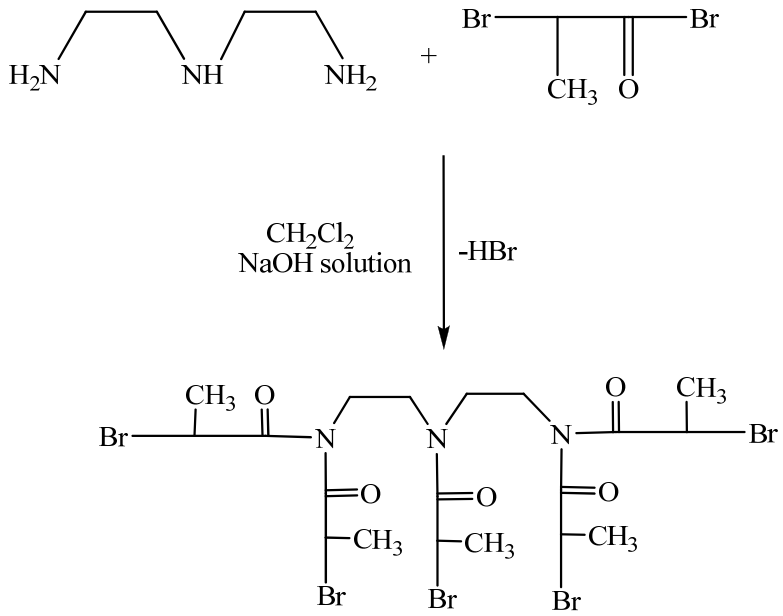

Figure 4.10 : Synthesis of penta-functional ATRP initiator (5-Br*) by Schotten-Baumann reaction.

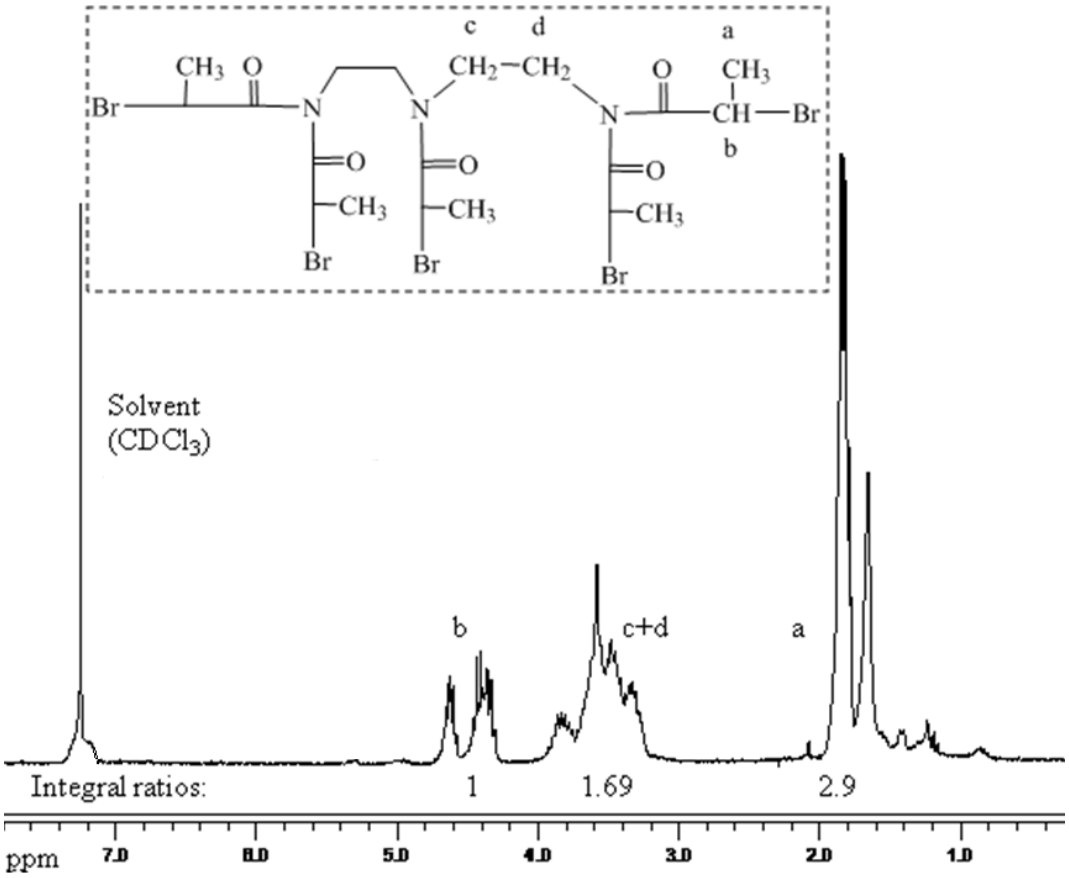

Figure 4.11 : ^{1}H NMR spectrum of 5-Br*.

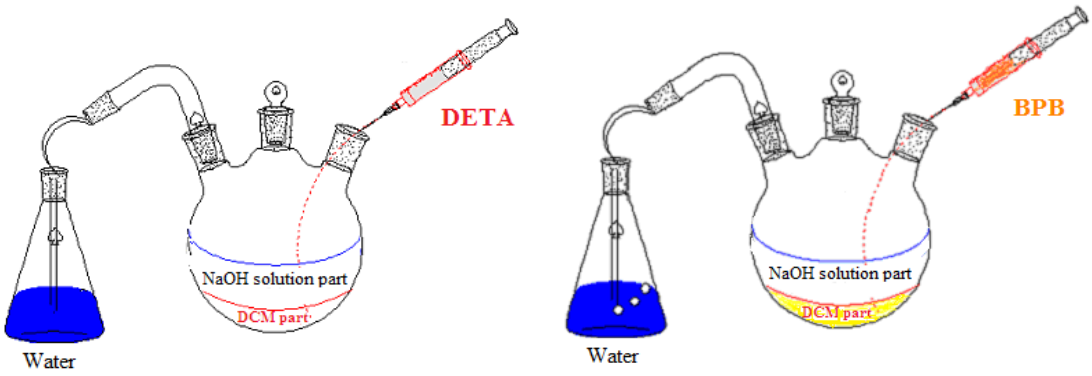

Figure 4.12 : Schematic representation for Schotten-Baumann synthesis of an amide reaction.

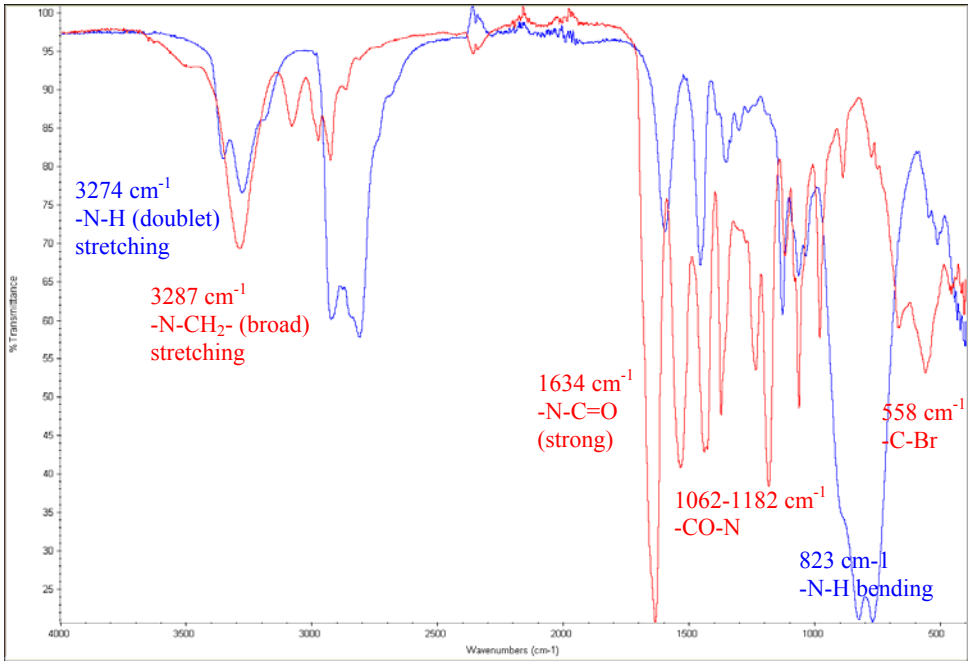

Figure 4.13 : FT-IR spectra of penta-functional ATRP initiator (5-Br*) and DETA.

4.1.5 Penta-OH functional initiator precursor by Michael addition reaction

Penta hydroxyl functional initiator precursor (5-OH*) was synthesized by Michael addition of amine to acrylate (Figure 4.14) in order to convert to ATRP initiator in the following step. As shown in Figure 4.11 5 in ^{1}H NMR spectrum ($CDCl_3$) the practical integral ratios are compatible with the theoretical values. Not observing any peaks at 5.6-6.6 ppm which belong to hydroxy ethyl acrylate's double bonds, is another proof of the formation of the initiator precursor. The observed from FT-IR measurement, the appearances of a new peak with high intensity at 3270 cm^{-1} (-CH_2-OH and -N-CH_2- stretching, broad), and the disappearance of =C-H bending peak at 800-980 cm^{-1} belongs to HEA and -N-H bending peak at 760 cm^{-1} that belongs to DETA confirmed that the reaction was proceeded.

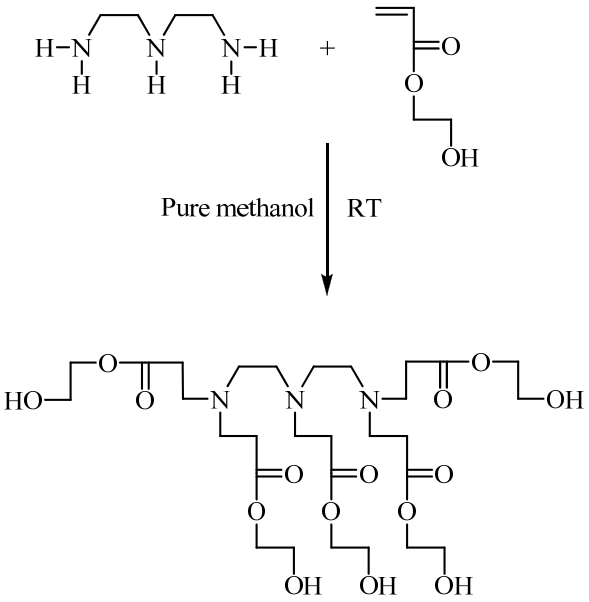

Figure 4.14 : Synthesis of penta-OH functional initiator precursor (5-OH*).

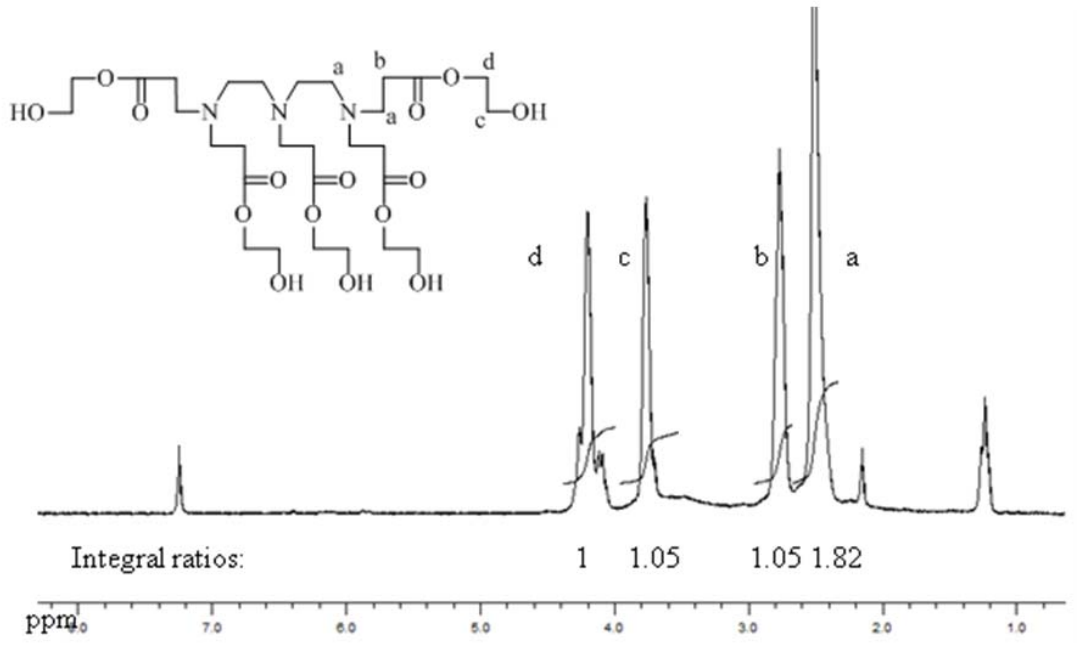

Figure 4.15 : ^{1}H NMR spectrum of 5-OH*.

The obtained product was used to synthesize penta-functional ATRP initiator. These are the representative examples for the synthesis of multifunctional initiator in versatile routes. Further information to synthesize different functional ATRP initiator can be found in the experimental part.

4.2 Synthesis of Linear Homopolymers and Star-shaped Polymers

Herein, well-defined PS-X, X-PS-X, X-PEHA-X linear homopolymers and $(PS\text{-}X)^{3*}$, $(PEHA\text{-}X)^{4*}$, $(PS\text{-}X)^{4*}$, $(PS\text{-}X)^{5*}$, $(PS\text{-}X)^{8*}$ star-shaped polymers were synthesized with appropriate mono-, di-, tri-, tetra-, penta- and octa- functional ATRP initiators.

4.2.1 Mono-functional polystyrene

Monofunctional polystyrenes (PS-X) were synthesized via ATRP using *N,N,N′,N″,N″*-pentamethyldiethylenetriamine (PMDETA) as the ligand for complexation with CuX halide salts. When this commercial available tridentate amine ligand was employed in ATRP, the rate of polymerization showed a significant increase for styrene, as compared to the corresponding bipyridine systems. Because of that a series of homo polystyrene with different molecular weights were obtained with this ligand as depicted in Table 4.1.

Some of these polymers were used as macroinitiators to synthesize block copolymer and also some of them were used as processing aid which will be further explained in the section of baroplastic as processing aid.

Table 4.1: Characteristics of the PS-X homopolymers.[a]

Run	$[M]_o$ (mol L^{-1})	$[M]_o$:$[I]_o$	Time (h)	Conv. (%)	$M_{n,GPC}$[b]	M_w/M_n[b]
P1[c]	5.24	48	18.00	85.0	6030	1.22
P2[c]	5.24	96	19.00	84.0	10800	1.13
P3[c]	5.24	192	19.00	72.2	17750	1.09
P4	7.91	100	26.50	94.0	21690	1.13
P5[c]	5.24	288	19.75	72.0	25950	1.10
P6[c]	5.24	480	19.50	50.5	27210	1.07
P7[c]	5.24	384	19.50	63.4	28940	1.09
P8	8.72	400	27.50	78.0	34840	1.17
P9[d]	7.91	432	21.50	90.4	37680	1.25
P10	6.00	200	17.50	95.0	38000	1.09
P11[d]	7.91	432	22.00	92.0	48220	1.23
P12	7.91	400	26.50	90.0	52410	1.12
P13[d]	8.72	609	18.00	89.5	57050	1.22
P14[d]	8.72	912	22.50	64.0	79480	1.27
P15	7.25	400	17.50	82.5	105780	1.39

[a] T: 110 °C, $[1\text{-}Br^*]_o$:$[CuBr]_o$:$[PMDETA]_o$= 1:1:1
[b] Measured by GPC with RI detector (calibration with linear PS standards in THF at 30 °C)
[c] T: 100 °C
[d] $[1\text{-}Br^*]_o$:$[CuCl]_o$:$[PMDETA]_o$= 1:1:1

4.2.2 Di-functional polystyrene

Polystyrenes (X-PS-X) with bromine or chloride end-terminals (Br-PS-Br or Cl-PS-Cl) were synthesized with different ligand and catalyst complexes. The bromine chain-end functionality of PS was prepared by activators regenerated by electron transfer for atom transfer radical polymerization (ARGET ATRP). The reason of employing this system in this research is to use a low concentration of an active Cu/ligand catalyst complex, so that it would be possible to decrease the occurrence of catalyst-based side reactions significantly and its removal or recycling would be unwarranted for most industrial applications as found in the literature [105-107]. Moreover, using alkylated linear amine ligands provide homogeneous and relatively fast polymerization reactions compared to most other ATRP ligands as discovered by our group. To obtain di-functional polystyrene normal ATRP, ARGET ATRP and homogeneous ATRP with ALALs were used to make a several alternatives to the synthetic procedures (Table 4.2).

Table 4.2: Characteristics of the X-PS-X homopolymers.[a]

Run	$[M]_o$ (mol L^{-1})	$[M]_o$:$[I]_o$	Time (h)	Conv. (%)	$M_{n,GPC}$[b]	M_w/M_n[b]
P16	8.72	200	16.50	44.5	9360	1.56
P17[c,d]	4.36	1000	125.00	12.2	11130	1.46
P18[c,d]	4.36	500	267.00	28.0	14670	1.44
P19	8.72	600	17.00	30.4	15600	1.19
P20[e]	2.90	300	72.00	65.0	17500	1.31
P21[f,d]	4.36	1000	47.00	11.0	17530	1.19
P22[d]	8.72	290	19.00	58.0	20010	1.24
P23[d]	8.72	300	22.00	46.0	24880	1.15
P24[g,d]	1.45	300	69.00	60.0	31150	1.42
P25	8.72	480	21.00	24.0	37320	1.18
P26[h]	7.94	288	3.50	94.0	42860	1.59
P27[h]	7.94	480	3.00	72.0	64500	1.31
P28[h]	8.72	800	17.00	92.0	107470	1.26
P29[h]	4.57	768	28.00	62.0	109350	1.20

[a] T: 110 °C, $[2\text{-Br*}]_o$:$[CuBr]_o$:$[Bipyr]_o$= 1:2:2
[b] Calculated from GPC calibrated with linear polystyrene standards
[c] $[2\text{-Br*}]_o$:$[CuCl]_o$:$[Bipyr]_o$= 1:2:2
[d] T: 100 °C
[e] $[2\text{-Br*}]_o$:$[CuBr_2]_o$:$[PMDETA]_o$:$[Ascorbic\ Acid]_o$= 1:0.2:2:2
[f] $[2\text{-Br*}]_o$:$[CuCl]_o$:$[PMDETA]_o$= 1:2:2
[g] $[2\text{-Br*}]_o$:$[CuBr]_o$:$[HPTETA]_o$= 1:2:2
[h] $[2\text{-Br*}]_o$:$[CuBr]_o$:$[PMDETA]_o$= 1:2:2

4.2.3 Di-functional poly(ethyl hexyl acrylate)

Vlcek and co-workers undertook a detailed study on the effect of alkali metal alkoxide in the living anionic polymerization of various acrylates. They performed the polymerization of 2-ethyl hexyl acrylate (EHA) using different initiators in the presence alkali metal alkoxide. Poor initiator efficiencies, low conversions and poly(EHA)s with very broad PDIs were obtained at low temperature and a moderate control in the polymerization of EHA was achieved [108-110]. The controlled synthesis of mono functional PEHA and derived random, block and blocky gradient copolymers via ATRP are described in the literature [111]. Linear P(EHA-co-MA) random copolymers were obtained with broad polydispersities as "all acrylate" block copolymers [112].

In this thesis, well defined di-functional PEHAs (X-PEHA-X) were obtained with different molecular weights via ATRP for the first time (Table 4.3).

Table 4.3: Characteristics of the X-PEHA-X homopolymers.[a]

Run	$[M]_o:[I]_o$	Time (h)	Conv. (%)	$M_{n,GPC}$[b]	M_w/M_n[b]	$M_{w,LS}$[c]
P30	80	-	15.5	28970	1.79	-
P31	300	28.50	73.5	50600	1.66	-
P32	300	2.50	46.0	71000	1.59	-
P33	300	5.50	69.5	114220	1.56	218210

[a] T: 100 °C, $[M]_o$= 4.8 mol L^{-1}, $[2\text{-Br*}]_o:[CuBr]_o:[Bipyr]_o$= 1:2:2
[b] Calculated from GPC calibrated with linear poly(methyl methacrylate) standards
[c] Absolute molecular weights were calculated with multi angle light scattering in THF and the *dn/dc* value for PEHA was used as 0.058 mL/g.

4.2.4 Tri-functional polystyrene

Tri-functional star shaped polystyrene was obtained via ATRP as given in Table 4.4 and it was used to acquire block copolymer in the following section.

Table 4.4: Characteristics of the $(PS\text{-}X)^{3*}$ star polymers.[a]

Run	$[M]_o:[I]_o$	Time (h)	Conv. (%)	$M_{n,GPC}$[b]	M_w/M_n[b]	$M_{w,LS}$[c]
P34	2000	116.00	19.6	35970	1.14	35240

[a] T: 100 °C, $[3\text{-Br*}]_o:[CuBr]_o:[Bipyr]_o$= 1:3:3, $[M]_o$= 2.98 mol L^{-1}
[b] Calculated from GPC calibrated with linear polystyrene standards
[c] Absolute molecular weights were calculated with multi angle light scattering in THF and the *dn/dc* value for PS was used as 0.185 mL/g.

4.2.5 Tetra-functional poly(ethyl hexyl acrylate)

The studies in literature about the synthesis of mono functional PEHA was explained in the synthesis of di-functional PEHA section. Additionally, 4-arm radial P(EHA-co-MA) random copolymers were obtained with very broad polydispersities (PDI:3) [112].

In this thesis, well defined four arm star shaped (PEHA-X)^4*s were achieved with different molecular weights via ATRP for the first time (Table 4.5).

Table 4.5: Characteristics of the (PEHA-X)^{4*} star polymers.[a]

Run	$[M]_o$ (mol L^{-1})	$[M]_o$:$[I]_o$	Time (h)	Conv. (%)	$M_{n,GPC}$[b]	M_w/M_n[b]	$M_{w,LS}$[c]
P64	1.74	216	28.50	74.0	13690	2.00	-
P65	1.73	400	52.50	53.4	20100	1.62	-
P66[d]	2.14	218	-	87.5	23440	1.45	46230
P67[e]	4.80	626	11.50	77.5	74210	1.46	-

[a] T: 100 °C, $[4\text{-Br*}]_o$:$[CuCl]_o$:$[Bipyr]_o$= 1:4:4,
[b] Calculated from GPC calibrated with linear poly(methyl methacrylate) standards
[c] Absolute molecular weights were calculated with multi angle light scattering in THF and the *dn/dc* value for PEHA was used as 0.058 mL/g.
[d] T: 100 °C, $[4\text{-Br*}]_o$:$[CuCl]_o$:$[Bipyr]_o$= 1:8:8
[e] $[4\text{-Br*}]_o$:$[CuBr]_o$:$[Bipyr]_o$= 1:6:6

4.2.6 Tetra-functional polystyrene

Star polymers with different numbers and lengths of polystyrene arms were obtained via atom transfer radical polymerization. To obtain 4-arm star polystyrene, (PS-X)^4*, heterogeneous and homogeneous ATRP with ALALs were used as the synthetic procedures (Table 4.6). The temperature, the catalyst systems and the initiator effects were investigated. In all cases, well defined star polymers were obtained. To ensure that the well defined polymers are obtained, light scattering measurements were performed for some polymers to compare the M_n values with the absolute M_w values and it was that the calculations were compatible.

Table 4.6: Characteristics of the (PS-X)$_{4}^{*}$ star polymers.[a]

Run	$[M]_o$ (mol L^{-1})	$[M]_o$:$[I]_o$	Time (h)	Conv. (%)	$M_{n,GPC}$ [b]	M_w/M_n [b]	$M_{w,LS}$ [c]
P35[d,f]	8.73	70	6.50	97.0	6680	1.27	-
P36[d,f]	1.74	400	3.00	-	7800	1.20	-
P37[d,f]	8.73	240	7.70	51.4	12930	1.23	-
P38[h]	1.74	400	2.00	-	15870	1.34	-
P39[e,i]	4.36	2000	97.50	12.4	17170	1.67	-
P40[d,f]	8.73	240	7.50	55.3	17170	1.32	-
P41[f]	8.73	240	7.70	61.0	18080	1.32	26010
P42[e,i]	4.36	1984	99.50	10.0	18850	1.58	29680
P43[e,i]	4.36	1984	99.50	15.0	27990	1.33	-
P44[e,h]	1.74	400	3.50	-	30600	1.84	-
P45[d,f]	8.73	480	7.75	41.0	31280	1.16	38460
P46[e,g]	1.45	2000	23.00	25.5	33390	1.73	-
P47[e,g]	3.87	2000	3.25	16.0	34300	1.22	-
P48[d,f]	8.73	480	7.00	61.0	34630	1.15	38310
P49[j,l]	0.79	2000	22.75	6.0	36290	1.66	-
P50[e,g]	3.87	4000	3.25	7.3	36370	1.24	43840
P51[d,f]	8.73	484	5.25	67.0	36920	1.16	-
P52[e,i]	4.36	2000	144.00	19.5	37200	1.37	-
P53[e,i]	4.36	2000	219.00	21.0	41400	1.57	-
P54[e,i]	4.36	2000	338.00	26.0	41700	1.44	50620
P55[d,f]	8.73	1000	23.25	41.0	58530	1.10	-
P56[d,f]	8.73	2000	101.00	24.0	73420	1.09	-
P57[h,l]	1.45	2000	59.00	23.0	75780	1.36	-
P58[g,l]	1.45	2000	22.00	34.0	81710	1.34	-
P59[e,k]	8.73	800	2.00	43.0	83950	1.59	-
P60[j,l]	1.45	2000	41.00	39.0	99280	1.60	-
P61[g,l]	1.45	2000	217.00	49.0	115850	1.42	-
P62[e,g]	3.87	2000	22.00	47.0	120980	1.32	-
P63[e,g]	3.87	4000	22.00	35.6	145690	1.43	-

[a] Initiator: 4-Br* (2′), T: 110 °C
[b] Calculated from GPC calibrated with linear polystyrene standards
[c] Absolute molecular weights were calculated with multi angle light scattering in THF and the *dn/dc* value for PS was used as 0.185 mL/g
[d] Initiator: 4-Br* (3′),
[e] T: 100 °C
[f] $[4\text{-Br}^*]_o:[CuBr]_o:[Bipyr]_o = 1:4:4$
[g] $[4\text{-Br}^*]_o:[CuBr]_o:[HPTETA]_o = 1:4:4$
[h] $[4\text{-Br}^*]_o:[CuBr]_o:[PMDETA]_o = 1:4:4$
[i] $[4\text{-Br}^*]_o:[CuCl]_o:[Bipyr]_o = 1:4:4$
[j] $[4\text{-Br}^*]_o:[CuBr]_o:[Butylatedpolyethyleneimine]_o = 1:4:4$
[k] $[4\text{-Br}^*]_o:[CuCl]_o:[PMDETA]_o = 1:4:4$
[l] T: 115 °C

4.2.7 Penta- and octa-functional polystyrene

Penta (5-Br*) functional initiator synthesized via Schotten-Baumann reaction was employed as a macroinitiator for the ATRP of polystyrene (Table 4.7).

In order to prove the controlled character of the polymerization of S using 5-Br* and 8-Br* as initiators with HPTETA as ligand, the relationship between time-conversion and molecular weight-conversion were studied. In principle, the characteristics of a controlled process are revealed through a first order kinetic plot of molecular weight and monomer conversion and a low polydispersity. As shown in Figure 4.16-a for pentafunctional polystyrene, a linear relationship is seen between $\ln([M]_0/[M])$ and reaction time, obeying first order kinetics, and indicating that the number of propagating species remained constant. Furthermore, one can observe from Figure 4.16-b, that the molecular weight increases rather linearly with conversion, and the polydispersity decreases from 1.54 to 1.48 over the same period. The increasement of molecular weight can be seen in GPC traces, Figure 4.17.

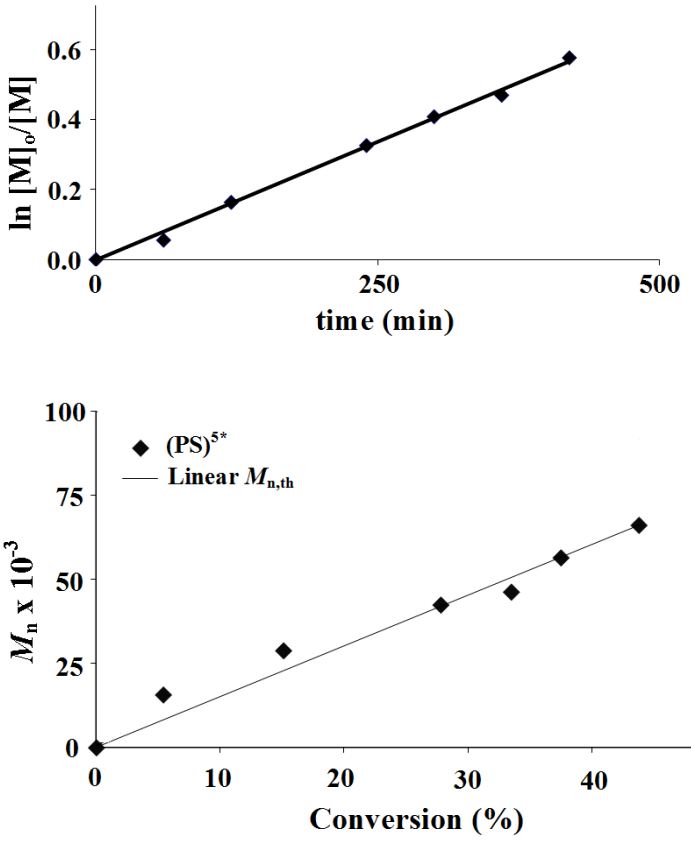

Figure 4.16 : a) First-order plot for ATRP of styrene with 5-Br* at 110 °C,
b) molecular weights versus conversions (by GPC) of penta-arm star PS (P78), $[Styrene]_o$: $[5\text{-}Br^*]_o$:$[CuBr]_o$:$[HPTETA]_o$ = 2000:1:5:5.

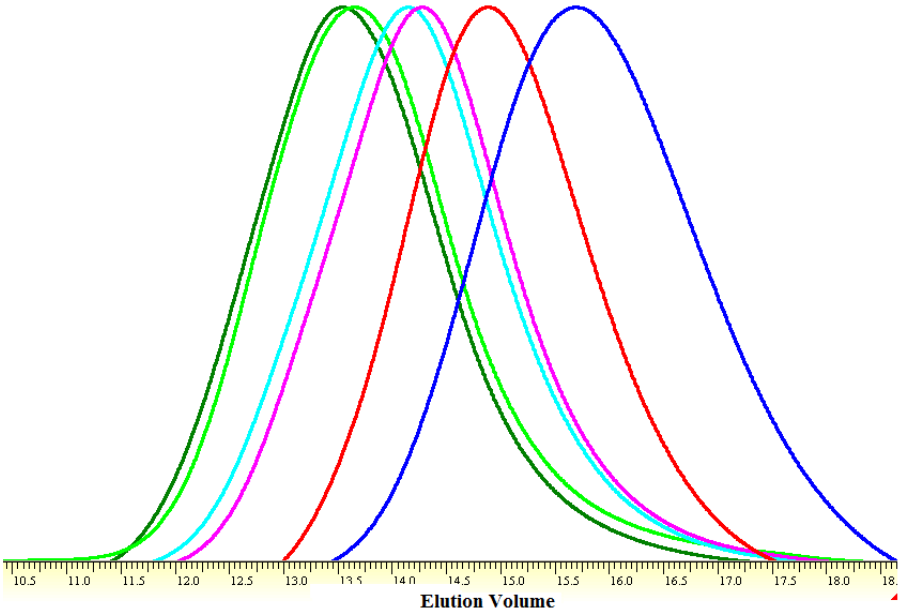

Figure 4.17 : GPC traces of penta-arm star-PS (P78) as a function of conversion.

Table 4.7: Characteristics of the (PS-X)^{5*} star polymers.[a]

Run	Time (h)	Conv. (%)	$M_{n,GPC}$ [b]	M_w/M_n [b]
P68	0.5	6	10870	1.57
P69	2	20	17510	1.45
P70	2	11	18000	1.69
P71	1	12	19490	1.36
P72	3	10	28000	1.56
P73	3	19	30490	1.69
P74	3.5	24	38290	1.46
P75	2	13	40160	1.28
P76	3	10	40630	1.46
P77	4	20	42700	1.53
P78 [c]	19.75	48	52350	1.48
P79	4	20	56260	1.47
P80[c]	24.58	-	56390	1.69
P81	6.17	28	62690	1.32
P82	24.33	21	83380	1.8
P83[c]	24.75	68	91000	1.48
P84[d]	0.83	22	114670	1.46

[a] T: 110 ^{o}C, $[M]_o$= 2.91 mol L^{-1} , $[M]_o$:$[5\text{-Br}^*]_o$:$[CuBr]_o$:$[HPTETA]_o$= 2000:1:5:5
[b] Calculated from GPC calibrated with linear polystyrene standards
[c] Kinetic work
[d] $[M]_o$= 4.36 mol L^{-1}

Octa functional initiator (8-Br*) synthesized via Schotten-Baumann reaction was employed as a macroinitiator for the ATRP of polystyrene (Table 4.8). The kinetics of S polymerization was investigated as well using 8-Br* as a initiator. The living character of the polymerization was also proven for that monomer by a linear relationship between $\ln([M]_o/[M])$ and reaction time (Figure 4.18-a), and also by the linear increase of the molecular weight with monomer conversion and the low polydispersities (Figure 4.18-b). However, the molecular weights measured by GPC versus Conversion% are slightly lower than the theoretical values for polymerization of 8 functional polystyrene. It seems possible that a small amount of transfer reaction takes place, which could be considered as breaking the kinetic chain.

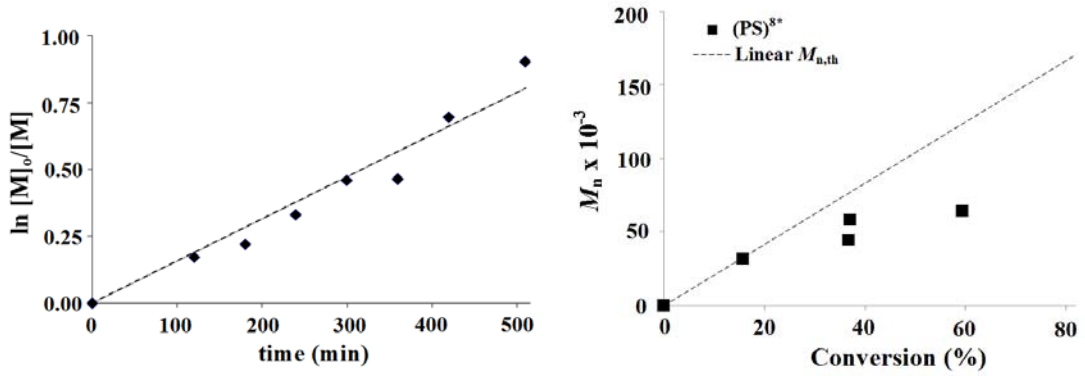

Figure 4.18 : a) Kinetics plot of the ATRP of S using octa-functional initiator, b) Effect of conversion during the ATRP of S on the molecular weight using octa- functional initiator.

Nevertheless, the linear kinetics plot and the low polydispersity confirmed that the ATRP of S proceeded in a living fashion under the conditions used and with octa-functional initiators and HPTETA as metal complex ligand.

Table 4.8 : Characteristics of the $(PS\text{-}X)^{8*}$ star polymers. [a]

Run	Time (h)	Conv. (%)	$M_{n,GPC}$ [b]	M_w/M_n [b]
P85	2.00	16	40770	1.68
P86	1.33	11	26310	1.78
P87	1.00	10	27400	1.96
P88	28.67	33	58990	2.02

[a] T: 110 °C, $[M]_o$= 2.9 mol L^{-1},
$[M]_o$:$[8\text{-}Br^*]_o$:$[CuBr]_o$:$[HPTETA]_o$= 2000:1:8:8
[b] Calculated from GPC calibrated with linear polystyrene standards

4.3 Synthesis of Block Copolymers by ATRP

ATRP allows block copolymer synthesis by sequential steps (one pot) [100] or by separated steps (two pots), where one component is polymerized in first batch, and then continued with the second monomer in the other batch after several purification steps [99]. In this thesis, well-defined PS-*b*-PEHA di-block, PS-*b*-PEHA-*b*-PS and PEHA-*b*-PS-*b*-PEHA tri-block, $(PS\text{-}b\text{-}PEHA)^{3*}$ 3-arm star-block, $(PEHA\text{-}b\text{-}PS)^{4*}$ and $(PS\text{-}b\text{-}PEHA)^{4*}$ 4-arm star-block, $(PS\text{-}b\text{-}PEHA)^{5*}$ 5-arm star-block, $(PS\text{-}b\text{-}PEHA)^{8*}$ 8-arm star-block copolymers were synthesized via ATRP (Figure 4.19).

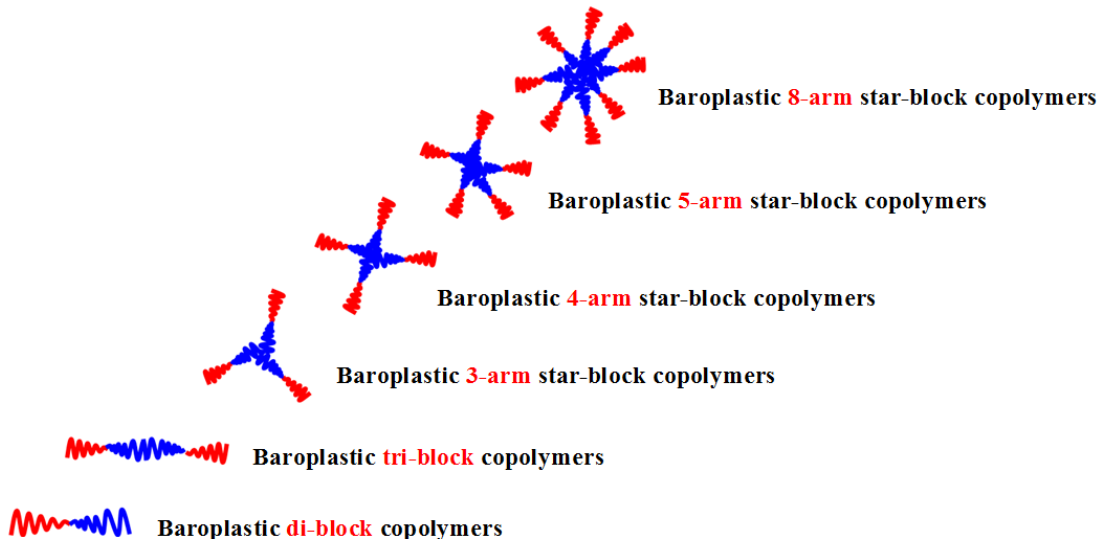

Figure 4.19 : Schematic representation of the synthesized block copolymers.

In the preparation of PS and PEHA with different functionalities as precursor for further use in the synthesis of block and star polymers, we applied different $[M]_o/[I]_o$ ratios were applied to obtain block copolymers having different chain lengths and compositions. Other results and conditions are given in appropiate tables. For all block copolymers, the molar compositions were calculated using ^1H NMR measurements according to the integration of characteristic peaks of corresponding segments. In order to compare the effect of structures on the baroplastic behavior, some block copolymers were obtained with the replacement of inner/outer soft segments.

4.3.1 PS-*b*-PEHA di-block copolymers

PS-*b*-PEHA diblock copolymers were synthesized using previously obtained homopolymer PS with PMDETA and CuBr or CuCl as catalyst (Table 4.9). The synthetic routes of the di-block copolymers are summarized in Figure 4.20.

Table 4.9: Characteristics of the PS-*b*-PEHA di-block copolymers.[a]

Run	$[M]_o$ (mol L^{-1})	$[M]_o$:$[I]_o$	Macro ini.	$M_{n,GPC}$ (MI)	Time (h)	Conv. (%)	$M_{n,GPC}$[b]	M_w/M_n[b]	Comp.[c] (PEHA,%)
B1[d]	0.77	150	P7	28940	64.50	49.0	43780	1.17	23
B2[e]	1.34	150	P3	17750	26.00	11.0	25800	1.40	37
B3[e]	1.85	850	P13	57050	26.50	8.5	83060	1.25	37
B4[g]	2.35	1000	P14	79480	24.00	56.0	132970	1.27	**41**
B5[f]	9.67	260	P7	28940	69.00	49.7	45600	1.17	**43**
B6[h]	1.37	308	P8	34840	20.00	59.0	57280	1.39	**43**
B7[i]	0.86	418	P11	48220	23.50	55.0	70860	1.28	**43**
B8[e]	1.62	200	P3	17750	17.00	56.0	35560	1.40	**50**
B9[g]	2.67	598	P8	34840	19.00	52.0	87130	1.44	**50**
B10[e]	2.04	250	P3	17750	26.00	-	21350	1.67	**51**

[a] T: 100 °C
[b] Calculated from GPC calibrated with linear poly(methyl methacrylate) standards
[c] Compositions were calculated by ^{1}H NMR analysis
[d] $[PS\text{-}X]_o$:$[CuCl]_o$:$[PMDETA]_o$= 1:1:1, [e] 1:2:3, [f] 1:3:3
[g] $[PS\text{-}X]_o$:$[CuBr]_o$:$[PMDETA]_o$= 1:5:5, [h] 1:3:3, [i] 1:4:4

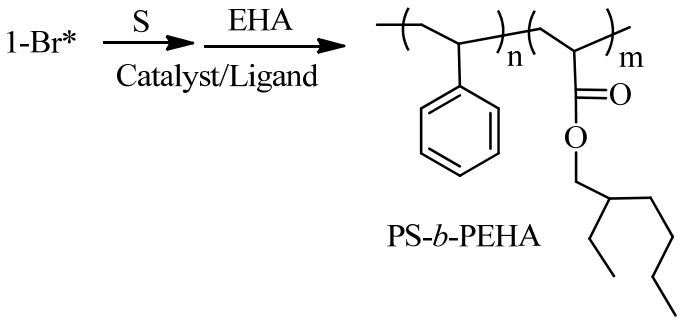

Figure 4.20 : Synthesis of PS-*b*-PEHA di-block copolymer.

4.3.2 PS-*b*-PIP di-block copolymers

The exhibited PS-*b*-PIP diblock copolymers in the literature synthesized via anionic polymerization were utilized as received (Table 4.10) [113].

Table 4.10: Characteristics of the PS-*b*-PIP di-block copolymers.[a]

Run	M_n [b] first block	M_n [b]	M_w/M_n [b]	Comp.[c] (PIP,%)
B11	8710	17170	1.32	58.3
B12	5800	16800	1.03	74.0
B13	11570	39090	1.79	81.6

[a] T: -30 °C, one-pot polymerization, $[M_1]_o:[M_2]_o:[BuLi]_o=100:500:1$
[b] Calculated from GPC calibrated with linear poly(methyl methacrylate) standards
[c] Compositions were calculated by ^{1}H NMR analysis

4.3.3 PEHA-*b*-PS-*b*-PEHA tri-block copolymers

Di-functional PS macroinitiators were further used to initiate the polymerization of EHA to afford the tri-block copolymers with various molecular weights and compositions (Table 4.11). Shown in Figure 4.21 are the synthetic routes of the tri-block copolymers.

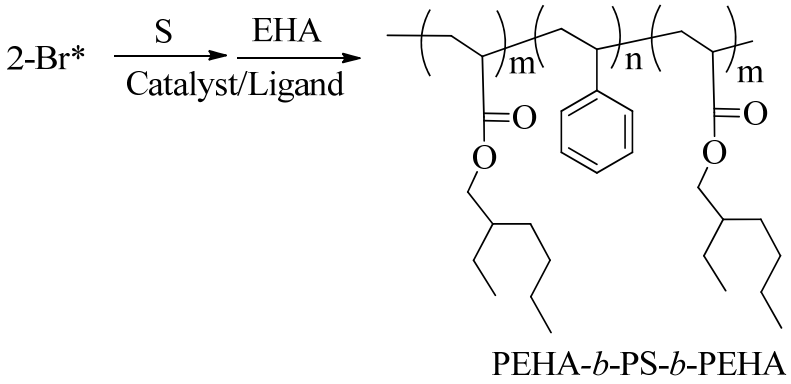

Figure 4.21 : Synthesis of PEHA-*b*-PS-*b*-PEHA tri-block copolymer.

Molecular weights and polydispersities of the block copolymers were traced by GPC to monitor the chain growth within the block and to confirm the continuation of the second block. This could be observed as a shift of the peak to lower elution time (higher molecular weights) representatively shown in Figure 4.22 for tri-block copolymer (51% PEHA, B18).

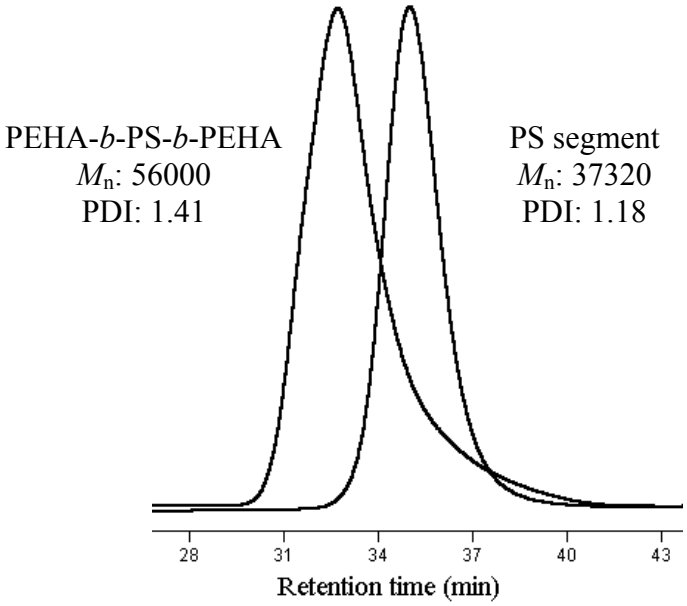

Figure 4.22 : GPC traces of the PS segment (P25) and PEHA-*b*-PS-*b*-PEHA tri-block copolymer (51% PEHA, B18).

Table 4.11 : Characteristics of the PEHA-*b*-PS-*b*-PEHA tri-block copolymers.[a]

Run	$[M]_o$ (mol L^{-1})	$[M]_o$:$[I]_o$	Macro Ini.	$M_{n,GPC}$ (MI)	Time (h)	Conv. (%)	$M_{n,GPC}$[b]	M_w/M_n[b]	$M_{w,LS}$[c]	Comp.[d] (PEHA,%)
B14[e]	0.83	1105	P29	109350	31.50	-	139920	1.16	-	16
B15[f]	0.96	1051	P29	109350	159.00	18.0	138000	1.14	-	26
B16[f]	1.22	899	P29	109350	20.00	39.0	141890	1.18	-	33
B17[g]	1.60	706	P18	14670	1.75	9.6	35650	1.43	35400	**50**
B18[h]	0.80	228	P25	37320	68.00	-	56000	1.41	65320	**51**
B19[g]	1.60	706	P18	14670	1.50	9.5	36000	1.35	38220	**51**
B20[i]	1.78	322	P23	24880	17.00	43.0	51630	1.59	75530	**52**
B21[g]	1.60	706	P18	14670	1.75	16.5	31770	1.54	41160	**53**
B22[i]	1.67	300	P23	24879	15.00	70.0	62470	1.87	-	**57**
B23[i]	1.78	322	P22	20010	20.00	26.0	58400	1.42	-	**59**

[a] T: 100 °C
[b] Calculated from GPC calibrated with linear poly(methyl methacrylate) standards
[c] Absolute molecular weights were calculated with multi angle light scattering in THF and the *dn/dc* value of blok copolymer= [X_{PS}*0.185 mL/g (*dn/dc* for PS)+X_{PEHA}*0.058 mL/g (*dn/dc* for PEHA)].
[d] Compositions were calculated by ^{1}H NMR analysis
[e] $[X\text{-}PS\text{-}X]_o$:$[CuBr]_o$:$[PMDETA]_o$ = 1:5:5, [f] 1:8:8, [g] 1:18.5:18.5, [h] 1:4:4, [i] 1:2:2

4.3.4 PS-*b*-PEHA-*b*-PS tri-block copolymers

The functionalized PEHA was employed as a macroinitiator for the ATRP of S. The PS-*b*-PEHA-*b*-PS tri-block copolymer was synthesized via one-pot or two-pot synthetic routes as shown in Figure 4.23 and the results are summarized in Table 4.12.

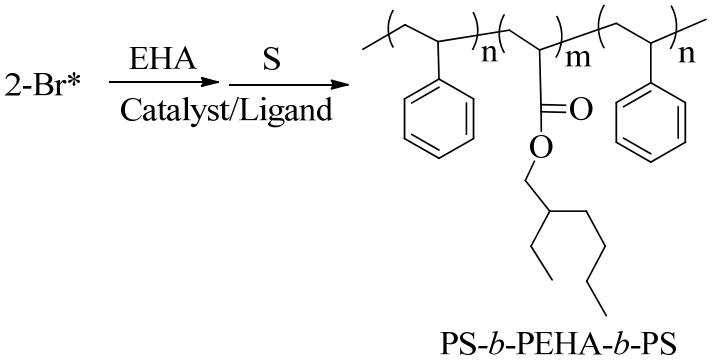

Figure 4.23 : Synthesis of PS-*b*-PEHA-*b*-PS tri-block copolymer.

Table 4.12: Characteristics of the PS-*b*-PEHA-*b*-PS tri-block copolymers.[a]

Run	$[M]_o$ (mol L^{-1})	$[M]_o$:$[I]_o$	Macro Ini.	$M_{n,GPC}$ (MI)	Time (h)	$M_{n,GPC}$ [b]	M_w/M_n [b]	$M_{w,LS}$ [c]	Comp.[d] (PEHA,%)
B24[e]	3.27	262	P31	50600	45.50	108090	1.42	-	27
B25[f]	2.18	500	P30	28970	89.50	58000	1.51	-	27
B26[e]	3.34	262	P31	50600	42.50	131070	1.33	-	28
B27[g]	1.95	98	-	13890	86.00	30290	1.27	33640	**40**
B28[h]	2.86	550	P31	50600	24.55	124290	1.30	134570	**40**
B29[g]	1.92	98	-	17780	17.00	36890	1.49	48090	**43**
B30[e]	1.86	620	P31	50600	24.00	94060	1.34	118380	**44**
B31[g]	1.92	98	-	19030	17.00	30780	1.46	40840	**45**
B32[g]	1.92	98	-	15000	25.00	41000	1.38	51870	**47**
B33[g]	1.92	98	-	14890	25.50	30130	1.44	38730	**48**
B34[g]	1.92	98	-	19030	18.00	38540	1.56	59580	**49**
B35[g]	1.92	98	-	18830	19.00	30150	1.49	37090	**50**
B36[i]	1.74	1000	P33	114220	22.25	150000	1.16	264450	**50**
B37[h]	1.44	1188	P33	114220	31.50	93280	1.67	-	**62**
B38[e]	2.40	446	P31	50600	18.50	81400	1.49	-	**64**

[a] T: 110 °C
[b] Calculated from GPC calibrated with linear polystyrene standards
[c] Absolute molecular weights were calculated with multi angle light scattering in THF and the *dn/dc* value of blok copolymer= [X_{PS}*0.185 mL/g (*dn/dc* for PS)+X_{PEHA}*0.058 mL/g (*dn/dc* for PEHA)]
[d] Compositions were calculated by ^{1}H NMR analysis
[e] $[X\text{-}PEHA\text{-}X]_o$:$[CuCl]_o$:$[PMDETA]_o$= 1:4:4, [h] 1:6:6
[f] $[X\text{-}PEHA\text{-}X]_o$:$[CuBr]_o$:$[PMDETA]_o$= 1:2:2, [i] 1:6:6
[g] $[2\text{-}Br^*]_o$:$[CuCl]_o$:$[Me_6TREN]_o$= 1:1.5:1.5, T: 70 °C, one-pot polymerization

4.3.5 PMMA-*b*-PEHA-*b*-PMMA tri-block copolymers

PMMA-*b*-PEHA-*b*-PMMA tri-block copolymers with one-pot synthetic route were achieved by ATRP (Figure 4.24, Table 4.13).

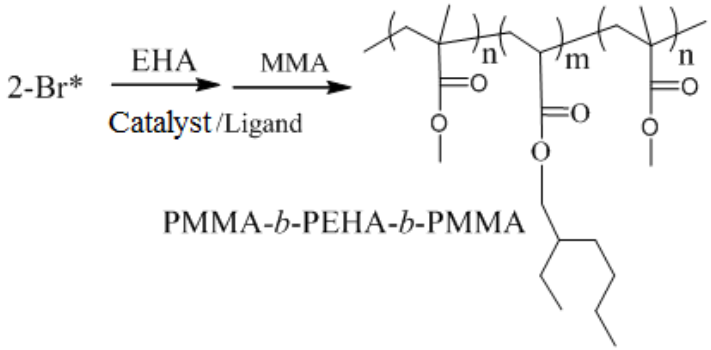

Figure 4.24 : Synthesis of PMMA-*b*-PEHA-*b*-PMMA tri-block copolymer.

Table 4.13: Characteristics of the PMMA-*b*-PEHA-*b*-PMMA tri-block copolymers.[a]

Run	$M_{n,GPC}$ first block	Time (h)	$M_{n,GPC}$[b]	M_w/M_n[b]	$M_{w,LS}$[c]	Comp.[d] (PEHA,%)
B39	21240	2.50	33680	2.07	-	15
B40	22695	1.00	30820	1.59	54920	**58**
B41	17010	1.00	24980	1.78	-	**61**
B42	19065	1.50	27560	2.10	-	**67**

[a] T: 70 °C, $[M_1]_o:[M_2]_o:[2\text{-Br*}]_o:[CuCl]_o:[Me_6TREN]_o$= 96:410:1:1.5:1.5
$[M]_o$=1.92 mol L^{-1}, one-pot polymerization
[b] Calculated from GPC calibrated with linear poly(methyl methacrylate) standards
[c] Absolute molecular weights were calculated with multi angle light scattering in THF and the *dn/dc* value of blok copolymer= [X_{PMMA}*0.076 mL/g (*dn/dc* for PMMA)+X_{PEHA}*0.058 mL/g (*dn/dc* for PEHA)]
[d] Compositions were calculated by ^{1}H NMR analysis

4.3.6 PMMA-*b*-PBA-*b*-PMMA tri-block copolymers

The synthesis of PMMA-*b*-PBA-*b*-PMMA tri-block copolymers were acquired with one-pot ATRP synthetic route were acquired (Figure 4.25). The details can be found in Table 4.14.

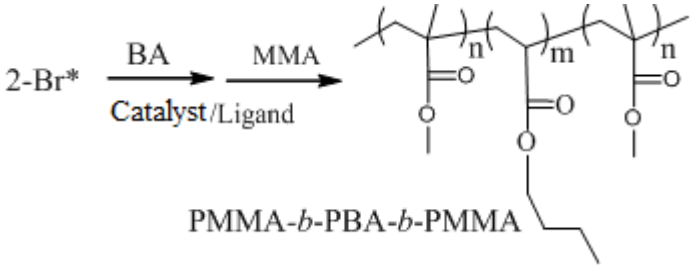

Figure 4.25 : Synthesis of PMMA-*b*-PBA-*b*-PMMA tri-block copolymer.

Table 4.14: Characteristics of the PMMA-*b*-PBA-*b*-PMMA tri-block copolymers.[a]

Run	$[M]_o$ (mol L^{-1})	$M_{n,GPC}$ first block	Time (h)	$M_{n,GPC}$[c]	M_w/M_n[c]	$M_{w,LS}$[d]	Comp.[e] (PBA,%)
B43	2.72	23000	73.00	71000	1.47	-	34.0
B44	2.38	43000	46.00	92000	1.51	-	40.8
B45[b]	4.00	36000	49.50	111000	1.29	-	41.3
B46[b]	4.00	40000	28.00	88000	1.74	155420	44.0

[a] T: 90 °C, $[M_1]_o$:$[M_2]_o$: $[2\text{-Br*}]_o$:$[CuBr]_o$:$[PMDETA]_o$= 260:660:1:1:1, one-pot polymerization
[b] $[M_1]_o$:$[M_2]_o$: $[2\text{-Br*}]_o$:$[CuCl]_o$:$[PMDETA]_o$= 260:660:1:1:1
[c] Calculated from GPC calibrated with linear poly(methyl methacrylate) standards
[d] Absolute molecular weights were calculated with multi angle light scattering in THF and the *dn/dc* value of blok copolymer= [X_{PMMA}*0.076 mL/g (*dn/dc* for PMMA)+X_{PBA}*0.057 mL/g (*dn/dc* for PBA)]
[e] Compositions were calculated by ^{1}H NMR analysis

4.3.7 (PS-*b*-PEHA)^3* tri-arm star-block copolymers

(PS-*b*-PEHA)^{3*} star block copolymers were produced using previously obtained tri-arm star polystyrenes with PMDETA and CuBr or CuCl complex catalyst system (Table 4.15). The synthesis of tri-armed star block copolymer is demonstrated in Figure 4.26.

Table 4.15: Characteristics of the (PS-*b*-PEHA)^{3*} tri-arm star-block copolymers.[a]

Run	$[M]_o$ (mol L^{-1})	$[M]_o$:$[I]_o$	Makro Ini.	$M_{n,GPC}$ (MI)	Time (h)	Conv. (%)	$M_{n,GPC}$[b]	M_w/M_n[b]	$M_{w,LS}$[c]	Comp.[d] (PEHA,%)
B47	0.89	176	P34	35970	23.00	8.9	56060	1.21	56500	27
B48[e]	1.35	248	P34	35970	160.00	62.0	71570	1.21	-	37
B49	1.17	284	P34	35970	48.00	51.0	154690	1.25	-	40
B50[e]	0.70	186	B49	56060	72.50	59.0	64030	1.23	65130	**50**

[a] T: 100 °C, $[PS^{3*}]_o$:$[CuCl]_o$:$[PMDETA]_o$= 1:3:3
[b] Calculated from GPC calibrated with linear poly(methyl methacrylate) standards
[c] Absolute molecular weights were calculated with multi angle light scattering in THF and the *dn/dc* value of blok copolymer= [X_{PS}*0.185 mL/g (*dn/dc* for PS)+X_{PEHA}*0.058 mL/g (*dn/dc* for PEHA)]
[d] Compositions were calculated by ^{1}H NMR analysis
[e] $[PS\text{-}X^{3*}]_o$:$[CuBr]_o$:$[PMDETA]_o$= 1:3:3

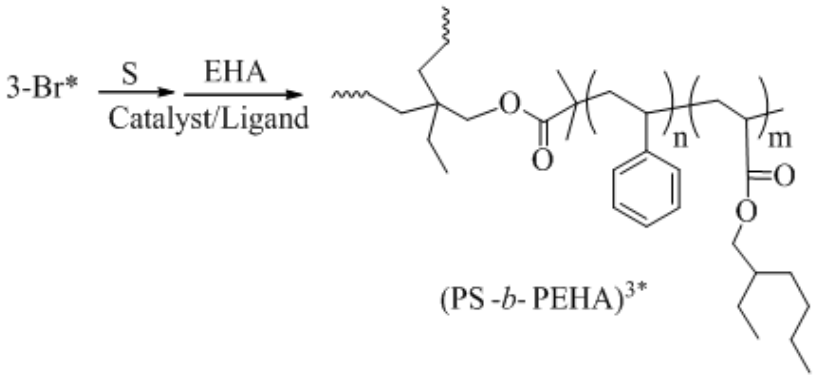

Figure 4.26 : Synthesis of (PS-*b*-PEHA)^{3*} tri-arm star-block copolymer.

4.3.8 (PS-*b*-PEHA)^{4}* four-arm star-block copolymers

With tetra functional polystyrene as macroinitiator, four-arm star-block copolymers, (PS-*b*-PEHA)^{4*}, were prepared and the arm lengths and compositions were controlled via ATRP (Figure 4.27, Table 4.16).

The block copolymer's composition was calculated using ^{1}H NMR measurements by integrating the characteristic peak of the PEHA segment (-C(O)O$\underline{CH_2}$-) at 3.9 ppm versus the aromatic peaks of the PS segment at 6.34-7.06 ppm. ^{1}H NMR spectrum of 4-arm star-block copolymer (B81) is shown in Figure 4.28. The signals of the methyl ester group were also assigned by means of ^{1}H NMR measurements confirming the incorporation of the PEHA blocks in the block copolymers. In GPC traces of the (PS-*b*-PEHA)^{4*} four-arm star-block copolymers a peak of the (PS)^{4*} shifted to the higher molecular weight region with increasing monomer conversion in the ATRP of EHA. Moreover, no peak was observed in the higher molecular weight region of the GPC traces which indicates the absence of the star-star coupling reaction.

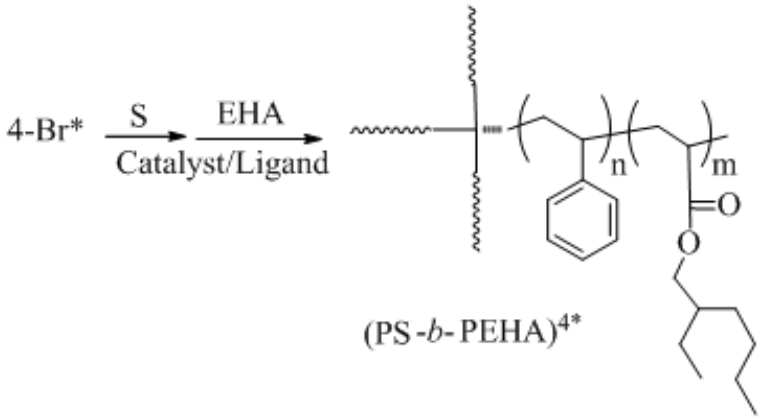

Figure 4.27 : Synthesis of (PS-*b*-PEHA)^{4*} four-arm star-block copolymer.

Table 4.16: Characteristics of the (PS-*b*-PEHA)^{4*} four-arm star-block copolymers.[a]

Run	$[M]_o$ (mol L^{-1})	$[M]_o$:$[I]_o$	Macro Ini.	$M_{n,GPC}$ (MI)	Time (h)	$M_{n,GPC}$ [b]	M_w/M_n [b]	$M_{w,LS}$ [c]	Comp.[d] (PEHA,%)
B51[e]	1.05	470	P53	41400	196.00	51190	1.42	-	-
B52[f]	1.08	535	P52	37200	364.00	50440	1.29	-	-
B53[g]	1.20	258	P48	34630	23.00	53310	1.19	-	-
B54[g]	0.80	300	P55	58530	72.00	87930	1.13	-	-
B55[h]	1.37	250	P45	31280	25.00	75900	1.25	-	-
B56[g]	1.20	258	P48	34630	65.00	79800	1.34	-	-
B57[i]	0.80	300	P55	58530	25.00	118760	1.34	-	-
B58[j]	1.20	296	P51	36920	102.00	73110	1.21	-	-
B59[k]	0.99	1189	P58	81710	16.00	94990	1.13	-	-
B60[g]	0.99	300	P40	17170	214.00	48140	1.27	-	-
B61[g]	0.69	200	P41	18080	69.00	28180	1.29	-	-
B62[e]	1.05	467	P53	41400	96.50	62160	1.39	-	7
B63[l]	1.10	189	P53	41400	45.00	52540	1.53	-	11
B64[i]	0.80	600	P56	73420	36.00	94000	1.09	-	13
B65[m]	0.83	639	P53	41400	47.25	57020	1.35	-	16
B66[h]	0.88	146	P43	27990	22.50	70400	1.29	-	23
B67[l]	1.10	194	P39	17170	25.00	30800	1.54	-	28
B68[n]	1.27	516	P39	17170	73.00	23590	1.66	-	31
B69[h]	1.15	200	P43	27990	23.00	64290	1.33	-	32
B70[i]	1.55	380	P50	36370	25.00	74340	1.20	78020	34
B71[k]	1.20	296	P51	36920	3.00	91910	1.42	-	35
B72[i]	1.99	258	P48	34630	69.00	81460	1.39	129410	**36**
B73[o]	1.45	1000	P57	75780	184.00	106940	1.20	100040	**36**
B74[i]	0.80	250	P45	31280	24.00	83830	1.29	94120	**39**
B75[g]	0.80	150	P41	18080	46.00	38800	1.33	50340	**39**
B76[i]	1.55	380	P50	36370	21.00	106270	1.34	138060	**47**
B77[i]	1.38	400	P54	41700	19.75	102900	1.21	102820	**48**
B78[g]	1.87	500	P48	34630	43.00	87590	1.28	106620	**48**
B79[i]	1.52	300	P43	27990	25.00	80000	1.28	106030	**49**
B80[i]	1.38	400	P54	41700	43.50	116000	1.16	100760	**49**
B81[i]	1.38	400	P54	41700	43.50	98000	1.33	114660	**51**
B82[i]	1.68	350	P43	27990	23.25	85650	1.35	101780	**51**
B83[i]	1.37	400	P54	41700	7.25	84610	1.31	107101	**56**
B84[i]	1.87	500	P48	34630	43.00	100000	1.31	128950	**57**
B85[g]	0.96	384	P42	18850	214.00	36340	1.72	63860	**62**

[a] T: 100 °C, $[PS\text{-}X^{4*}]_o$:$[CuCl]_o$:$[Bipyr]_o$= [e] 1:3.2:3.2, [f] 1:4.2:4.2, [l] 1:3.5:3.5, [m] 1:5.2:5.2, [n] 1:4:2.55
[g] $[PS\text{-}X^{4*}]_o$:$[CuBr]_o$:$[Bipyr]_o$= 1:4:4, [j] 1:5:5
[h] $[PS\text{-}X^{4*}]_o$:$[CuCl]_o$:$[PMDETA]_o$= 1:4:4
[i] $[PS\text{-}X^{4*}]_o$:$[CuBr]_o$:$[PMDETA]_o$= 1:4:4, [k] 1:6.6:6.6, [o] 1:8:8
[b] Calculated from GPC calibrated with linear poly(methyl methacrylate) standards
[c] Absolute molecular weights were calculated with multi angle light scattering in THF and the *dn/dc* value of blok copolymer= [X_{PS}*0.185 mL/g (*dn/dc* for PS)+X_{PEHA}*0.058 mL/g (*dn/dc* for PEHA)]
[d] Compositions were calculated by ^{1}H NMR analysis

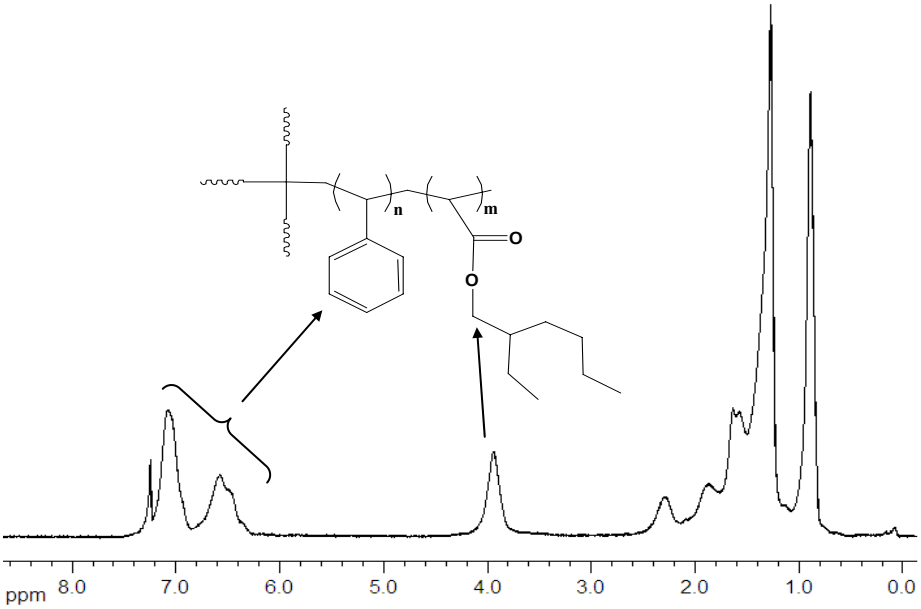

Figure 4.28 : ^{1}H NMR spectrum of ($PS_{0.49}$-*b*-$PEHA_{0.51}$)^{4*} four-arm star-block copolymer (B81) in $CDCl_3$.

4.3.9 (PEHA-*b*-PS)^{4}* four-arm star-block copolymers

Polymerization conditions for the synthesis of (PEHA-*b*-PS)^{4*} star-block copolymers with the PEHA block as the core with different compositions and molecular weights are displayed in Table 4.17 and the reaction scheme is illustrated in Figure 4.29.

Table 4.17: Characteristics of the (PEHA-*b*-PS)^{4*} four-arm star-block copolymers.[a]

Run	$[M]_o$ (mol L^{-1})	$[M]_o$:$[I]_o$	Macro Ini.	$M_{n,GPC}$ (MI)	Time (h)	$M_{n,GPC}$ [b]	M_w/M_n [b]	$M_{w,LS}$ [c]	Comp.[d] (PEHA,%)
B86	1.47	220	P64	13690	19.00	85000	3.60	-	-
B87[e]	1.96	527	P64	13690	24.00	19650	1.56	-	-
B88[f]	1.44	536	P65	20100	92.75	25330	1.95	-	-
B89[g]	2.17	300	P66	23440	21.50	174000	2.41	-	34
B90[h]	1.96	500	P66	23440	267.00	49330	1.26	52450	**41**
B91[g]	1.44	750	P67	74210	92.00	270000	1.48	953910	42
B92[i]	1.94	220	-	31000	2.00	74150	1.71	155250	**48**
B93	3.06	300	P65	20100	13.00	34390	1.97	80380	**52**

[a] T: 100 °C, $[PEHA\text{-}X^{4*}]_o$:$[CuBr]_o$:$[Bipyr]_o$ =1:4:4
[b] Calculated from GPC calibrated with linear polystyrene standards
[c] Absolute molecular weights were calculated with multi angle light scattering in THF and the *dn/dc* value of blok copolymer= [X_{PS}*0.185 mL/g (*dn/dc* for PS)+X_{PEHA}*0.058 mL/g (*dn/dc* for PEHA)].
[d] Compositions were calculated by ^{1}H NMR analysis
[e] $[PEHA\text{-}X^{4*}]_o$:$[CuCl]_o$:$[Bipyr]_o$ = 1:4.7:4.7, [f] 1:4.3:4.3, [h] 1:4:4
[g] $[PEHA\text{-}X^{4*}]_o$:$[CuBr]_o$:$[PMDETA]_o$ =1:4:4, [i] 1:6:12, one-pot polymerization

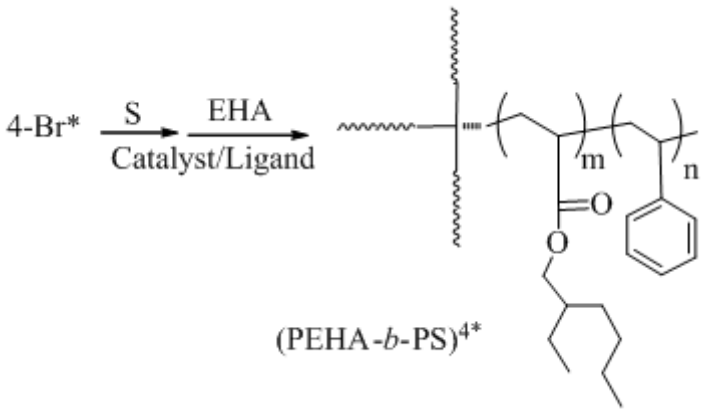

Figure 4.29 : Synthesis of (PEHA-*b*-PS)^{4*} four-arm star-block copolymer.

To obtain (PEHA-*b*-PS)^{4*} star-block copolymer, the EHA and S polymerization was followed by GC, the semi-logarithmic kinetic plot ($\ln([M]_o/[M])$ versus time) of ATRP reaction of EHA is given in Figure 4.30 as representative example. The "livingness" of this polymerization process can be ascertained from a linear first-order kinetic plot.

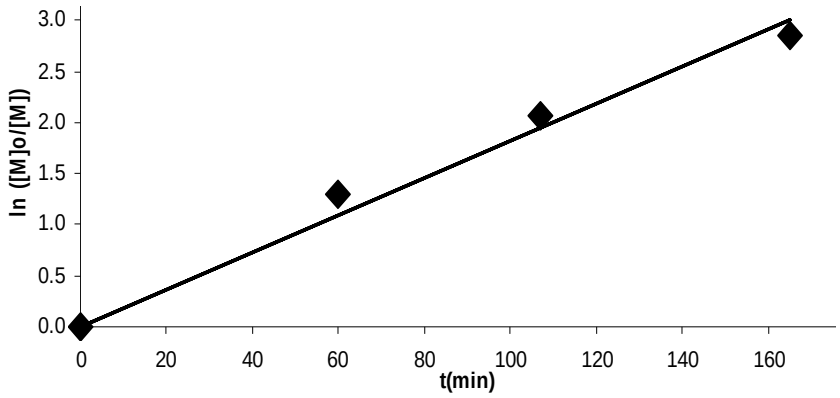

Figure 4.30 : Semi-logarithmic kinetic plot for ATRP of EHA using 4-Br* as an initiator. $[EHA]_o$:[4-Br*]$_o$:$[CuBr]_o$:$[PMDETA]_o$= 220:1:6:12, [EHA] : 1.95 mol L^{-1}, EHA/Toluene: 0.70/1 (v/v).

4.3.10 Penta- and octa-functional star-block copolymers

ATRP has been applied to prepare penta- and octa-functional star-block copolymers as in Figure 4.31 and 4.32. The experimental conditions and results are shown in Table 4.18 for penta-functional and in Table 4.19 for octa-functional star-block copolymers. Alkylated linear amine ligand (HPTETA) was used to make the polymerization faster in controlled manner.

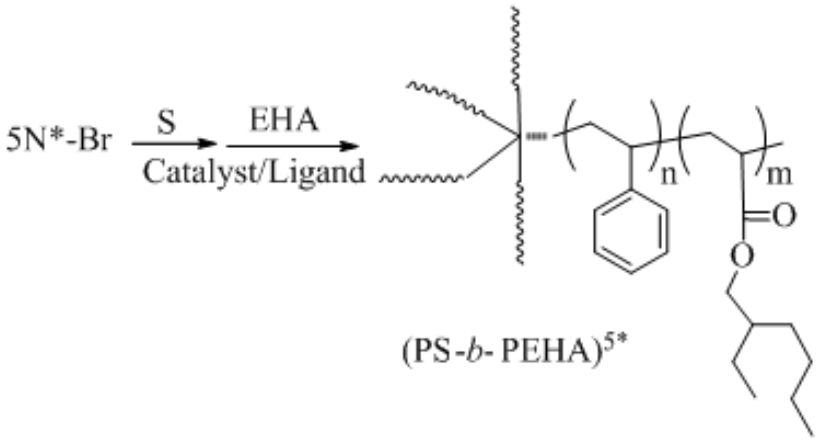

Figure 4.31 : Synthesis of five-arm star-block copolymer.

Table 4.18: Characteristics of the (PS-*b*-PEHA)^{5*} five-arm star-block copolymers. [a]

Run	$[M]_o$ (mol L^{-1})	$[M]_o$:$[I]_o$	Macro Ini.	$M_{n,GPC}$ (MI)	Time (h)	Conv. (%)	$M_{n,GPC}$ [b]	M_w/M_n [b]	$M_{w,LS}$ [c]	Comp.[d] (PEHA,%)
B94	0.17	1000	P70	18000	1.67	8	28970	1.3	-	17
B95	0.45	1000	P77	42700	6.33	25	65550	1.25	-	23
B96	0.51	1000	P69	17510	1.00	11	25680	1.32	-	31
B97[e]	0.44	1193	P75	40160	3.00	19	52320	1.31	-	31
B98	0.42	1200	P77	42700	39.5	-	67250	1.22	-	31
B99	0.55	1055	P72	28000	8.00	-	41550	1.29	-	35
B100	0.45	1000	P76	40630	71.00	-	56000	1.27	-	35
B101	0.73	1000	P71	19490	2.00	14	31310	1.25	-	38
B102	0.75	1193	P73	30490	2.00	28	62000	1.27	-	38
B103	0.79	1200	P71	19490	3.00	24	40820	1.23	-	**40**
B104	0.55	1193	P72	28000	18.5	-	50570	1.26	40580	**48**
B105[e]	0.89	1193	P70	18000	6.00	27	36800	1.28	-	**60**

[a] T: 110 °C, $[PS\text{-}Br^{5*}]_o$:$[CuBr]_o$:$[HPTETA]_o$= 1:10:10
[b] Calculated from GPC calibrated with linear poly(methyl methacrylate) standards
[c] Absolute molecular weights were calculated with multi angle light scattering in THF and the *dn/dc* value of blok copolymer= [X_{PS}*0.185 mL/g (*dn/dc* for PS)+X_{PEHA}*0.058 mL/g (*dn/dc* for PEHA)]
[d] Compositions were calculated by ^{1}H NMR analysis
[e] $[PS\text{-}Br^{5*}]_o$:$[CuBr]_o$:$[HPTETA]_o$= 1:5:5

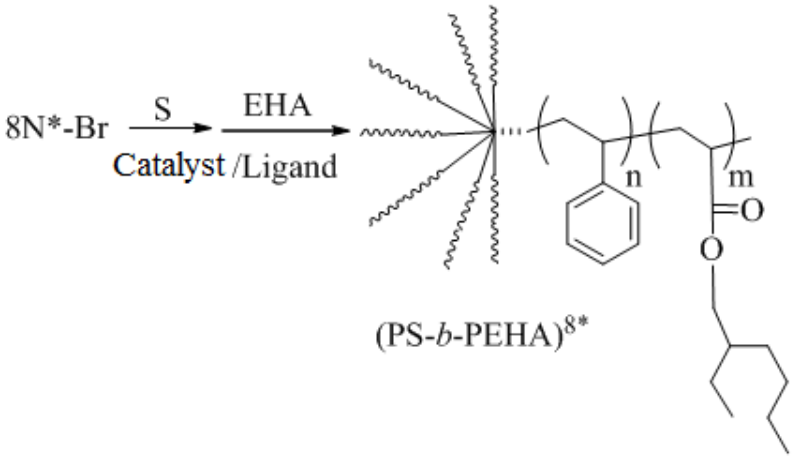

Figure 4.32 : Synthesis of eight-arm star-block copolymer.

Table 4.19: Characteristics of the (PS-*b*-PEHA)^{8*} eight-arm star-block copolymers. [a]

Run	Macro Ini.	$M_{n,GPC}$ (MI)	Time (h)	Conv. (%)	M_n [b]	M_w/M_n [b]	Comp.[c] (PEHA,%)
B106	P86	26310	2	22	41220	1.36	**77**

[a] $[M]_o$= 0.54 mol L^{-1}, $[M]_o$:$[PS^{8*}]_o$:$[CuBr]_o$:$[HPTETA]_o$= 1000:1:10:10, T: 110 ^oC
[b] Calculated from GPC calibrated with linear poly(methyl methacrylate) standards
[c] Compositions were calculated by ^1H NMR analysis

4.3.11 Random copolymers

In brief, to synthesize random block copolymers, the mixture of monomers (S/BA or S/EHA) in different ratios, AIBN and toluene was charged in a 50 mL round bottom flask, degassed with nitrogen, then the mixtures was heated to 100 ^oC. Polymer was recovered as a precipitate from a large excess of methanol and thoroughly dried. The experimental conditions with feed ratios of both monomers and results are depicted in Table 4.20 for PS-*r*-PBA and in Table 4.21 for PS-*r*-PEHA. Copolymer compositions were calculated using ^1H NMR measurements according to the integration of characteristic peaks of corresponding segments.

Table 4.20: Synthesis of PS-*r*-PBA random copolymers.

Polymer	Monomer feed ratio (PBA %)	Time (h)	$[PBA]_o/[I]_o$	I_o (mol)	Solvent/ monomer	Copolymer composition (PBA %)
R1	20	96	125	0.053600	8.00	16
R2	28	119	211	0.053600	5.00	25
R3	34	72	209	0.000330	4.00	28
R4	29	16	250	0.053600	2.50	28
R5	29	10	250	0.026800	2.50	29
R6	37	44	157	0.053600	2.60	35
R7	44	2	237	0.000436	2.60	42
R8	44	47	237	0.000436	0.67	43

Table 4.21: Synthesis of PS-*r*-PEHA random copolymers.

Polymer	Monomer feed ratio (PEHA %)	Time (h)	$[PEHA]_o/[I]_o$	I_o (mol)	Solvent/ monomer	Copolymer composition (PEHA %)
R9	27	72	145	0.000330	4.00	16
R10	20	96	125	0.053600	5.80	16
R11	22	118	147	0.053600	5.00	18
R12	49	11	250	0.026800	2.35	31
R13	33	17	250	0.053600	2.35	32
R14	49	65	176	0.053600	0.83	40
R15	35	2	165	0.000436	2.67	-
R16	42	47	165	0.000436	0.67	40
R17	50	28	200	0.053600	0.73	49
R18	60	24	200	0.053600	0.80	52

4.4 Processing of Baroplastic Materials

As mentioned in the theoretical part, the polymers should exhibit pressure-induced miscibility due to a hard (high T_g) and a soft (low T_g) components which are immiscible at ambient temperature to be considered as baroplastic materials. From this point forward, the obtained block copolymers were processed via compression or extrusion molds to prove baroplastic behaviors. For compression molding, a Shimadzu manual press (Figure 4.33-a) having up to 10 ton at 600 kg cm^{-2} capacity was utilized and a special ordered, heat and pressure controlled Hursan hydraulic press having up to 40 ton at 250 kg cm^{-2} capacity was used (Figure 4.33-b).

As shown in Figure 4.34, block copolymers in the powder forms were introduced into the compression mold (IR pellet mold), which then was closed carefully, placed in the center region of the press and pressed at room temperature (6 ton, 300 kg cm^{-2}).

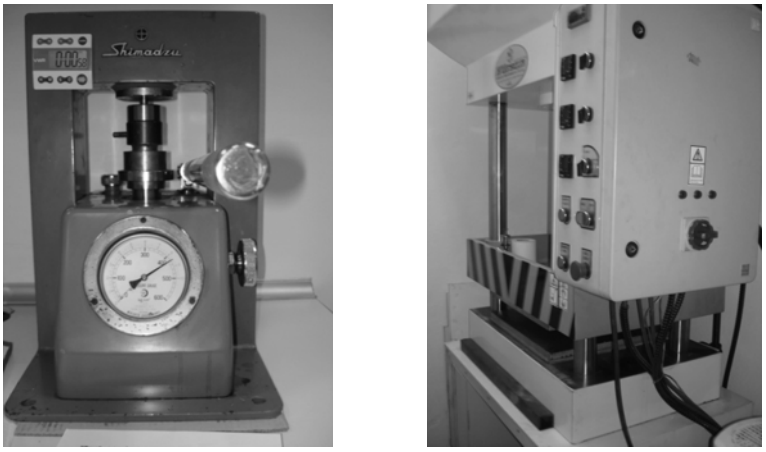

a b

Figure 4.33 : a) Manual press (Shimadzu), b) hydraulic press (Hursan).

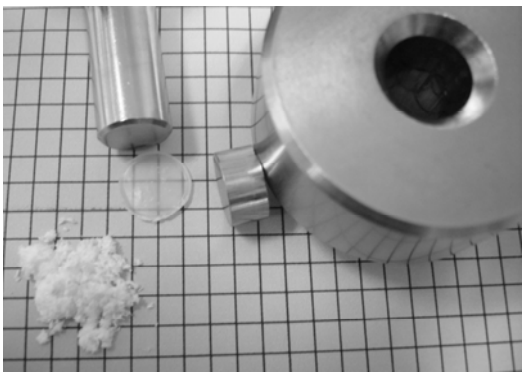

Figure 4.34 : The pictures of transparent processed baroplastic material with the peaces of the mold and unprocessed powder tri-block copolymer (PS-*b*-PEHA-*b*-PS, 48% PEHA, B33).

In the processing of the synthesized polymers, it is observed that the polymeric material, which is initially in the powder form, takes the shape of the mold and becomes transparent after being processed under pressure at room temperature. The reason of that is; when pressure is applied, the low T_g component acts as a sort of solvent for the high T_g component at room temperature. The transparent material obtained at room temperature is the first proof that the polymer shows pressure induced flow property, therefore, it and they can be named as baroplastics.

The block copolymers, which can show the baroplastic properties was indicated as in bold character in each table's composition columns, in the synthesis of the polymer part in the experimental section. The further provements of baroplasticity will be explained in the following sections.

4.4.1 The effect of sample weight on processing

In order to understand the influence of the material quantity on processing block copolymers in the pellet pattern, different amounts of different molecular weighted polystyrene homopolymers (P3 and P11) were taken and processed at 8 ton (400 kg cm^{-2}) for 10 minutes. Although, polystyrene cannot be processed at room temperature, transparent image was obtained below 0.05 g weight of polymers as shown in Figure 4.35. In that case, to ensure the processing of baroplastics, 0.1 g was taken as the minimum amount of polymer.

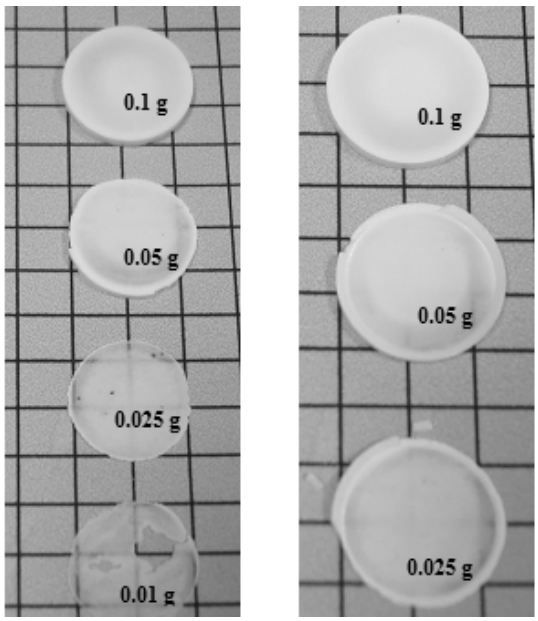

Figure 4.35 : Processed polystyrene (P3: 17K and P11: 48K) in different weights.

4.4.2 Transparency measurement by spectroscopic methods

In order to investigate the pressure effect on the light permeability (transparency) of the polymer, 0.1 g of PS-*b*-PEHA-*b*-PS baroplastic tri-block copolymer (47% PEHA, B32) was placed between two plates and processed under pressure. Disc shaped transparent films were obtained after this process. The IR and UV results of these films are given below. The following UV spectra in Figure 4.36-a and 4.36-b, were taken from two different halfs of the disc films obtained at the end of the process.

The comparison of UV measurement and absorbances in the UV-visible region for the first half of the baroplastic films processed under various pressures is shown in Figure 4.36-a. and the comparison of UV measurement and absorbances in the UV-visible region for the other half of the baroplastic films processed under similar conditions with first half film is shown in Figure 4.36-b. The comparison between the baroplastic materials processed at different pressures can be concluded that any relation between the pressure and light transmittance can not be expressed, even some trend can be observed at 450-520 nm region (Figure 4.36-b), due to unrepeatable results.

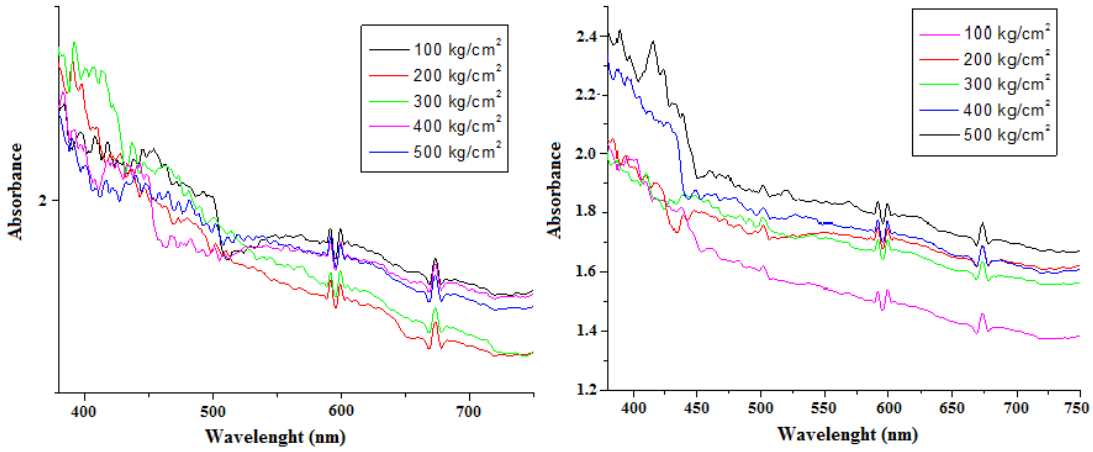

Figure 4.36 : a) The comparison of UV measurement for the first half of the baroplastic films, b) for the other half of the baroplastic films (PS-*b*-PEHA-*b*-PS, 47% PEHA, B32).

Using FT-IR instrument, the light transmittance were compared for the baroplastic materials (PS-*b*-PEHA-*b*-PS, 47% PEHA, B32) processed at different pressures as shown in Table 4.22. According to the results obtained, the light transmittance percentage of the material was increased hence the pressure increasing. But because of the unrepeated results, no relation can be obtained between pressure and light transmittance for FT-IR measurements.

Table 4.22: The FT-IR measurement comparison of light transmittance of baroplastic materials processed at different pressures.

Pressure (kg cm^{-2})	Transmittance %
200	98.10
300	98.15
500	98.50

4.4.3 Transparency measurement by optical method

Haze is the result of scattered light when it passes through a transparent material. Haze gives information about the transparency of the material. Because of the fact that repeatable results can not be taken from FT-IR and UV-Vis instruments, the baroplastic material in powder form was placed between two plates, after the applied pressure, 21 mm diameter circular films were obtained. Haze% and transmittance% values of these films were measured with hazemeter. From the pressure-transmittance% graph in Figure 4.37 and 4.38-a, similar results were obtained by FT-IR measurements.

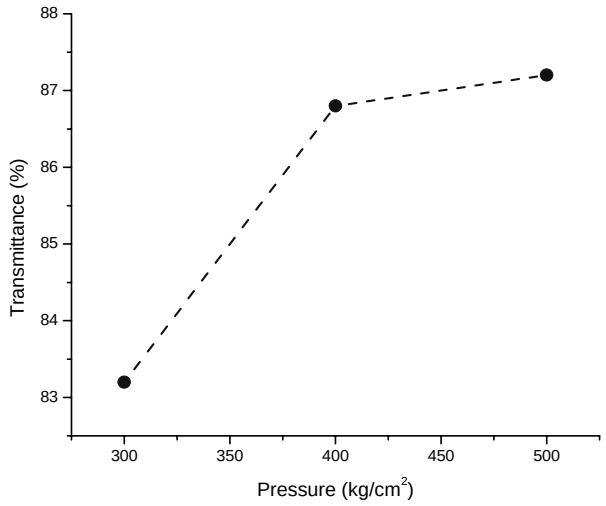

Figure 4.37 : Transmittance (%) changes of baroplastic tri-block copolymer (PS-*b*-PEHA-*b*-PS, 48% PEHA, B33) measured by hazemeter at different pressures.

When the pressure is increased, the transmittance percentage increased. Similarly, from the Haze-pressure% graph in Figure 4.38-b, it is concluded that when the pressure is increased, haze percentage is decreased. However, these changes are not significant, the obtained result, also observed by DSC measurements in the following sections, supports the fact that the process pressure is an ineffective on the transparency of the material.

It can be concluded that the processed transparent materials can be made by applying even very little pressure in the process.

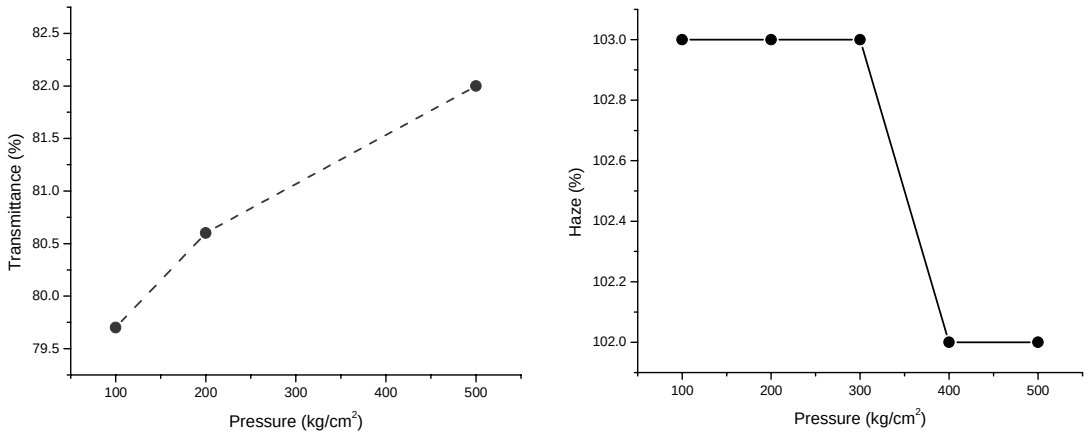

Figure 4.38 : a) Transparency, b) haze changes of baroplastics tri-block copolymer films of PS-*b*-PEHA-*b*-PS (47% PEHA, B32) obtained at different pressures.

4.4.4 Mold design for processing

The processing of baroplastic materials is similar to the processing of industrial plastics but high temperatures are required for shaping commodity plastics whereas baroplastic materials can be shaped at room temperature. The extrusion molds used for baroplastics are in similar design with the molds used for industrial plastics.

To test the possibility of processing of baroplastics by extrusion, a custom-made "extrusion pistons-wire and strip process mold" were fabricated that one side from which the polymer can flow when subjected to pressure from the piston to obtained wire or strip shaped films. By the molds that are used in our study, strips of 8 mm x 1 mm and wires of 1mm diameter can be obtained in order to analyze the dynamic mechanical properties.

During the research, due to the problems encountered, mold design has been improved. The main problem encountered was the separation of piston from the mold due to getting stuck especially after processing (applying pressure). The strip mold used in the early stages of our study is shown in Figure 4.39-a, in order to avoid getting stuck, a spring is inserted to the mold which would push the piston back as seen in Figure 4.39-b.

a b

Figure 4.39 : a) The first design for a strip mold, b) a strip mold with a spring.

But this improvement was not sufficient to solve the problem of the piston getting stuck. Also, in addition to the applied force for the process, extra force was required to overcome the force that the spring generated. These problems lead to another mold design. The most effective solution to ensure the separation of the piston from the mold was designing a new mold which consists of two parts that can be easily separated after the process (Figure 4.40-a).

In this design, it was foreseen that the mold consisting of two body parts will tend separate from each other under the influence of pressure. To avoid this, an outer ring of steel was used to hold the mold parts together tightly (Figure 4.40-b). The same mechanism was applied to the wire process mold as well (Figure 4.41).

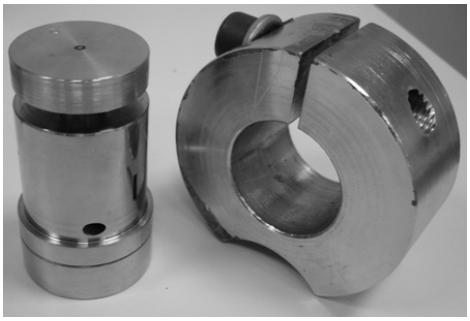

a b

Figure 4.40 : a) A strip process mold with two body parts, b) a strip mold body and the body of the circle clamp.

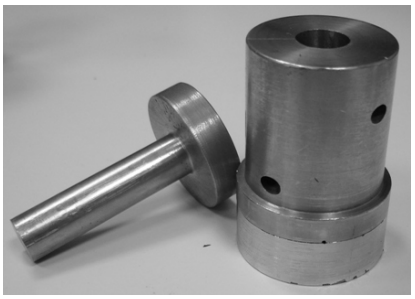

Figure 4.41 : The wire process mold.

Another problem encountered was the unstable flow of the polymer melt at the mold exit. The sharp edges of the mold were rounded to overcome this problem (Figure 4.42).

a b

Figure 4.42 : The revision of the mold, a) before the revision, b) after the revision.

While using the processing molds, the metal contamination problem was occurred on the processed material because of the increased number of processing. To overcome this problem, the inner surface of the mold was covered with chromium nitride coating by physical vapour deposition (PVD) method [114]. The fact that PVD Cr–N has good hardness and toughness and its excellent chemical stability makes it difficult to remove the coating as well as reducing the surface roughness.

Finally, a new mold was designed which can be covered all the above solutions and has the temperature control unit in addition (Figure 4.43). An advantage of this new mold is that, its design is similar to the capillary rheometry instrument. The processed polymer starts flowing from the bottom of the mold. Thus, the tought was to investigate the viscosity behaviours of the baroplastics priorly in the laboratory scale then the industrial machines would be used.

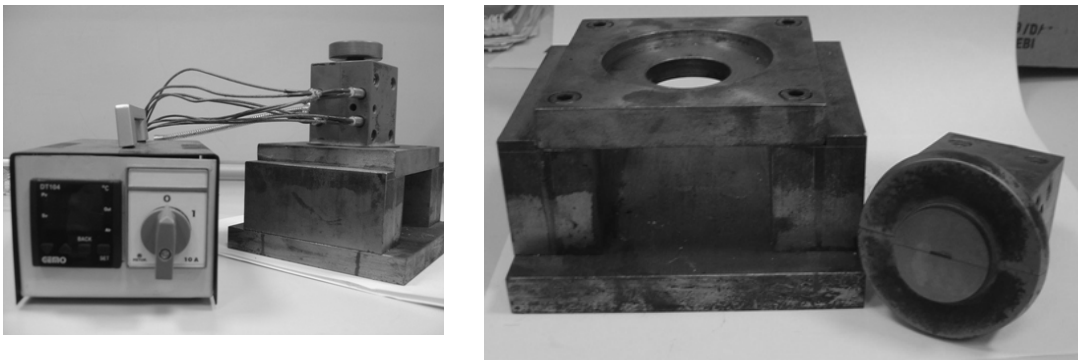

Figure 4.43 : New mold design.

4.4.4.1 Basic extrusion tests

Basic extrusion test was applied on the block copolymers having different inner segment with using the related special designed mold after the transparent films were obtained in the pellet mold. As shown in Figure 4.44 and 4.45, polymers in the powder forms were introduced into the mold which then was closed carefully, placed in the center region of the press and pressed at room temperature. To get strip shaped film, basic extrusion test was applied on PEHA-*b*-PS-*b*-PEHA (53% PEHA, B21) tri-block copolymer having hard inner segment polymer as shown in Figure 4.44. To get wire shaped film, basic extrusion test was also applied on PS-*b*-PEHA-*b*-PS tri-block copolymer having soft inner segment (47% PEHA, B32) (Figure 4.45).

Although the internal or external segments of the block copolymers contain soft segment, in both cases they can be easily extruded from the molds. This situation is advantageous in terms of a wide range of baroplastic block copolymer synthesis.

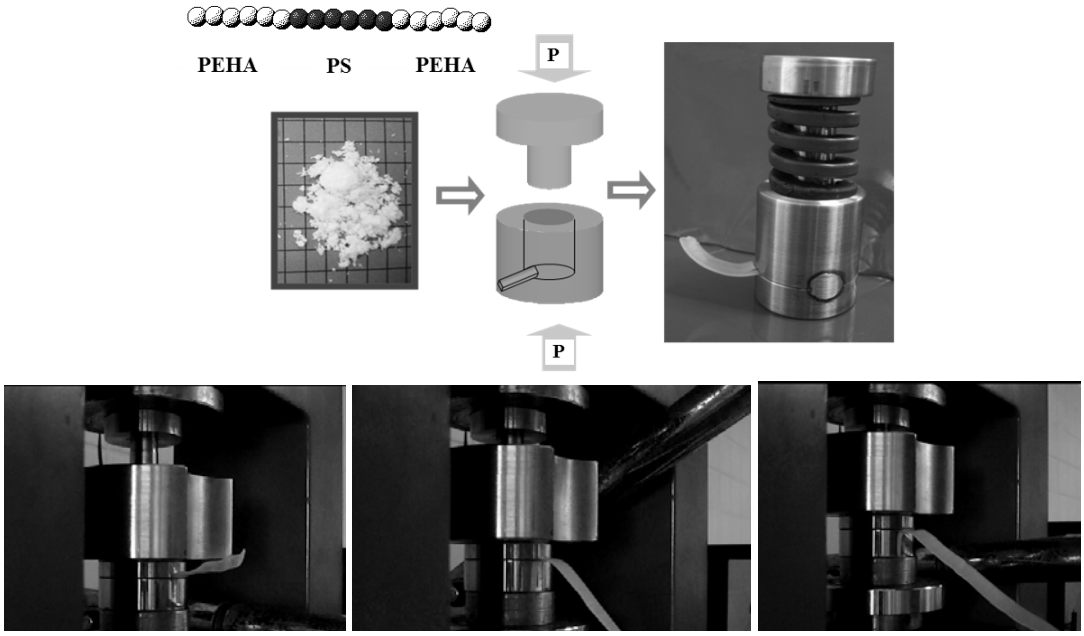

Figure 4.44 : The pictures of strip shaped baroplastic (PEHA-*b*-PS-*b*-PEHA, 53% PEHA, B21) flowing from a strip process mold extrusion piston.

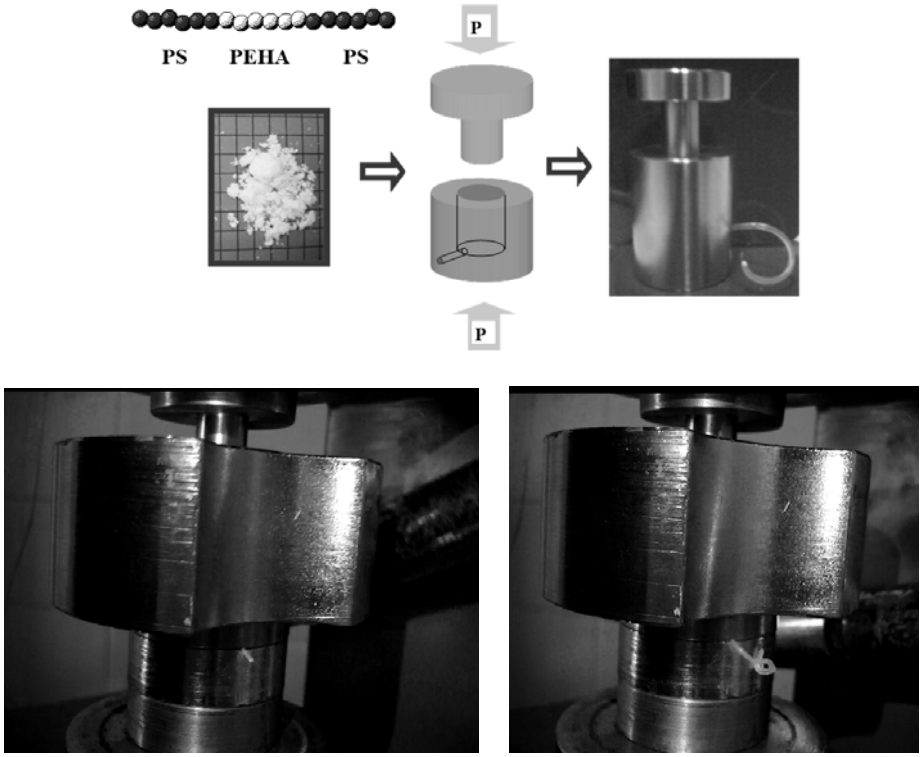

Figure 4.45 : The pictures of squared shaped polymer (PS-*b*-PEHA-*b*-PS, 47% PEHA, B32) flowing from a wire process mold extrusion piston.

4.4.4.2 Application of imprinting technique by compression mold

We have investigated the imprinting performance of baroplastics by investigating the ambient imprinting temperature. Imprinting experiments were performed for PS-*b*-PEHA-*b*-PS (40% PEHA, B27) tri-block copolymer by applying a pressure of 2 ton (100 kg cm^{-2}) for 5 min. As a result, baroplastics can be imprinted at room temperature without having to apply much force. The mold apparatus for imprinting and the embossed material with our university's initials are shown in Figure 4.46.

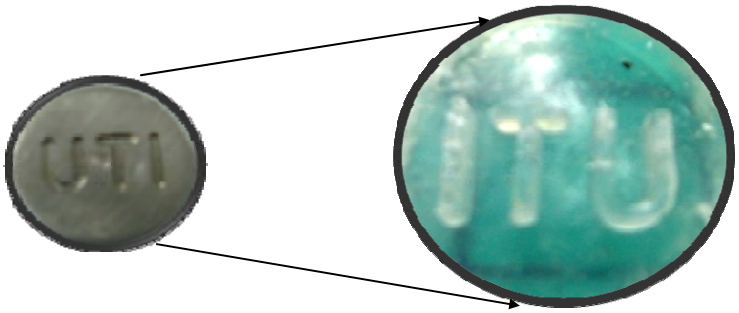

Figure 4.46 : The mold apparatus for imprinting and the processed baroplastic material with **I**stanbul **T**echnical **U**niversity's initials.

4.4.4.3 Coloring of baroplastics and processing by extrusion mold

As one of the scope of applicability of baroplastic materials in industrial areas is to give color to the materials. Industrial dye pigments were added into the polymer solution and then, polymer was precipitated. Obtained powder polymers (PS-*b*-PEHA-*b*-PS, 47% PEHA, B32) of different colors have also been successfully processed (Figure 4.47).

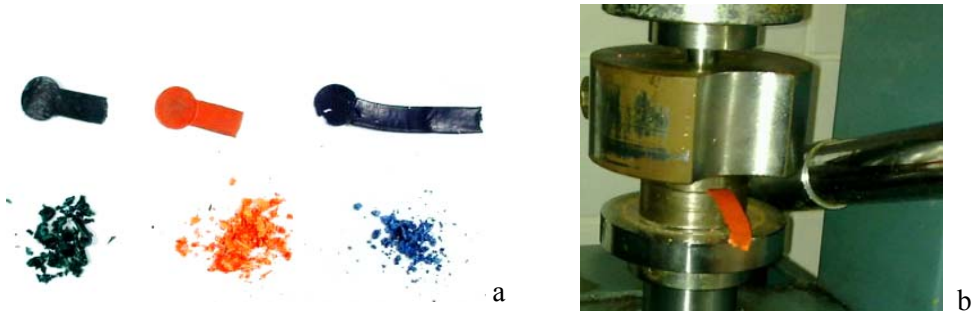

a b

Figure 4.47 : a) Green, orange, blue before processing as powder and after processing as strip shaped, b) orange colored baroplastics flowing from a strip process mold (extrusion piston).

4.4.5 Controlling tests for processing

So far, we have mentioned about the processing of block copolymers. The processing effect on the thermal, morphological, rheological and mechanical properties of baroplastic materials will be described in more detail below. To provide useful control for examining the role of pressure enhanced mixing, blend polymers, random copolymers and PS-*b*-PIP di-block copolymers were processed at room temperature.

4.4.5.1 Processibility of blends

It has been previously reported that PBA and PS exhibit pressure-induced miscibility; when pressure is applied, the two components become more miscible as they were in block copolymer structure [12]. To compare with the PS-*b*-PBA baroplastic di-block copolymers, having low T_g poly(*n*-butylacrylate) (PBA) and high T_g polystyrene (PS) homopolymers were synthesized via ATRP and different weight compositions of them were mixed as given in Table 4.23. To check the processibility of blends at room temperature, they were processed at 6 ton (300 kg cm^{-2}) for 15 min.

Table 4.23: Weight fractions of PS and PBA for blends.

No	PBA (B43-first segment) g (wt%)	PS (P11) g (wt%)
1	0.45 (90%)	0.05 (10%)
2	0.35 (70%)	0.15 (30%)
3	0.25 (50%)	0.25 (50%)
4	0.15 (30%)	0.35 (70%)
5	0.05 (10%)	0.45 (90%)

The images of processed blends having 10-90% PS content are shown in Figure 4.48, respectively. However, it was found just from these results that flow at room temperature is not the case for blend polymer systems, the further investigation will be carried out at higher temperatures. Because in the literature, a study was carried out through a simple emulsion blending and heterocoagulation method, poly ethyl acrylate/PMMA with unmodified montmorillionite nanocomposites were prepared which could be repeatedly processed at 40 ^{o}C [81].

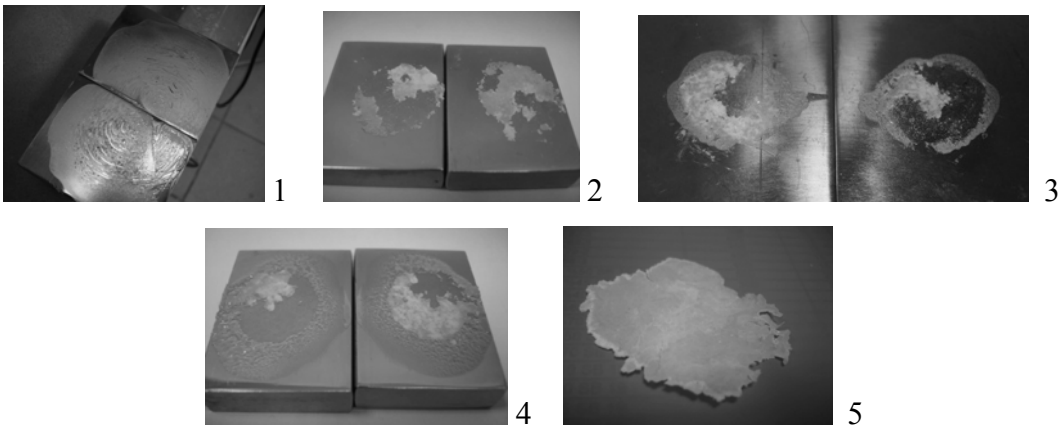

Figure 4.48 : The images of processed blends of PS and PBA having different weight compositions.

4.4.5.2 Processibility of random polymers

Random copolymers, PS-*r*-PBA and PS-*r*-PEHA was tried to be processed. However some of them were very brittle, whereas the others were very soft while processing. Because of that it was not possible to give the images of the processed random polymers. To be certain further research is being carried out on this subject.

4.4.5.3 Processibility of polystyrene-*b*-polyisoprene block copolymers

To control the tendency for some polymers to demix upon the application of pressures, the di-block copolymer having PS (T_g: 100 ^oC) and PIP (T_g: -50 ^oC) segments with different compositions were processed by compression molding. As shown in Figure 4.49, it was found that they were not showing baroplastic behaviors even in the presence of soft segment with high composition (81.6% PIP, B13). Because the PS and PIP segments exhibit attributable to the weak interface and not met with the CRS model as explained in the theoretical part.

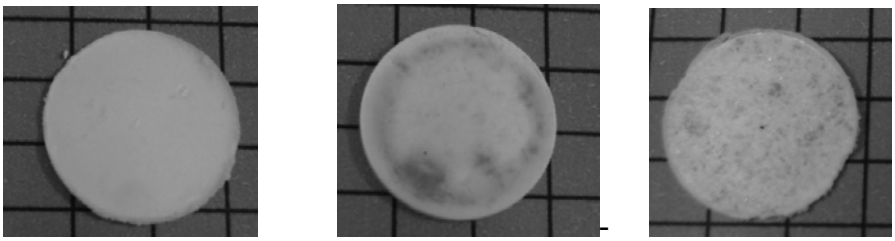

B11 B12 B13

Figure 4.49 : The images of processed PS-*b*-PIP di-block copolymers (~0.1 g).

These findings supported the literature work [12] that any segment cannot be choosen to obtain block copolymer as used as baroplastics. The segments in block copolymers should be suitable with the conditions in CRS model.

4.4.6 Investigation of thermal behaviour by DSC measurements

Block copolymer structures that were introduced as baroplastics, consist of two immiscible phases. After processing at room temperature, a third (mixed) phase, is generated, which is attributed to the interphase of the two components. The main reason of that is the conversion of immiscible phases in unprocessed polymers to partly miscible phases under the influence of pressure. Thus, after processing, both miscible and immiscible phases exist within the same structure. This phenomenon was first introduced to the literature by baroplastic concept i.e. pressure induced flow. In order to understand this transition (mixed phase), some characterizations can be carried out by optical tests, investigation of morphology by AFM or measurement of glass transition temperature (T_g) by DSC and DMA. Optical tests and information about morphology measurements can be found in the following part. In this section, the use of DSC measurement to identify the thermal transiton of the mixed phase were discussed.

In the DSC measurements, the glass transition temperature of each segment of block copolymers was observed for unprocessed baroplastic materials ($T_{g,PS}$ and $T_{g,PEHA}$). The measured T_g values wasn't corresponded exactly to the pure homopolymer values (-75 ^oC for PEHA and 105 ^oC for PS), as expected in immissible block copolymers, this is most probably due to a certain degree of intermixing between the components that shifted the T_g's to intermediate values, a phenomenon commonly observed in block copolymers. In addition to the already existing two T_g's, after processing a new T_g belonging to the two immissible segments appeared among the existing T_g's as expected in ordered structure which is demonstrated in Figure 4.50. As an illustrative example, the endotherm at 44.9 ^oC, indicated in the DSC curve associated with the mixings' transition temperature ($T_{g,mix}$) could belong to the mixture of two segments that corresponds to the disordered phase.

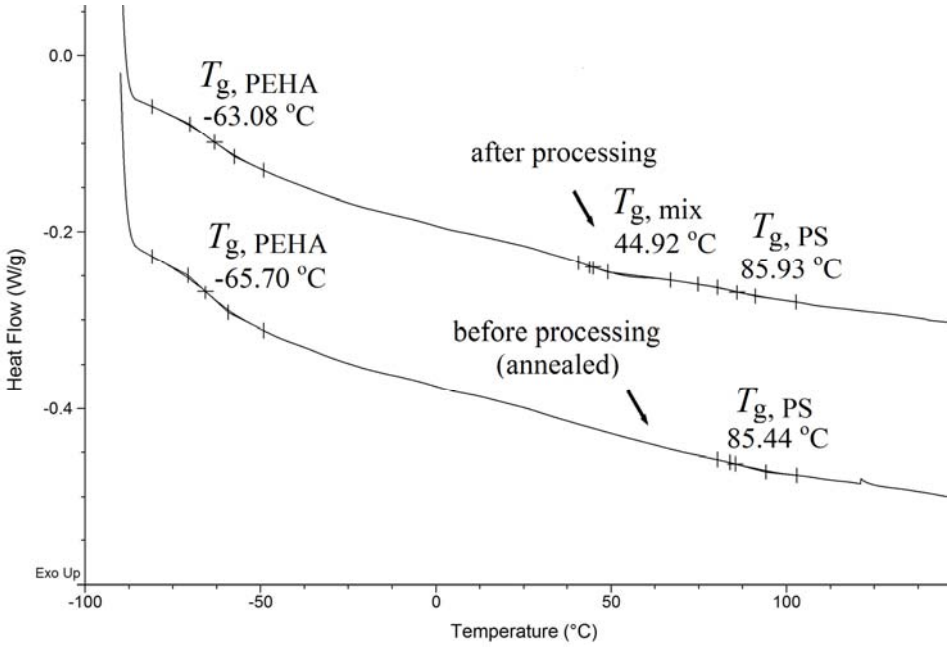

Figure 4.50 : DSC thermograms of PS-*b*-PEHA-*b*-PS baroplastic tri-block copolymer (47% PEHA, B32) before and after processing with pellet mold.

4.4.6.1 The effect of annealing

As we have known from the literature that the regularity and style of alignment of the phase domain were highly influenced by the annealing temperature. In the literature, Crawford et. al observed that DSC experiments on a series of polyurethane block copolymers revealed three prominent thermal transitions. It was concluded that the lower temperature endothermic transitions (60-72 °C) is related to the disruption of soft and hard segment bonds or disruption of short range order within the hard segment length [115-117].

Herein, in the DSC measurements, $T_{g,mix}$ appeared for powder polymer although no pressure was applied (Figure 4.51, the first heating) beside other T_g's corresponding to the two segments. It is assumed that this phase is formed due to the internal tensions arising during the "dissolve-precipitate" method applied to obtain powder form polymer after the synthesis. Another common situation is the disappearance of $T_{g,mix}$ in the same measurements. For sample B32 (47% PEHA, PS-*b*-PEHA-*b*-PS), $T_{g,mix}$ can be observed at the first heating cycle that is from room temperature to 150 °C, but after cooling to -90 °C and re-heating up to 150 °C, no heat flow was observed at the point which $T_{g,mix}$ was previously observed (Figure 4.51, the second heating).

This shows that the first heating caused annealing. The mixed phase is separated to its constituent phases, which means the thermal history is erased.

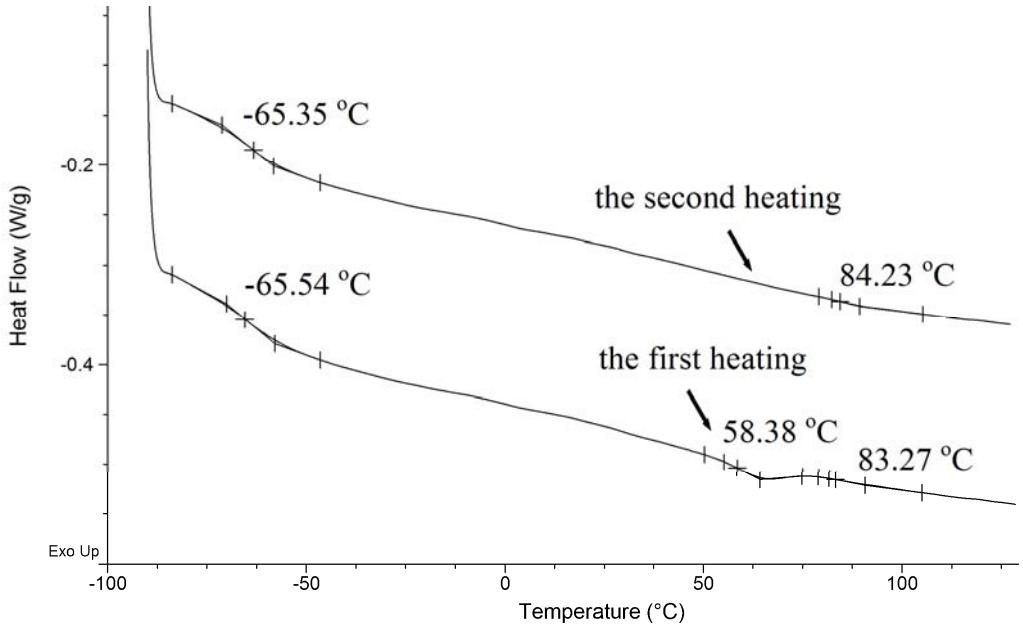

Figure 4.51 : Comparison of DSC thermograms for PS-*b*-PEHA-*b*-PS baroplastic tri- block copolymer (47% PEHA, B32) in the first and second heatings.

From the above findings, it is concluded that the baroplastic materials should be annealed before processing. Thus, the $T_{g,mix}$ observed in the DSC thermogram of the processed material is ensured to be only due to the mixed phase caused by the applied processing pressure. As a result of systematic measurements, the annealing temperature is determined as 120 °C that are used for recycling and other processing studies in the following parts.. This temperature is above the T_g's of both segments. The optimum applied annealing time is found to be 60 minutes.

4.4.6.2 The effect of time and pressure

To optimize the processing conditions on baroplastic polymers with different topologies, pressure and time effects were studied. Same processing procedure was applied to the two type block copolymers at different pressures for 5 minutes and found that 1 ton (50 kg cm^{-2}) pressure is enough for the processing (Figure 4.52-a and 4.53-a).

After optimization was complete for pressure effect, different processing times were applied on the same polymers at 1 ton (50 kg cm^{-2}) pressure (Figure 4.52-b and 4.53-b). After both process treatments, it was found that even application of 1 ton (50 kg cm^{-2}) pressure for 1 min was enough to process baroplastic block copolymers at 25 ^{o}C. The size of processed materials from the pellet mold can be seen in Figure 4.53-c.

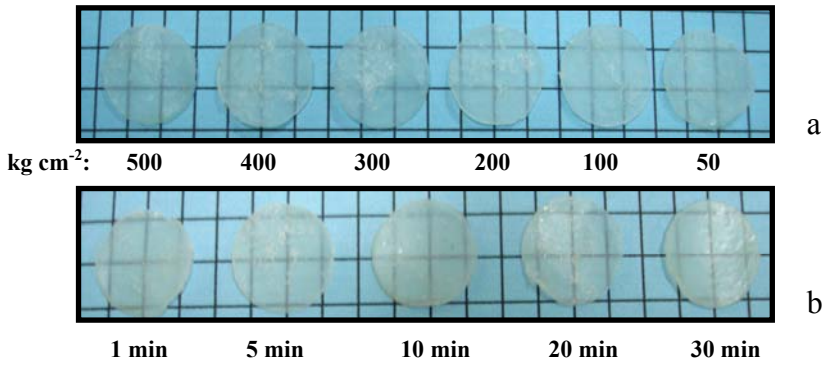

Figure 4.52: The pictures of processed tri-block copolymers (48% PEHA, B33), a) for different pressures at 5 min and 25 ^{o}C, b) for different times at 1 ton (50 kg cm^{-2}) and 25 ^{o}C.

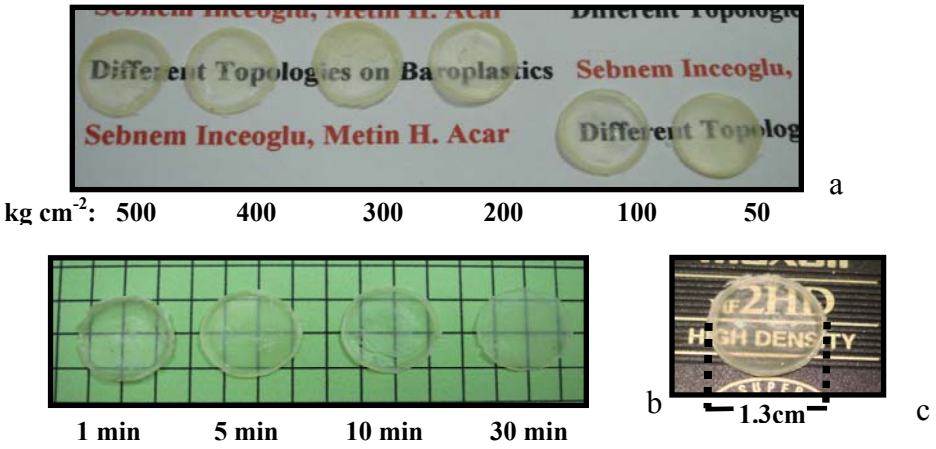

Figure 4.53 : The pictures of processed four-arm star-block copolymer (48% PEHA, B92), a) for different pressures at 5 min and 25 ^{o}C, b) for different times at 2 tons (100 kg cm^{-2}) and 25 ^{o}C, c) the size of processed materials for 5 min at 2 tons (100 kg cm^{-2}) and 25 ^{o}C.

The pressure or time values were increased for processing with pellet mold, DSC measurements were performed with the first cooling cycle to -90 °C and heating up to 150 °C (10 ^{o}C/min). DSC measurements show that no significant changes in the $T_{g,mix}$ values were observed as shown in Table 4.24 and Table 4.25, respectively.

Supporting the above findings, minimum 1 ton pressure for 1 minute is sufficient to obtain polymers of the desired shapes according to the results obtained from the DSC measurements of various kinds of block copolymers. This situation is advantageous for achieving the processing in mild conditions.

Table 4.24: $T_{g,mix}$ values of PEHA-*b*-PS-*b*-PEHA tri-block copolymer (48% PEHA, B33) and four-arm star-block copolymer (PEHA-*b*-PS)^{4*} (48% PEHA, B92) processed at different pressures for 5 minutes at 25 ^{o}C.

Processing condition ton (kg cm^{-2})	$T_{g,mix}$ (^{o}C)	
	B33	B92
1 (50)	69.23	65.48
2 (100)	70.07	64.12
4 (200)	69.86	63.86
6 (300)	69.97	64.55
7 (350)	69.10	64.14
8 (400)	69.17	62.63
10 (500)	70.42	65.59

Table 4.25: $T_{g,mix}$ values of PEHA-*b*-PS-*b*-PEHA tri-block copolymer (48% PEHA, B33) and four-arm star-block copolymer (PEHA-*b*-PS)^{4*} (48% PEHA, B92) processed at 1 ton (50 kg cm^{-2}) and 25 ^{o}C for different times.

Processing time (min)	$T_{g,mix}$ (^{o}C)	
	B33	B92
1	70.36	65.35
5	69.23	65.48
10	69.93	-
20	69.63	65.05
30	70.10	67.08

4.4.6.3 The effect of polymer composition

Baroplastic block copolymers of different compositions were also tested for processability under the same conditions. Block copolymers having a lower PS content (30>PS%), which resulted in a soft and tacky material. Although the material is phase separated (as confirmed by DSC) and it is easily deformed by the application of pressure, it lacks strength and cohesion to form a useful solid object.

It was difficult to remove from the mold due to adhesiveness and poor mechanical properties. Samples with higher PS content were also tested for processability. Block copolymers with PS content higher than 65%, were processed at room temperature and resulted in an opaque object, resembling more a compacted powder object rather than a cohesive and processed specimen. For this composition PS lacks the mobility that the soft component provides. The mobile low T_g phase also seems to be necessary as a "binder" between the rigid domains to hold.

These results suggest that there is a defined window in composition where the low temperature processing of block copolymers is possible. To show pressure-induced mixing is highly dependent on the soft to hard component ratio. It was found that well-defined objects were generally obtained at room temperature when starting from the powdery precipitate in a PEHA composition range from ~35-65 %.

To test the composition effect, PS-*b*-PEHA-*b*-PS tri-block copolymers having different compositions were synthesized. When the extrusion molds are used, the process pressure varies depending on the structure of the polymers that have been identified (Table 4.26). The increasement in the amount of soft phase (PEHA) in baroplastic block copolymers, naturally causes the material to be softer and thus this allows the material to be shaped easier under lower pressure. This situation can be considered that the PEHA transferred from their individual phase to the mixed phase is increased by the increasing the PEHA segment, may result in the decreasing of the mix T_g.

However, in reality, $T_{g,mix}$ is not a feature that causes the structure to be shaped easily, it depends on the ratio of the PEHA and PS in the mixed phase obtained after applied pressure and the material is a feature independent from the ratio of the seperated phases. Therefore, in the DSC measurements with different compositions, no significant changes were achieved in $T_{g,mix}$ values as the same tendency was mentioned in the effect of time and pressure section.

Table 4.26: Processing conditions and thermal behaviours of PS-*b*-PEHA-*b*-PS tri-block copolymers with different compositions.

Polymer	PEHA%	$M_{w,LS}$	$T_{g,mix}$	Process pressure Ton (kg cm^{-2})
B27	40	33.6K	51.32	3.0 (150)
B29	43	48.1K	51.48	6.0 (300)
B31	45	40.8K	62.09	4.0 (200)
B32	47	51.9K	52.67	2.0 (100)
B33	48	38.7K	63.75	2.0 (100)
B34	49	59.6K	63.03	1.5 (75)
B35	50	37.3K	60.08	1.5 (75)

When the PMMA-*b*-PEHA-*b*-PMMA and PMMA-*b*-PBA-*b*-PMMA tri-block copolymers are compared, it is also to be noted that materials of PEHA are easier to process than PBA materials. PEHA has the advantage of having a lower T_g than PBA, which may give rise to this difference. Another reason for the ease of processing and recycling of PEHA containing block copolymer may be that it is predicted to be more miscible with PS or PMMA than PBA. Because of that reason PEHA was mostly used as low T_g segment in the experiments.

4.4.6.4 The effect of molecular weights and topologies

The block copolymers were synthesized with various topologies. The below statements are concluded according to the investigation of the molecular weights and compositions of the block copolymers after processing under pressure.

In (PEHA-*b*-PS)^{4*} star-block copolymers, containing 41% PEHA (B90, M_n = 49.3) segmented polymer while processing, PEHA containing 42% (B91, M_n = 270 K) polymer could not be processed. So, higher than the 200K molecular weighted block copolymers cannot be used as baroplastics.

For PS-b-PEHA di-block copolymers, containing 41% PEHA (M_n = 133K, B4), for PS-*b*-PEHA-*b*-PS tri-block copolymers containing 40% PEHA (M_n = 124.3K, B28) and for (PS-*b*-PEHA)^{4*} star-block copolymers PEHA containing 36% (M_n = 107K, B73) could be processed. It was concluded that to process star-block copolymers the lower soft segment is required than for the linear polymer. This result can be considered as advantages of star block copolymers.

4.4.6.5 The effect of recycling

To manufacture plastic products in industry, the raw material are being processed at high temperatures (e.g. 200 ^{o}C) with high hydraulic pressure. During this process, because of the high-temperature, energy consumption and degradation of recycled polymers can not be ignored. Therefore, quality of product was decreased. Although the use of plastic is increased every day, the recycling of thermoplastics is limited today because of the above reasons. As an alternative to this limitation, baroplastic block copolymers can be recycled multiple times under pressure at room temperature. During processing, very little energy is spent and recycled materials do not undergo degradation.

Herein, in addition to the existing baroplastics, we have shown that baroplastic block copolymers can be recycled for 5 times at 8 ton (400 kg cm^{-2}) for 30 min as shown in Figure 4.54 for star-block copolymer, representatively.

Figure 4.54 : Images of starting polymer, processed and 5 times recycled (PEHA-*b*-PS)^{4*} four-arm star-block copolymer (48% PEHA, B92).

Additionaly, the recycle number was increased for another polymer. The recycling of B32 (PS-*b*-PEHA-*b*-PS, 47% PEHA) was achieved by chopping and extruding at 3 tons (150 kg cm^{-2}) which was repeated for 20 times. In Figure 4.55, five different recycled strip shaped baroplastic tri-block copolymers can be seen respectively. In this case, the strip process mold was used and faced with the metal contamination problem of the processed material from the mold was encountered due to the increase in the number of recycling. To overcome this problem, the inner surface of the mold was covered with more durable materials as mentioned in the mold design section. The fact that the resulting material is still remoldable is a clear indication of the recyclability of the material.

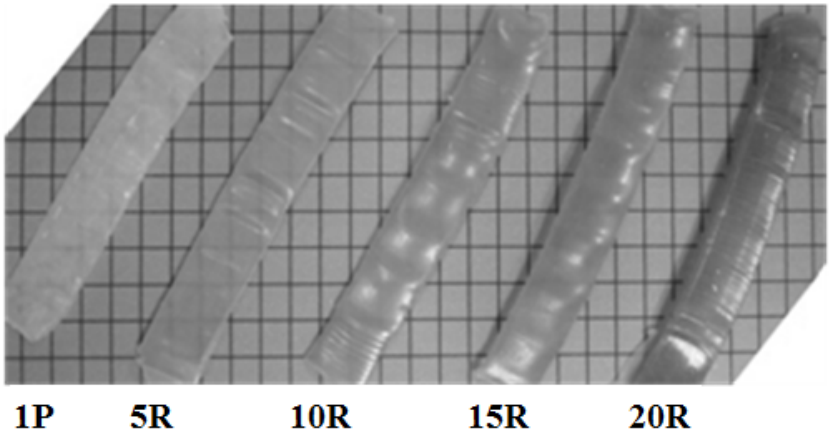

Figure 4.55 : 1, 5, 10, 15 and 20 times recycled strip shaped baroplastic tri-block copolymers (PS-*b*-PEHA-*b*-PS, 47% PEHA, B32).

As known, recyclability is limited for thermoplastic elastomers because of the energy consumption associated with the heating of the TPE to form a melt an, this energy may result as a potential for thermal degradation.

The GPC measurements of the virgin and the recycled baroplastic materials show no significant change in M_n and polydispersity indicating that the processing was carried out without any degradation. Representative chromatogram of the GPC traces can be seen in Figure 4.56 for tri-block copolymer (B32).

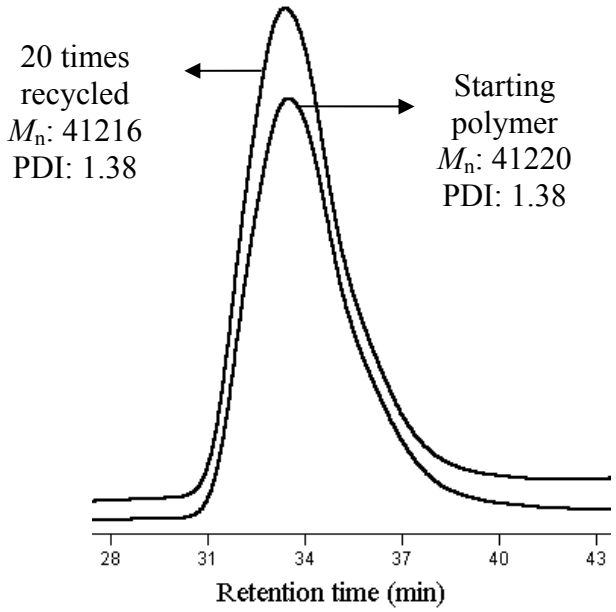

Figure 4.56 : GPC traces of virgin and 20 times recycled PS-*b*-PEHA-*b*-PS tri-block copolymers (47% PEHA, B32).

DSC heat flow of all of the recycled strip-shaped materials show both components' T_g's and a mixed-phase T_g similar to the initial processed material (Figure 4.57). This observation also indicates that the recycled baroplastic materials maintain a mixed morphology (the mixture of ordered and disordered structure) supported by AFM phase images that will be discussed later.

As can be seen in Figure 4.57, the $T_{g,mix}$ value has shifted towards the soft phase's T_g ($T_{g,PEHA}$) with increasing number of processes. With the approach developed from this behaviour, it is concluded that the PEHA transferred from their individual phase to the mixed phase is increased by the influence of applied pressure during processing. This situation has been evaluated using the following Fox-equation (4.1).

$$\frac{1}{T_{g,mix}} = \frac{x_{PS}}{T_{g,PS}} + \frac{x_{PEHA}}{T_{g,PEHA}} \qquad \textbf{(4.1)}$$

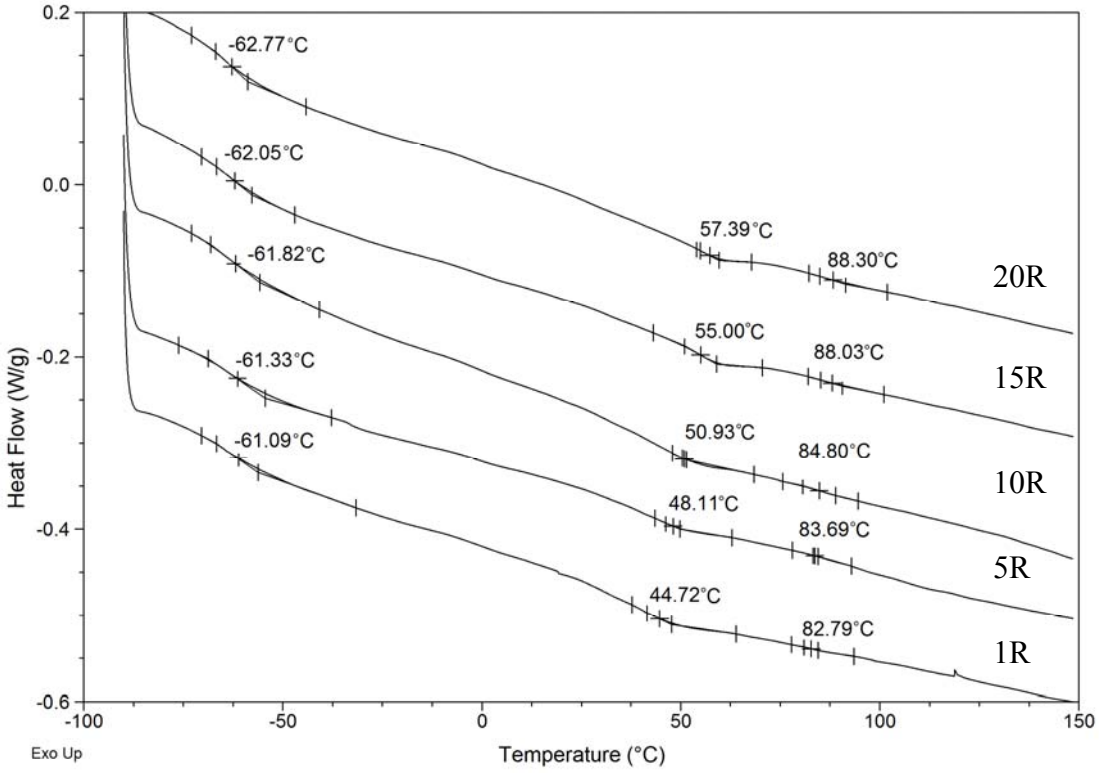

Figure 4.57 : DSC thermograms of 1 to 20 times recycled PS-*b*-PEHA-*b*-PS tri-block copolymers (47% PEHA, B32).

The percent ratios of PS and PEHA in the mixed phase can be calculated when the $T_{g,mix}$ values (obtained from the DSC analysis) are substituted into the Fox equation.

Additionally, it can be predicted that in an "n" times processed polymer, the entire individual phases will be transformed to the mixed phase. In this case, the $T_{g,mix}$ values of "n" times processed block copolymers can be calculated by substituting the weight fraction of PS as 0.53 and PEHA as 0.47 in the block copolymer composition (Table 4.27). Using this thought, maximum recyling number can be calculated as 118 from both of the equations obtained from the plot of the processing number versus either $1/T_{g,mix}$ or PS wt% values in mixed phase, respectively (Figure 4.58).

This result is based only on the number of processing for the same materials without annealing in each processing time. Beside of this concern, annealed materials at any stage/usage cycle can be shown almost the same behavior as the virgin materials. Therefore, the recycling possibility under pressure can be extended to the infinite by annealing.

Table 4.27: The variation of $T_{g,mix}$ and PS content in the mixed phase with the number of processing for PS-*b*-PEHA-*b*-PS baroplastic tri-block copolymer (47% PEHA, B32).

Recycling number	**$T_{g,mix}$ (^{o}C)**	**PS (wt%)**
1	57.39	84.15
5	55.00	83.23
10	50.93	81.64
15	48.11	80.51
20	44.72	79.13
n	-8.16	53.00

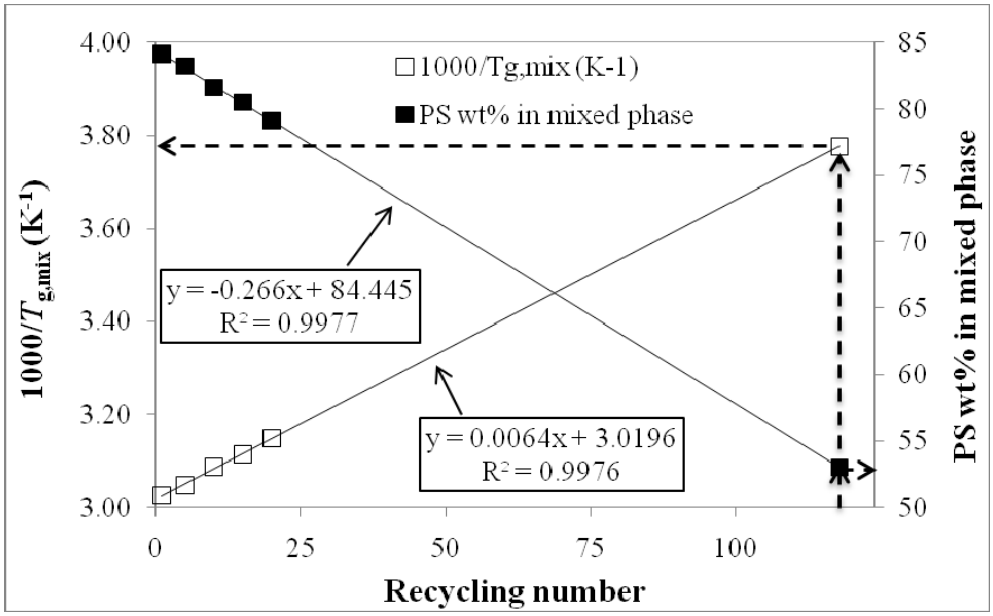

Figure 4.58 : Processing times versus $T_{g,mix}$ values and PS wt% content in mixed phase for PS-*b*-PEHA-*b*-PS, baroplastics tri-block copolymer (47% PEHA, B32).

4.4.7 Investigation of morphology by AFM measurements

To probe the influences of processing at room temperature on morphology, atomic force microscopy (AFM) characterization was performed in the tapping mode. In the literature, just for core-shell nanoparticles, the points where two adjacent core-shell particles break and combine was seen after processing operations, consistent with the proposed flow mechanism [13].

Herein, for AFM measurements, the block copolymer films were prepared by solution casting using dichloromethane on mica surface at room temperature. The solution concentration of block copolymers was adjusted around ~ 5% (w/v). The types of films were used in the measurements are; solvent cast, annealed and pressure applied. In all cases, to eliminate the thermal history and thus to reach the thermodynamic equilibrium, the block copolymer films were annealed overnight at 120 °C after solvent casting which is well above the glass transition temperatures of each polymer segment. The morphology of the solution casted (unannealed) films and only the phase images of annealed and pressure applied films were investigated by Tapping Mode AFM.

Since the AFM phase images of the annealed films showed more organized lamellar structure than the solution casted films, only annealed and pressured films phase images were compared. The images were analyzed further to identify the soft and hard segments. In literature, it was stated that for low- and high-density parts of a micro layered polyethylene sample and for a polydiethylsiloxane sample on Si, the phase angle shift is larger for hard segment and smaller for soft segment at moderate tapping regimes (r_{sp}=0.4-0.7) (27). Although the tapping was performed at lighter regimes (r_{sp}=0.8-0.9), according to the above statement in literature, it is most probable that in our case, phase angle shift at around 1 to 2° for bright parts and -3 to -4° for dark parts which were measured along the two lines (upper left part in Figure 4.59) corresponds to lamellae of soft (PEHA) and hard (PS) segments, respectively. As shown in Figure 4.59, AFM phase images belongs to 500 and 250 nm were taken for baroplastic tri-block copolymer film prepared on mica.

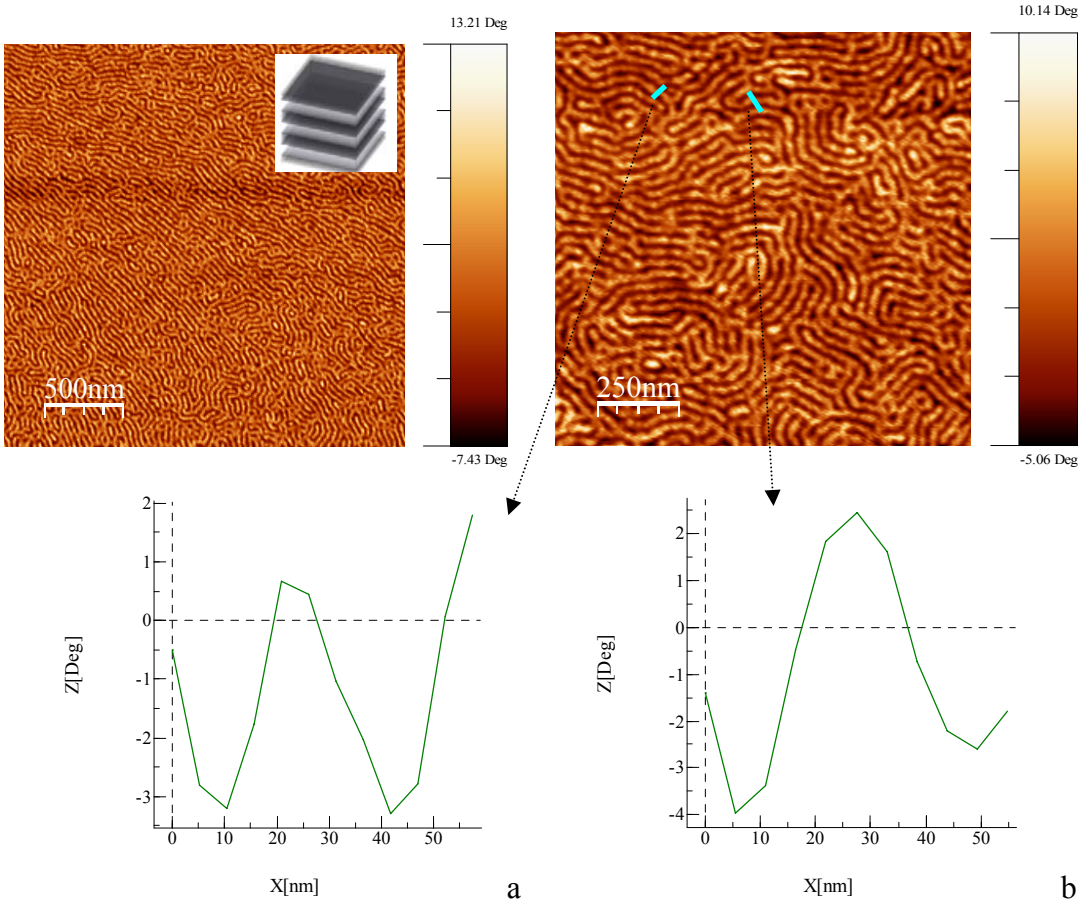

Figure 4.59 : AFM phase images of annealed films of PEHA-*b*-PS-*b*-PEHA tri-block copolymer (52% PEHA, B20) and phase profile along a) the left, b) the right line in AFM phase image (250 nm).

Before applying pressure, annealed film displays a strong orientation of the lamellar structure for tri-block copolymer (PEHA-*b*-PS-*b*-PEHA, 52% PEHA, B20) (Figure 4.60-a). By applying pressure, this periodical distribution changes into a mixed morphology that represent the mixture of both ordered (phase-separated) and disordered (non-phase separated, mixed phase) structures (Figure 4.60-b). The formation of mixed morphology (diminishing of phase separation), supported by both AFM and DSC results, may suggest a rheological flow, which could be responsible for the baroplastic behavior. To investigate the processing effect on morphology, different block copolymers of various molecular weight and topologies were chosen. The comparison was performed with the baroplastic block copolymers before (annealed) (Figure 4.60-a to Figure 4.65-a) and after applying pressure at 6 tons (300 kg cm^{-2}) for 5 min (processed) (Figure 4.60-b to Figure 4.65-b). Different kind of polymers was chosen for AFM studies to show the pressure-induced miscibility in each sample. In ordered state they have shown different morphologies (lamellae, gyroid, cylindrical, etc.) depends on their topologies and compositions. After processing, the AFM phase images clearly demonstrate the reduced microphase separation (transition from ordered to disordered structure).

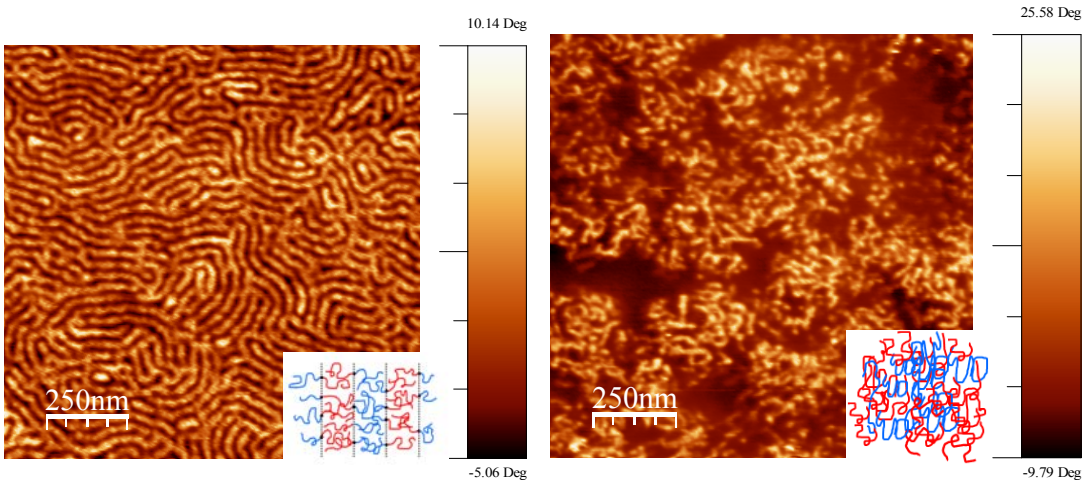

a b

Figure 4.60 : AFM phase images of PEHA-*b*-PS-*b*-PEHA tri-block copolymer (52% PEHA, B20) films, a) before and, b) after processing at 6 tons (300 kg cm^{-2}) for 5 min.

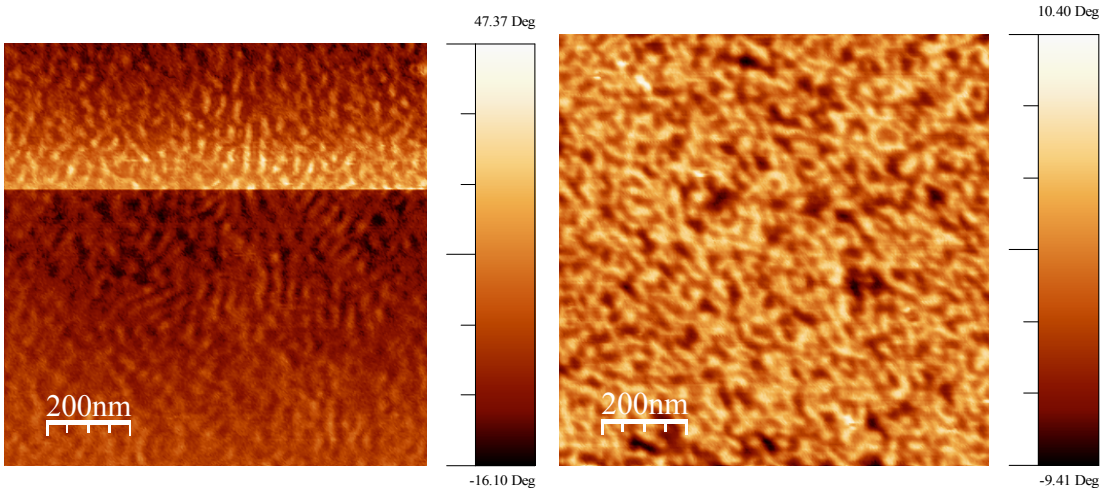

a b

Figure 4.61 : AFM phase images of PEHA-*b*-PS-*b*-PEHA tri-block copolymer (50% PEHA, B17) films, a) before and, b) after processing at 6 tons (300 kg cm^{-2}) for 5 min.

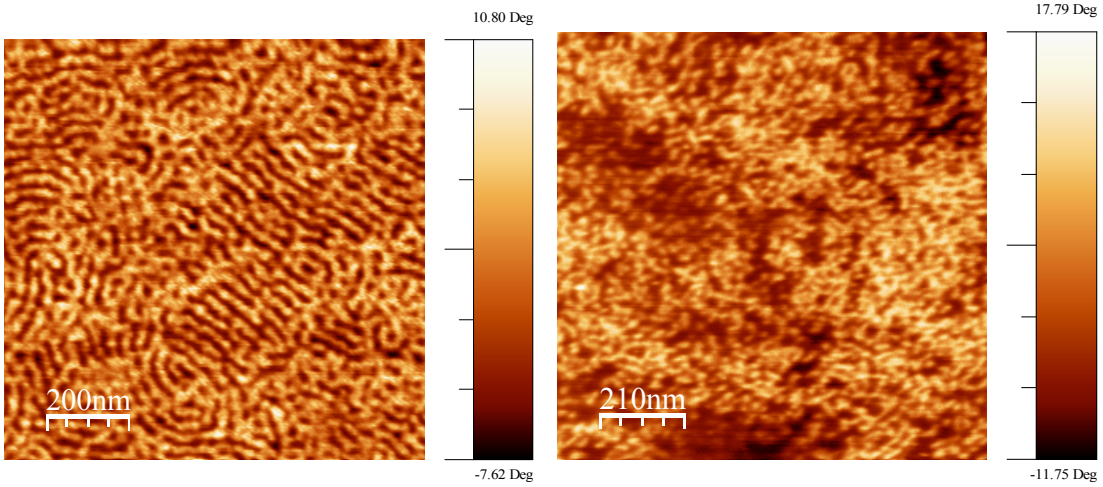

a b

Figure 4.62 : AFM phase images of PS-*b*-PEHA-*b*-PS tri-block copolymer (47% PEHA, B32) films, a) before and, b) after processing at 6 tons (300 kg cm^{-2}) for 5 min.

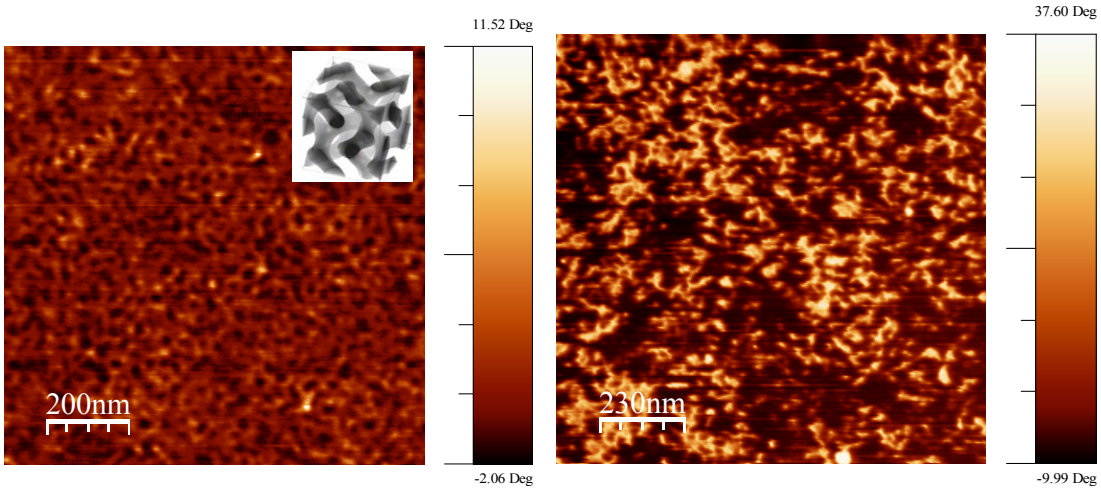

a b

Figure 4.63 : AFM phase images of (PS-*b*-PEHA)^{4*} 4-arm star-block copolymer (48% PEHA, B78) films, a) before and, b) after processing at 6 tons (300 kg cm^{-2}) for 5 min.

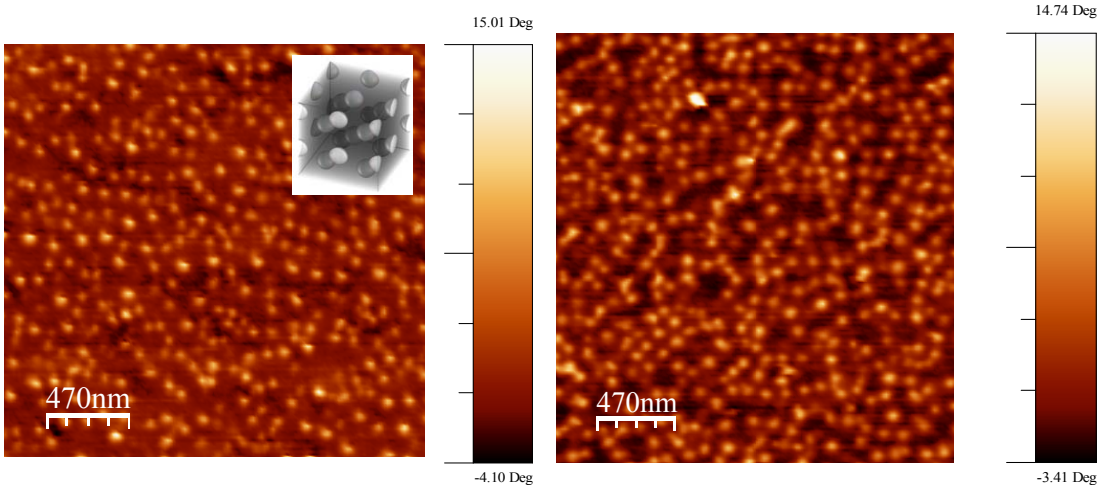

a b

Figure 4.64 : AFM phase images of (PS-*b*-PEHA)^{4*} 4-arm star-block copolymer (36% PEHA, B73) films, a) before and, b) after processing at 6 tons (300 kg cm^{-2}) for 5 min.

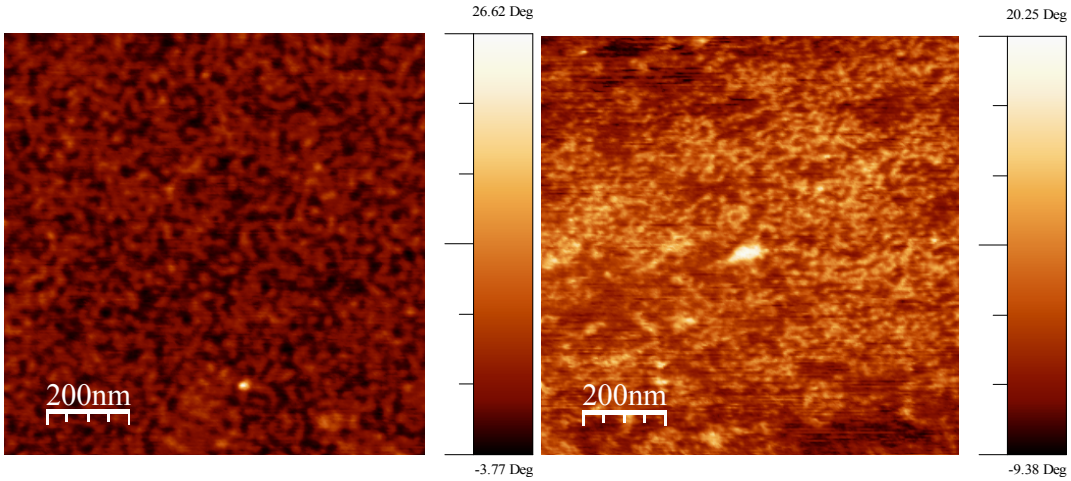

a b

Figure 4.65 : AFM phase images of (PEHA-*b*-PS)^{4*} 4-arm star-block copolymer (52% PEHA, B93) films, a) before and, b) after processing at 6 tons (300 kg cm^{-2}) for 5 min.

From AFM and DSC experiments two important features became clear about the processing mechanism. Firstly, that mixing is actually occurring during the processing by the application of pressure, at least at the interphase level. Secondly that the mixing is not complete during pressurization, and distinct domains are always present even after several processing cycles. The obtained results suggest that the molecular mechanism underlying this phenomenon involve pressure-induced partial intermixing of dissimilar phase domains, where the low T_g acrylate domains serve as a mobile layer to the rigid PS domains, allowing flow and molding into a new shape.

4.4.8 Investigation of rheological behaviour

The main objective of this study is the processing of polymers at room temperature, thus the flow behavior of polymers were investigated at ambient temperatures using capillary rheometer instrument that is already being used in industry. In literature all reology studies were carried out for high temperature processing of polymers. As there are no publications related with rheometer measurements at room temperature, the initial measurements were made at 43 ^{o}C considering the resistance of the instrument. As a result of measurements at 43 ^{o}C, capillary rheometer instrument was used at room temperature as first impression. Baroplastic materials exhibits an unusual deformation and flow behavior due to their viscoelastic behaviour. The deformation of a polymer is due to stresses imposed to it.

The capillary die used was 2 mm in diameter and 0 mm in length and an entrance angle of 180°, which was fitted into the left-hand barrel. During extrusion processes with capillary rheometer at 43 °C, PS-*b*-PEHA-*b*-PS (43% PEHA, B29 and 49% PEHA, B34) baroplastic tri-block copolymers were exposed to shear stresses that is increasing with increasing shear rates as shown in Figure 4.66 and 4.67. In addition, viscosity is reduced with increasing shear rate that causes the material to be extruded from the mold more quicker. The meaning of the curves of each process (i.e., recycling) are identical, materials can be recycled multiple times without degradation.

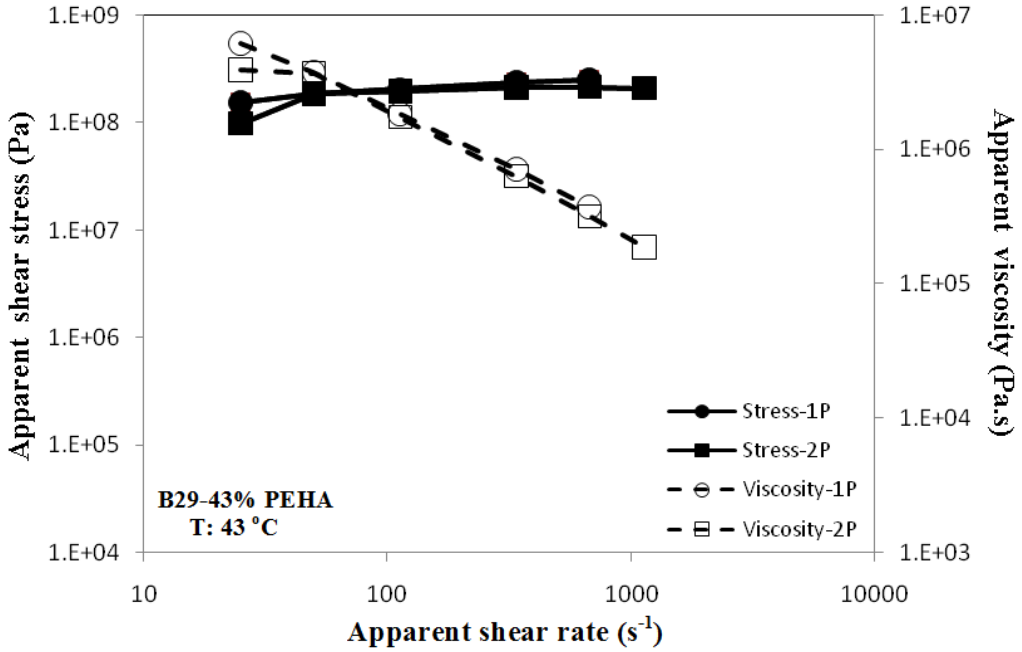

Figure 4.66 : The chart of appearent shear rate versus appearent viscosity and appearent shear stress for PS-*b*-PEHA-*b*-PS (43% PEHA, B29) baroplastic tri-block copolymer (T: 43 °C, die l/d: 0/2 mm).

In order to examine the effect of the flow behavior on recycling of baroplastic block copolymers, materials taken from capillary rheometer's die (l/d: 0:2 mm) were chopped into granules and measured again.

In Figure 4.68, 1, 2,3 and 4 times of recycled wire shaped baroplastic tri-block copolymers can be seen respectively. A more uniform extrudate is obtained with increasing processing steps beginning from the powder, consistent with the higher degree of mixing shown by DSC and AFM with increased processing time.

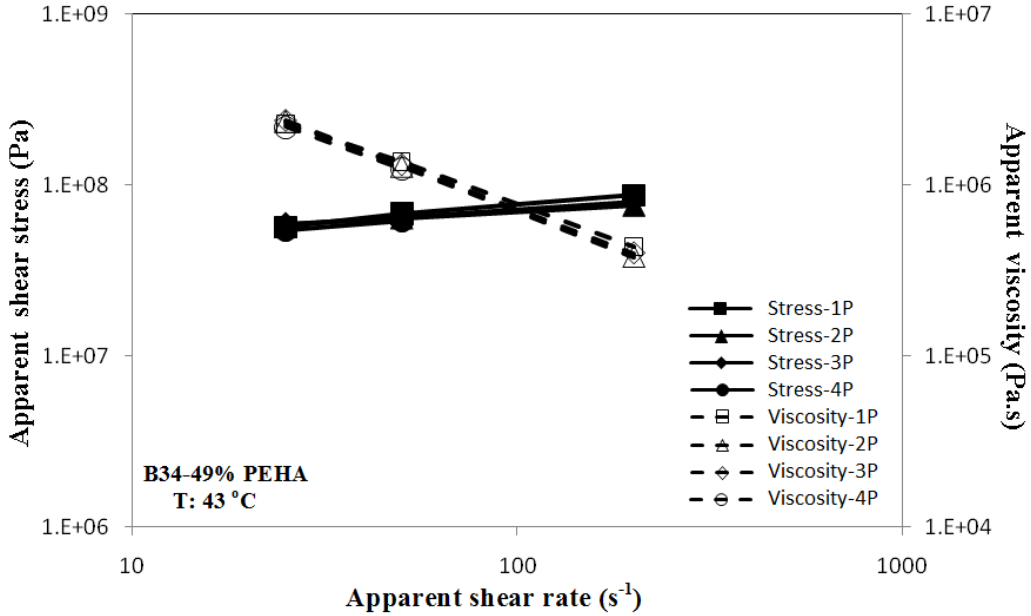

Figure 4.67 : The chart of appearent shear rate versus appearent viscosity and appearent shear stress for PS-*b*-PEHA-*b*-PS (49% PEHA, B34) baroplastic tri-block copolymer (T: 43 °C, die l/d: 0/2 mm).

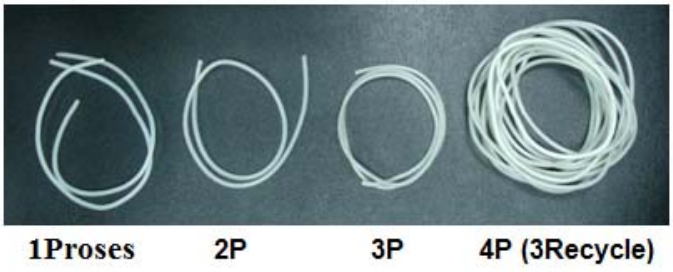

Figure 4.68 : Baroplastic tri-block copolymer PS-*b*-PEHA-*b*-PS (49% PEHA, B34): from process to recycle at capillary rheometry instrument (T:43 °C, P: 65 bar, die l/d: 0/2 mm).

AFM phase images belonging to PS-*b*-PEHA-*b*-PS baroplastic tri-block copolymer (49% PEHA, B34) after 1 and 4 times processing from capillary rheometry instrument is shown in Figure 4.69.

Before applying the pressure, PS-*b*-PEHA-*b*-PS baroplastic tri-block copolymer displayed a strong orientation of the lamellar structure (go to Figure 4.59). In the first processing, the periodical distribution was changing by application of pressure and ended up in a mixed morphology that represent the mixture of both ordered (phase-separated) and disordered (non-phase separated) structures (Figure 4.69-a). It can be seen from AFM phase images of 4 times processed material, the diminished microphase separation (increasing of disordered structure) is clearly demonstrated by increasing process (recycle) time by capillary rheometry instrument (Figure 4.69-b).

As can be seen in Figure 4.70, DSC heat flows of from 1 to 4 times processed (recycled) wire-shaped material show both components' T_g's and a mixed-phase T_g similar to the initial processed material. The formation of mixed morphology (the mixture of ordered and disordered structure and reduction of the phase separation), supported by both AFM and DSC results, may suggest a rheological flow, which could be responsible for the baroplastic behavior. These results corroborate the results which were explained in the effect of recycling part.

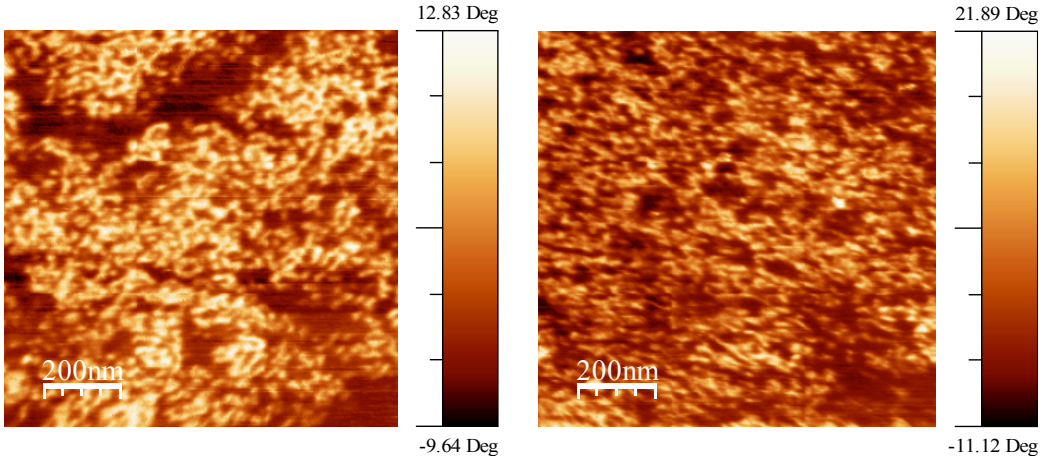

Figure 4.69 : AFM phase images of PS-*b*-PEHA-*b*-PS tri-block copolymer (49% PEHA, B34) after, a) 1 processing and, b) 4 times processing at 43 °C from capillary rheometry instrument (die l/d: 0/2 mm).

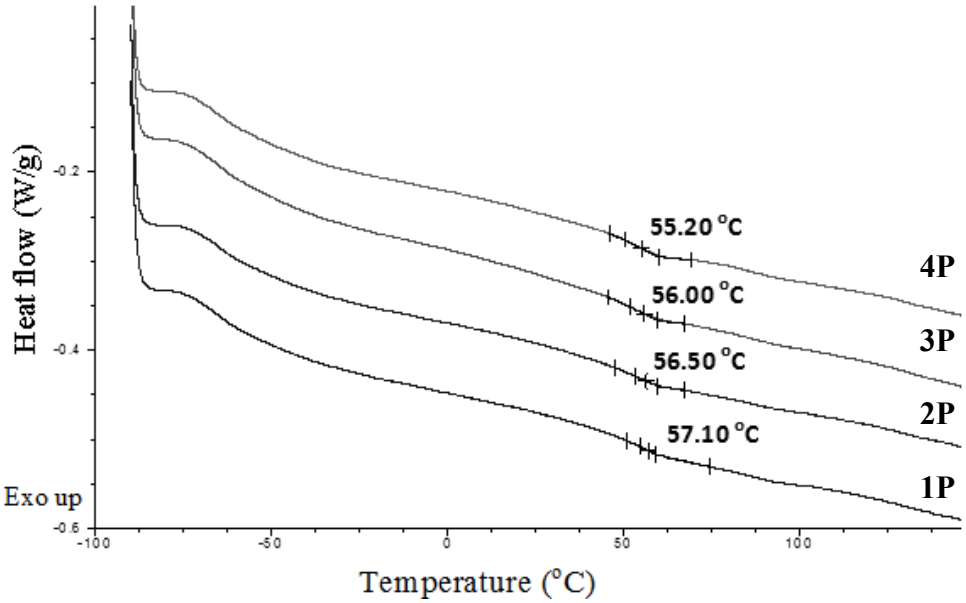

Figure 4.70 : DSC thermograms of 1 to 4 times processed tri-block copolymer (PS-*b*-PEHA-*b*-PS, 49% PEHA, B34) in capillary rheometry.

To evaluate the effect of composition on processing, capillary rheometer measurements were applied on block copolymers having the same structure with different compositions. Comparing the apparent viscosity of baroplastic block copolymers with two different compositions, the higher ratio belongs to the sample having more PS blocks (Figure 4.71). This result could be expected because the increasing PEHA segment provides mobility to the material that causes to use less pressure values to process the material as shown in the Table 4.29.

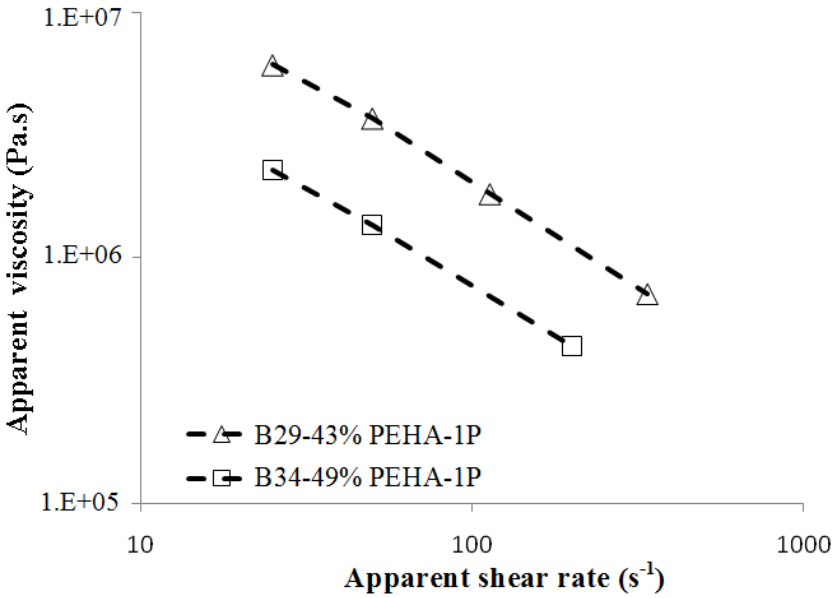

Figure 4.71 : The chart of appearent shear rate versus appearent viscosity for baroplastic tri-block copolymers with different compositions (B29 and B34) (T: 43 ^{o}C, die l/d: 0/2 mm).

The main goal of this thesis, is to examine the process conditions at room temperature. Capillary rheometer measurements were performed on PS-*b*-PEHA-*b*-PS block tri-block copolymer (43% PEHA, B29) at 28 ^{o}C. The same trend was obtained at 43 ^{o}C by reological measurements. As illustrated in Figure 4.72, baroplastic tri-block copolymers were exposed to shear stress that is almost constant with increasing shear rates. Moreover, viscosity is decreasing with increasing shear rate that causes the material to be extruded from the mold fluently.

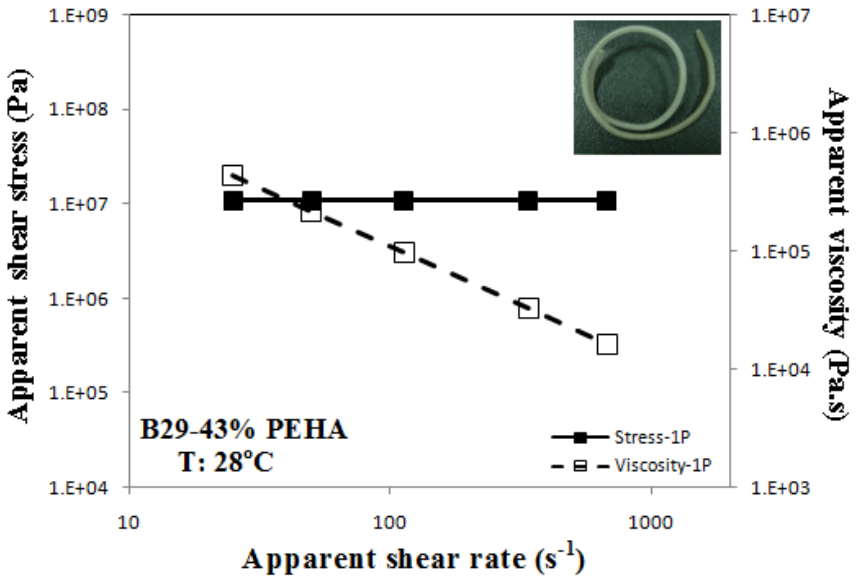

Figure 4.72 : The chart of appearent shear rate versus appearent shear stress and appearent viscosity for PS-*b*-PEHA-*b*-PS baroplastic tri-block copolymer (43% PEHA, B29) (T: 28 ^{o}C, die l/d: 0/2 mm).

To investigate the composition effect on processing, room temperature capillary rheometer measurements was also applied to PS-*b*-PEHA-*b*-PS baroplastic tri-block copolymer (50% PEHA, B35). Again the same tendency to decrease the appearent viscosity with increasing appearent shear rate was observed (Figure 4.73). In addition, no degradation was observed by process cycle. Using the wire shaped-films obtained in each process, ITU initials was written schematically (Figure 4.74). As depicted in Table 4.28, increasing number of recycling processes results in a decrease on the T_g of the mixed phase (but not significant) and the process pressure whereas it results as an increase on the strength of the material. The same trend was observed in the effect of processing part. Elastic modulus values of PS-*b*-PEHA-*b*-PS (50% PEHA, B35) was obtained by Zwick instrument.

The data given in Table 4.29 belong to the 25 s^{-1} shear rate when flow was first observed in 2 mm die. When the values that were achieved from the capillary rheomety measurements for PS-*b*-PEHA-*b*-PS baroplastic tri-block copolymers with different PEHA compositions were compared, the pressure is observed to decrease with increasing PEHA% in the block copolymers. Besides, for the case of almost similar PEHA contents (B34 and B35), pressure is increasing with decreasing of processing temperature (Table 4.29).

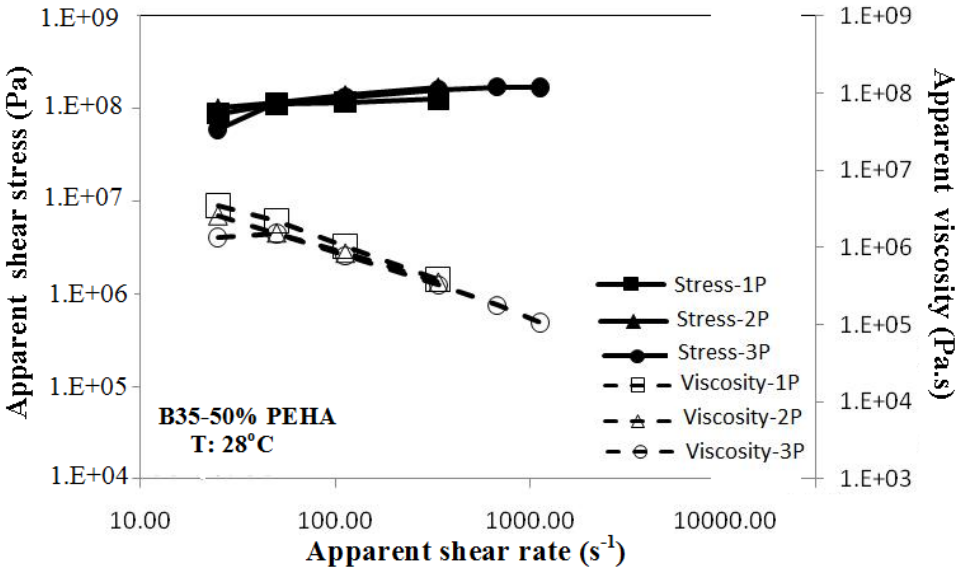

Figure 4.73 : The chart of appearent shear rate versus appearent shear stress and appearent viscosity for PS-*b*-PEHA-*b*-PS baroplastic tri-block copolymer (50% PEHA, B35) (T: 28 °C, die l/d: 0/2 mm).

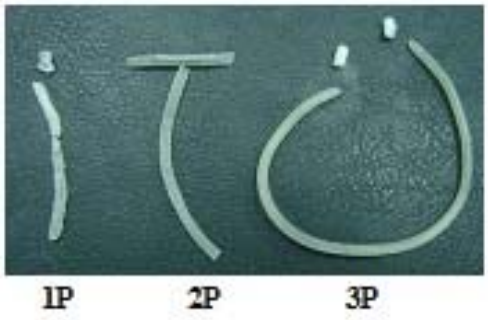

Figure 4.74 : Schematic illustration of 3 times processed PS-*b*-PEHA-*b*-PS baroplastic tri-block copolymer (50% PEHA, B35) in capillary rheometer.

Table 4.28 : Thermal and mechanical properties of PS-*b*-PEHA-*b*-PS baroplastic tri-block copolymer (50% PEHA, B35) for 1-3 times processing (T: 28 °C, appearent shear rate: 25 s^{-1}).

Polymer	$T_{g,mix}$ [a]	E [b] (MPa)	Process pressure [c] (bar)
B35-1p	49.03	15.44	176
B35-2p	48.50	31.36	127
B35-3p	48.48	43.42	68

[a] DSC measurement
[b] Zwick tensile test
[c] Capillary rheometer

Table 4.29 : Processing conditions for PS-*b*-PEHA-*b*-PS baroplastic tri-block copolymer with different PEHA contents at 25 s^{-1} shear rate in capillary rheometer measurement.

Polymer	PEHA%	Process conditions	
		T (°C)	P (bar)
B29	43	43	280
B34	49	43	114
B35	50	28	176

For all cases, T_g values were also obtained in the same trend by dynamic mechanical analysis that the method will be explained in the following section.

GPC measurements of the virgin and the 3 time processed (recycled) PS-*b*-PEHA-*b*-PS baroplastic tri-block copolymer (50% PEHA, B35) showed almost no significant change in M_w (exact weight avarage molecular weight) measured with light scattering dedector indicating that processing with capillary rheometer can be carried out without any degradation as can be seen in the GPC overlays in Figure 4.75.

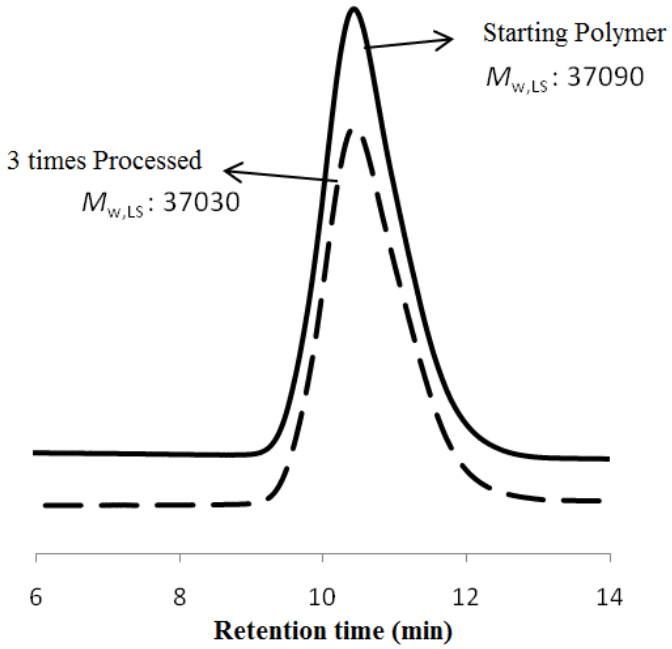

Figure 4.75 : GPC overlays of starting and 3 times processed PS-*b*-PEHA-*b*-PS tri-block copolymers (50% PEHA, B35) in capillary rheometer (T: 28 °C, appearend shear rate: 25 s^{-1}).

In order to reveal T_{ODT} of the triblock copolymer used, measurements were performed on a rotational rheometer. Two methods were used to determine T_{ODT}. The first method was to perform dynamic temperature sweeps with temperatures decreasing or increasing. A second method is to plot G' versus G´´. For a given polymer microstructure, data at different temperatures should fit on a single curve. The presence of two curves indicates an ODT in the case of block copolymers, and the temperature where data shift from one curve to the other is T_{ODT}. After gab calibration of the rotational rheometer**,** PS-*b*-PEHA-*b*-PS tri-block copolymer (49% PEHA, B34) generated in disc form were placed between 20 mm diameter parallel plates. Samples were then heated above the annealing temperature (to 120 ^{o}C) and allowed to remain for 1 hour at that temperature. The purpose of holding at 120 ^{o}C is to eliminate the thermal history of the block copolymer used that was explained in the effect of annealing part. This was done so that rotational rheometer measurements deliver repeatable results. Then various rheological studies were performed as described below. Dynamic amplitude sweeps were performed on the samples at frequencies of 1, 10, and 100 rad/s to determine the linear viscoelastic regime for the sample at the desired temperature. The amplitude sweeps show that the linear viscoelastic region extends to between $8E^{-4}$ and $6E^{-3}$ for PS-*b*-PEHA-*b*-PS block tri-block copolymer (49% PEHA, B34) (Figure 4.76). Dynamic frequency sweeps from 0.05 rad/s up to 100 rad/s were performed at different temperatures by using a strain value of $3E^{-3}$ (Figure 4.77). Dynamic temperature sweep experiments were carried out with different frequencies (0.1, 1, 10, 50, 100 Hz) in iner viscoelastic region (i.e., γ: 3E-3).

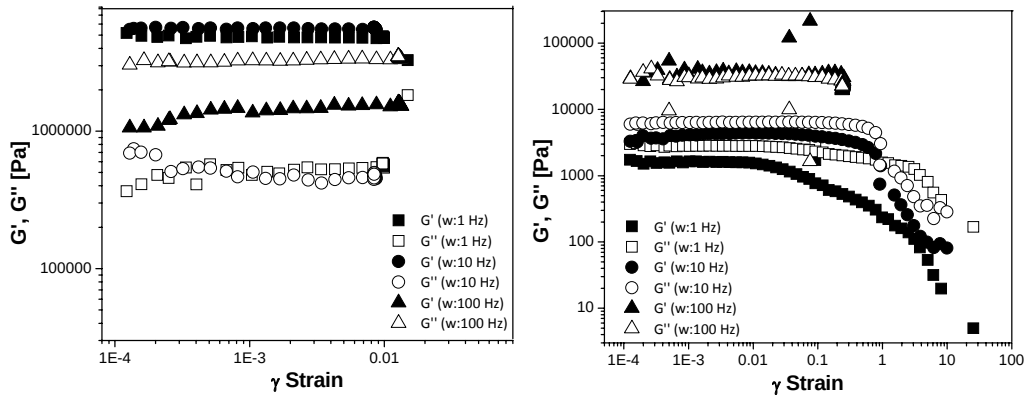

a b

Figure 4.76 : Amplitude sweep experiments with different frequencies at a) 20 ^{o}C and b) 160 ^{o}C.

According to prelimenary frequency sweeps, G' and G" change as of 120 ^{o}C. In order to detect the exact temperature, where the change in G' and G" begins, the temperature range of 100-120 ^{o}C was investigated (Figure 4.77). Both Figure 4.77 and Figure 4.78 show that a change was observed as of 110 ^{o}C, which is denoted as order-disorder transition temperature.

Temperature sweeps are shown in Figures 4.79. Employing different heating rates deliver the same curves (Figure 4.79-a). Hence, the highest heating rate of 5 ^{o}C/min was used. The disordering process is much faster than the ordering process, so supercooling is likely at this temperature ramp rate. Superheating is less likely, so the heating curves give a better estimate of the thermodynamic T_{ODT} (Figure 4.79-b). According to temperature sweep experiments, a sharp and a mild drop were observed at 82 ^{o}C and 110 ^{o}C, respectively. Theoretical studies of block copolymer morphology anticipate order–order transitions (OOT) in the vicinity of the order-disorder transition (ODT) [118]. Considering this fact and that the glass transition temperature of PS component of the triblock copolymer is 81 ^{o}C, it's revealed that the first change in G' and G" corresponds to order-order transition temperature. The second change at 110 ^{o}C shows the order-disorder temperature, which is in accordance with the results obtained by the frequency sweep results (Figure 4.78).

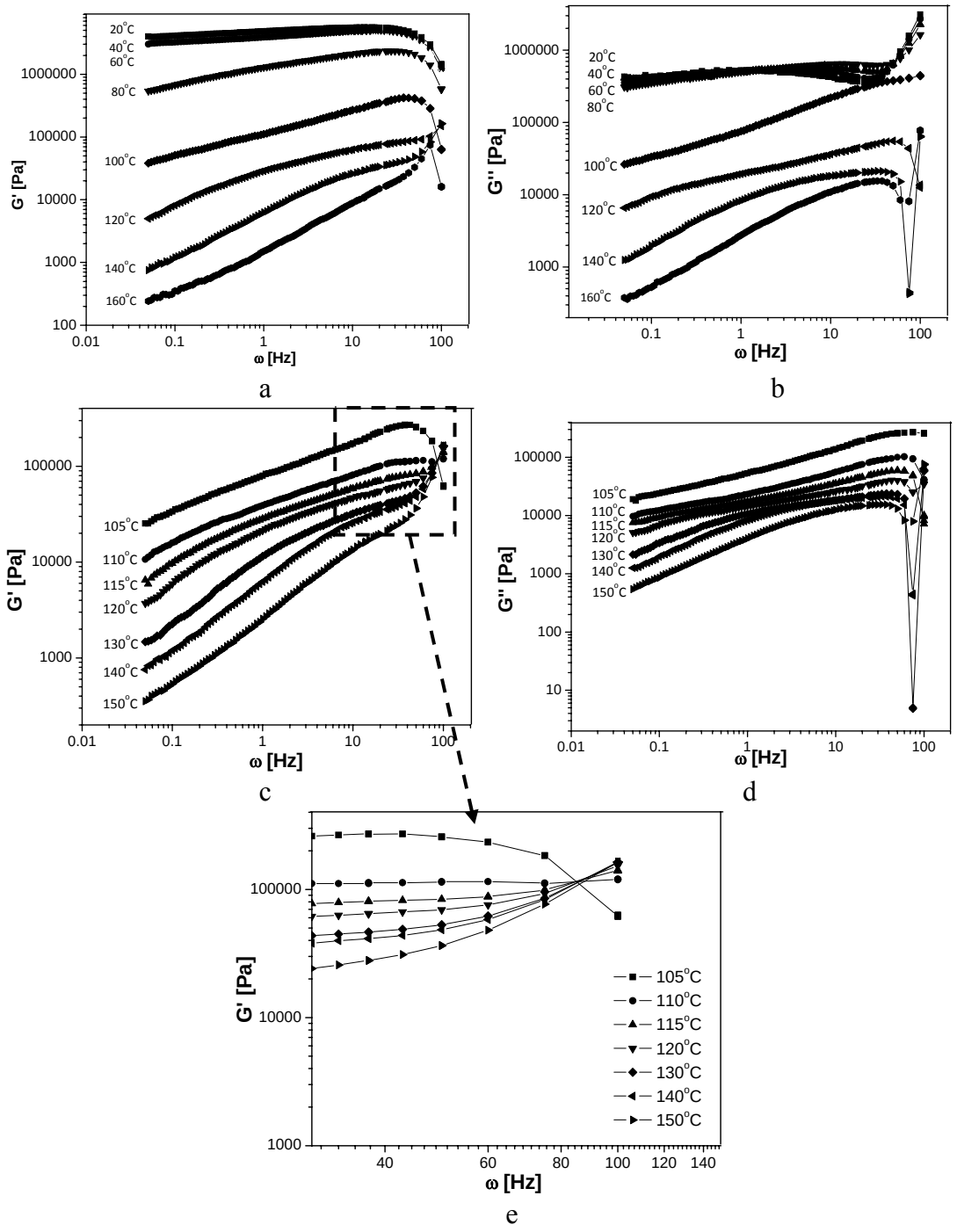

Figure 4.77 : Elastic (G') and viscous modulus (G") obtained with frequency sweep experiments at different temperatures (γ :3E^{-3}).

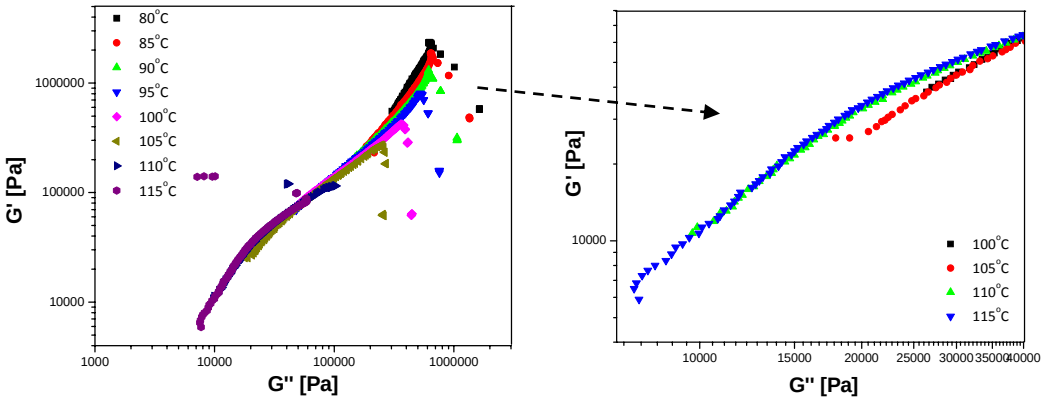

Figure 4.78 : G' versus G" graph for stress for PS-*b*-PEHA-*b*-PS tri-block copolymer (49% PEHA, B34) and enlargement of graph.

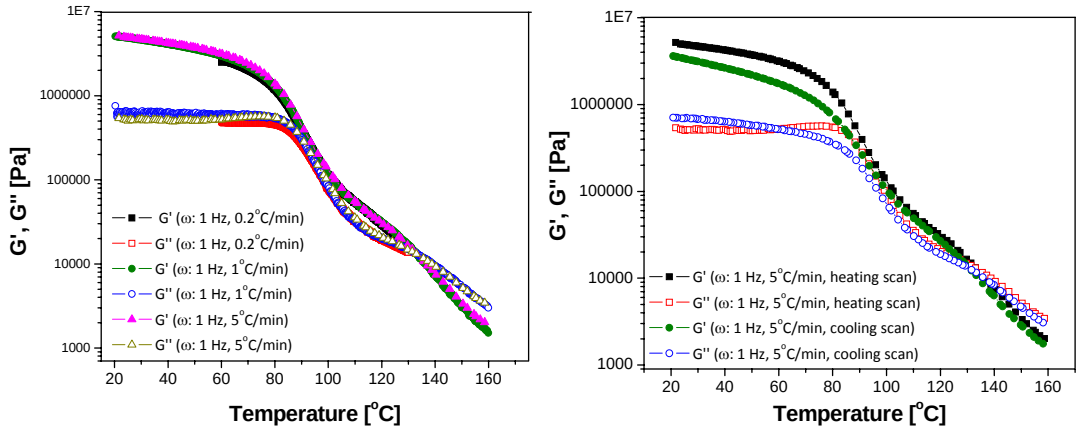

a b

Figure 4.79 : a)Temperature dependance of G' and G" at a frequency of 1 Hz with different heating rates (0.2, 1, and 5 °C/min) and a strain value of $3E^{-3}$, b) G' and G" as a function of temperature during increasing and decreasing temperature sweeps with ramp rates of 5 °C/min, a frequency of 1 Hz, and a strain value of $3E^{-3}$.

Additionally, melt shear viscosity measurements of the neat PS-*b*-PEHA-*b*-PS tri-block copolymer (49% PEHA, B34) in powder form were carried out at constant shear rate test with a Rosand RH-10 twin-bore, high-pressure capillary rheometer. Testing temperatures were betwen 60-120 °C. The range of shear rate was between 100 and 2000 s^{-1}. The capillary rheometer used has two pressure transducers located on the left hand barrel (10,000 psi) and on the right hand barrel (1500 psi). The capillary die used was 1 mm in diameter and 16 mm in length with an L/D ratio of 16 and an entrance angle of 180°, which was fitted into the left-hand barrel. In addition, the orifice die (pin hole with negligible L/D ratio) has dimensions of 0.5 mm (diameter of the die) x 0.25 mm (shear length) x 180° (entry angle), which was fitted into the right-hand barrel.

For reliability of the results, tests were performed according to the practical working range from 5% to 95% of the pressure transducers. The purposes of working on the the capilary rheometer are: (i) to determine whether the synthesized PS-*b*-PEHA-*b*-PS could be processed at low temperatures in the shear rate range which is seen in common plastics processing equipment, (ii) to determine whether morphology of the triblock copolymer is transformed from ordered into disordered state with processing at different temperatures, (iii) to reveal whether the triblock copolymer shows Cox-Merz relationship. In order to determine any morphological change, measurements of the neat PS-*b*-PEHA-*b*-PS were performed at different temperatures (60-120 ^{o}C) with two different shear rates, i.e. 100 and 1000/s. Measurements below 60 ^{o}C weren't able to be carried out by using 1 mm die. On the other hand, PS-*b*-PEHA-*b*-PS tri-block copolymer (49% PEHA, B34) could be processed at 28 and 43 ^{o}C on a different capillary rheometer by using a die with 2 mm diameter as explained previously. This is a clear indication that the tri-block copolymer synthesized could be processed at low temperatures in common plastic processing equipment. Shear viscosity values drop to a large extent especially after 80 ^{o}C (Figure 4.80). Additionally, forces generated during experiments are shown in Figure 4.81. Because of low temperatures PS-*b*-PEHA-*b*-PS tri-block copolymer (49% PEHA, B34) is forced to a larger extent at 60 ^{o}C. The images of wire shaped films can be seen in Figure 4.82.

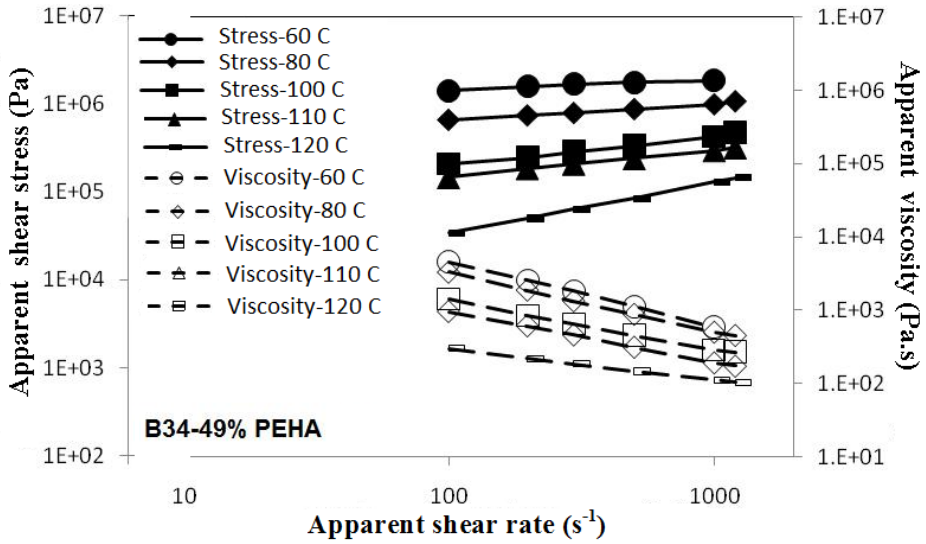

Figure 4.80 : The chart of appearent shear rate versus appearent viscosity and appearent shear stress for PS-*b*-PEHA-*b*-PS tri-block copolymer (49% PEHA, B34) at different temperatures from capillary rheometry instrument (die l/d: 1/0.8 mm).

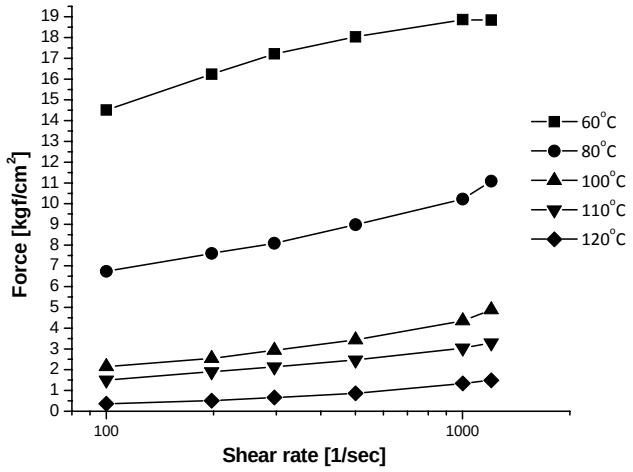

Figure 4.81 : Forces generated during capillary rheometer experiments at different temperatures stress for PS-*b*-PEHA-*b*-PS baroplastic tri-block copolymer (49% PEHA, B34).

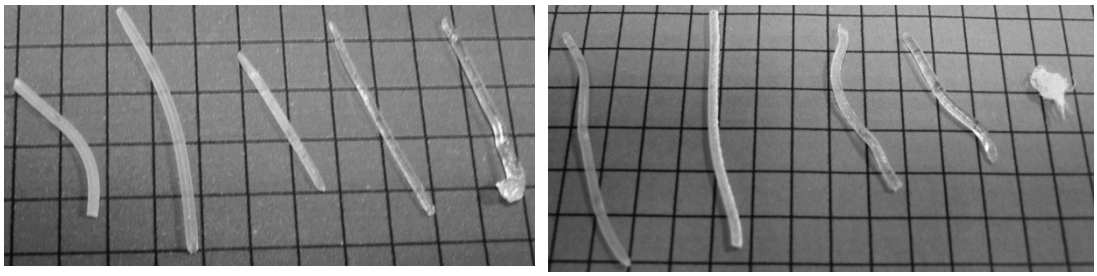

60°C 80°C 100°C 110°C 120°C **60°C 80°C 100°C 110°C 120°C**

a b

Figure 4.82 : The wire shaped films of PS-*b*-PEHA-*b*-PS tri-block copolymer (49% PEHA, B34) after processing from 1mm die capillary rheometer measurements at, a)100 and, b)1000 s^{-1} shear rate at different temperatures.

The Cox-Merz rule requires that;

$$\eta\ (\omega) = \eta\ (\dot{\gamma}) \quad for \quad \omega = \dot{\gamma} \tag{4.2}$$

and is generally found to be applicable for homopolymers. In fact, for the unfilled disordered liquidlike block copolymer, the empirical Cox-Merz rule is also applicable [119]. We observe that application of small-amplitude oscillatory shear results in a drop of dynamic viscosity at high frequencies. And at high shear rates (> 100/s), shear viscosity exceeds the complex viscosity. Besides, the tri-block copolymer examined at 110 °C results in the failure of the empirical Cox-Merz rule as demonstrated in Figure 4.83. According to these results, it's highly probable that the rheological properties change in the vicinity of order-disorder transition temperature, which also show themselves by leading to a failure in Cox-Merz rule.

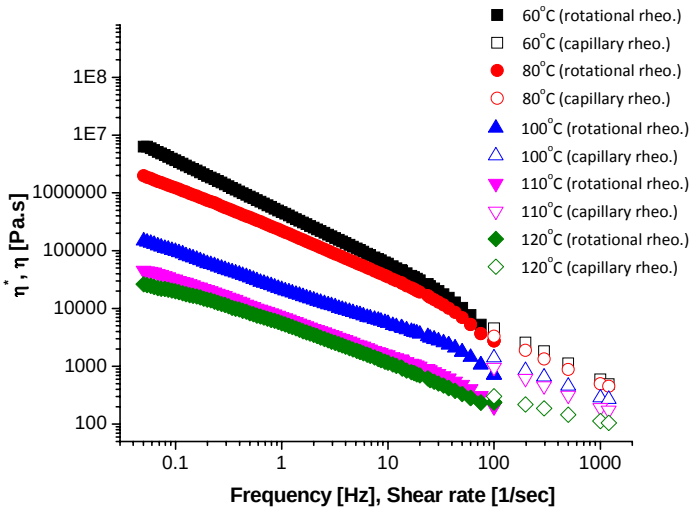

Figure 4.83 : Viscosity values of PS-*b*-PEHA-*b*-PS triblock copolymer obtained with rotational and capillary rheometer at different temperatures for establishing the Cox-Merx relationship (a strain value of $3E^{-3}$ used for rotational rheometer, a die of 1 mm diameter used for capillary rheometer).

Morphology of the samples generated were investigated by employing AFM (Figure 4.84). Processing at 60 °C, periodical distribution is changing by the applied pressure ended up in a mixed morphology. It can be seen from AFM phase images of processed material at 110 °C, reduced microphase separation (increasing of disordered structure) is clearly demonstrated by increasing process temperature (Figure 4.84-b).

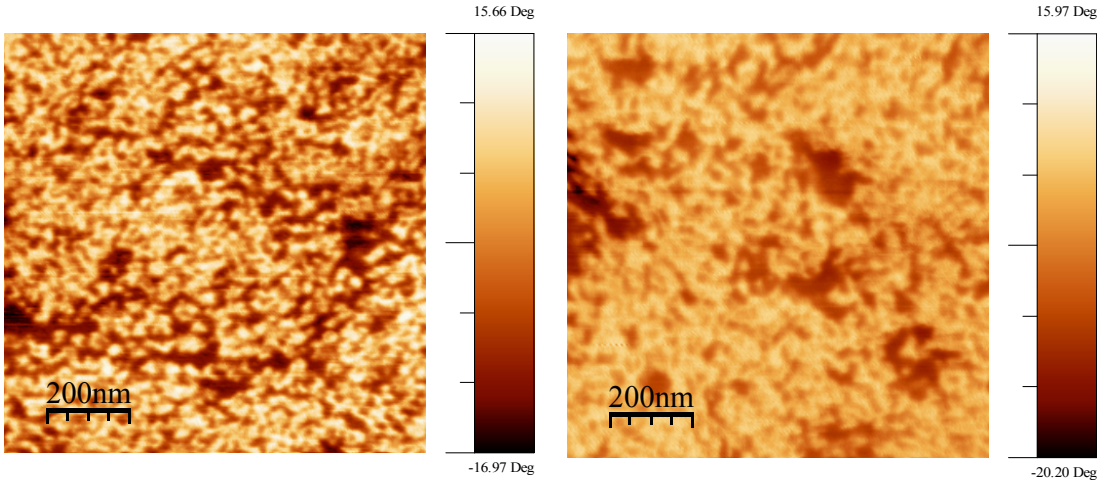

Figure 4.84 : AFM images of PS-*b*-PEHA-*b*-PS baroplastic tri-block copolymer (49% PEHA, B34) after capillary rheometer measurements at a) 60 °C and b) 110 °C.

Furthermore, because the temperature is higher than the glass transition temperature of polystyrene segments, PS domains (light part) can become dominated in mixed morphology as seen in microscopy image.

The formation of mixed morphology supported by AFM was approved by the DSC measurements when the mixed T_g is found to belong to mixture of ordered and disordered segments and the values of $T_{g,mix}$ and processing conditions are given in Table 4.30.

Table 4.30: Thermal and processing properties of PS-*b*-PEHA-*b*-PS baroplastic tri-block copolymer (49% PEHA, B34) at different temperatures.

Processing Temperature (^oC)	**100 s^{-1} shear rate**		**1000 s^{-1} shear rate**	
	Pressure (MPa)	**$T_{g,mix}$ (^oC)**	**Pressure (MPa)**	**$T_{g,mix}$ (^oC)**
60	46.43	50.79	60.00	51.92
80	21.55	51.09	32.69	58.95
100	6.87	51.64	13.93	51.13
110	4.82	52.22	9.73	57.80
120	1.15	56.58	4.28	58.25

To summarize briefly, it was understood from the measurements, polymers can be shaped at room temperature under pressure instead of using high temperatures (Figure 4.85).

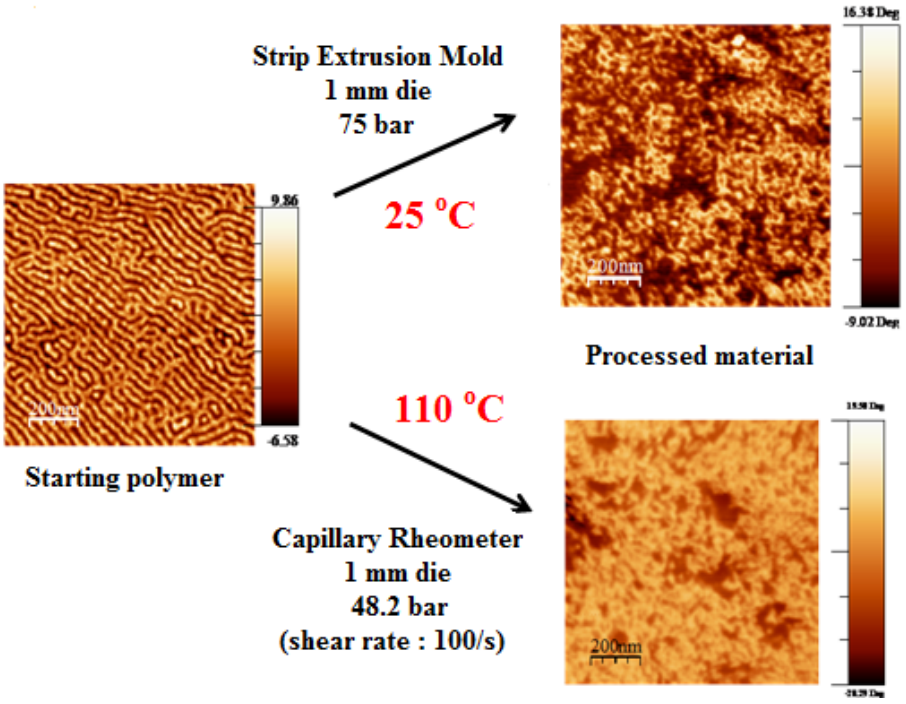

Figure 4.85 : AFM phase images of PS-*b*-PEHA-*b*-PS tri-block copolymer (49% PEHA, B34) after processing at 25 °C from extrusion mold and at 110 °C from capillary rheometry instrument.

When the use of pressure is considered instead of temperature, the phase separation is partially decreased that was confirmed by the AFM study. When high and low temperature processing were compared, the equipment that is used for the manufacturing of the current commercial plastics could be suitable for baroplastic processing as well, since the room temperature processing does not require high pressure.

4.4.9 Investigation of mechanical properties

4.4.9.1 Glass transition temperature measurements by dynamic mechanical analysis

To identify glass transition temperature (T_g), DSC methods are widely used and we have discussed the results for baroplastics in the previous parts. Thus it is of interest to compare and prove the results obtained by DMA and DSC. Both methods have usefulnesses and limitations. In this section, the use of DMA methods to characterize T_g is discussed. DSC uses very small samples (5 to 10 mg) and yields quantitative thermodynamic data for ΔC_p at T_g but it has relatively poor sensitivity.

In order to improve resolution for measuring T_g one frequently increases sample size and heating rate (above 10 ^oC) in order to sharpen the baseline shift. Identifying T_g's using DSC is particularly a problem when T_g is a relatively minor event such as in multicomponent systems where more than one T_g exists as encountered in these experiments. DMA signal strength is approximately 1000 times greater for detecting T_g (Figure 4.88) and the technique also provides useful mechanical property data. But in our cases, it is limited to obtain large scale solid material for all kind of polymers, hence we have shown a representative result to calculate T_g with DMA measurement. After extrusion processes, the transparent strip film images of PS-*b*-PEHA-*b*-PS baroplastic tri-block copolymers of different compositions is shown in Figure 4.86. DMA measurements were practiced with these films or wire films which were extruded from capillary rheometer. Due to the thermal gradient problems, heating rates in DMA was applied as 2 ^oC/min. However, the data obtained for T_g at a fixed frequency are independent of scanning rate in the absence of system thermal gradients. The final image of the strip films between the clamps after the tension test for T_g analysis by DMA can be seen in Figure 4.87. In DMA measurement, typical curves (storage modulus, loss modulus and tan δ) were obtained and the T_g values are close to each other and the temperature of tan δ_{max} is higher than the modulus as expected. "Inflection (start-end)" method for DSC analysis and the "Onset of Storage Modulus" method were used for DMA analysis of the obtained baroplastic materials. As a result from of both measurements, no significant difference in T_g values was noticed between DSC and DMA overlay curves as seen in Figure 4.88. In detail, the T_g values obtained by DSC was a little lower than the DMA values as mentioned in literature [120].

PEHA, %:	40	43	45	47	48	49	50

Figure 4.86 : The strip film images of PS-*b*-PEHA-*b*-PS baroplastic tri-block copolymers (PEHA%,40-50, B27-35) in different compositions obtained by extrusion process.

Figure 4.87 : The measured strip film images of PS-*b*-PEHA-*b*-PS (40% PEHA, B27) baroplastic tri-block copolymers by DMA.

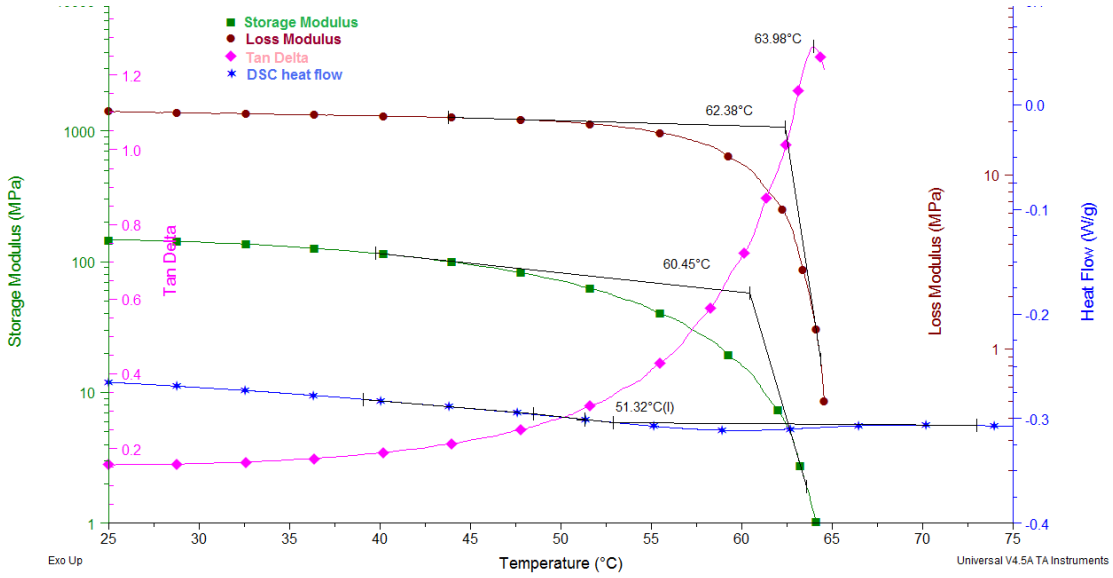

Figure 4.88 : DMA and DSC overlay graphs of PS-*b*-PEHA-*b*-PS tri-block copolymer (40% PEHA, B27).

Moreover, the DMA measurement was performed with higher molecular weight of PS-*b*-PEHA-*b*-PS tri-block copolymer (50% PEHA, B36, M_n = 150K) than the polymer shown in the previous graph (40% PEHA, B27, M_n = 30K). As the strip film resistance is high due to the higher molecular weight, higher temperatures could be measured; the T_g value of the PS could be obtained in addition to $T_{g,mix}$ value (Figure 4.89).

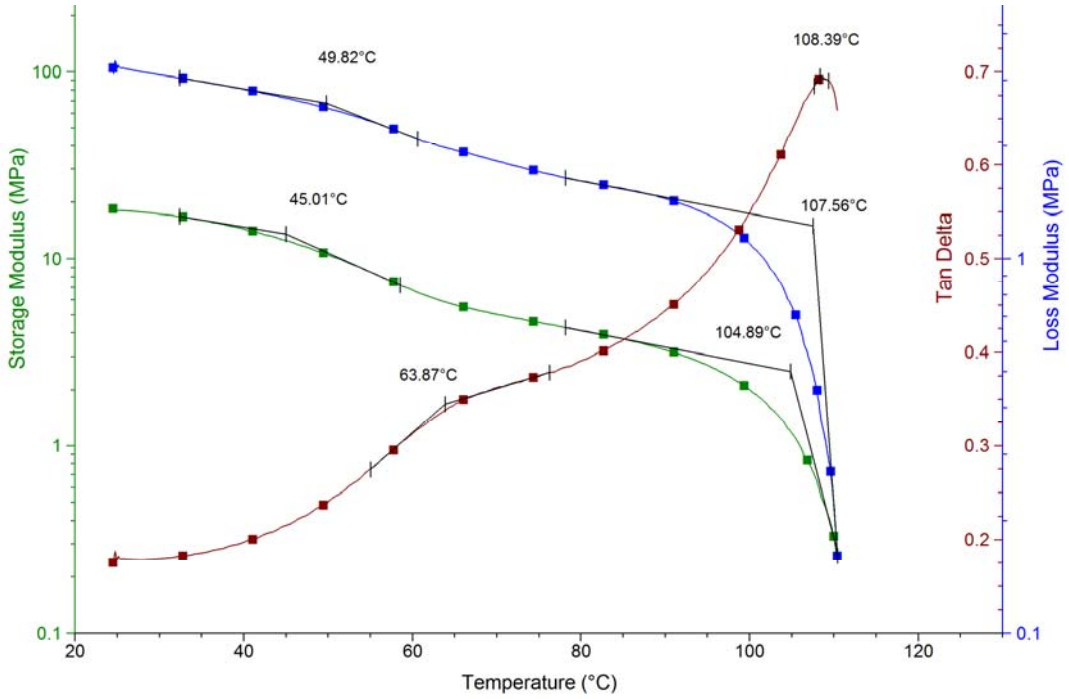

Figure 4.89 : DMA overlay graphs of PS-*b*-PEHA-*b*-PS tri-block copolymer (50% PEHA, B36).

The $T_{g,mix}$ values for baroplastic PS-*b*-PEHA-*b*-PS tri-block copolymers of different compositions are provided in Table 4.31. When the PEHA contents were increased, no significant changes in the $T_{g,mix}$ values have been observed as shown in Table 4.31. The same behavior was also explained in the effect of polymer composition section.

Table 4.31: Comparison of $T_{g,mix}$ values for PS-*b*-PEHA-*b*-PS tri-block copolymers in different compositions.

Polymer	% PEHA	$M_{w,LS}$	$T_{g,mix}$	
			DSC	DMA
B27	40	33.6K	51.32	60.45
B29	43	48.1K	51.48	51.69
B31	45	40.8K	62.09	64.78
B32	47	51.9K	52.67	-
B33	48	38.7K	63.75	51.46
B34	49	59.6K	63.03	73.13
B35	50	37.1K	60.08	64.72

Consequently, the diminishing of phase separation and the presence of the $T_{g,mix}$ after processing baroplastics was also proved by the DMA measurements which are also evident from the DSC and AFM measurements.

4.4.9.2 Mechanical tests

To characterize and quantify the effects of the processing on the materials, tension tests on processed objects were carried out. Obtained strip-shaped films from special designed extrusion piston was attached to the tension film clamp as shown in Figure 4.90 to perform stress/relaxation test.

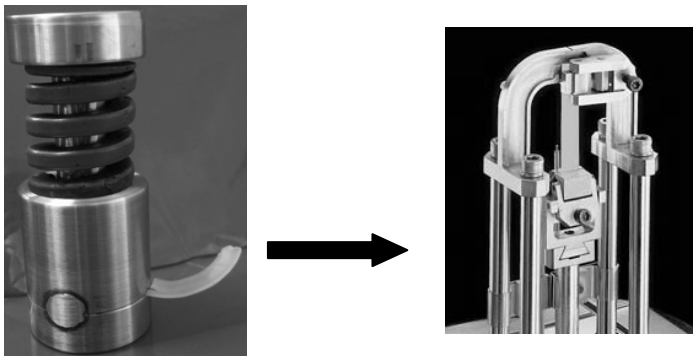

Figure 4.90 : Extruder piston with obtained strip shape film and tension test clamps for DMA.

In the DMA instrument, the clamps were not suitable design for elastomeric metarials because the top holding clamp is very sharp. During the measurements, the clamps cut the obtained films because of the softness of the films and the measurements had to be ended. When the clamps screws were loosened the films slipped through the clamps. Despite all the problems have been attempting to make measurements. Nevertheless, it can be clearly seen from the initial part of stress-strain testing curves in the Figure 4.91 and the young modulus values as 13.68 Mpa (PS-*b*-PEHA-*b*-PS, 40% PEHA, B27), 3.87 MPa (PS-*b*-PEHA-*b*-PS, 47% PEHA, B32) and 2.071 Mpa (PEHA-*b*-PS-*b*-PEHA, 53% PEHA, B21), that the soft segment was used as outer segment the material behaves as much more elastomeric than the soft segment used as inner segment. It was made inferences from the Figure 4.91 and 4.92 that when the soft segment was decreased the materials become more rigid. The same trend was seen as expected between the PS-*b*-PEHA-*b*-PS baroplastic tri-block copolymers having 43% and 45% PEHA segment. The young modulus values was found as 38.10 MPa for B29 and 28.46 MPa B31, respectively.

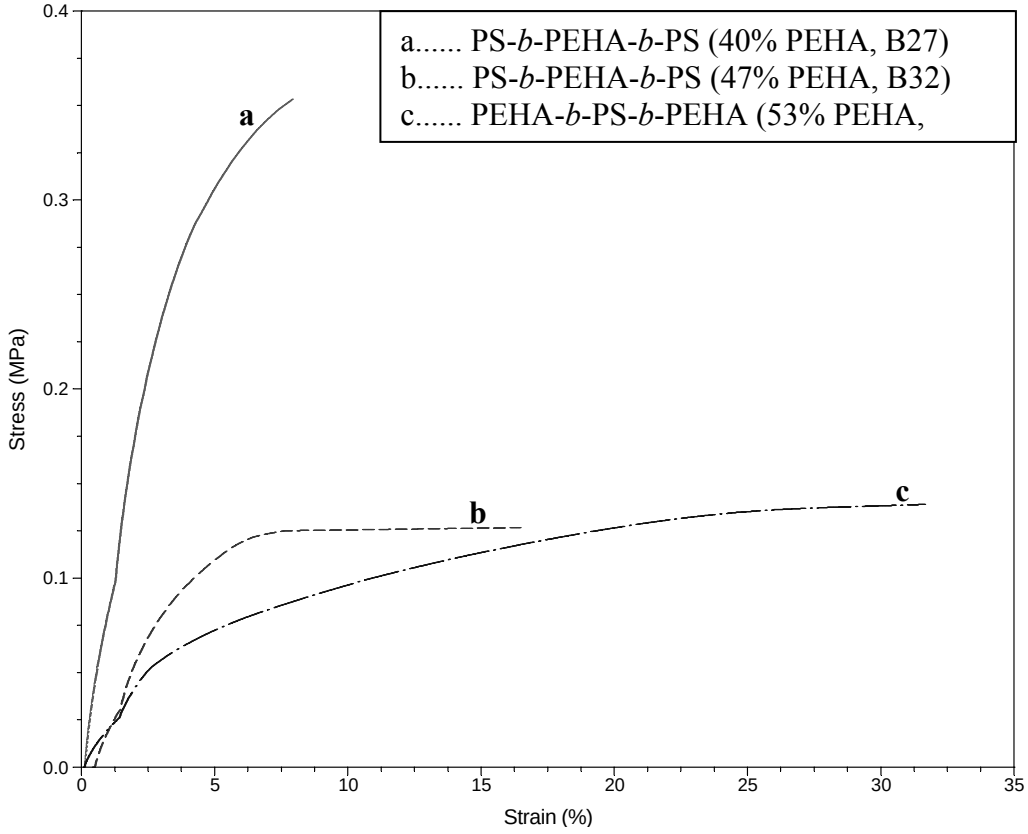

Figure 4.91 : Stress-strain curves of PS-*b*-PEHA-*b*-PS (40% PEHA, B27 and 47% PEHA, B32) and PEHA-*b*-PS-*b*-PEHA (53% PEHA, B21).

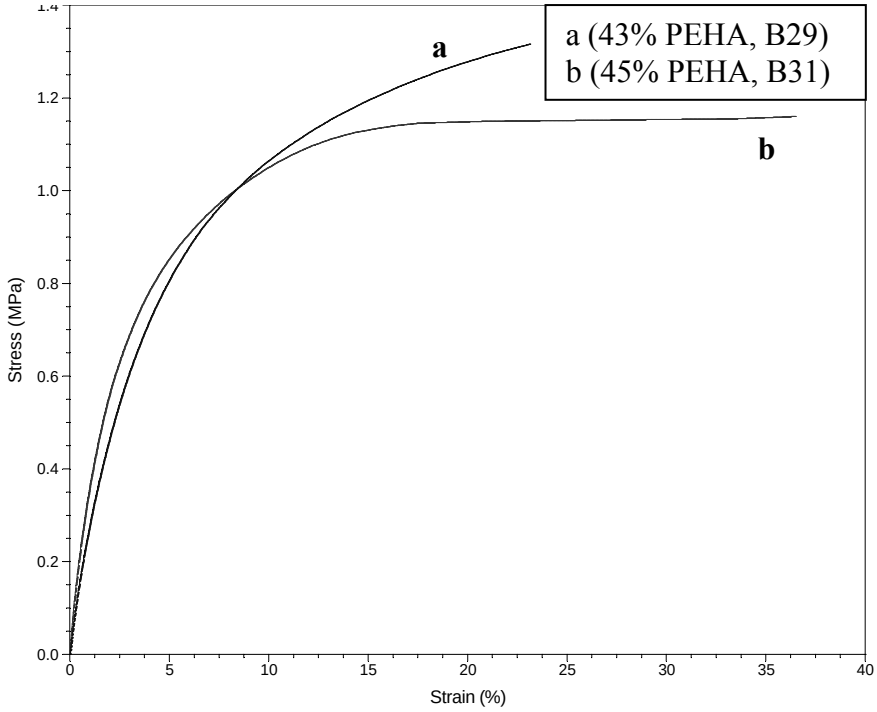

Figure 4.92 : Stress-strain curves of PS-*b*-PEHA-*b*-PS (43% PEHA, B29 and 45% PEHA, B31) tri-block copolymers.

Stress-relaxation tests were applied to four-arm star-block polymers with different inner segments and the young modulus were found as 11.35 MPa for (PEHA-*b*-PS)^{4*} (48% PEHA, B92) and 5.25 MPa for (PS-*b*-PEHA)^{4*} (51% PEHA, B82) (Figure 4.93). It was found that the results were comparible with the core-shell nanoparticle baroplastics (core/shell size: 201 nm, young modulus: 4.36 Mpa) [11].

Due to the clamps' problem, elastic modulus of this strip films were determined by tensile tests with Zwick instrument with appropriate clamps for elastomeric materials and the results for baroplastic PS-*b*-PEHA-*b*-PS tri-block copolymers of different compositions are given in Table 4.32. As mechanical properties, hardness values were determined with a Shore A and D handy portable hardness device with analog display. The results also revealed that the material strength and hardness was increased by decreasing PEHA, % rate as evaluated from Table 4.32. Hereby, the baroplastics with desired properties can be synthesized and will be used in considered applications.

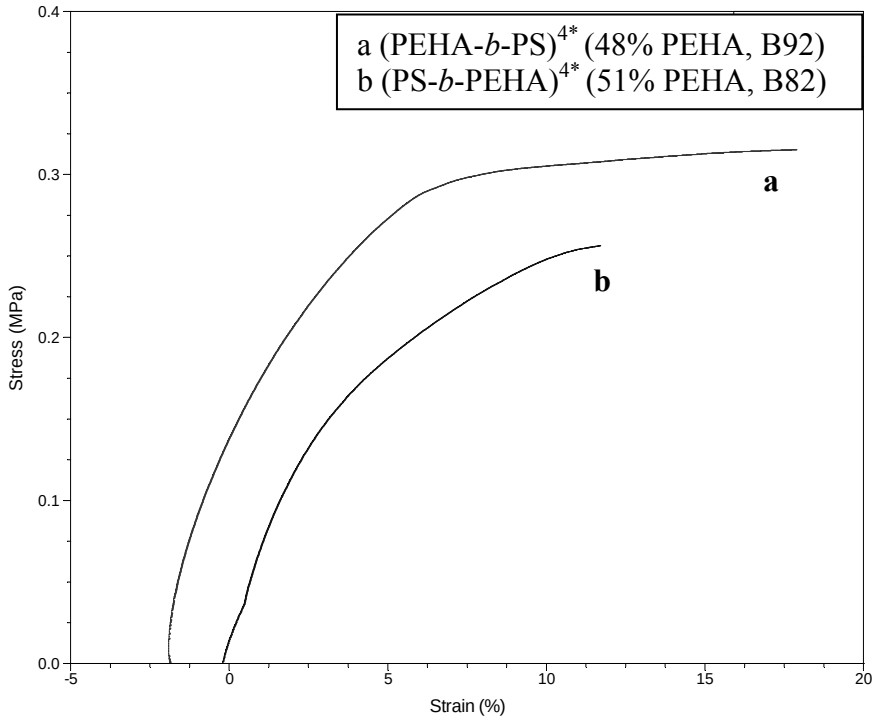

Figure 4.93 : Stress-strain curves of (PEHA-*b*-PS)^{4*} (48% PEHA, B92) and (PEHA-*b*-PS)^{4*} (51% PEHA, B82) four-arm star-block copolymers.

Table 4.32: Comparison of mechanical properties for PS-*b*-PEHA-*b*-PS tri-block copolymers in different compositions.

Polymer	PEHA%	Young's Modulus (MPa)	Shore A	Shore D
B27	40	-	91	-
B29	43	~90	93	32
B31	45	~60	90	28
B32	47	-	72	-
B33	48	~50	70	-
B34	49	-	75	15
B35	50	~20	70	-

4.4.10 Baroplastic as processing aid

It was also shown that baroplastic materials can be used as a processing aid to process high T_g homopolymer such as polystyrene (PS) at room temperature. To optimize the conditions, polystyrene and baroplastic materials in powder form were blended at different compositions and pressed using compression or extrusion mold at room temperature.

Different topologies of baroplastics were also studied to determine the contribution of baroplastic materials for the processibility of homopolymers. Additionally, the T_g value shifts due to the composition of the baroplastic block copolymer and homopolymer polystyrene were examined. Also the time and pressure effect were examined. The important thing here is that the blends should be prepared homogeneously. Otherwise the comparison with the DSC results will not be valid because of the heterogeneity of the prepared samples.

To prepare a homogenous blend, the powder polymers were dissolved in CH_2Cl_2 than precipitated in MeOH. After drying in the vacuum oven, the blends were annealed. Finally they were processed with a compression or extrusion mold. In case of a blend of baroplastics with polystyrene homopolymers it is expected the baroplastic material to drag the polystyrene chains to form the required shape as well. After a couple of experiments, it was shown that polystyrene can not be processed and results in a brittle material after processing at room temperature. On the other hand, when the PS was blended with baroplastic block copolymer, it could be processed. An illustrative example can be seen for baroplastic tri-bock copolymer that is used as processing aid to process PS with pellet mold (Figure 4.94).

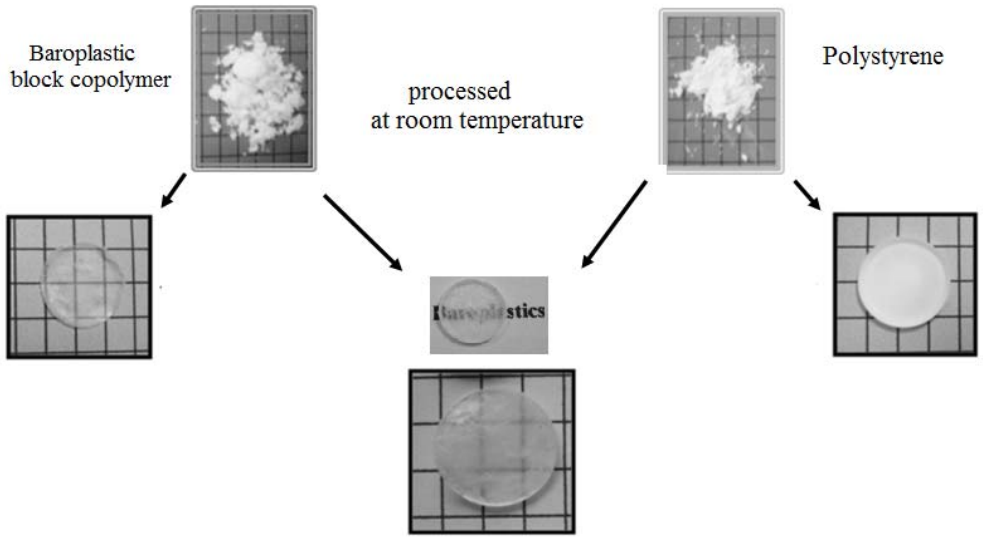

Figure 4.94 : Images of processed PS homopolymer (P11), baroplastic tri-block copolymer (48% PEHA, B33) blend of them (50 wt%) in pellet form.

For the all cases, samples from obtained pellets or strip films were measured via DSC set with a procedure of temperature increase up to 150 ^{o}C starting from -90 ^{o}C with a 10 ^{o}C/min ramp rate. As the process results with immiscible phases of PEHA and PS domains of the block copolymers and the endothermic T_g peak of PS homopolymer, a miscible phase $T_{g,mix}$ appears in the measurements. DSC thermograms can be seen in Figure 4.95 for the 45 wt% blend of baroplastic tri-block copolymer (48% PEHA, B33) and PS (P11) belongs to after processing, representatively.

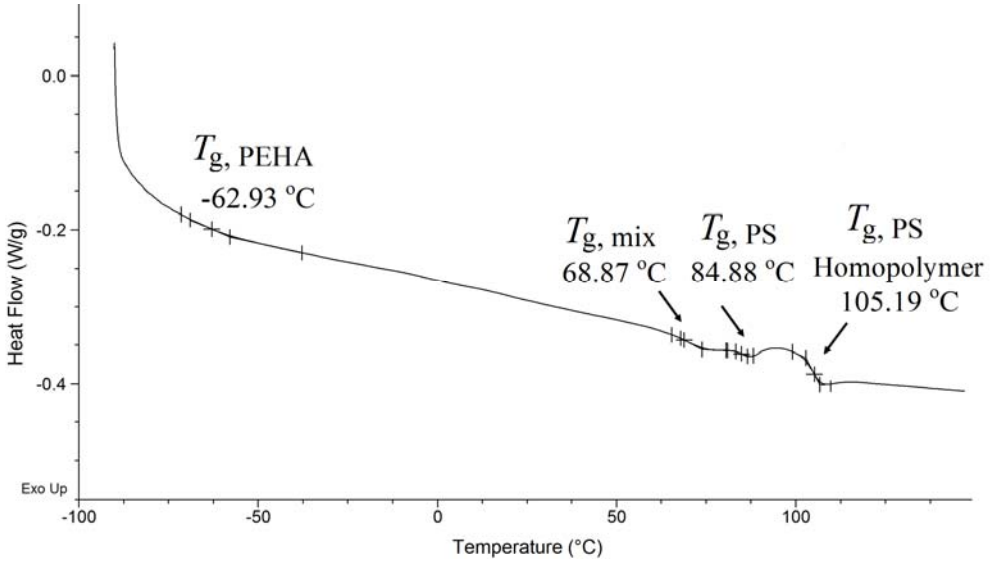

Figure 4.95 : DSC measurement of baroplastic block copolymer (48% PEHA, B33) blended polystyrene (P11) after processed at 10 tons (500 kg cm^{-2}) for 10 min.

4.4.10.1 The effect of processing aid composition

It is observed that, polystyrene cannot be processed as in the literature so far, even so the blend of baroplastics with PS could be processed easily at room temperature as we achieved. From that all, to optimize the processing conditions different composition ratios were studied systematically for different topologies of baroplastics. In Figure 4.96, the pictures of processed blends of PS (P11, 48K) with baroplastic four-arm star-block copolymer (48% PEHA, B33, 30K) in different weight percent ratios can be seen as a representative example that showed us as low as 30 wt% baroplastic (BP) is enough to process polystyrene at room temperature (8 tons, 400 kg cm^{-2} for 30 min).

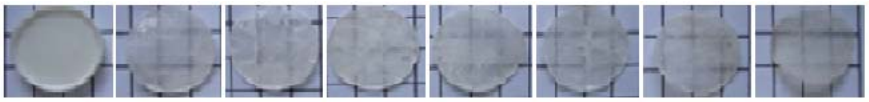

BP:	0%	30%	40%	45%	50%	60%	70%	100%
$T_{g,mix}$:	-	71.25	69.85	68.87	70.58	68.48	69.75	69.66

Figure 4.96 : The pictures of processed blends of PS (P11, 48K) and baroplastic tri-block copolymer (PS-*b*-PEHA-*b*-PS) (48% PEHA, B33, 30K).

When the blends were prepared heterogeneously, in the $T_{g,mix}$ values for the transition obtained from the DSC analysis were no significant changes with the corporation of either processing aid amount. These inaccurate results were obtained, because of the heterogenenity. When the blends are prepared homogeneously, the results will be valid for the DSC measurements. Because of this reason, the measurements were performed for the homogeneous blends of baroplastic di-block copolymer and polystyrene. The increase in the content of baroplastics caused an increase in the interaction between the phases leading to a decrease in the mixed-phase T_g towards to the endotherm of the PEHA segment as shown in Figure 4.97. In contrast, the increase in the content of PS led to a separation between the rigid and flexible phases because of the formation of the rigid areas with less mobility inducing the temperature observed for mixed-phase. This results show that the composition is important to process the PS with baroplastics at room temperature, above 30 wt% baroplastic composition the polystyrene can be processed.

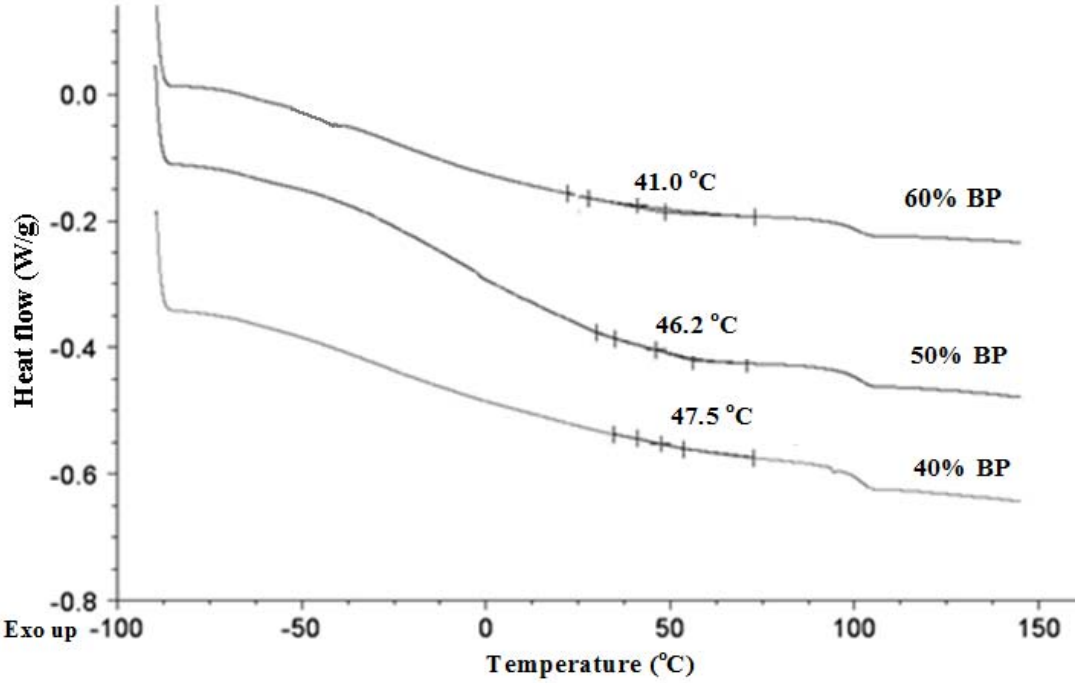

Figure 4.97 : DSC thermograms of the homogeneous blended PS-*b*-PEHA di-block copolymer (50% PEHA, B8, 36K) and polystyrene (P4, 22K) in different mixing ratio, processed under 10 tons (500 kg cm^{-2}) pressure.

So, this is an extraordinary result that room temperature processing of polystyrene is possible with a small amount of baroplastics.

4.4.10.2 The effect of time and pressure

For optimizing the duration of process, baroplastic tri-block copolymers (B8) and a polystyrene homopolymer (P13) 50 wt% were blended homogenously by means of dissolving in a beaker with CH_2Cl_2 and precipitation in methanol. After the preperation of the homogenous blend, a set of polymer blend is processed for miscellaneous times (2, 5, 10, 20 minutes) at 10 tons (500 kg cm^{-2}). In Table 4.33, it is possible to see that from DSC results there is almost no shift in $T_{g,mix}$ depending on the processing time of blends, thus it is beneficial to carry out the least possible process time to maximize the productivity which is 2 minutes between the performed process times in this case. This expected behaviour was explained before.

Table 4.33: $T_{g,mix}$ values of 50 wt% blended PS (P13, 57K) and baroplastic tri-block copolymer (50% PEHA, B8, 36K) after processing at 10 tons for different times.

Pressure time (min)	$T_{g,mix}$ (^{0}C)
2	49.6
5	49.1
10	49.4
20	49.2

To investigate the effect of pressure on processing, PEHA-*b*-PS-*b*-PEHA baroplastic tri-block copolymer (57% PEHA, B22, 62.4K) and polystyrene (P11, 48K) were blended (70 wt% of PS) homogenously and processed at 2 and 10 tons (100 and 500 kg cm^{-2}) in pellet mold. Comparing the $T_{g,mix}$ in the DSC thermograms that belong to different pressures, the more clear peak was observed for processing at the higher pressure value (Figure 4.98). From these results, for processing aid experiments the optimum conditions are determined as 2 tons (500 kg cm^{-2}) pressure for 2 minutes.

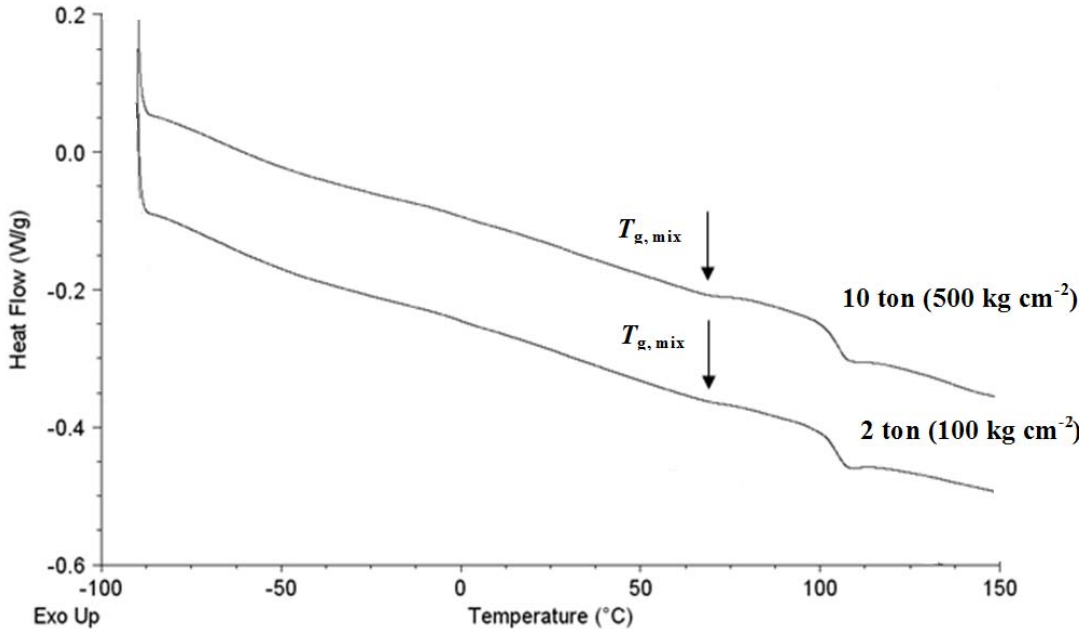

Figure 4.98 : DSC thermograms of blended PEHA-*b*-PS-*b*-PEHA baroplastic tri-block copolymer (57% PEHA, B22, 62K) and polystyrene (P11, 48K) (70 wt% of PS) after processing at 2 and 10 tons (100 and 500 kg cm^{-2}).

4.4.10.3 The usage of polymers with different topologies

To investigate the effect of polymer topologies, polystyrenes were blended with di-block, tri-block and star block copolymers, respectively.

In Table 4.34, baroplastic di-block copolymers and their blends with different homopolymer polystyrenes are shown. It was found that the increase in the content of baroplastics caused a decrease in the mixed-phase T_g. When the baroplastic content is increased, the processibility of PS needs a lower pressure. The increase in the molecular weight of homopolymer promoted a little increase in the $T_{g,\,mix}$ values, allowing the formation of bigger hard domains when compared with the PS with the low molecular weight.

Table 4.34: $T_{g,mix}$ values of blended PS-*b*-PEHA baroplastic di-block copolymer (50% PEHA, B8, 36K) with different molecular weight polystyrenes (P4: 22K and P13: 57K).

B8 (50% PEHA) (wt%)	PS (wt%)	2 Tons pressure		10 Tons pressure	
		Process	$T_{g,mix}$ (^oC)	Process	$T_{g,mix}$ (^oC)
40	P4 (60)	⊖	55.85	⊖	54.98
50	P4 (50)	☑	54.94	☑	54.26
60	P4 (40)	☑	52.89	☑	52.94
40	P13 (60)	⊖	59.78	☑	58.86
50	P13 (50)	☑	55.24	☑	54.66
60	P13 (40)	☑	55.38	☑	54.10

☑ : Processed, ⊖: partially processed

In Table 4.35, blends of baroplastic tri-block copolymer with polystyrene homopolymer are shown. The same result was obtained that the increase in the content of baroplastics caused a decrease in the mixed-phase T_g. The another observation is that the increase in the processing pressure brings the decrease in $T_{g,mix}$ values. So, it can be stated that the soft segment of the baroplastic reduced the formation of rigid domains and it gave the mobility to the PS segment.

Table 4.35: $T_{g,mix}$ values of blended PEHA-*b*-PS-*b*-PEHA baroplastic tri-block copolymer (56% PEHA, B22, 62K) and its blend with homopolymer polystyrene (P12, 52K).

B22 (56% PEHA) (wt%)	PS-P12 (wt%)	Pressure	
		2 Tons	10 Tons
		$T_{g,mix}$ (^oC)	$T_{g,mix}$ (^oC)
30	70	64.58	58.22
40	60	63.57	55.13
50	50	56.74	54.50
70	30	52.71	47.49

In Table 4.36, $T_{g,mix}$ values of blended polystyrene with baroplastic four-arm star-block copolymer are shown.

Table 4.36: $T_{g,mix}$ values of (PS-*b*-PEHA)^{4*} baroplastic four-arm star-block copolymer (48 % PEHA, B92) and polystyrene (P12, 52K) blends after processing.

B92 (48% PEHA) (wt%)	PS-P12 (wt%)	8 Tons pressure
		$T_{g,mix}$ (^oC)
30	70	66.78
50	50	66.36
60	40	64.23
70	30	63.75

As can be understood from the results, when the baroplastic percentage was increased $T_{g,mix}$ value has decreased and slid towards to $T_{g,PEHA}$ value. The reason for this is an increase of PEHA content in the mixed phase under pressure.

4.4.10.4 The extrusion test of baroplastics in the usage of processing aid

After the observation of shaping the polystyrene in the presence of baroplastics, extrusion tests were also examined for these mixtures. For processing aid studies, to avoid problems with extruder mold, 50 wt% composition were chosen (Table 4.37). Figure 4.99 shows that the homogeneous blend of PS with di-, tri- and 4-arm star-block copolymers can be extruded at 8 tons (400 kg cm^{-2}) pressure yielding a strip film, individually.

Table 4.37: $T_{g,mix}$ values of homogeneous blends of polystyrene with baroplastic di-, tri- and four-arm star-block copolymers after processing.

Polymer mixtures (50 wt%)	$T_{g,mix}$ (°C)
B8+P13	55.24
B22+P11	54.50
B73+P11	69.55

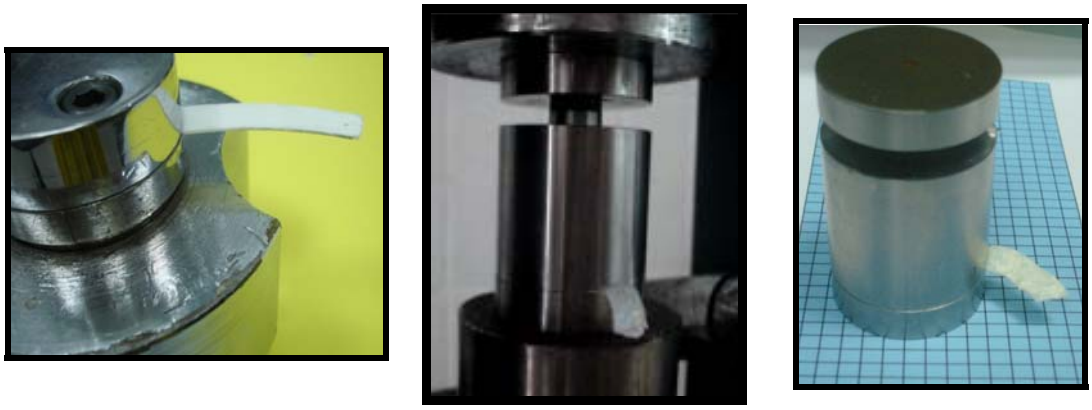

a b c

Figure 4.99 : Images of processed PS homopolymer (P4) and baroplastic, a) PS-*b*-PEHA di- block copolymer (50% PEHA, B8), b) PS-*b*-PEHA-*b*-PS tri- block copolymer (57% PEHA, B22), c) $(PS\text{-}b\text{-}PEHA)^4$* four-arm star-block copolymer (36% PEHA, B73) blend (50 wt%) in strip extrusion mold.

The resultant AFM images result should be emphasized, the phase separation of baroplastic block copolymer diminishes with the pressure after processing which is also supported by DSC (Figure 4.100).

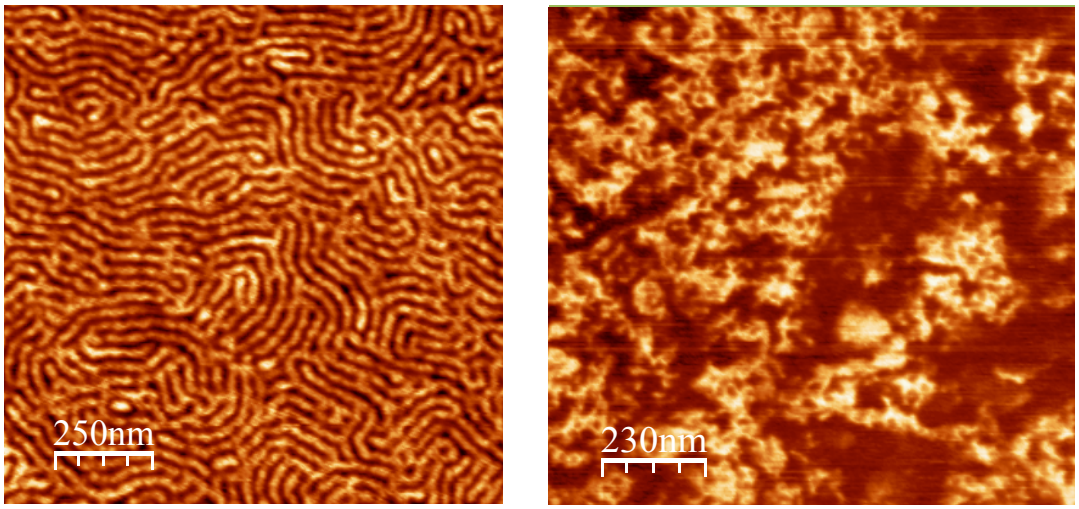

Figure 4.100 : AFM phase images of a) PEHA-*b*-PS-*b*-PEHA baroplastic tri-block copolymer (57% PEHA, B22) and b) its blend with polystyrene (P13) after processing.

5. CONCLUSION

This thesis focused on obtaining well-defined block copolymers of different topologies with the goal of expanding the range of existing baroplastics and pressure induced processability and recyclability of the obtained polymers which were investigated by thermal, morphological, rheological and mechanical properties.

From this point of view, first of all, suitable di-, tri-, tetra-, penta- and octa-functional initiators were synthesized by different methods. To synthesize the initiators in addition to a method used in the literature, three versatile alternative routes were proposed. In order to synthesize well defined di-, tri block and tetra, penta, octa armed star-block copolymers, starting from obtained initiators, well-defined homopolymers and star polymers with different compositions and molecular weights were synthesized via atom transfer radical polymerization, and from them well-defined block copolymers were successfully achieved with different topologies.

It was determined that the resulting block copolymers, depending on their compositions and topologies, showed baroplastic feature. The first proof of baroplasticity was to observe transparent images after the block copolymers were pressed in the pellet mold as well as extruded in the wire or strip mold at room temperature. For extrusion molding, “custom-made” molds were designed through trial- errors to improve the processing at room temperature. In addition, the role of pressure-induced miscibility was studied by the use of a copolymer control experiment that exhibits pressure induced demixing. Additionally, the imprinting and coloring of baroplastic block copolymers were demonstrated.

The changes of internal or external segments of the tri- block and four-arm star-block copolymers showed no difference in the processing, whereas thermoplastic elastomers that containing only inner soft segment. These results provide advantages in terms of various synthesis In general, it was concluded that to process star-block copolymers, soft segments lower than that of linear polymers are required. This result can be considered as an advantage of star-block copolymers.

In order to understand the -baroplasticity- transition from ordered to disordered structure by applying pressure at room temperature, optical tests, investigation of morphology by AFM and glass transition temperature measurement by DSC and DMA were examined. It was seen that the generation of a third (mixed) phase attributed to the interphase of the two immiscible phases which belongs to block copolymers was caused by the influence of pressure at room temperature. It can be clearly seen that the $T_{g,mix}$ concept of baroplastics were supported by the both DSC and DMA results.

It was demonstrated that baroplastic materials can be recycled 100% after multiple recycling times (20 cycle) without any degradation (with properties equivalent to that of the virgin material which are supported by GPC measurements). The calculation from the thermal characterization results showed that the baroplastic materials may be used for infinity times. These results suggest a longer recycling life that could substantially reduce the amount of waste generation. Also, a material with this processing advantage would save energy and time since no heating and cooling are involved.

For baroplastics to become more comparable to commercial thermoplastic elastomers, triblock copolymers were deeply investigated. Capillary rheometer measurements were performed for processing at room temperature. When high and low temperature processing were compared, the equipment that is used for the manufacturing of the current commercial plastics was found to be suitable for baroplastic processing as well, since the room temperature processing does not require high pressure. This finding was supported with the AFM studies.

The mechanical property measurement results also revealed that the material strength and hardness was increased by decreasing the soft segment ratios. This result showed that the baroplastic materials with different mechanical properties can be obtained for different purposes.

Moreover, possibility of using baroplastic materials as processing aid in order to process under pressure at room temperature was demonstrated with polystyrene which is a high temperature processing commodity polymer.

It can be summarized from the results, baroplastics offer a variety of practical advantages over conventional thermoplastic elastomers:

* *Lower energy consumption* as a result of *processing at room temperature*.

* *Low processing cost*. Baroplastics have the processing simplicity of a thermoplastic elastomers and significantly lower processing cost because of the low processing temperature [14].

* *No degradation* and *discoloration*.

* *Multiple lifetimes*, safe nature (100% recyclability). The regrind from baroplastic processing can be recycled to give finished parts with *the same properties as virgin material*.

* *No additives*. Most baroplastics are fully formulated and ready for use as received.

* *Shorter fabrication times*. Molding cycles of baroplastics is commonly measured as 15 seconds that is 150 seconds for thermoplastic elastomers.

* *Same technology*. Any significant innovation requires the communication of at least some new technology. However, the equipment required for baroplastics is familiar with the thermoplastic elastomers fabricators.

* *Varied number of hardness*. The great majority of commercially available thermoplastic elastomers have a hardness above 80 Shore A. Below a hardness 60 Shore, the number of available thermoplastic elastomers is quite limited.

* *Coloration and imprinting of the material* is the same as thermoplastic elastomers.

* *Processing of polystyrene at room temperature*, by adding baroplastic as processing aid.

As a result, baroplastic material opens the door for a class of plastic materials that become processable with the application of pressure at greatly reduced temperatures relative to traditional thermoplastic processing.

REFERENCES

[1] **Url-1** *<http://www.plasticsportal.net/wa/plastics~en_GB/portal>*, accessed at 16.02.1010.

[2] **Callister, W. D.,** 2006. *Materials Science and Engineering: An Introduction*, *7th ed.*, John Wiley&Sons, University of Utah.

[3] **Url-2** *<http://www.plasticsresource.com>*, accessed at 16.02.2010.

[4] **Url-3** *<http://en.wikipedia.org/wiki/Plastic>*, accessed at 16.02.2010.

[5] **Drobny, J. G.,** 2007. *Handbook of Thermoplastic Elastomers*, William Andrew Inc., United States of America.

[6] **Url-4** *<http://en.wikipedia.org/wiki/Thermoplasticelastomer>*, accessed at 16.02.2010.

[7] **Walker, B. M. and Rader, C. R.,** 1988. *Handbook of Thermoplastic Elastomers*, Van Nostrand Reinhold Company Inc., United States of America.

[8] **Hopewell, J., Dvorak, R. and Kosior, E.,** 2009. Plastics recycling: challenges and opportunities*, Philosophical Transactions the Royal Society B*, **364,** 2115-2126.

[9] **Acar, M. H., Gonzalez, J. A. and Mayes, A. M.,** 2002. Synthesis of baroplastic elastomer by ATRP*, Abstracts of Papers of the American Chemical Society*, **224,** 331-POLY.

[10] **Acar, M. H., Gonzalez-Leon, J. A. and Mayes, A. M.,** 2003. Pressure dependence phase transition in block copolymers*, Polymeric Materials: Science and Engineering*, **88**, 159.

[11] **Gonzalez-Leon, J. A.,** 2005. Low Temperature Processing of Baroplastic Core-Shell Nanoparticles and Block Copolymers*, PhD Thesis*, MIT, Cambridge, MA.

[12] **Gonzalez-Leon, J. A., Acar, M. H., Ryu, S-W., Ruzette, A. V. G. and Mayes, A. M.,** 2003. Low-temperature processing of 'baroplastics' by pressure-induced flow*, Nature*, **426** (6965), 424-428.

[13] **Gonzalez-Leon, J. A., Ryu, S-W., Hewlett, S. A., Ibrahim, S. H. and Mayes, A. M.,** 2005. Core-shell polymer nanoparticles for baroplastic processing*, Macromolecules*, **38** (19), 8036-8044.

[14] **Ibrahim, S. H.,** 2005. Evaluation of the Economic Feasibility of Core-Shell Baroplastic Polymers and a Comparison to Traditional Thermoplastic Elastomer, *MSc Thesis*, MIT, Cambridge, MA.

[15] **Lovell, N. G.,** 2005. The Design, Synthesis and Properties of Pressure-Processable Biodegradable Block copolymers*, MSc Thesis*, MIT, Cambridge, MA.

[16] **Mayes, A. M., Ryu, S-W., Acar, M. H., and Gonzalez, J. A.,** 2009. Structured baroplastic materials*, U.S. Patent*, US 7,538,157 B2 dated 26.05.2009.

[17] **Mayes, A. M., Ruzette, A. V., and Russell, T. P.,** 2003. Baroplastic Materials*, U.S. Patent*, US 6,632,883 B2 dated 2003.

[18] **Ryu, S. W., Gonzalez, J. A., Acar, M. H. and Mayes, A. M.,** 2003. Core-shell structured nano-particles for baroplastic processing*, Abstracts of Papers of the American Chemical Society*, **226**, U530.

[19] **Ryu, S. W., Gonzalez-Leon, J. A., Acar, M. H. and Mayes, A. M.,** 2003. Core-shell structured nanoparticles baroplastic processing*, Polymeric Materials: Science and Engineering*, **89**, 770.

[20] **Pollard, M., Russell, T. P., Ruzette, A. V., Mayes, A. M. and Gallot, Y.,** 1998. The effect of hydrostatic pressure on the lower critical ordering transition in diblock copolymers*, Macromolecules*, **31** (19), 6493-6498.

[21] **Ruzette, A. V. G., Banerjee, P., Mayes, A. M. and Russell, T. P.,** 2001. A simple model for baroplastic behavior in block copolymer melts*, Journal of Chemical Physics*, **114** (18), 8205-8209.

[22] **Ruzette, A. V. G. and Mayes, A. M.,** 2001. Simple free energy model for weakly interacting polymer blends*, Macromolecules*, **34** (6), 1894-1907.

[23] **Ruzette, A. V. G., Mayes, A. M., Pollard, M., Russell, T. P. and Hammouda, B.,** 2003. Pressure effects on the phase behavior of styrene/n-alkyl methacrylate block copolymers*, Macromolecules*, **36** (9), 3351-3356.

[24] **Ryu, D. Y., Jeong, U., Kim, J. K. and Russell, T. P.,** 2002. Closed-loop phase behaviour in block copolymers*, Nature Materials*, **1** (2), 114-117.

[25] **Ryu, D. Y., Lee, D. J., Kim, J. K., Lavery, K. A., Russell, T. P., Han, Y. S., Seong, B. S., Lee, C. H. and Thiyagarajan, P.,** 2003. Effect of hydrostatic pressure on closed-loop phase behavior of block copolymers*, Physical Review Letters*, **90** (23), 235501.1-235501.4.

[26] **Kim, H. J., Bin Kim, S., Kim, J. K. and Jung, Y. M.,** 2008. Hydrostatic pressure effect on the phase transitions of a closed-loop type block copolymer by using 2D FT-IR correlation spectroscopy*, Journal of Physical Chemistry B*, **112** (48), 15295-15300.

[27] **Lee, D. H., Kim, H. J. and Kim, J. K.,** 2006. Closed-loop phase behavior and baroplasticity of deuterated polystyrene-block-poly(n-pentyl methacrylate) copolymer investigated by SANS and FTIR spectroscopy*, Macromolecular Symposia*, **240**, 123-129.

[28] **Ruzette, A. V.,** 2002. Block copolymers-copolymers close the loop*, Nature Materials*, **1** (2), 85-87.

[29] **Hasegawa, H., Sakamotoa, N., Takenoa, H., Jinnaia, H., Hashimotoa, T., Schwahnb, D., Frielinghausb, H., Janβenb, S., Imaic, M. and Mortensend, K.,** 1999. Small-angle neutron scattering studies on phase behavior of block copolymers*, Journal of Physics and Chemistry of Solids*, **60** (8-9), 1307-1312

[30] **Frielinghaus, H., Schwahn, D., Mortensen, K., Almdal, K. and Springer, T.,** 1996. Composition fluctuations and coil conformations in a poly(ethylene-propylene)-poly(ethylethylene) diblock copolymer as a function of temperature and pressure*, Macromolecules*, **29,** 3263-3271.

[31] **Schwahn, D., Frielinghaus, H., Mortensen, K. and Almdal, K.,** 1996. Temperature and pressure dependence of the order parameter fluctuations, conformational compressibility, and the phase diagram of the PEP-PDMS diblock copolymer*, Physical Review Letters*, **77** (15), 3153-3156.

[32] **Russell, T. P., Karis, T. E., Gallot, Y. and Mayes, A. M.,** 1994. A lower critical ordering transition in a diblock copolymer melt*, Nature*, **368** (6473), 729-731.

[33] **Tsitsilianis, C.,** 2007. Multisegmental Block/Graft Copolymers in *Macromolecular Engineering: Precise Synthesis, Materials Properties, Applications*, **2,** Chapter 4, 839-873, Eds. K. Matyjaszewski, Y. Gnanou ve L. Leibler, John Wiley & Sons.

[34] **Hadjichristidis, N., Pispas, S. and Floudas, G.,** 2003. in *Block copolymers, Synthetic Strategies, Physical Properties and Applications*, John Wiley&Sons.

[35] **Hadjichristidis, N., Pitsikalis, M. and Iatrou, H.,** 2005. Block copolymer I, Synthesis of Block copolymers, in *Advances in Polymer Science*, **189,** 1-124, Springer.

[36] **Bahadur, P.,** 2001. Block copolymers–their microdomain formation (in solid state) and surfactant behaviour (in solution)*, Special Section: Soft Condenced Matter*, **80** (8), 1002-1007.

[37] **Patten, T. E. and Matyjaszewski, K.,** 1998. Atom transfer radical polymerization and the synthesis of polymeric materials*, Advanced Materials*, **10** (12), 901-915.

[38] **Hadjichristidis, N., Pitsikalis, M. and Iatrou, H.,** 2007. Polymers with Star-related structures, in *Macromolecular Engineering, Precise Synthesis, Materials Properties, Applications*, **2,** Chapter 6, 909-972, Eds. Matyjaszewski, K., Gnanou, Y. and Leibler, L., John Wiley & Sons.

[39] **Hadjichristidis, N., Pitsikalis, M., Pispas, S. and Iatrou, H.,** 2001. Polymers with complex architecture by living anionic polymerization*, Chemical Reviews*, **101** (12), 3747-3792.

[40] **Gnanou, Y. and Taton, D.,** 2002. Macromolecular Engineering by Controlled/Living Radical Polymerization, in *Handbook of radical polymerization*, Chapter 14, 775-844, Eds. Matyjaszewski, K. and Davis, T.P., John Wiley&Sons.

[41] **Angot, S., Murthy, K. S., Taton, D. and Gnanou, Y.,** 1998. Atom transfer radical polymerization of styrene using a novel octa-functional initiator: Synthesis of well-defined polystyrene stars, *Macromolecules*, **31** (21), 7218-7225.

[42] **Hawker, C. J.,** 1995. Architectural control in living free radical polymerization-preparation of star and graft polymers. *Angewandte Chemie-International Edition in English*, **34** (13-14), 1456-1459.

[43] **Matyjaszewski, K., Miller, P. J., Fossum, E. and Nakagawa, Y.,** 1998. Synthesis of block, graft and star polymers from inorganic macroinitiators, *Applied Organometallic Chemistry*, **12** (10-11), 667-673.

[44] **Matyjaszewski, K., Miller, P. J., Pyun, J., Kickelbick, G. and Diamanti, S.,** 1999. Synthesis and characterization of star polymers with varying arm number, length, and composition from organic and hybrid inorganic/organic multifunctional initiators, *Macromolecules*, **32** (20), 6526-6535.

[45] **Mayadunne, R. T. A., Jeffery, J., Moad, G. and Rizzardo, E.,** 2003. Living free radical polymerization with reversible addition-fragmentation chain transfer (RAFT polymerization): Approaches to star polymers, *Macromolecules*, **36** (5), 1505-1513.

[46] **Ueda, J., Matsuyama, M., Kamigaito, M. and Sawamoto, M.,** 1998. Multifunctional initiators for the ruthenium-mediated living radical polymerization of methyl methacrylate: Di- and trifunctional dichloroacetates for synthesis of multiarmed polymers, *Macromolecules*, **31** (3), 557-562.

[47] **Baek, K. Y., Kamigaito, M. and Sawamoto, M.,** 2001. Star-shaped polymers by metal-catalyzed living radical polymerization. 1. Design of Ru(II)-based systems and divinyl linking agents, *Macromolecules*, **34** (2), 215-221.

[48] **Barner-Kowollik, C., Davis, T. P., Heuts, J. P. A., Stenzel, M. H., Vana, P. and Whittaker, M.,** 2003. RAFTing down under: Tales of missing radicals, fancy architectures, and mysterious holes, *Journal of Polymer Science Part A-Polymer Chemistry*, **41** (3), 365-375.

[49] **Bosman, A. W., Vestberg, R., Heumann, A., Frechet, J. M. J. and Hawker, C. J.,** 2003. A modular approach toward functionalized three-dimensional macromolecules: From synthetic concepts to practical applications, *Journal of the American Chemical Society*, **125** (3), 715-728.

[50] **Gao, H. F. and Matyjaszewski, K.,** 2006. Structural control in ATRP synthesis of star polymers using the arm-first method, *Macromolecules*, **39** (9), 3154-3160.

[51] **Gao, H. F., Tsarevsky, N. V. and Matyjaszewski, K.,** 2005. Synthesis of degradable miktoarm star copolymers via atom transfer radical polymerization, *Macromolecules*, **38** (14), 5995-6004.

[52] **Matyjaszewski, K.,** 2003. The synthesis of functional star copolymers as an illustration of the importance of controlling polymer structures in the design of new materials, *Polymer International*, **52** (10), 1559-1565.

[53] **Moad, G., Mayadunne, R. T. A., Rizzardo, E., Skidmore, M. and Thang, S. H.,** 2003. Synthesis of novel architectures by radical polymerization with reversible addition fragmentation chain transfer (RAFT polymerization), *Macromolecular Symposia*, **192**, 1-12.

[54] **Xia, J. H., Zhang, X. and Matyjaszewski, K.,** 1999. Synthesis of star-shaped polystyrene by atom transfer radical polymerization using an "arm first" approach, *Macromolecules*, **32** (13), 4482-4484.

[55] **Zhang, X., Xia, J. H. and Matyjaszewski, K.,** 2000. End-functional poly(*tert*-butyl acrylate) star polymers by controlled radical polymerization, *Macromolecules*, **33** (7), 2340-2345.

[56] **Gao, H. F. and Matyjaszewski, K.,** 2006. Synthesis of star polymers by a combination of ATRP and the "click" coupling method, *Macromolecules*, **39** (15), 4960-4965.

[57] **Shipp, D. A.,** 2005. Living radical polymerization: Controlling molecular size and chemical functionality in vinyl polymers, *Journal of Macromolecular Science-Polymer Reviews*, **45** (2), 171-194.

[58] **Matyjaszewski, K. and Spanswick, J.,** 2005. Controlled/living radical polymerization, in *Handbook of Polymer Synthesis*, Chapter 17, 895, Eds. Kricheldorf, H.R., Nuyken O. and Swift, G., Marcel Dekker Publication, New York, USA.

[59] **Coessens, V., Pintauer, T. and Matyjaszewski, K.,** 2001. Functional polymers by atom transfer radical polymerization, *Progress in Polymer Science*, **26** (3), 337-377.

[60] **Pintauer, T. and Matyjaszewski, K.,** 2005. Structural aspects of copper catalyzed atom transfer radical polymerization, *Coordination Chemistry Reviews*, **249** (11-12), 1155-1184.

[61] **Matyjaszewski, K. and Xia, J. H.,** 2001. Atom transfer radical polymerization, *Chemical Reviews*, **101** (9), 2921-2990.

[62] **Matyjaszewski, K. and Xia, J. H.,** 2002. Fundamentals of Atom Transfer Radical Polymerization, in *Handbook of radical polymerization*, Eds. Matyjaszewski, K. and Davis, T.P., John Wiley & Sons.

[63] **Kamigaito, M., Ando, T. and Sawamoto, M.,** 2001. Metal-catalyzed living radical polymerization, *Chemical Reviews*, **101** (12), 3689-3745.

[64] **Braunecker, W. A. and Matyjaszewski, K.,** 2007. Controlled/living radical polymerization: Features, developments, and perspectives, *Progress in Polymer Science*, **32** (1), 93-146.

[65] **Wang, J. S. and Matyjaszewski, K.,** 1995. Controlled living radical polymerization-halogen atom transfer radical polymerization promoted by a Cu(I)/Cu(II) redox process, *Macromolecules*, **28** (23), 7901-7910.

[66] **Wang, J. S. and Matyjaszewski, K.,** 1995. Controlled living radical polymerization-atom transfer radical polymerization in the presence of transition-metal complexes*, Journal of the American Chemical Society*, **117** (20), 5614-5615.

[67] **Matyjaszewski, K. and Spanswick, J.,** 2005. Controlled/living radical polymerization*, Materials Today*, **8** (3), 26-33.

[68] **Matyjaszewski, K.,** 1998. Mechanistic Aspects of Atom Transfer Radical Polymerization, in *Controlled Radical Polymerization, ACS Symposium Series*, **685,** Chapter 16, 258-283, John Wiley & Sons.

[69] **Qui, J.,** 2000. Atom transfer radical polymerization in aqueous dispersed media*, PhD Thesis*, Carnegie-Mellon University, Pittsburgh, PA., USA.

[70] **Url-5** <*http://www.chem.cmu.edu/groups/maty/*>, accessed at 18.02.2010.

[71] **Buschnakowski, M., Adhikari, R., Michler, G. H. and Knoll, K.,** 2007. Influence of the extrusion process on the morphology and micromechanical behavior of polystyrene-block(polystyrene-co-butadiene)-block-polystyrene star block copolymer/homopolystyrene blends*, Journal of Applied Polymer Science*, **106** (3), 1939-1949.

[72] **Leibler, L.,** 1980. Theory of microphase separation in block copolymers*, Macromolecules*, **13** (6), 1602-1617.

[73] **Url-6** <*www.princeton.edu/~polymer*>, accessed at 18.02.2010.

[74] **Thomas, E. L. and Lescanec, R. L.,** 1994. Phase morphology in block-copolymer systems*, Philosophical Transactions of the Royal Society of London Series a-Mathematical Physical and Engineering Sciences*, **348** (1686), 149-166.

[75] **Abetz, V. and Simon, P. F. W.,** 2005. Phase behaviour and morphologies of block copolymers, in *Block Copolymers I*, **189,** 125-212.

[76] **Sakurai, S., Okamoto, S. and Sakurai, K.,** 2004. Melt Behaviour of Block Copolymers in *Developments in Block Copolymer Science and Technology*, Eds. Hamley, I.W., John Wiley & Sons.

[77] **West, P. E.,** 2006. *Introduction to Atomic Force Microscopy: Theory, Practice, Applications,* Pacific Nanotechnology, Santa Clara, USA.

[78] **Nelson, B., Bonilla, J. V. B. and Lobo, H.,** 2003. General Introduction to Plastics Analysis, in *Handbook of plastic analysis*, Chapter 1, Marcel Dekker Inc., New York.

[79] **Url-7** <*http://pslc.ws/macrog/tg.htm*>, accessed at 18.02.2010.

[80] **Menczel, J. D. and Prime, R. B.,** 2009. in *Thermal analysis of polymers: fundamentals and applications*, Wiley, New Jersey.

[81] **Xu, Y. J., Brittain, W. J., Vaia, R. A. and Price, G.,** 2006. Improving the physical properties of PEA/PMMA blends by the uniform dispersion of clay platelets*, Polymer*, **47** (13), 4564-4570.

[82] **Nelson, B., Bonilla, J. V. B. and Lobo, H.,** 2003. Capillary rheometry, in *Handbook of plastic analysis*, Chapter 2, Marcel Dekker Inc., New York.

[83] **Url-8 <***http://www.polydynamics.com/Role_of_Rheology_in Extrusion.PDF*>, accessed at 18.02.2010.

[84] **Vlachopoulos, J. and Wagner, J. R.,** 2001. The SPE Guide on Extrusion Technology and Troubleshooting, in *Society of Plastics Engineers*, Brookfield, CT

[85] **Cogswell, F. N.,** 1996. *Polymer Melt Rheology*, Woodhead Publishing, Cambridge, England.

[86] **Macosko, C. W.,** 1994. *Rheology: Principles, Measurements and Applications*, VCH Publishers, New York.

[87] **Adams, J. L., Graessley, W. M. and Register, R. A.,** 1994. Rheology and the microphase separation transition in styrene-isoprene block-copolymers*, Macromolecules*, **27** (21), 6026-6032.

[88] **Ciolino, A. E., Gomez, L. R., Vega, D. A., Villar, M. A. and Valles, E. M.,** 2008. Synthesis and physicochemical characterization of a well-defined poly(butadiene 1,3)-block-poly(dimethylsiloxane) copolymer*, Polymer*, **49** (24), 5191-5194.

[89] **Chanda, M. and Roy, S. K.,** 1998. Plastics Properties and Testing, in *Plastics Technology Handbook (Plastics Engineering)*, **47**, Marcel Dekker, Inc., New York.

[90] **ACS,** 1999. ASTM Annual Book of Standards, in *American Society for Testing and Materials*, **08.02**, West Conshohocken, PA.

[91] **Gahleitner, M.,** 2001. Melt rheology of polyolefins*, Progress in Polymer Science*, **26** (6), 895-944.

[92] **Klompen, E. T. J.,** 2005. Constitutive modelling of long and short term behaviour, in *Mechanical properties of solid polymers*, University Press Facilities, Technische Universiteit Eindhoven, The Netherlands, Eindhoven.

[93] **Menard, K. P.,** 1999. A Practical Introduction, in *Dynamic Mechanical Analysis*, CRC Press, Florida.

[94] **Url-9** <*http://www.hanser-publishers.com/*>, accessed at 18.02.2010.

[95] **Acar, M. H., Becer, C. R., Ondur, H. A. and Inceoglu, S.,** 2006. Alkylated linear amine ligands for homogeneous ATRP, in *Controlled/ Living Radical Polymerization: From Synthesis to Materials, ACS Symposium Series Book*, **994,** Eds. Matyjaszewski, K., Washington, DC.

[96] **Idota, N., Kikuchi, A., Kobayashi, J., Akiyama, Y. and Okano, T.,** 2006. Thermal modulated interaction of aqueous steroids using polymer-grafted capillaries*, Langmuir*, **22** (1), 425-430.

[97] **Inceoglu, S., Olugebefola, S. C., Acar, M. H. and Mayes, A. M.,** 2004. Atom transfer radical polymerization using poly(vinylidene fluoride) as macroinitiator*, Designed Monomers and Polymers*, **7** (1-2), 181-189.

[98] **Queffelec, J., Gaynor, S. G. and Matyjaszewski, K.,** 2000. Optimization of atom transfer radical polymerization using Cu(I)/tris(2-(dimethylamino)ethyl)amine as a catalyst*, Macromolecules*, **33** (23), 8629-8639.

[99] **Cassebras, M., Pascual, S., Polton, A., Tardi, M. and Vairon, J. P.,** 1999. Synthesis of di- and triblock copolymers of styrene and butyl acrylate by controlled atom transfer radical polymerization*, Macromolecular Rapid Communications*, **20** (5), 261-264.

[100] **Matyjaszewski, K., Shipp, D. A., McMurtry, G. P., Gaynor, S. G. and Pakula, T.,** 2000. Simple and effective one-pot synthesis of (meth)acrylic block copolymers through atom transfer radical polymerization*, Journal of Polymer Science Part A-Polymer Chemistry*, **38** (11), 2023-2031.

[101] **Horcas, I., Fernandez, R., Gomez-Rodriguez, J. M., Colchero, J., Gomez-Herrero, J. and Baro, A. M.,** 2007. WSXM: A software for scanning probe microscopy and a tool for nanotechnology, *Review of Scientific Instrument*, **78,** 013705.

[102] **Lecolley, F., Waterson, C., Carmichael, A. J., Mantovani, G., Harrisson, S., Chappell, H., Limer, A., Williams, P., Ohno, K. and Haddleton, D. M.,** 2003. Synthesis of functional polymers by living radical polymerisation*, Journal of Materials Chemistry*, **13** (11), 2689-2695.

[103] **Clayden, J., Greeves, N., Warren, S. and Wothers, P.,** 2001. *Organic Chemistry*, Chapter 12, 285, Oxford University Press.

[104] **Mather, B. D., Viswanathan, K., Miller, K. M. and Long, T. E.,** 2006. Michael addition reactions in macromolecular design for emerging technologies*, Progress in Polymer Science*, **31** (5), 487-531.

[105] **Jakubowski, W., Kirci-Denizli, B., Gil, R. R. and Matyjaszewski, K.,** 2008. Polystyrene with improved chain-end functionality and higher molecular weight by ARGET ATRP*, Macromolecular Chemistry and Physics*, **209** (1), 32-39.

[106] **Jakubowski, W., Min, K. and Matyjaszewski, K.,** 2006. Activators regenerated by electron transfer for atom transfer radical polymerization of styrene*, Macromolecules*, **39** (1), 39-45.

[107] **Min, K., Gao, H. F. and Matyjaszewski, K.,** 2005. Preparation of homopolymers and block copolymers in miniemulsion by ATRP using activators generated by electron transfer (AGET)*, Journal of the American Chemical Society*, **127** (11), 3825-3830.

[108] **Baskaran, D.,** 2003. Strategic developments in living anionic polymerization of alkyl (meth)acrylates*, Progress in Polymer Science*, **28** (4), 521-581.

[109] **Vlcek, P.,** 1990. Anionic polymerization of acrylates 1. Polymerization of 2-ethyl hexyl acrylate in nonpolar solvents, *Journal of Polymer Science Part a-Polymer Chemistry*, **28** (11), 2917-2922.

[110] **Vlcek, P., Otoupalova, J. and Kriz, J.,** 1993. The anionic polymerization of acrylates controlling the molecular weights in the polymerization of 2-ethyl hexyl acrylate initiated by the mixed initiator lithium ester-enolate lithium tert-butoxide, *Makromolekulare Chemie-Macromolecular Chemistry and Physics*, **194** (3), 841-847.

[111] **Vidts, K. R. M., Dervaux, B. and Du Prez, F. E.,** 2006. Block, blocky gradient and random copolymers of 2-ethylhexyl acrylate and acrylic acid by atom transfer radical polymerization, *Polymer*, **47** (17), 6028-6037.

[112] **Jeusette, M., Leclere, P., Lazzaroni, R., Simal, F., Vaneecke, J., Lardot, T. and Roose, P.,** 2007. New "all-acrylate" block copolymers: Synthesis and influence of the architecture on the morphology and the mechanical properties, *Macromolecules*, **40** (4), 1055-1065.

[113] **Acar, M. H. and Matyjaszewski, K.,** 1999. Block copolymers by transformation of living anionic polymerization into controlled/"living' atom transfer radical polymerization, *Macromolecular Chemistry and Physics*, **200** (5), 1094-1100.

[114] **Fuentes, G. G., Rodriguez, R., Avelar-Batista, J. C., Housden, J., Montala, F., Carreras, L. J., Cristobal, A. B., Damborenea, J. J. and Tate, T. J.,** 2005. Recent advances in the chromium nitride PVD process for forming and machining surface protection, *Journal of Materials Processing Technology*, **167** (2-3), 415-421.

[115] **Crawford, D. M., Bass, R. G. and Haas, T. W.,** 1998. Strain effects on thermal transitions and mechanical properties of thermoplastic polyurethane elastomers, *Thermochimica Acta*, **323** (1-2), 53-63.

[116] **Fang, H. X., Feng, L. B., You, B. and Wu, L. M.,** 2007. Effect of annealing on the microphase separated behavior and properties of PDMS-MDI-PEG multiblock copolymer films, *Journal of Polymer Science Part B-Polymer Physics*, **45** (2), 208-217.

[117] **Saiani, A., Rochas, C., Eeckhaut, G., Daunch, W. A., Leenslag, J. W. and Higgins, J. S.,** 2004. Origin of multiple melting endotherms in a high hard block content polyurethane. 2. Structural investigation, *Macromolecules*, **37** (4), 1411-1421.

[118] **Ryu, C. Y., Lee, M. S., Hajduk, D. A. and Lodge, T. P.,** 1997. Structure and viscoelasticity of matched asymmetric diblock and triblock copolymers in the cylinder and sphere microstructures, *Journal of Polymer Science Part B-Polymer Physics*, **35** (17), 2811-2823.

[119] **Ren, J. X. and Krishnamoorti, R.,** 2003. Nonlinear viscoelastic properties of layered-silicate-based intercalated nanocomposites, *Macromolecules*, **36** (12), 4443-4451.

[120] **Cassel, B. and Twombly, B.,** 1991. Glass-transition determination by thermomechanical analysis, a dynamic mechanical analyzer and a differential scanning calorimeter, in *Materials Characterization by Thermomechanical Analysis*, Eds. Riga, A.T., and Neag, C.M., 108-119, ACS, Philadelphia, USA.

CIRRUCULUM VITAE

Candidate's full name **:** Şebnem İNCEOĞLU

Place and Date of Birth **:** 12.06.1978

Permanent Adress **:** ITU

Universities attended **:** ITU Polymer Science and Technology

Publications **:**

- "Novel Baroplastic Materials" **S. Inceoglu**, M. H. Acar, Progress in Controlled/Living Radical Polymerization, ACS Symposium Series Book; Matyjaszewski, K., Ed, Philadelphia, PA, Materials Prepared by ATRP, Chapter 21, 313, (2009).
- "Baroplastic in different topologies and used as compatibilizer" M. H. Acar, **S. Inceoglu**, Abst. Paper Am. Chem. Soc. 236, 270 (2008) Polym. Preprint 49(2), 30 (2008).
- "Alkylated Linear Amine Ligands for Homogeneous Atom Transfer Radical Polymerization" M. H. Acar, C. R. Becer, H. A. Ondur, **S. Inceoglu**, In Controlled/ Living Radical Polymerization: From Synthesis to Materials, ACS Symposium Series Book; Matyjaszewski, K., Ed, Washington, DC, 994, Chapter 97 (2006).
- "Synthesis of alkylated linear amine ligands and their effect on homogeneous ATRP" M. H. Acar, C. R. Becer, H. A. Ondur, **S. Inceoglu**, Abst. Paper Am. Chem. Soc. 230, 242 (2005) Polym. Preprint, 46(2), 433 (2005).
- "Synthesis of styrene-methyl methacrylate graft and graft-block copolymers via combination of ATRP and SFRP" **S. Inceoglu**, U. Tunca, G. Hızal, Designed Monomers and Polymers, 7, 203 (2004).
- "Atom Transfer Radical Polymerization using poly(vinylidene fluoride) as macroinitiator" **S. Inceoglu**, S. C. Olugebefola, M. H. Acar, A. M. Mayes, Designed Monomers and Polymers, 7, 181 (2004).

Awards :

- Oral Presentation Award (2nd): Nanomats2009, 10-13 August 2009
- Poster Presentation Award (3rd): NATO-ASI, 1-12 September 2008
- Poster Presentation Award (2nd): NanoTr4, 9-13 June 2008
- Oral Presentation Award (1st, Best young speaker): CLP07, 25-29 Oct. 2007
- Poster Presentation Award (1st): APME03, 1-26 June 2003

Projects :

- Tubitak 107M323 (November 2007-November 2009) "Baroplastic Elastomer: New method for plastic processing and recycling" Istanbul Technical University.
- Tubitak 104M409 (November 2005-November 2007) "Synthesis of new polymeric membranes for proton exchange membrane fuel cells" Istanbul Technical University and Sabancı University.
- MIT (February 2003-July 2003) "Ultrafiltration polymeric membranes" Massachusetts Institute of Technology.

Proceedings :

International

- "Plastics Processing: Energy saving without heating" **S. Inceoglu**, M. H. Acar, 11th Pasific Polymer conference, PPC11, Cairns, Avustralya (6-10 December 2009), oral presentation.
- "Decreasement of nanophase separation on plastics" **S. Inceoglu**, M. H. Acar, International Conference on Nanomaterials and Nanosystems, NanoMats, ITU, Istanbul, Turkey, (10-13 August 2009).
- "Baroplastic: Synthesis, characterization and application" **S. Inceoglu**, M. H. Acar, Nanoscience and Nanotechnology Conference, NanoTR4, ITU, Istanbul, Turkey, (9-13 June 2008), poster presentation.
- "Baroplastics in different topologies and their compatibilizer behaviour" **S. Inceoglu**, M. H. Acar, Nanoscience and Nanotechnology Conference, NanoTR4, ITU, Istanbul, Turkey, (9-13 June 2008), poster presentation.
- "Baroplastics in different topologies and their compatibilizer", M. H. Acar, **S. Inceoglu**, Controlled/Living Radical Polymerization, at the National Meeting of the American Chemical Society in Philadelphia, PA, USA (17-21 August 2008), invited speaker, oral presentation.
- "Baroplastic elastomers" **S. Inceoglu**, New Smart Materials via Metal Mediated Macromolecular Engineering: From Complex to Nano Structures, NATO Advanced Study Institute (ASI), Antalya, Turkey, (1-12 September 2008), oral presentation.

▪ "Baroplastic Elastomer: In Different Topologies and used as Compatibilizer" **S. Inceoglu**, M. H. Acar, The Polymer Processing Society 24th Annual Meeting, PPS24, Salerno, Italy, (15-19 June 2008), oral presentation.

▪ "Baroplastics in Different Topologies and Used as Compatibilizer" **S. Inceoglu**, M. H. Acar, Controlled/Living Polymerization: From synthesis to applications, CLP'07, Antalya, Turkey, (25-29 October 2007), oral presentation.

▪ "Synthesis of PVDF-based copolymers" N. Bozok, **S. Inceoglu**, B. Saner, B. Birkan, Y. Z. Menceloglu, M. H. Acar, Controlled/Living Polymerization: From synthesis to applications, CLP'07, Antalya, Turkey, (25-29 October 2007), poster presentation.

▪ "The effect of stirring rate on heterogeneous ATRP" N. Bozok, **S. Inceoglu**, M. H. Acar, Controlled/Living Polymerization: From synthesis to applications, CLP'07, Antalya, Turkey, (25-29 October 2007), poster presentation.

▪ "Alkylated polyethyleneimine ligand for homogeneous atom transfer radical polymerization" A. Zorvaryan, **S. Inceoglu**, M. H. Acar, Controlled/Living Polymerization: From synthesis to applications, CLP'07, Antalya, Turkey, (25-29 October 2007), poster presentation.

▪ "Different topologies on baroplastic elastomers" **S. Inceoglu**, M. H. Acar, 1st European Chemistry Congress, EuChems06, Budapest, Hungary, (27-31 August 2006), poster presentation.

▪ "Atom transfer radical polymerization: homogeneous or heterogeneous?" M. H. Acar, C. R. Becer, H. A. Ondur, A. Zorvaryan, O. Deniz, M. Bekmez, N. Bozok, **S. Inceoglu**, 1st European Chemistry Congress, EuChems06, Budapest, Hungary, (27-31 August 2006), oral presentation.

▪ "Alkylated polyethyleneimine ligand (APEI) for homogeneous atom transfer radical polymerization" A. Zorvaryan, **S. Inceoglu**, M. H. Acar, 1st European Chemistry Congress, EuChems06, Budapest, Hungary, (27-31 August 2006), poster presentation.

▪ "Design and synthesis of novel polymeric materials for proton exchange membrane fuel cell applications", B. Birkan, **S. Inceoglu**, Y. Z. Menceloglu, M. H. Acar, 2005 International Hydrogen Energy Congress, (IHEC'2005), İstanbul, Turkey (13-15 July 2005), oral presentation.

▪ "Synthesis of alkylated linear amine ligands and their effect on homogeneous ATRP", M. H. Acar, C. R. Becer, H. A. Ondur, **S. Inceoglu**, Fall National ACS meeting, Washington, D. C., ABD (27 August-1 September 2005), oral presentation.

▪ "Atom Transfer Radical Polymerization using PVDF as macroinitiator" **S. Inceoglu**, S. C. Olugebefola, M. H. Acar, A. M. Mayes, 40th IUPAC International Symposium on Macromolecules World Polymer Congress, Macro2004 (4-9 July 2004), poster presentation.

▪ "Synthesis of styrene-methyl methacrylate graft and graft-block copolymers via combination of ATRP and SFRP" **S. Inceoglu**, U. Tunca, G. Hızal, The 5th International Conference on Advanced Polymer via Macromolecules Engineering, APME5, (21-26 June 2003), poster presentation.

▪ "Alkyl Floride as an initiator in ATRP" **S. Inceoglu**, S. Aras, M. H. Acar, A. M. Mayes, The 5th International Conference on Advanced Polymer via Macromolecules Engineering, APME5, (21-26 June 2003), poster presentation.

National

▪ "Synthesis and characterization of PVDF-based proton conductive copolymers" H. Kocaturk, **S. Inceoglu**, B. Birkan, S. U. Celik, A. Bozkurt, Y. Z. Menceloglu, M. H. Acar , IV. National Hydrojen Energy Congress and Exhibition, UHK 2009, Kocaeli University, (15-16 October 2009), oral presentation.

▪ "Baroplastic: New approach for plastic processing" **S. Inceoglu**, New Polymeric Materials and Technology Workshop, NPMT, Çanakkale, Turkey, Çanakkale 18 Mart University, (17-19 April 2009), invited speaker, oral presentation.

▪ "Proton değişim membran yakıt pilleri için yeni polimerik mebran sentezi" H. Kocaturk, **S. Inceoglu**, M. H. Acar, New Polymeric Materials and Technology Workshop, NPMT, Çanakkale, Turkey, Çanakkale 18 Mart University, (17-19 April 2009), oral presentation.

▪ "Recycling and thermal characterization of baroplastic" A. S. Bilal, **S. Inceoglu**, M. H. Acar, New Polymeric Materials and Technology Workshop, NPMT, Çanakkale, Turkey, Çanakkale 18 Mart University, (17-19 April 2009), oral presentation.

▪ "New synthetic approach for star and star- block (co)polymers" C. Catlı, **S. Inceoglu**, M. H. Acar, New Polymeric Materials and Technology Workshop, NPMT, Çanakkale, Turkey, Çanakkale 18 Mart University, (17-19 April 2009), oral presentation.

▪ "Baroplastic as processing aid" E. Buyukaslan, **S. Inceoglu**, M. H. Acar, oral New Polymeric Materials and Technology Workshop, NPMT, Çanakkale, Turkey, Çanakkale 18 Mart University, (17-19 April 2009), oral presentation.

▪ "Homogeneous ATRP with alkylated linear amine ligands" **S. Inceoglu**, 1st National Science and Technology Congress, ODTU, Ankara, Turkey (21-23 June 2006) oral presentation

▪ "Design of new polymeric membranes for hydrogen fuel cells" D. Kösker, **S. Inceoglu**, B. Birkan, Y. Z. Menceloğlu, M. H. Acar, 1st National Science and Technology Congress, ODTU, Ankara, Turkey (21-23 June 2006), (2nd poster design award) poster presentation.

- "Synthesis of ethylated polyethyleneimine ligand and using in homogeneous atom transfer radical polymerization" A. Zorvaryan, **S. Inceoglu**, M. H. Acar, 1st National Science and Technology Congress, ODTU, Ankara, Turkey (21-23 June 2006), poster presentation.

- "Synthesis of three dentate linear amine ligands and using in homogeneous atom transfer radical polymerization" M. Bekmez, **S. Inceoglu**, M. H. Acar, 1st National Science and Technology Congress, ODTU, Ankara, Turkey (21-23 June 2006), poster presentation.

- "Effect of stirring rate in heterogeneous atom transfer radical polymerization" N. Bozok, **S. Inceoglu**, M. H. Acar, 1st National Science and Technology Congress, ODTU, Ankara, Turkey (21-23 June 2006), poster presentation.

- "Synthesis of tetra dentate linear amine ligands and using in homogeneous atom transfer radical polymerization" O. Deniz, **S. Inceoglu**, M. H. Acar, 1st National Science and Technology Congress, ODTU, Ankara, Turkey (21-23 June 2006), poster presentation.

- "2-Fenil-2-[2,2,6,6-tetrametilpiperidiniloksi]-etil-2-metakrilat monomerinin sentezi ve yaşayan polimerizasyon yöntemleri ile aşı blok kopolimerlerinin eldesi" **S. Inceoglu,** Tunca, U., Hızal, G., XVI. National Chemistry Congress, Konya, Turkey (10-13 September 2002.) oral presentation.